Fermionic Superfluids: From Cold Atoms to High Density QCD

Gapless (Breached Pair) Superfluidity and Kaon Condensation

by

Michael McNeil Forbes

B.Sc., The University of British Columbia, 1999
M.Sc., The University of British Columbia, 2001

Submitted to the Department of Physics
in partial fulfillment of the requirements for the degree of

Doctor of Philosophy

at the

Massachusetts Institute of Technology

3 June 2005

Signature of Author .....
Department of Physics
May 17, 2005

Certified by .....
Frank Wilczek
Herman Feshbach Professor of Physics
Thesis Supervisor

Accepted by .....
Thomas Greytak
Professor and Associate Department Head for Education

Fermionic Superfluids: From Cold Atoms to High Density QCD

Gapless (Breached Pair) Superfluidity and Kaon Condensation

by

Michael McNeil Forbes

Submitted to the Department of Physics
on May 18, 2005, in partial fulfillment of the
requirements for the degree of
Doctor of Philosophy

Abstract

In this thesis, we explore aspects of fermionic superfluidity through a mean-field approximation. Our framework is extremely general, includes both pairing and Hartree-Fock contributions, and is derived rigorously from a variational principle. This framework allows us to analyze a wide range of fermionic systems. In this thesis, we shall consider two-species non-relativistic atomic systems with various types of interactions, and relativistic QCD systems with $3 \times 3 \times 4 = 36$ different quark degrees of freedom (3 colours, 3 flavours, and 4 relativistic degrees of freedom).

We discuss properties of a new state of matter: gapless (Breached Pair) superfluidity, and include a summary of potential experimental realizations. We also present numerical results for a completely self-consistent approximation to the NJL model of high-density QCD and use these results to demonstrate a microscopic realization of kaon condensation. We describe how to match the mean-field approximation to the low-energy chiral effective theory of pseudo-Goldstone bosons, and we extract the numerical coefficients of the lowest order effective potential.

Thesis Supervisor: Frank Wilczek
Title: Herman Feshbach Professor of Physics

Contents

List of Tables

List of Figures

Preface

The goal of this thesis is to provide the reader with a solid foundation for the theory of fermionic superfluidity, and to use this foundation to examine some novel phenomena in both condensed matter physics and particle physics. The basic formalism is based on a mean-field approximation: This approximation, however, is firmly founded on a variational method. By couching our analysis firmly in a variational principle, I hope to remove much of the mystery behind the use of the mean-field method.

I present the variational method in a very general manner using a matrix formalism. This allows the same technique to approximate both non-relativistic condensed matter physics, and relativistic models of QCD.

The overall structure of this document is thus: First some background is given to set the stage. I subsequently develop the mean-field formalism in Part I, apply this to non-relativistic systems in Part II, and extend this to relativistic QCD in Part III. For those of you who are experts, I would suggest glancing through the formalism, and then heading straight to the heart of the relevant material in Part II (for the condensed matter physics) and Part III (for the high-energy physics). Details have been relegated to the Appendix IV to clarify the presentation.

All of the work in this thesis is my own, although some of the background reflects other presentations as noted. The bulk of the novel and original work is centred about two of my recent publications: My work on the "Stability Criteria for Breached Pair Superfluidity" with Elena Gubankova, W. Vincent Liu, and Frank Wilczek [1] forms the basis for Part II, and my work on "Kaon Condensation in an NJL Model at High Density" [2] forms the basis of Part III. I developed the matrix formalism as a background to study both of these topics. In addition, I have included partial discussions of several topics that represent ongoing work and suggest future directions.

Acknowledgements

First of all, I would like to thank my adviser Frank Wilczek for his encouragement, support, and insight throughout the course of my Ph.D. It has been an honour and pleasure to work with him. I am also extremely grateful to Krishna Rajagopal for sharing his time, support, and advice, and for treating me like one of his own students. I would also like to thank Ariel Zhitnitsky for many discussions, and much candid advice.

For reading and commenting on this thesis, I would like to thank my thesis committee: Frank, Krishna and Young Lee. I also extend special appreciation to my colleagues Wensheng Vincent Liu and Elena Gubankova with whom I spent many hours discussing and working details of the Breach Pair states.

Thanks to Ian Affleck, Mark Alford, Ryan Barnett, Gordon Baym, Paulo Bedaque, Roberto Casalbuoni, Brian Fore, Kenji Fukushima, Tamar Friedmann, Umut Gursoy, Alan Guth, Walter Hoffstetter, Deog Ki Hong, David Kaplan, Chris Kouvaris, Joydip Kundu, Andrei Kryjevski , Björn Lange, Keith Seng Mun Lee, Michael Levin, Sonny Mantry, Vivek Mohta, Sanjay Reddy, Sean Patrick Robinson, Martin Savage, Thomas Schäfer, Andreas Schmitt, Rishi Sharma, Jessie Shelton, Martin Savage, Igor Shovkovy, Dam Son, Iain Stewart, Ari Turner, and Wesley Wong for many useful discussions about physics related to this thesis. I would also like to thank Molly Bright and David Lopez Mateos for comments on the introduction of this thesis.

Finally, I would like to thank my wife Katheryn Buble, and my parents for being so supportive of my work, and for proofreading sections of this thesis.

This research was supported in part by the Natural Sciences and Engineering Research Council (NSERC) of Canada Postgraduate Scholarship program, and by funds provided by the U. S. Department of Energy (D.O.E.) under cooperative research agreement #DF-FC02-94ER40818. I am also grateful for the Institute for Nuclear Theory (I.N.T.) at the University of Washington, Seattle for their hospitality and support.

Chapter 1

Introduction

1.1 Why Fermions?

Why are we interested in systems of fermions? It turns out that all of the observed "matter" in the universe is composed fundamentally of fermions. Thus, fermions are ubiquitous, and their fundamental nature is key to understanding how the world works. Perhaps we should start by answering the question of just what a fermion *is*?

The term "fermion" characterizes one class of particles: the "stuff" comprised by the universe. More generally, the presently accepted fundamental theory of the universe characterizes all "stuff" as particles, and allows for two classes of particles: bosons and fermions. This classification follows from a fundamental property of quantum field-theory that particles are fundamentally indistinguishable. This indistinguishability is not simply a statement that all particles of a certain type have the same physical properties (such as mass, charge, etc.), but that one must even *count* the particles as if they were completely indistinguishable. The counting becomes important when considering the thermodynamics of particles as the statistical mechanical framework is predicated on determining how many accessible states are available with a certain energy. Thus, indistinguishability has a profound consequence on the "statistics" of fundamental particles: bosons are counted with "Bose-Einstein" statistics, fermions are counted with "Fermi-Dirac" statistics, and distinguishable particles are counted with "Maxwell-Boltzmann" statistics. At large enough temperatures, both "Bose-Einstein", and "Fermi-Dirac" reduce to "Maxwell-Boltzmann" statistics: it is only at low temperatures that the quantum distinctions are important.

Consider two particles: In quantum mechanics, the state of a system is described by a "wave-function" $\psi(\vec{\mathbf{r}}_1, \vec{\mathbf{r}}_2)$ that describes the "probability amplitude" that one particle will be found (measured) at position $\vec{\mathbf{r}}_1$ and that the other will be found (simultaneously measured) at position $\vec{\mathbf{r}}_2$. (The actual probability is governed by the square of the amplitude: $p = |\psi|^2$.) If the particles are distinguishable, then the two wave-functions $\psi_{12} = \psi(\vec{\mathbf{r}}_1, \vec{\mathbf{r}}_2)$ and $\psi_{21} = \psi(\vec{\mathbf{r}}_2, \vec{\mathbf{r}}_1)$, which differ by exchanging the particles, could be

different: $|\psi_{12}|^2 \neq |\psi_{21}|^2$. This would allow one, in principle, to identify each particle.

Fundamental indistinguishability requires that there be no such way of identifying the particles. Mathematically, this implies that the wave-function transform by only a phase under the exchange of particles. Coupled with the dimensionality[1] of our space-time, two possibilities are permitted:

Bosons: The wave function for bosons does not change under particle exchange:

$$\psi_B(\vec{\mathbf{r}}_1, \vec{\mathbf{r}}_2) = \psi_B(\vec{\mathbf{r}}_2, \vec{\mathbf{r}}_1). \tag{1.1}$$

In particular, two particles can be in the same state: $\psi_B(\vec{\mathbf{r}}_1, \vec{\mathbf{r}}_1) \neq 0$. This possibility admits the phenomena of Bose-Einstein condensation. At low temperatures, a macroscopic number of bosons occupy the ground state forming a single quantum state of macroscopic size. This state is called a Bose-Einstein Condensate (BEC). Bose-Einstein condensation appears to be responsible for most superfluid phenomena.

Fermions: The wave function for fermions changes sign under particle exchange:

$$\psi_F(\vec{\mathbf{r}}_1, \vec{\mathbf{r}}_2) = -\psi_F(\vec{\mathbf{r}}_2, \vec{\mathbf{r}}_1). \tag{1.2}$$

This implies that particles can *not* be in the same state: $\psi_F(\vec{\mathbf{r}}_1, \vec{\mathbf{r}}_1) = -\psi_F(\vec{\mathbf{r}}_1, \vec{\mathbf{r}}_1) = 0$. This is the famous Pauli exclusion principle, and it leads to very different physics at low-temperatures.

Consider a collection of bosons: as the temperature is lowered, more and more of the bosons will try to occupy the lowest energy state. Nothing stands in their way. The result is that, at extremely low temperatures, virtually all of the bosons will occupy a single quantum state, and the system can be well described by a single, coherent wave-function.

If the matter in the universe were fundamentally composed of bosons, such a collapse would be catastrophic. Although the Heisenberg uncertainty principle would prevent complete collapse, bulk matter composed only of bosons could not be stable. As Dyson pointed out, were bulk matter primarily bosonic, even the simple act of bringing together two macroscopic objects would release huge amounts of energy comparable to a thermonuclear explosion [4].

[1] Mathematically this is related to the topology of the group SO(3) of rotations: $\pi_1(\mathrm{SO}(3)) = \mathbb{Z}_2$. In two spatial dimensions where $\pi_1(\mathrm{SO}(2)) = \mathbb{Z}$ one may have many different types of particles with fractional statistics called "anyons". See for example [3].

Fortunately, all of the observed, stable, non-relativistic matter in the universe has turned out to be fermionic.[2] Pauli's famous exclusion principle comes to the rescue and permits bulk matter to be stable. (Note that, although this is trivially observed through our existence, and the lack of fireworks whenever we clap our hands, it is not at all trivial to show formally: see for example [6, 7] and the references therein.)

Massive bosons do appear in nature: many atoms, for example, are bosonic. Bose-Einstein condensation can thus play an important role in cold systems of atoms. Fundamentally, however, these bosons are composite collections of an even number of fermions. (One must count the total number of protons, neutrons and electrons: if the sum is even, the atom will be a boson; if it is odd, the atom will be a fermion). Although composite bosons may condense, eventually, these composite bosons will get close enough together that their constituent fermions start to interact. At this point, the Pauli principle kicks in and the collapse of matter is fortuitously arrested.

One of the reasons to study the properties of fermions is that, not only are the responsible for the stability of matter, but they form the basis of bulk matter. In many contexts, the exclusion principle plays a fundamental role in the dynamics. We shall focus our attention here on degenerate Fermi systems: systems in which the fermions would like to collapse into a single state, but in which the exclusion principle creates a "degeneracy" pressure that stabilizes the system. Here are a few examples:

Electronics: In metals, and semiconductors, the electrons are the fundamental degrees of freedom (the nuclei are typically fixed firmly in a lattice). The electron interactions are dominated by the exclusion principle, and many properties of metals are well described as a "Fermi liquid".

Superconductors: At low enough temperatures, systems of degenerate fermions may undergo a phase transition and become a superconductor:

[2] As discussed in Section 6.1.4, it appears that virtually all fundamental particles—other than the massless gauge bosons which mediate the forces—are fermions. There is one notable exception: the Higgs boson. Although it is a cornerstone for the Standard Model of particle physics, (see Section 6.1.7), the Higgs has not been conclusively detected. Even if it does exist, the Higgs is not stable and thus does not enter into the stability arguments discussed here.

As for the gauge bosons: they are massless. Being massless, they can never be at rest and thus cannot accumulate in low-energy matter. It should be mentioned, however, that, despite being massless, the gauge bosons that bind quarks together—the gluons—have energy, and are responsible for the majority of the visible mass in the universe via $m = E/c^2$. See for example [5].

a material with no electrical resistance. This phenomenon is ultimately due to pairs of fermions acting like bosons and condensing to form a BEC. The microscopic theory for the simplest type of superconductor was first developed by Bardeen, Cooper, and Schrieffer [8]. Materials described by this model are referred to as BCS superconductors.

Atomic Physics: Recently, there has be a great deal of interest in systems of cold atoms (typically alkali metals). If the atoms are bosons, then one may obtain a BEC. If the atoms are fermions, one may obtain a BCS like state.[3] Materials described as either a BEC or by BCS theory are generally referred to as "superfluids". Even in the case of atomic BECs, the effects of the exclusion principle can play an important role in the dynamics.

One of the "hottest" areas of research in this field is to study the transition from a BEC to a BCS phase. This occurs in systems of fermions. As the interacting is increased, the fermions bind to form bosons. These systems can thus exhibit properties of both BCS and BEC states. For a weakly attractive interaction, the exclusion principle dominates and one has a BCS superfluid state. As one increases the interactions, molecular bound states form, and at strong enough coupling, the fermions pair to form tightly bound bosons which condense in a BEC. It is generally believed that this transition is actually a smooth crossover, and that the two phases are different manifestations of the same physics.

Compact Stellar Objects: The consequence of nature's choice for fermions as fundamental particles is perhaps nowhere better emphasize than in compact stellar objects: white dwarfs and neutron stars. These are the last stages of stellar evolution. When enough of a massive star's light elements have fused into iron, the star can no longer efficiently generate energy from the fusion processes. The star starts to cool and the thermal pressure is no-longer sufficient to prevent further gravitational collapse.

As the stars cool, the atoms fall closer and closer together. If the fundamental constituents of matter were bosons, all old stars would quickly collapse into black holes. If the star is not too massive, however, then the collapse is arrested by the Pauli exclusion principle between the electrons. This suffices to stabilize the white dwarf as long as it is less than about 1.4 solar masses. Many properties of white dwarfs are well modelled as a

[3]These states are very similar to superconductors, but, unlike the electrons in a superconductor, the atoms in a trap are neutral. Thus, these states are better described as BCS superfluids.

degenerate Fermi liquid of electrons.

If the original star was extremely massive, however, its demise may be cataclysmic rather than slow cooling, with much of the star's matter being blown away in a supernova explosion. The remnants of massive supernova are still too massive for the electron degeneracy pressure to stabilize. Gravity compresses the stellar remnant to such an extent that the electrons are crushed into the protons. The resulting object—a "neutron" star—is typically of about 10 km radius and may be thought of as a single gigantic nucleus! At this point, the collapse is arrested by the exclusion principle between the protons and neutrons. Some properties of this proton-neutron fluid may be well described as a degenerate Fermi liquid, and is typically thought to be superfluid.

In the cores of neutron stars, however, the pressure may be so great that even the protons and neutrons are crushed together. The collapse is once again arrested by the exclusion principle—this time by the exclusion pressure of the quarks. Even in this extremely dense regime, the physics may once again be described as a degenerate Fermi liquid.

The same techniques used to study conventional superconductivity may be used to study this extremely dense quark matter with the role of the electrically-charged electrons being assumed by the coloured quarks. As we shall discuss later, such matter may also be a superfluid: a "colour" superconductor.

The universal applicability of a single theory of degenerate fermions to physics spanning over more than 9 orders of magnitude is surely one of nature's marvels.

Part I

Formalism and Background

Chapter 2

Variational Mean-Field Method

The technical core for the analysis in this thesis is based on the application of a variational method due to Feynman [9]. With this method, we shall provide a rigorous foundation for the "mean-field" approximation that is to follow. We shall derive this mean-field method for rather arbitrary fermionic systems, starting with simple two-component systems and proceeding to study models of QCD that contain nine species of quarks, each with four relativistic components. We hope that this formulation provides the reader with a solid basis for the resulting mean-field approximation. Although these techniques appears often in the literature, they are seldom properly explained or justified.

Consider a system described by a Hamiltonian $\widehat{\mathbf{H}}$. As we discuss in Appendix A, all of the thermodynamic information is given in the appropriate partition function

$$Z = e^{-\beta F} = \mathrm{Tr}[e^{-\beta \widehat{\mathbf{H}}}] \tag{2.1}$$

where the operator $\widehat{\mathbf{H}}$ and resulting thermodynamic potential F are chosen to produce the desired ensemble. (In this case, $\widehat{\mathbf{H}}$ is the Hamiltonian, and F is the Helmholtz free-energy: this expression is for the macro-canonical ensemble at fixed temperature $T = 1/(k_B\beta)$.)

The basic principle behind the mean-field approximation is to use the solution for some exactly solvable model $\mathbf{H}_0$ to approximate the desired model. This idea comes from a variational method discussed by Feynman [9] which we state here without proof:

Th$^{\underline{\mathbf{m}}}$ 2.0.1: *The thermodynamic potential F of a given system described by the Hamiltonian $\widehat{\mathbf{H}}$ is bounded:*

$$F \leq F_0 + \langle \widehat{\mathbf{H}} - \widehat{\mathbf{H}}_0 \rangle_0 \tag{2.2}$$

where F_0 is the free energy of the system described by Hamiltonian $\widehat{\mathbf{H}}_0$ and

the average is performed with respect to the thermal ensemble of $\widehat{\mathbf{H}}_0$*:*

$$\langle \widehat{\mathbf{A}} \rangle_0 = \frac{\mathrm{Tr}\left[\widehat{\mathbf{A}} e^{-\beta \widehat{\mathbf{H}}_0}\right]}{\mathrm{Tr}\, e^{-\beta \widehat{\mathbf{H}}_0}}. \tag{2.3}$$

To use this, we consider a family of solvable Hamiltonian for which we can compute the right hand side. We then vary the parameters of this Hamiltonian to minimize the right side, thereby obtaining an upper bound for the true thermodynamic potential on the left. Using the thermodynamic relationship $\widehat{\boldsymbol{\rho}}_0 = \exp(-\beta \widehat{\mathbf{H}}_0)/Z_0$, which follows from the principle of maximum entropy, we have

$$F_0 = E - TS = \langle \widehat{\mathbf{H}}_0 \rangle_0 - T\,\mathrm{Tr}[\widehat{\boldsymbol{\rho}}_0 \ln \widehat{\boldsymbol{\rho}}_0]. \tag{2.4}$$

Thus, the variational procedure is equivalent to the standard thermodynamic minimization,

$$F \leq \min_{\widehat{\boldsymbol{\rho}}_0} \left(\langle \widehat{\mathbf{H}} \rangle_0 - TS(\widehat{\boldsymbol{\rho}}_0) \right), \tag{2.5}$$

over a set of ensembles $\widehat{\boldsymbol{\rho}}_0$ is defined by the choice of exactly solvable Hamiltonians $\widehat{\mathbf{H}}_0$.

In this thesis we shall work primarily in the grand-canonical ensemble where we fix the temperature, and the chemical potentials. We thus typically redefine our "Hamiltonian" so as to include the chemical potential:

$$\widehat{\mathbf{H}} \equiv \widehat{\mathbf{H}} - \mu \widehat{\mathbf{N}}. \tag{2.6}$$

In this case, the relevant thermodynamic potential $\Omega = -PV$ is proportional to the negative pressure of the system. In this grand-canonical ensemble, the mean-field calculation now is equivalent to the minimization

$$\Omega[\mu] \leq \min_{\widehat{\boldsymbol{\rho}}_0} \left(F(\widehat{\boldsymbol{\rho}}_0) - \mu \langle \widehat{\mathbf{N}} \rangle_0 \right). \tag{2.7}$$

This has some important consequences. In particular, as discussed in Appendix A.4.1, the computed bound for $\Omega[\mu]$ is a convex function of its arguments. This is true for any source (chemical potential or background field) added linearly to the "Hamiltonian". Thus, if a bunch of chemical potentials μ_a are introduced, the matrix

$$[\mathbf{M}]_{a,b} = \frac{\partial^2 \Omega}{\partial \mu_a \partial \mu_b} \tag{2.8}$$

is negative semi-definite. This condition is a necessary condition for thermodynamic equilibrium and follows directly from the principle of maximal entropy.

In our case, we choose the exactly solvable models to be purely quadratic. The resulting approximation is thus Gaussian, and completely described by two-point correlations: Higher order correlations are completely described in terms of the two-point correlations through Wick's theorem. For example, the four-point function is given by

$$\langle \hat{\mathbf{a}}\hat{\mathbf{b}}\hat{\mathbf{c}}\hat{\mathbf{d}} \rangle_0 = \langle \hat{\mathbf{a}}\hat{\mathbf{b}} \rangle \langle \hat{\mathbf{c}}\hat{\mathbf{d}} \rangle_0 + \langle \hat{\mathbf{a}}\hat{\mathbf{d}} \rangle \langle \hat{\mathbf{b}}\hat{\mathbf{c}} \rangle_0 \pm \langle \hat{\mathbf{a}}\hat{\mathbf{c}} \rangle \langle \hat{\mathbf{b}}\hat{\mathbf{d}} \rangle_0 . \tag{2.9}$$

The sign of the last term depends on the statistics of the particles. The order of the operators in this term is an odd permutation of the original interaction. For fermions, this term thus acquires a relative minus sign. For non-Gaussian states, this decomposition is not exact as there are generally more than just two-body correlations.

One can think of this as replacing the operator combination $\hat{\mathbf{a}}\hat{\mathbf{b}} \rightarrow \langle \hat{\mathbf{a}}\hat{\mathbf{b}} \rangle_0$ with its "mean' value, hence the term "mean-field". If one has access to more general solvable models, then these may also be used to obtain generalized "mean-field" approximations. (In this case, the term "mean-field" may not be very appropriate.) Exactly solvable models, however, are generally hard to come by.[1] In this thesis, we shall restrict our discussion to approximation by quadratic models.

[1]Note, however, that the original BCS model admits an exact solution due to Richardson [10]. This is part of a class of exactly solvable models classified by a Gaudin algebra. See [11, 12, 13] for more details. We shall not use these solutions here.

Chapter 3

Matrix Formulation

3.1 Fermions

The basis of our variational mean-field calculation will be systems of fermions with purely quadratic interactions. We start by presenting some simple results for these systems.

3.1.1 Thermodynamic Potential

Consider the quantum mechanics of a single fermionic degree of freedom described by the Hamiltonian

$$\widehat{\mathbf{H}} = \omega\left(\widehat{\mathbf{a}}^\dagger\widehat{\mathbf{a}} - \tfrac{1}{2}\right) + h_0. \tag{3.1}$$

The partition function for this system can be computed using the complete two-dimensional basis $\{|0\rangle, |1\rangle\}$:

$$\begin{aligned} e^{-\beta\Omega} &= \mathrm{Tr}[e^{-\beta[\omega(\widehat{\mathbf{a}}^\dagger\widehat{\mathbf{a}}-1/2)+h_0]}], &(3.2)\\ &= e^{-\beta[h_0-\omega/2]}\left(\langle 0|e^{-\beta\omega\widehat{\mathbf{a}}^\dagger\widehat{\mathbf{a}}}|0\rangle + \langle 1|e^{-\beta\omega\widehat{\mathbf{a}}^\dagger\widehat{\mathbf{a}}}|1\rangle\right), \\ &= 2\cosh(\beta\omega/2)e^{-\beta h_0}. &(3.3)\end{aligned}$$

The thermodynamic potential is thus

$$\Omega = -\frac{1}{\beta}\ln(Z) = -\frac{1}{\beta}\ln[2\cosh(\beta\omega/2)] + h_0. \tag{3.4}$$

The formal structure of a Hamiltonian with more degrees of freedom

$$\widehat{\mathbf{H}} = \sum_n \omega_n\left(\widehat{\mathbf{a}}_n^\dagger\widehat{\mathbf{a}}_n - \tfrac{1}{2}\right) \tag{3.5}$$

is a diagonal tensor product of similar terms:

$$e^{-\beta\widehat{\mathbf{H}}} = \bigotimes_n e^{-\beta\omega_n\left(\widehat{\mathbf{a}}_n^\dagger\widehat{\mathbf{a}}_n - \frac{1}{2}\right)}. \tag{3.6}$$

The resulting partition function is thus

$$Z = e^{-\beta\Omega} = \prod_n 2\cosh(\beta\omega_n/2), \tag{3.7}$$

and the free-energy is

$$\Omega = \frac{-1}{\beta}\sum_n \ln[2\cosh(\beta\omega_n/2)]. \tag{3.8}$$

To move from this quantum mechanical example to a quantum field theory, we take the continuum limit. In this case, the index $n \to \vec{\mathbf{p}}$ becomes a continuous degree of freedom and the sum becomes an integral. There are several issues that arise when considering an uncountable number of degrees of freedom that technically complicate the study of quantum field theory (leading to divergences etc.). For condensed matter systems, however, one may always in principle consider large but finite systems—for example, by placing the system in a finite size box, or on a lattice etc.— and take this continuum limit carefully at the end of the calculation to verify that everything works out properly. Thus, we proceed with a discussion of finite systems, and postpone the continuum limit until Chapter 3.3.

Consider, for example, a single fermionic degree of freedom in the grand-canonical ensemble at fixed temperature and chemical potential. The appropriate "Hamiltonian" is

$$\widehat{\mathbf{H}} = \omega\left(\hat{\mathbf{a}}^\dagger\hat{\mathbf{a}} - \tfrac{1}{2}\right) - \mu\widehat{\mathbf{N}} = (\omega-\mu)\left(\hat{\mathbf{a}}^\dagger\hat{\mathbf{a}} - \tfrac{1}{2}\right) - \frac{\mu}{2}. \tag{3.9}$$

The free-energy is thus

$$\Omega = \frac{-1}{\beta}\ln[2\cosh(\beta(\omega-\mu)/2)] + \frac{\mu}{2}. \tag{3.10}$$

From this result, we can use the thermodynamic relationships to extract other quantities. For example, the occupation number $n = \langle\hat{\mathbf{a}}^\dagger\hat{\mathbf{a}}\rangle$ can be found using the standard thermodynamic relationship:

$$n = -\partial\Omega/\partial\mu = \frac{1-\tanh(\beta(\omega-\mu)/2)}{2} = f_\beta(\omega-\mu) \tag{3.11}$$

where

$$f_\beta(E) = \frac{1-\tanh(\beta E/2)}{2} = \frac{1}{1+e^{\beta E}} \tag{3.12}$$

is the Fermi-Dirac distribution function.

3.1.2 Quadratic Hamiltonians

We now consider a very general quadratic Hamiltonian which we may write:[1]

$$\widehat{\mathbf{H}} = \widehat{\psi}^{\dagger}\mathbf{E}\widehat{\psi} \tag{3.13}$$

where $\widehat{\psi}$ may contain several fermionic operators:

$$\widehat{\psi} = \begin{pmatrix} \widehat{\mathbf{a}}_1 \\ \widehat{\mathbf{a}}_2 \\ \vdots \\ \widehat{\mathbf{a}}_n \end{pmatrix}, \tag{3.14}$$

and satisfies canonical anti-commutation relations

$$\{\widehat{\psi}_a, \widehat{\psi}_b^*\} = \delta_{ab}, \qquad \{\widehat{\psi}_a^*, \widehat{\psi}_b^*\} = \{\widehat{\psi}_a, \widehat{\psi}_b\} = 0. \tag{3.15}$$

This Hamiltonian can be diagonalized using a unitary transformation $\mathbf{U}$:

$$\widehat{\mathbf{H}} = \sum_n \omega_{j=1}^n \left(\widehat{\mathbf{c}}_j^{\dagger}\widehat{\mathbf{c}}_j\right) \tag{3.16}$$

where

$$\widehat{\mathbf{c}} = \mathbf{Q}^{\dagger}\widehat{\psi}, \qquad \text{and} \qquad \mathbf{Q}^{\dagger}\mathbf{E}\mathbf{Q} = \begin{pmatrix} \omega_1 & & & \\ & \omega_2 & & \\ & & \cdots & \\ & & & \omega_n \end{pmatrix}. \tag{3.17}$$

From this diagonal form, we can compute all properties of the ensemble. For example, the thermodynamic potential is simply

$$\Omega = \frac{1}{\beta}\sum_{j=1}^{n} \ln[f_\beta(-\omega_n)], \tag{3.18}$$

and the quadratic expectation values are

$$\langle\widehat{\mathbf{c}}_a^*\widehat{\mathbf{c}}_b\rangle = \delta_{ab}f_\beta(\omega_a), \quad \langle\widehat{\mathbf{c}}_a\widehat{\mathbf{c}}_b^*\rangle = \delta_{ab}f_\beta(-\omega_a), \quad \langle\widehat{\mathbf{c}}_a\widehat{\mathbf{c}}_b\rangle = \langle\widehat{\mathbf{c}}_a^*\widehat{\mathbf{c}}_b^*\rangle = 0, \tag{3.19}$$

[1] In this section, we sketch rather briefly the general method for dealing with general quadratic systems. There are quite a few subtle technical details that must be considered when actually implementing this scheme. These are discussed, along with the truly general analysis, in Appendix B.

where f_β is the Fermi-distribution (3.12). From these, using the inverse transformation $\mathbf{Q}$, we can reconstruct the expectation value of the original operators. We express these in matrix form:

$$\langle \widehat{\psi}^* \widehat{\psi}^T \rangle = [\mathbf{F}^+]^T, \qquad \text{and} \qquad \langle \widehat{\psi} \widehat{\psi}^\dagger \rangle = [\mathbf{F}^-], \tag{3.20}$$

where

$$\mathbf{F}^\pm = \frac{\mathbf{1}}{\mathbf{1} + e^{\pm \beta \mathbf{E}}}. \tag{3.21}$$

From these, the two-point functions can be computed.[2] Higher-order functions are simply expressed in terms of the appropriate Wick contractions. Finally, we point out that the thermodynamic potential can be written in terms of the original matrix as

$$\Omega = \frac{1}{\beta} \operatorname{Tr} \ln[\mathbf{F}^-]. \tag{3.22}$$

3.2 Interactions

We now consider adding interactions to our quadratic model. As a specific example (and because the models we shall study later have this form) consider the Hamiltonian

$$\widehat{\mathbf{H}} = \widehat{\psi}^\dagger \boldsymbol{\varepsilon} \widehat{\psi} + g(\widehat{\psi}^\dagger \boldsymbol{\Gamma}^\dagger \widehat{\psi})(\widehat{\psi}^\dagger \boldsymbol{\Gamma} \widehat{\psi}). \tag{3.23}$$

The matrices $\boldsymbol{\Gamma}$ specify the type of interaction—in this case, a four-fermion interaction. We proceed with this example, but note that the results generalize trivially to interaction with more operators, or that contain a sume of terms like this.

3.2.1 Variational Hamiltonian

The variational Hamiltonian that will provide the upper bound (2.2) for our ensemble is

$$\widehat{\mathbf{H}}_0 = \widehat{\boldsymbol{\Psi}}^\dagger (\boldsymbol{\varepsilon} + \boldsymbol{\Sigma}) \widehat{\boldsymbol{\Psi}} = \widehat{\boldsymbol{\Psi}}^\dagger \mathbf{E} \widehat{\boldsymbol{\Psi}}. \tag{3.24}$$

[2]The formalism here does not allow for non-zero correlations of the form $\langle \widehat{\psi} \widehat{\psi} \rangle$. These can be dealt with using the generalized formalism presented in Appendix B. It may seem that this precludes the study of superfluidity because the pairing correlation is often written $\langle \widehat{\psi} \widehat{\psi} \rangle$. Recall, however, that the operators $\widehat{\psi}$ have two components. We will choose these to be $\widehat{\mathbf{a}}$ and $\widehat{\mathbf{b}}^\dagger$ so that the off-diagonal elements of $\langle \widehat{\psi}_2^\dagger \widehat{\psi}_1 \rangle = \langle \widehat{\mathbf{b}} \widehat{\mathbf{a}} \rangle$ contain exactly the superfluid correlations. What we are neglecting are the $\langle \widehat{\mathbf{a}}^\dagger \widehat{\mathbf{b}} \rangle$ correlations.

The variational parameters are the elements of the matrix $\mathbf{\Sigma}$ which should be thought of as the matrix of "self-energy" corrections. This matrix must be constrained to be Hermitian: $\mathbf{\Sigma} = \mathbf{\Sigma}^\dagger$.

The quadratic portion of the free energy is given by (3.22) while the expectation of the difference $\langle \widehat{\mathbf{H}} - \widehat{\mathbf{H}}_0 \rangle_0$ is

$$\langle \widehat{\mathbf{H}} - \widehat{\mathbf{H}}_0 \rangle_0 = \langle \widehat{\mathbf{H}}_{\text{int}} \rangle_0 + \text{Tr}[\langle \widehat{\mathbf{\Psi}}^* \widehat{\mathbf{\Psi}}^T \rangle_0 \mathbf{\Sigma}^T], \tag{3.25}$$

$$= \langle \widehat{\mathbf{H}}_{\text{int}} \rangle_0 - \text{Tr}[\mathbf{\Sigma}\mathbf{F}^+], \tag{3.26}$$

and the expectation of the interaction is[3]

$$\langle \widehat{\mathbf{H}}_{\text{int}} \rangle_0 = g \left(\text{Tr}[\mathbf{\Gamma}^\dagger \mathbf{F}^+] \, \text{Tr}[\mathbf{\Gamma}\mathbf{F}^+] + \text{Tr}[\mathbf{\Gamma}^\dagger \mathbf{F}^- \mathbf{\Gamma}\mathbf{F}^+] \right).$$

In total, we have

$$\Omega \leq \Omega[\mathbf{\Sigma}] = \frac{1}{\beta} \text{Tr} \ln[\mathbf{F}^-] - \text{Tr}[\mathbf{\Sigma}\mathbf{F}^+] + \\ + g \left(\text{Tr}[\mathbf{\Gamma}^\dagger \mathbf{F}^+] \, \text{Tr}[\mathbf{\Gamma}\mathbf{F}^+] + \text{Tr}[\mathbf{\Gamma}^\dagger \mathbf{F}^- \mathbf{\Gamma}\mathbf{F}^+] \right). \tag{3.27}$$

3.2.2 Self-Consistent Schwinger-Dyson Equations

The usual self-consistency conditions follow from (3.27) by varying the right hand side with respect to the variational parameters. It is difficult, however, to directly compute the derivative with respect to $\mathbf{\Sigma}$.[4] Instead, we perform the variation with respect to $\mathbf{F}^+$, using the relation

$$\mathbf{\Sigma} = \boldsymbol{\varepsilon} - \frac{1}{\beta} \ln \left[(\mathbf{F}^+)^{-1} - \mathbf{1} \right] = \boldsymbol{\varepsilon} - \frac{1}{\beta} \left(\ln[\mathbf{F}^+] - \ln[\mathbf{F}^-] \right). \tag{3.28}$$

We also use the fact that, for analytic matrix functions $\mathbf{f}(\mathbf{X})$,

$$\frac{d\text{Tr}[\mathbf{A}\mathbf{X}]}{d\mathbf{X}} = \mathbf{A}^T, \qquad \text{and} \qquad \frac{d\text{Tr}[\mathbf{f}(\mathbf{X})]}{d\mathbf{X}} = \mathbf{f}'(\mathbf{X})^T. \tag{3.29}$$

As long as we work at finite temperature, the function $\mathbf{F}^+(\mathbf{E})$ is invertible, and so the result of varying with respect to $\mathbf{F}^+$ will differ by an overall factor

[3] For a fully self-consistent analysis, we should include the term $-g \langle \hat{\psi}^\dagger \hat{\psi}^\dagger \rangle \langle \hat{\psi}\hat{\psi} \rangle$. This simplified analysis does not include these correlations: They are included in Appendix B.

[4] The difficulty lies in computing the derivative of $f(\boldsymbol{\varepsilon} + \mathbf{\Sigma})$ and in computing the derivative of the interaction terms. Unless one can assume that $\boldsymbol{\varepsilon}$, $\mathbf{\Sigma}$ and $\mathbf{\Gamma}$ all commute—and in general they do not—the result is a mess of commutators.

of the non-singular Jacobian matrix. The $T \to 0$ limit, however, must be taken *after* the self-consistency conditions are derived.

Proceeding to compute the derivative of the first two terms of (3.27) and noting that $\mathbf{F}^- = \mathbf{1} - \mathbf{F}^+$ we have $-\mathbf{\Sigma}^T$. Taking the transpose, we have the full set of self-consistency conditions—the Schwinger-Dyson equations:

$$\mathbf{\Sigma} = g\left(\mathbf{\Gamma}^\dagger \operatorname{Tr}[\mathbf{\Gamma}\mathbf{F}^+] + \mathbf{\Gamma} \operatorname{Tr}[\mathbf{\Gamma}^\dagger\mathbf{F}^+] + \mathbf{\Gamma}^\dagger\mathbf{F}^-\mathbf{\Gamma} - \mathbf{\Gamma}\mathbf{F}^+\mathbf{\Gamma}^\dagger\right). \tag{3.30}$$

We make a few comments about this equation:

- Since (3.21) is in general invertible for non-zero temperature, we may use either $\mathbf{\Sigma}$ or $\mathbf{F}^+$ as variational parameters. Specifying $\mathbf{\Sigma}$ amounts to specifying the properties of the "variational Hamiltonian" while specifying $\mathbf{F}^+$ amounts to specifying all of the two-point correlations. For Gaussian systems, there is a one-to-one correspondence between these two. At zero temperature, the variational bound reduces to $\Omega \leq \langle \widehat{\mathbf{H}} \rangle_0$ where the expectation values is in the ground state of the Hamiltonian $\widehat{\mathbf{H}}_0$. In this sense, one simply has a variational state. This allows for an easy extension to variational states beyond the quadratic Gaussian approximation by using more complicated variational states. Note that this only works for zero temperature: At finite temperatures, one must specify the "variational ensemble" which is most concisely expressed in terms of a solvable Hamiltonian. At present, we are not sure of any other appropriate generalization to finite temperature of the notion of a variational state.

- As a matrix equation, (3.30) is generally valid. In particular, one simply needs include momentum or position "indices" to account for continuous dimensions. These "matrices", however, become infinite-dimensional and one thus encounters the problems of: a) infinitely many variational parameters and, b) manipulating (inverting etc.) infinite dimensional matrices. One solution is to use finite-volumes and/or lattices. The matrices then become finite (though large) and may be manipulated numerically.

- Since the Schwinger-Dyson equation (3.30) has been derived by varying with respect to $\mathbf{F}^+$, one may simply impose variational constraints on the parameters of $\mathbf{F}^+$ if these are treated as variational parameters (rather than considering $\mathbf{\Sigma}$ as the variational parameters). For example, one might consider restricting attention to variational ensembles where $\mathbf{F}^+$ is diagonal. In this case, one need only consider the equations specified by the diagonals in (3.30). The off-diagonal equations

will likely not be satisfied, but they may be safely ignored when considering only this restricted subset. Ignoring certain parameters in $\mathbf{F}^+$ is thus justified as a minimization over a restricted subset of Gaussian states with only the specified form of two-body correlations $\mathbf{F}^+$.

Unfortunately, because of the non-trivial relationship between $\boldsymbol{\Sigma}$ and $\mathbf{F}^+$, making similar restrictions on $\boldsymbol{\Sigma}$ will not work with the present form of self-consistency conditions.

3.2.2.1 Free Energy

Finally, note that there is a simpler expression for the free-energy bound at the stationary point. One uses the Schwinger-Dyson equation (3.30) to eliminate $\boldsymbol{\Sigma}$ from (3.27):

$$\Omega[\mathbf{F}^+] = \frac{1}{\beta}\operatorname{Tr}\ln[\mathbf{F}^+] - g\left(\operatorname{Tr}[\boldsymbol{\Gamma}^\dagger\mathbf{F}^+]\operatorname{Tr}[\boldsymbol{\Gamma}\mathbf{F}^+] - \operatorname{Tr}[\boldsymbol{\Gamma}^\dagger\mathbf{F}^+\boldsymbol{\Gamma}\mathbf{F}^+]\right). \quad (3.31)$$

Note that this only holds at the variational solution and does *not* necessarily form a valid variational function.

3.2.2.2 Parameter "Renormalization"

We pause here to discuss a few matters related to thermodynamic relationships and the self-consistent "renormalization" of parameters. What we mean here is that the variational ensemble is described by certain parameters that are the coefficients of quadratic (bi-linear) combinations of the fermion fields.[5] These quadratic parameters may differ from the quadratic parameters in original Hamiltonian. We refer to the variational parameters as "renormalized" parameters: These renormalized parameters defined the variational Hamiltonian $\widehat{\mathbf{H}}_0$ and thus parametrize the variational state. In contrast, we shall call the parameters in the physical Hamiltonian $\widehat{\mathbf{H}}$ "bare" parameters.

In terms of our formalism, the matrix $\boldsymbol{\epsilon}$ contains the "bare" parameters, the matrix $\mathbf{E} = \boldsymbol{\epsilon} + \boldsymbol{\Sigma}$ contains the "renormalized" parameters, and the matrix $\boldsymbol{\Sigma}$ contains the "renormalizations". The renormalizations are determined self-consistently through the Schwinger-Dyson equation. In QCD, for example, this distinction is the distinction between the "current" quark masses, (which appear in the model Hamiltonian, for example, $m_u \sim 4$

[5] Actually, since we only consider Gaussian states, all of the parameters are quadratic, but this is not the general case.

MeV), and the "constituent" quark masses (which are typically much larger: $M_u \sim 300$ MeV. See, for example, Table E.3 or [14].)

In particular, consider a model where the grand-canonical "Hamiltonian" $\widehat{\mathbf{H}}(\mu_0) = \widehat{\mathbf{F}} - \mu_0 \widehat{\mathbf{N}}$ depends on a (bare) chemical potential μ_0. The Schwinger-Dyson determines a self-consistent renormalization $\delta\mu$ in Σ and the state is parametrized by the renormalized chemical potential $\mu_R = \mu_0 + \delta\mu$.

3.2.2.3 Thermodynamic Relationships

In order to use the computed thermodynamic potential to generate other thermodynamic quantities, it is important to perform the minimization properly. For example, consider determining the average particle number $N = \langle \widehat{\mathbf{N}} \rangle_0$ in a given state. For pure states, this should follow from the thermodynamic relationship

$$-\frac{\partial \Omega}{\partial \mu_0} = N. \tag{3.32}$$

This follows only if Ω is computed properly:

$$\Omega[\mu_0] = \min_{\rho}[F(\rho) - \mu_0 N(\rho)], \tag{3.33a}$$

$$= F[\rho(\mu)] - \mu_0 N[\rho(\mu_0)] \tag{3.33b}$$

where the implicit dependence $\rho[\mu_0]$ is determined to satisfy the minimization. The thermodynamic relationship to extract the particle number suggests computing:

$$\frac{\partial \Omega}{\partial \mu_0} = \left(\frac{\partial F}{\partial \rho} - \mu_0 \frac{\partial N}{\partial \rho}\right) \frac{\partial \rho}{\partial \mu_0} - N[\rho(\mu_0)]. \tag{3.33c}$$

If the minimization was not properly performed, the first term does not vanish, and the thermodynamic relationship (3.32) is not satisfied. Such relationships only hold at stationary points where $F' = \mu_0 N'$.

Consider relationship (3.32) in our formalism. The state is characterized by $\mathbf{F}^+(\mu_R)$ which depends on the renormalized parameter μ_R. The gap equation determines $\mathbf{\Sigma}(\mu_R)$ which explicitly determines the renormalizations $\delta\mu$. Ω thus has the following form (after minimizing with respect to other parameters, such as Δ as described in Section 4.2):

$$\Omega = \Omega_0[\mu_R] + H[\mu_0, \mu_R] - H_0[\mu_R] \tag{3.34}$$

where $H[\mu_0, \mu_R] = \langle \widehat{\mathbf{H}} \rangle_0$, etc. The dependence on $\mu_R(\mu_0, \delta\mu)$ is determined by the minimization condition for the other variational parameters, such as

Δ. Note that there is an explicit dependence on the bare parameter μ_0 in the term $H[\mu_0, \mu_R]$.

The Schwinger-Dyson equation for the remaining variational parameter $\delta\mu$ gives:

$$\frac{\partial\Omega_0[\mu_R]}{\partial\mu_R} + \frac{\partial H[\mu_0,\mu_R]}{\partial\mu_R} - \frac{\partial H_0[\mu_R]}{\partial\mu_R} = 0 \tag{3.35}$$

through which one may determine $\delta\mu(\mu_0)$. Thus, in principle, one must determine all the parameters $\delta\mu$ self-consistently for a given μ_0. Typically, however, the relationship between μ_R and μ_0 is trivial:[6] $\mu_R = \mu_0 + \delta\mu$ with $\delta\mu$ being determined explicitly as a function of μ_R through the gap equation. Thus, one may simply specify μ_R, solve the gap equations for the other parameters, and then, at the end of the day, be confident that one has the correct solution, by setting the bare parameter value to $\mu_0 = \mu_R - \delta\mu$. In this way, one may "ignore" the bare value μ_0 and effectively specify the renormalized value that parametrize the state.

The thermodynamic relationships such as (3.32), however, are only valid when one differentiates with respect to the *bare* parameters. In particular, even though the expression (3.27) depends only on $\mathbf{F}^+$ and thus only on μ_R, the following does not correctly compute the particle number

$$\begin{aligned}\frac{\partial\Omega}{\partial\mu_R} = \frac{\partial\Omega_0[\mu_R]}{\partial\mu_R} + \frac{\partial H[\mu_0,\mu_R]}{\partial\mu_R} - \frac{\partial H_0[\mu_R]}{\partial\mu_R} + \frac{\partial H[\mu_0,\mu_R]}{\partial\mu_0}\frac{\mathrm{d}\mu_0}{\mathrm{d}\mu_R}, \\ = \frac{\partial H[\mu_0,\mu_R]}{\partial\mu_0}\frac{\mathrm{d}\mu_0}{\mathrm{d}\mu_R} = -\langle\widehat{\mathbf{N}}\rangle_0\frac{\mathrm{d}\mu_0}{\mathrm{d}\mu_R},\end{aligned} \tag{3.36}$$

unless $\mathrm{d}\mu_0/\mathrm{d}\mu_R = 1$. Expression (3.32) may be used with the renormalized parameters, however, if one can arrange the interaction so that the solution to the Schwinger-Dyson equation is $\delta\mu = 0$. This is often possible and explains why many works in the literature that neglect the chemical potential and other self-energy renormalizations are still self-consistent. If the interaction cannot be arranged to ensure that $\delta\mu = 0$, however, then one must include this parameter in the self-consistency relations in order to properly reproduce the thermodynamic relations.

3.3 Momentum Dependence

In the previous sections, we showed how to solve rather arbitrary fermionic problems using the variational mean-field approach. Unfortunately, we

[6] This is not always true, as we shall see when we include a momentum dependence.

would like to consider systems with infinitely many degrees of freedom that arise through the consideration of continuous fields. In this case one must work with infinite (even uncountably infinite) dimensional matrices. The previous results become useless without some simplifying assumptions.[7]

In principle, one can simply introduce position or momentum labels $\vec{\mathbf{x}}$ and $\vec{\mathbf{p}}$ as additional indices, but if one allows arbitrary cross-terms, even the quadratic model becomes intractable. One solution is to limit restrict the variations to a limited subset of possible solutions. In this thesis we shall primarily limit our attention to homogeneous and isotropic states as discussed in Section 3.3.2.

3.3.1 Conventions

The results of the previous sections are extended to continuum theories by promoting the sums, traces, etc., to integrals. For example, the Hamiltonian for a single species of non-relativistic fermions in d dimensions is

$$\widehat{\mathbf{H}} = \int \mathrm{d}^d\vec{\mathbf{x}}\, \widehat{\mathbf{a}}^\dagger(\vec{\mathbf{x}}) \left(-\frac{\nabla^2}{2m} - \mu\right) \widehat{\mathbf{a}}(\vec{\mathbf{x}}) = V \int \text{đ}^d\vec{\mathbf{p}}\, \widehat{\mathbf{a}}^\dagger_{\vec{\mathbf{p}}} \left(\frac{p^2}{2m} - \mu\right) \widehat{\mathbf{a}}_{\vec{\mathbf{p}}}. \quad (3.37)$$

We use this to point out a few conventions: First, we use natural units where $\hbar = k_B = c = 1$. Second, we use the shorthand notation $\text{đ}p = \mathrm{d}p/(2\pi)$ in momentum space and keep all of our factors of 2π in the momentum integrals of our Fourier transforms:

$$\widehat{\mathbf{a}}(\vec{\mathbf{x}}) = \int \text{đ}^d\vec{\mathbf{p}}\, e^{i\vec{\mathbf{x}}\cdot\vec{\mathbf{p}}}\, \frac{\widehat{\mathbf{a}}_{\vec{\mathbf{p}}}}{\sqrt{V}} = \int \frac{\mathrm{d}^d\vec{\mathbf{p}}}{(2\pi)^d}\, e^{i\vec{\mathbf{x}}\cdot\vec{\mathbf{p}}}\, \frac{\widehat{\mathbf{a}}_{\vec{\mathbf{p}}}}{\sqrt{V}} \quad (3.38)$$

To maintain consistent notations with our formal developments, we include a factor of the volume with our definition of the momentum space operators so that they are dimensionless $[\widehat{\mathbf{a}}_{\vec{\mathbf{p}}}] = 0$. Thus, the momentum is simply a label and the operators $\widehat{\mathbf{a}}_{\vec{\mathbf{p}}}$ directly correspond to the operators $\widehat{\mathbf{a}}_a$ in (3.14). To be consistent, we use a subscript for the momentum dependence to emphasize that this is an index. This also helps distinguish between a field and its Fourier transform: $\widehat{\psi}(\vec{\mathbf{x}})$ should be thought of as a dimensionful "field" $[\widehat{\psi}(\vec{\mathbf{x}})] = d/2$ in position while $\widehat{\psi}_{\vec{\mathbf{p}}}$ should be thought of as a dimensionless creation operator with a momentum label. The volume factor in the momentum space representation follows from $V = (2\pi)^d\delta^{(d)}(0)$.

[7] One place where the previous sections may be of direct use is when performing an analysis in the basis of harmonic oscillator states as one might do when studying finite systems in an atomic trap. One may also be able to directly use the equations to solve the problem on a lattice in a finite, or periodic volume.

The thermodynamic potential density for this gas is simply

$$\frac{\Omega}{V} = -\frac{1}{\beta}\int \mathrm{đ}^d\vec{\mathbf{p}} \ln\left[2\cosh\left(\beta\frac{p^2/(2m)-\mu}{2}\right)\right] + \int \mathrm{đ}^d\vec{\mathbf{p}}\frac{p^2/(2m)-\mu}{2},$$
$$= \frac{1}{\beta}\int \mathrm{đ}^d\vec{\mathbf{p}} \ln\left[f_\beta\left(\mu - \frac{p^2}{2m}\right)\right] \tag{3.39}$$

where $f_\beta(E)$ is the Fermi-Dirac distribution function (3.12). From this we can compute the occupation number $n_{\vec{\mathbf{p}}} = \langle \hat{\mathbf{a}}^\dagger_{\vec{\mathbf{p}}}\hat{\mathbf{a}}_{\vec{\mathbf{p}}}\rangle = f_\beta(\omega_{\vec{\mathbf{p}}})$ from the thermodynamic relationship (3.32):

$$\frac{N}{V} = -\frac{\partial\Omega/V}{\partial\mu} = \int \mathrm{đ}^d\vec{\mathbf{p}}\, n_{\vec{\mathbf{p}}} = \int \mathrm{đ}^d\vec{\mathbf{p}}\, f_\beta\left(\frac{p^2}{2m}-\mu\right). \tag{3.40}$$

We note that for spatially homogeneous and isotropic states, $\langle \hat{\mathbf{a}}^\dagger_{\vec{\mathbf{p}}}\hat{\mathbf{a}}_{\vec{\mathbf{q}}}\rangle = \delta_{\vec{\mathbf{p}},\vec{\mathbf{q}}}n_p$ where $\delta_{\vec{\mathbf{p}},\vec{\mathbf{q}}}n_p$ is a Kronecker delta so that it makes sense to write $n_p = \langle \hat{\mathbf{a}}^\dagger_{\vec{\mathbf{p}}}\hat{\mathbf{a}}_{\vec{\mathbf{p}}}\rangle$.

3.3.2 Homogeneous and Isotropic States

In this thesis, we shall only consider homogeneous and isotropic states. This means that all quadratic terms must have net momentum zero and we need only consider the following types of terms:

$$\hat{\psi}^\dagger_{\vec{\mathbf{p}}}\hat{\psi}_{\vec{\mathbf{p}}}, \qquad\qquad \hat{\psi}_{\vec{\mathbf{p}}}\hat{\psi}_{-\vec{\mathbf{p}}}, \tag{3.41}$$

and their conjugates. In terms of the variational states, we only consider states such that the correlations have the following forms:

$$\langle \hat{\psi}_{\vec{\mathbf{p}}}\hat{\psi}^\dagger_{\vec{\mathbf{q}}}\rangle_0 \propto \delta_{\vec{\mathbf{p}},\vec{\mathbf{q}}}, \qquad\qquad \langle \hat{\psi}_{\vec{\mathbf{p}}}\hat{\psi}_{\vec{\mathbf{q}}}\rangle_0 \propto \delta_{\vec{\mathbf{p}},-\vec{\mathbf{q}}}. \tag{3.42}$$

Our momentum dependent models have the following Hamiltonian density:

$$\hat{\mathcal{H}} = \frac{\hat{\mathbf{H}}}{V} = \int \mathrm{đ}^3\vec{\mathbf{p}}\, \hat{\psi}^\dagger_p(\varepsilon_p - \mu)\hat{\psi}_p + g\int_\Lambda (\hat{\psi}^\dagger\mathbf{\Gamma}^\dagger\hat{\psi})(\hat{\psi}^\dagger\mathbf{\Gamma}\hat{\psi}). \tag{3.43}$$

The momentum structure of the interaction must include some sort of ultraviolet cutoff to regulate the theory. The general form of the interaction is as a sum of terms of the form:

$$\frac{\hat{\mathbf{H}}_I}{V} = g\int \mathrm{đ}^3\vec{\mathbf{p}}\, \mathrm{đ}^3\vec{\mathbf{p}}'\, \mathrm{đ}^3\vec{\mathbf{q}}\, \mathrm{đ}^3\vec{\mathbf{q}}'\, V(\vec{\mathbf{p}},\vec{\mathbf{p}}',\vec{\mathbf{q}},\vec{\mathbf{q}}')(\hat{\psi}^\dagger_{\vec{\mathbf{p}}}\mathbf{\Gamma}^\dagger_A\hat{\psi}_{\vec{\mathbf{p}}'})(\hat{\psi}^\dagger_{\vec{\mathbf{q}}}\mathbf{\Gamma}_A\hat{\psi}_{\vec{\mathbf{q}}'}). \tag{3.44}$$

The regulation is included in the interaction structure $V(\vec{\mathbf{p}}, \vec{\mathbf{p}}', \vec{\mathbf{q}}, \vec{\mathbf{q}}')$. For simplicity, we discuss here models with separable potentials and use an explicit cutoff. More general and realistic models will be discussed later in Section 5.3.1. The separable interactions we consider in Sections 5.3.1 and 7.3 have the following explicit form[8]

$$V(\vec{\mathbf{p}}, \vec{\mathbf{p}}', \vec{\mathbf{q}}, \vec{\mathbf{q}}') = V\Lambda_p\Lambda_{p'}\Lambda_q\Lambda_{q'}(2\pi)^3\delta^{(3)}(\vec{\mathbf{p}} - \vec{\mathbf{p}}' + \vec{\mathbf{q}} - \vec{\mathbf{q}}'). \tag{3.45}$$

The function Λ_p acts as an ultraviolet cutoff. This is similar to the type of interaction arrived at in the original BCS model [8] for example, where the cutoff function Λ_p mimics a Debye screened phonon interaction, but also includes the Hartree-Fock contributions. To analyze QCD in Part III we will choose a cutoff that goes to zero for large momenta to simulate asymptotic freedom.

We note that the separable interactions generally have some horrible features—they are non-local, violate most gauge invariance, etc.—but proceed because it leads to some very simple results and delivers many of the qualitative features found with more complicated interactions. We shall consider rectifying some of these deficiencies in Section 5.2. We also note that the dimension of the coupling is $[g] = -2$.

It will turn out that, with this separable interaction, all of the non-trivial momentum dependence will arise from the functions Λ_p. To see this, we first write the bound on the thermodynamic potential density:

$$\begin{aligned}\frac{\Omega}{V} \leq \int \text{đ}^3\vec{\mathbf{p}} \left(\frac{1}{\beta}\operatorname{Tr}\ln[\mathbf{F}^-_{\vec{\mathbf{p}}}] - \operatorname{Tr}[\mathbf{\Sigma}_{\vec{\mathbf{p}}}\mathbf{F}^+_{\vec{\mathbf{p}}}]\right) + \\ + g\left(\operatorname{Tr}[\mathbf{\Gamma}^\dagger\mathbf{F}^+_{\int}]\operatorname{Tr}[\mathbf{\Gamma}\mathbf{F}^+_{\int}] + \operatorname{Tr}[\mathbf{\Gamma}^\dagger\mathbf{F}^-_{\int}\mathbf{\Gamma}\mathbf{F}^+_{\int}]\right)\end{aligned} \tag{3.46}$$

where

$$\mathbf{F}^\pm_{\int} = \int \text{đ}^3\,\vec{\mathbf{p}}\Lambda_p^2\mathbf{F}^\pm_{\vec{\mathbf{p}}}. \tag{3.47}$$

Note that $\mathbf{F}^\pm_{\vec{\mathbf{p}}}$ are dimensionless variational parameters:

$$\mathbf{F}^-_{\vec{\mathbf{p}}} = \langle\widehat{\psi}_{\vec{\mathbf{p}}}\widehat{\psi}^\dagger_{\vec{\mathbf{p}}}\rangle \tag{3.48}$$

for example, but that $[\mathbf{F}^\pm_{\int}] = 3$ is not dimensionless. These integrated parameters are convenient to work with, but cannot be treated as variational

[8]We include a volume factor here to ensure that the result is an energy density, corresponding with the Hamiltonian density in equation (3.43).

parameters. Note also that

$$\mathbf{F}_{\int}^{+} + \mathbf{F}_{\int}^{-} = \mathbf{V}_p = V_p \mathbf{1} = \int \text{đ}^3\vec{\mathbf{p}}\, \Lambda_p^2 \mathbf{1} \tag{3.49}$$

where V_p is the "volume" of momentum space. Varying as before, we obtain the momentum space Schwinger-Dyson equations:

$$\mathbf{\Sigma}_{\vec{\mathbf{p}}} = g\Lambda_p^2 \left(\mathbf{\Gamma}^\dagger \operatorname{Tr}[\mathbf{\Gamma}\mathbf{F}_{\int}^{+}] + \mathbf{\Gamma} \operatorname{Tr}[\mathbf{\Gamma}^\dagger \mathbf{F}_{\int}^{+}] + \mathbf{\Gamma}^\dagger \mathbf{F}_{\int}^{-} \mathbf{\Gamma} - \mathbf{\Gamma}\mathbf{F}_{\int}^{+}\mathbf{\Gamma}^\dagger \right). \tag{3.50}$$

We see explicitly that all of the momentum dependence of $\mathbf{\Sigma}_{\vec{\mathbf{p}}}$ is given by the cutoff function:

$$\mathbf{\Sigma}_{\vec{\mathbf{p}}} = \Lambda_p^2 \mathbf{\Sigma}. \tag{3.51}$$

Using the Schwinger-Dyson equation, we can eliminate $\mathbf{\Sigma}$ from the expression for the free-energy as before:

$$\begin{aligned} \frac{\Omega[\mathbf{F}^{+}]}{V} = \int \text{đ}^3 p\, \frac{1}{\beta} \operatorname{Tr} \ln[\mathbf{F}_{\vec{\mathbf{p}}}^{-}] + \\ - g \left(\operatorname{Tr}[\mathbf{\Gamma}^\dagger \mathbf{F}_{\int}^{+}] \operatorname{Tr}[\mathbf{\Gamma}\mathbf{F}_{\int}^{+}] + \operatorname{Tr}[\mathbf{\Gamma}^\dagger \mathbf{F}_{\int}^{+} \mathbf{\Gamma} \mathbf{F}_{\int}^{+}] \right). \end{aligned} \tag{3.52}$$

At this point, we the reader may wish to take a peak at Section 4.2 to see how this formalism is applied to standard BCS style superfluidity. More complicated, but realistic, examples of momentum dependence are discussed in Section 5.3.1.

Part II

Breached Pair Superfluids

Chapter 4

Theory of Fermionic Superfluidity

4.1 History of Breached Pair Superfluids

The general idea of Breached Pair superfluidity arises quite naturally by considering standard BCS superfluidity where the two components have different dispersions. These are sometimes referred to as "asymmetric" superfluids. For certain parameter values, a solution to the Schwinger-Dyson equation exists with the characteristic properties of a Breached Pair state. The challenge with the Breached Pair state is ensuring that it is stable. Although this solution is a stationary point, it is not always a minimum of the thermodynamic potential. The stability of these phases is one of the main points addressed in this thesis. In particular, we demonstrate models where stable Breached Pair states may exist.

The interesting feature of Breached Pair superfluids is that the superfluid state retains gapless fermionic excitations. With dominant S-wave interactions, these states are also homogeneous and isotropic. Consequently the gapless modes occupy entire Fermi-surfaces, not just nodal points or planes as is the case with several other "gapless" superfluids.[1] The simultaneous existence of superfluid properties with gapless excitations in a homogeneous fluid is a novel feature of the Breached Pair state.

The origin of these states goes back to at least 1963 when Sarma considered a gapless Schwinger-Dyson solution for a superconductor in an external magnetic field [16]. The field provides an asymmetry by shifting the relative chemical potentials of the two spin states. For certain fields, an additional solution to the gap equation may be found, but this state is unfavoured energetically to the fully gapped BCS solution. Similar results were considered in the context of colour superconductivity [17], again concluding that these states are not stable.

This phenomenon of gapless superfluidity was re-examined by Liu and

[1] For example, consider the A phases of ^{4}He [15].

Wilczek [18] where they considered a splitting due to a large mass ratio and coined the term "interior gap" superfluidity for the situation where the primary pairing takes place about the inner Fermi-surface. This paper drew criticism from Wu and Yip [19], who argued that the state was unstable to quantum fluctuations.

Further possibilities for gapless superfluids were reconsidered in the QCD context [20, 21] where a similar state was stabilized by a gauge charge neutrality condition for electric and colour charges. Wilczek, Liu, and Gubankova [22] also considered a more generic case where pairing could occur about either Fermi-surface and decided that the state was best described by the term "Breached Pair" (BP). They argued that the stability of the state depended on fixing particle numbers (working in the micro-canonical ensemble): the previous instabilities were all noted for fixed chemical potentials in the grand-canonical ensemble.

The claim that one may stabilize the system by fixing the particle number comes from noting that the Breached Pair states admit different number densities whereas the BCS state enforces equal densities (see Section 5.1.2). Thus, fixing a particle number asymmetry precludes the formation of the BCS state. One can then compare the free energies (rather than the thermodynamic potentials) and find that the Breached Pair state is favoured over the normal state.

The problem with this argument, however, is that one is only considering two possible competing states: a uniform normal phase and a uniform Breached Pair phase. Bedaque, Caldas and Rupak [23] showed that a third possibility exists that can compete energetically with the Breached Pair state. They considered a heterogeneous mixed phase consisting of an inhomogeneous mixture of BCS and normal states. The constraint of total particle asymmetry is maintained by the normal phase. Bedaque, Caldas and Rupak found for several cases, that the energy of such a mixed phase was lower than that of the Breached Pair state.

The energetic preference of a mixture in the macro-canonical ensemble over a pure phase that is unstable in the grand-canonical ensemble is quite generic. For extensive systems in the thermodynamic (large volume) limit, this follows from the convexity of the thermodynamic potentials (see Appendix A.4.2). Thus, for extensive systems, one may only consider states that are stable in the grand-canonical ensemble: all mixtures found the other ensembles will comprise various pure phases found in the grand-canonical ensemble. Wu and Yip's calculation [19] is simply a statement that the Breached Pair state considered is not stable at fixed chemical potentials: the negative superfluid density they calculate is just the positive curvature

of the thermodynamic potential as a function of the appropriate sources.

Details of this argument were discussed in [1] where we also provided two models that exhibit stable Breached Pair superfluidity at fixed chemical potential. We shall discuss the details of this stability in Section 5.2. It seems to require a large mass ratio and a finite range interaction. Reddy and Carlson [24] have recently suggested that these restrictions may relax as one moves to stronger coupling.

In the QCD context, progress is still being made under the assumption that charge neutrality conditions stabilize the state (see for example [21, 25, 26, 27, 28]). Calculations of the gluon screening masses, however, find a negative square of the Meissner mass, suggesting that, even with the neutrality constraints, the state may be unstable [29, 30, 31]. This is presently unresolved, though an attempt will be made to address this situation in Section 5.2.

4.1.1 Mismatched Fermi Surfaces

In this chapter, we shall consider systems of two species that, in the absence of interactions, would have two distinct Fermi surfaces. The natural BCS pairing is thus strained. In the presence of an attractive interaction, several possibilities arise.

Normal: If the interaction is too weak, the Fermi-surfaces will be slightly modified, but no pairing will be induced. The phase will remain a "normal" Fermi-liquid. Heuristically, the reason is that the low-energy excitations which might participate in pairing are isolated at separate Fermi-surfaces and the interaction is insufficient to overcome the kinetic energy required to overcome the separation.

A useful image is to consider "promoting" particles from one Fermi-surface to the other to form a pair. The energy costs for this are determined by the dispersion relationships.

BCS: If the interactions are strong enough over all momenta, then the aforementioned promotions will be allowed, and the pairing will equalize the densities, forming a conventional BCS superfluid.

LOFF: One way of reducing the kinetic cost is to pair unequal momenta. In this way, particles do not need to be promoted, but there is also only a limited amount of pairing: this is limited to the regions of momentum

space where the displaced Fermi surfaces overlap, and is dimensionally reduced. Such states will not be homogeneous and isotropic, but rather, will have a preferred direction or crystalline structure and are commonly referred to as LOFF (or LOFF in the condensed matter community) states after the originators, Larkin, Ovchinnikov [32], Fulde, and Ferrell [33]. This possibility has also been considered in the QCD context (see for example [34, 35, 36, 37, 38, 39, 40]).

To perform a complete analysis, one should consider this possibility, but the LOFF analysis is quite challenging and beyond the scope of the present work. In this thesis, we consider only homogeneous and isotropic states.

Breached Pairing: Another way of reducing the kinetic energy cost is to flatten the energy bands by increasing the masses of the fermions. In this way, promoting particles to admit pairing costs little energy.[2] In addition, if the interaction has a non-trivial momentum structure, then it is possible for pairing to occur only about one of the Fermi-surfaces. These are the conditions that seem to be required for stable extensive Breached Pair superfluids at weak coupling: some heavy particles are promoted to the light particle Fermi surface where they pair—this is where the interaction is dominant. The other Fermi surface remains essentially unpaired because of the momentum structure of the interaction.

In the following sections we shall present the details which support this picture and characterize the Breached Pair superfluids. We start by describing our model, deriving the general gap equation, and calculating some physical properties in Section 4.2. We then discuss the standard BCS state, the asymmetric BCS state, and finally the Breached Pair state in Sections 4.2.2, 4.2.3, and Chapter 5 respectively.

4.2 Fermionic Superfluidity

We start our discussion by deriving some mean-field results for BCS [8] superfluids. This will serve to illustrate the formalism developed in Section 3.1 and provide a basis for understanding the Breached Pair state.

We start with the model defined by the following Hamiltonian density:

$$\widehat{\mathcal{H}} = \int \mathrm{d}^3\vec{\mathbf{p}} \left(\widehat{\mathbf{a}}^\dagger_{\vec{\mathbf{p}}} \varepsilon^a_p \widehat{\mathbf{a}}_{\vec{\mathbf{p}}} + \widehat{\mathbf{b}}^\dagger_{\vec{\mathbf{p}}} \varepsilon^b_p \widehat{\mathbf{b}}_{\vec{\mathbf{p}}} \right) + g \int \widehat{\mathbf{a}}^\dagger \widehat{\mathbf{b}}^\dagger \widehat{\mathbf{b}} \widehat{\mathbf{a}}. \tag{4.1}$$

[2] Note, however, that a flat band becomes much more sensitive to finite temperature effects, and the corresponding critical temperatures is lowered [41] (4.46).

This is a model for two species of spinless fermions with annihilation operators $\widehat{\mathbf{a}}$ and $\widehat{\mathbf{b}}$. In the usual BCS model, these two species are just the spin-up and spin-down states of the electron. Here we would like to consider particles with potentially different properties such as their mass. This is why we use the two species notation.

For now we leave the dispersion relationships ε_p^a and ε_p^b arbitrary, though we have in mind non-relativistic dispersions $p^2/(2m) - \mu$. Note that we have included the bare chemical potentials in these dispersion relationships to simplify the notation. Complicated dispersions might arise in systems where the electrons are in two different bands interact. In QCD, the dispersion are relativistic $\sqrt{p^2 + m^2} - \mu$.

We shall also not specify the exact nature of the four-fermion interaction: In general, this will need regularization, but, to simplify this presentation, we shall defer this discussion until Section 5.2. For now, consider a contact interaction regulated with a hard three-momentum cutoff as discussed in Section 3.3 in Equation (3.45).

The first step is to rewrite the Hamiltonian density in terms of a two-component spinor of definite momentum:[3]

$$\widehat{\psi}_{\vec{\mathbf{p}}} = \begin{pmatrix} \widehat{\mathbf{a}}_{\vec{\mathbf{p}}} \\ \widehat{\mathbf{b}}^\dagger_{-\vec{\mathbf{p}}} \end{pmatrix}. \tag{4.2}$$

In terms of this spinor, the Hamiltonian density has the the form (3.43):

$$\widehat{\mathcal{H}} = \int \mathrm{d}^3\vec{\mathbf{p}} \left(\widehat{\psi}^\dagger_{\vec{\mathbf{p}}} \boldsymbol{\varepsilon}_p \widehat{\psi}_{\vec{\mathbf{p}}} + \varepsilon_p^b \right) + g \int (\widehat{\psi}^\dagger \boldsymbol{\Gamma}^\dagger \widehat{\psi})(\widehat{\psi}^\dagger \boldsymbol{\Gamma} \widehat{\psi})$$

where

$$\boldsymbol{\varepsilon}_p = \begin{pmatrix} \varepsilon_p^a & 0 \\ 0 & -\varepsilon_p^b \end{pmatrix}, \qquad \text{and} \qquad \boldsymbol{\Gamma} = \begin{pmatrix} 0 & 0 \\ 1 & 0 \end{pmatrix}. \tag{4.3}$$

The extra ε^b results from the anti-commutation relations and the reordering of the operators $\widehat{\mathbf{b}}$. We note now that, for homogeneous and isotropic states, everything is diagonal in momentum space, and we simply drop all momentum dependency in our presentation: The back-to-back scattering that leads to the correlations $\langle \widehat{\mathbf{a}}_{\vec{\mathbf{p}}} \widehat{\mathbf{b}}_{-\vec{\mathbf{p}}} \rangle$ is naturally provided by the spinor

[3] In this simple two-species system, one can either have pairing of the form $\langle \widehat{\mathbf{a}}_{\vec{\mathbf{p}}} \widehat{\mathbf{b}}_{-\vec{\mathbf{p}}} \rangle$ or of the form $\langle \widehat{\mathbf{a}}_{\vec{\mathbf{p}}} \widehat{\mathbf{b}}^\dagger_{\vec{\mathbf{p}}} \rangle$ depending on the sign of the interaction. As long as the sign of the interaction is constant, however, these are mutually exclusive. This allows us to use the simplified formalism discussed in Section 3.1. More complicated models require the full formalism discussed in Appendix B to deal with both types of condensates simultaneously.

structure (4.2). We shall be more careful with the momentum structure in Section 5.3.1, but wish to keep the present presentation clean. We point out that the interaction is the normal ordered form of $g\widehat{\mathbf{a}}^\dagger\widehat{\mathbf{a}}\widehat{\mathbf{b}}^\dagger\widehat{\mathbf{b}}$ and is thus attractive if $g < 0$ and repulsive if $g > 0$.

We shall effect a mean-field upper bound on the thermodynamic potential with the following quadratic Hamiltonian density:

$$\widehat{\mathcal{H}}_0 = \int \mathrm{d}^3\vec{\mathbf{p}} \left(\widehat{\psi}^\dagger \mathbf{E} \widehat{\psi} + E_b\right) \tag{4.4}$$

where

$$\mathbf{E} = \boldsymbol{\varepsilon} + \boldsymbol{\Sigma} = \begin{pmatrix} \varepsilon^a - \delta\mu_a & \Delta \\ \Delta^* & -\varepsilon^b + \delta\mu_b \end{pmatrix} = \begin{pmatrix} E_a & \Delta \\ \Delta^* & -E_b \end{pmatrix} \tag{4.5}$$

and the variational parameters are

$$\boldsymbol{\Sigma} = \begin{pmatrix} -\delta\mu_a & \Delta \\ \Delta^* & \delta\mu_b \end{pmatrix}. \tag{4.6}$$

One may think of the parameters $\delta\mu$ as chemical potential "renormalizations" such that the renormalized dispersions are

$$E = \varepsilon - \delta\mu = \frac{p^2}{2m} - (\mu + \delta\mu) \tag{4.7}$$

with the renormalized chemical potential $\mu_R = \mu + \delta\mu$. The parameters Δ might also be thought of as a renormalization, but since there is no corresponding bare parameter, this is better thought of as a spontaneously induce symmetry breaking term: The original theory has a global U(1) symmetry where $\widehat{\mathbf{a}} \to e^{i\alpha}\widehat{\mathbf{a}}$ and $\widehat{\mathbf{b}} \to e^{i\alpha}\widehat{\mathbf{b}}$. This symmetry is explicitly broken by the variational parameter Δ. If Δ is found to be non-zero after minimization, then this symmetry is said to be spontaneously broken by the state. All of the solutions $e^{2i\alpha}\Delta$ will be degenerate, but physically equivalent. This phenomenon of a spontaneously broken symmetry is responsible for many superfluid properties and will be discussed in Section 5.4. For now we simply note that, on account of this symmetry, we may take Δ to be real.

The variational bound on the free energy is now given by (3.46).[4] The

[4]There is a slight complication from the terms $\varepsilon^b_{\vec{\mathbf{p}}}$ and $E^b_{\vec{\mathbf{p}}}$ that arise from the arrangement of the operators $\widehat{\mathbf{b}}$. The free-energy Ω_0 picks up a term $E^b_{\vec{\mathbf{p}}}$ while the term $\langle\widehat{\mathcal{H}} - \widehat{\mathcal{H}}_0\rangle_0$ picks up the term $\varepsilon^b_{\vec{\mathbf{p}}} - E^b_{\vec{\mathbf{p}}}$. The net result $\varepsilon^b_{\vec{\mathbf{p}}}$ is independent of the variational parameters and thus does not affect the Schwinger-Dyson equations.

result is now

$$\frac{\Omega}{V} \leq \int \mathrm{d}^3\vec{\mathbf{p}} \left(\frac{1}{\beta} \operatorname{Tr} \ln[\mathbf{F}^-_{\vec{\mathbf{p}}}] - \operatorname{Tr}[\mathbf{\Sigma}_{\vec{\mathbf{p}}} \mathbf{F}^+_{\vec{\mathbf{p}}}] + \varepsilon^b_{\vec{\mathbf{p}}} \right) + \\ + g \left(\operatorname{Tr}[\mathbf{\Gamma}^\dagger \mathbf{F}^+_\int] \operatorname{Tr}[\mathbf{\Gamma} \mathbf{F}^+_\int] + \operatorname{Tr}[\mathbf{\Gamma}^\dagger \mathbf{F}^-_\int \mathbf{\Gamma} \mathbf{F}^+_\int] \right) \quad (4.8)$$

and the Schwinger-Dyson equation is[5]

$$\mathbf{\Sigma} = g \left(\mathbf{\Gamma}^\dagger \operatorname{Tr}[\mathbf{\Gamma} \mathbf{F}^+_\int] + \mathbf{\Gamma} \operatorname{Tr}[\mathbf{\Gamma}^\dagger \mathbf{F}^+_\int] + \mathbf{\Gamma}^\dagger \mathbf{F}^-_\int \mathbf{\Gamma} - \mathbf{\Gamma} \mathbf{F}^+_\int \mathbf{\Gamma}^\dagger \right). \quad (4.9)$$

This expression is probably a bit foreign, so we shall express this in terms of more physical quantities under the assumption that the interaction is separable as discussed in Section 3.3.2. We start by defining the integrated two-body correlations $n_a \sim \langle \widehat{\mathbf{a}}^\dagger \widehat{\mathbf{a}} \rangle$, $n_b \sim \langle \widehat{\mathbf{b}}^\dagger \widehat{\mathbf{b}} \rangle$, and $\Phi \sim \langle \widehat{\mathbf{b}} \widehat{\mathbf{a}} \rangle$:

$$\mathbf{F}^+_\int = \begin{pmatrix} n_a & -\Phi \\ -\Phi & 1 - n_b \end{pmatrix} = \int \mathrm{d}^3\vec{\mathbf{p}} \Lambda^2_{\vec{\mathbf{p}}} \begin{pmatrix} \langle \widehat{\mathbf{a}}^\dagger_{\vec{\mathbf{p}}} \widehat{\mathbf{a}}_{\vec{\mathbf{p}}} \rangle & \langle \widehat{\mathbf{b}}_{-\vec{\mathbf{p}}} \widehat{\mathbf{a}}_{\vec{\mathbf{p}}} \rangle \\ \langle \widehat{\mathbf{a}}^\dagger_{\vec{\mathbf{p}}} \widehat{\mathbf{b}}^\dagger_{-\vec{\mathbf{p}}} \rangle & \langle \widehat{\mathbf{b}}_{-\vec{\mathbf{p}}} \widehat{\mathbf{b}}^\dagger_{-\vec{\mathbf{p}}} \rangle \end{pmatrix}. \quad (4.10)$$

Note that n_a is not actually the total density if the cutoff is not sharp, but, rather, the density as it couples in the interaction. (The true density should be integrated without a cutoff.) The free-energy bound now has the form

$$\frac{\Omega}{V} \leq \int \mathrm{d}^3\vec{\mathbf{p}} \left(\frac{1}{\beta} \ln[f_\beta(-\omega^-_{\vec{\mathbf{p}}}) f_\beta(-\omega^+_{\vec{\mathbf{p}}})] + E^b_{\vec{\mathbf{p}}} \right) + \\ + \delta\mu_a n_a + \delta\mu_b n_b + 2\Delta\Phi + g \left(n_a n_b + \Phi^2 \right) \quad (4.11)$$

and the Schwinger-Dyson equation gives

$$\Delta = -g\Phi, \qquad \delta\mu_a = -g n_b, \qquad \delta\mu_b = -g n_a. \quad (4.12)$$

Note that this appears to follow by varying (4.11) with respect to n_a, n_b and Φ, but one must actually vary the momentum-dependent quantities because of the implicit momentum dependence in the kinetic terms. The additional terms generated, however, cancel as discussed in Section 3.2.2. Using the Schwinger-Dyson equation, we obtain the following thermodynamic potential density *at the stationary point*:

$$\frac{\Omega}{V} \approx \int \mathrm{d}^3\vec{\mathbf{p}} \left(\frac{1}{\beta} \ln[f_\beta(-\omega^-_{\vec{\mathbf{p}}}) f_\beta(-\omega^+_{\vec{\mathbf{p}}})] + E^b_{\vec{\mathbf{p}}} \right) - g \left(n_a n_b + \Phi^2 \right). \quad (4.13)$$

[5] Recall that $\mathbf{F}^+ \int$ contains the integrated two-body correlations (3.47).

To proceed further, we must perform some evaluations. First, we diagonalize the quadratic Hamiltonian density:

$$\mathbf{E} = \mathbf{Q} \cdot \begin{pmatrix} \omega^+ & 0 \\ 0 & \omega^- \end{pmatrix} \cdot \mathbf{Q}^\dagger, \qquad \begin{pmatrix} \widehat{\mathbf{c}}_+ \\ \widehat{\mathbf{c}}_- \end{pmatrix} = \mathbf{Q}^\dagger \begin{pmatrix} \widehat{\mathbf{a}} \\ \widehat{\mathbf{b}}^\dagger \end{pmatrix}. \tag{4.14}$$

This is easily achieved with the following transformation

$$\mathbf{Q} = \mathbf{Q}^\dagger = \begin{pmatrix} \cos\phi & \sin\phi \\ \sin\phi & -\cos\phi \end{pmatrix} \tag{4.15}$$

where

$$2\cos\phi\sin\phi = \frac{\Delta}{\sqrt{E_+^2 + \Delta^2}}. \tag{4.16}$$

As these quantities will appear frequently, we define some terms which we shall use throughout this thesis:

$$E_\pm = \frac{E_a \pm E_b}{2}, \qquad \eta = \sqrt{E_+^2 + \Delta^2}, \qquad \xi = E_+/\eta. \tag{4.17}$$

In terms of these parameters, the eigenvalues of $\mathbf{E}$, which determine the quasiparticle spectrum of fermionic excitations, are given by:

$$\omega_\pm = E_- \pm \eta = E_- \pm \sqrt{E_+^2 + \Delta^2}. \tag{4.18}$$

The unitary transformation, $\mathbf{Q}$ is expressed in terms of the "coherence factors" $u = \cos\phi$ and $v = \sin\phi$. They satisfy the following relationships:

$$\cos^2\phi = \frac{1+\xi}{2}, \qquad \sin^2\phi = \frac{1-\xi}{2}, \qquad 2\cos\phi\sin\phi = \frac{\Delta}{\eta}. \tag{4.19}$$

The main results follow from the computation of $\mathbf{F}^+_{\vec{\mathbf{p}}}$:

$$\mathbf{F}^+_{\vec{\mathbf{p}}} = f_\beta(\mathbf{E}_{\vec{\mathbf{p}}}) = \mathbf{Q} \cdot \begin{pmatrix} f_\beta(\omega_+) & 0 \\ 0 & f_\beta(\omega_-) \end{pmatrix} \cdot \mathbf{Q}^\dagger. \tag{4.20}$$

To simplify this, and to foreshadow the familiar $T \to 0$ limit, we define

$$\theta_\pm = 1 - f_\beta(\omega_\pm) = \frac{1 + \tanh(\beta\omega_\pm/2)}{2}. \tag{4.21}$$

In the $T \to 0$ limit these become step functions

$$\lim_{T\to 0} \theta_\pm = \theta(\omega_\pm). \tag{4.22}$$

The result is

$$\mathbf{F}^{+}_{\vec{\mathbf{p}}} = \begin{pmatrix} 1-\theta_+\cos^2\phi-\theta_-\sin^2\phi & -(\theta_+-\theta_-)\cos\phi\sin\phi \\ -(\theta_+-\theta_-)\cos\phi\sin\phi & 1-\theta_-\cos^2\phi-\theta_+\sin^2\phi \end{pmatrix} \tag{4.23}$$

Properties of the variational ensemble can now be extracted from $\mathbf{F}^{+}_{\vec{\mathbf{p}}}$. For example, the densities follow from the definition of $\mathbf{F}^{+}_{\vec{\mathbf{p}}}$ as a quadratic correlation: $[\mathbf{F}^{+}_{\vec{\mathbf{p}}}]_{11} = \langle \widehat{\mathbf{a}}^\dagger \widehat{\mathbf{a}} \rangle = n_a$ and $[\mathbf{F}^{+}_{\vec{\mathbf{p}}}]_{22} = \langle \widehat{\mathbf{b}}\widehat{\mathbf{b}}^\dagger \rangle = 1 - n_b$:

$$n_a = 1-\theta_+\cos^2\phi-\theta_-\sin^2\phi = \frac{(2-\theta_+-\theta_-)-\xi(\theta_+-\theta_-)}{2}, \tag{4.24a}$$

$$n_b = \theta_-\cos^2\phi+\theta_+\sin^2\phi = \frac{(\theta_++\theta_-)-\xi(\theta_+-\theta_-)}{2}. \tag{4.24b}$$

Note that the sum and differences take a particularly nice form:

$$n_a + n_b = 1-\xi(\theta_+-\theta_-) = 1-\frac{\xi}{2}[\tanh(\beta\omega_+/2)-\tanh(\beta\omega_-/2)], \tag{4.24c}$$

$$n_a - n_b = 1-(\theta_++\theta_-) = -\frac{1}{2}[\tanh(\beta\omega_+/2)+\tanh(\beta\omega_-/2)]. \tag{4.24d}$$

We can also write the self-consistency conditions from the components of the Schwinger-Dyson equation:

$$\Delta = -g\int \mathrm{d}^3\vec{\mathbf{p}} \frac{\Delta}{2\sqrt{E_+^2+\Delta^2}}(\theta_+-\theta_-), \tag{4.25a}$$

$$\delta\mu_a = -g\int \mathrm{d}^3\vec{\mathbf{p}} \frac{(\theta_++\theta_-)-\xi(\theta_+-\theta_-)}{2} = -gn_b, \tag{4.25b}$$

$$\delta\mu_b = -g\int \mathrm{d}^3\vec{\mathbf{p}} \frac{(2-\theta_+-\theta_-)-\xi(\theta_+-\theta_-)}{2} = -gn_a. \tag{4.25c}$$

We note that the interpretation of the chemical potential renormalizations is particularly simple: if the interaction is attractive ($g < 0$), then a net density of one species increases the chemical potential of the other because of the attraction.

Generally, the "gap equation" (4.25a) needs ultraviolet regulation because, for large momenta, $E_+ \sim p^\alpha$. For relativistic dispersions, $\alpha = 1$, and for non-relativistic dispersions, $\alpha = 2$. In either case, the integral diverges in three dimensions as $\int p^{2-\alpha}\mathrm{d}p$. Details of this will be discussed later in Section 5.2. For now, simply imagine that there is a hard momentum cutoff in the integrals.

4.2.1 Order Parameter

Note how the variational parameters relate to the order parameter. In the literature (especially the QCD literature), one usually sees the parameter Δ defines as an order parameter:

$$\Delta_{\text{OP}} \equiv g \langle \widehat{\mathbf{\Delta}} \rangle \tag{4.26a}$$

where

$$\widehat{\mathbf{\Delta}} = \int \text{đ}^3\vec{\mathbf{p}}\, \Lambda_p^2 \widehat{\mathbf{b}}_{\vec{\mathbf{p}}} \widehat{\mathbf{a}}_{-\vec{\mathbf{p}}}. \tag{4.26b}$$

This definition corresponds to the right-hand side of the gap equation (4.25a) where Δ is our variational parameter from the quadratic Hamiltonian density $\widehat{\mathcal{H}}_0$. At the stationary point, these are equivalent, but away from the stationary point, they are different. Thus, one may consider an additional variational method

$$\frac{\Omega(\Delta_{\text{OP}})}{V} = \min_{\langle\theta|\widehat{\mathbf{\Delta}}|\theta\rangle = \Delta_{\text{OP}}} \langle\theta|\widehat{\mathcal{H}} - \mu_a \widehat{\mathbf{n}}_a - \mu_b \widehat{\mathbf{n}}_b|\theta\rangle\,, \tag{4.27}$$

where we minimization over all BCS style ansatz $|\theta\rangle$ with given expectation Δ_{OP}. However, it is difficult to actually compute this explicitly since all expressions are in terms of Δ rather than Δ_{OP}. This was carefully done in [1] where both Ω and Δ_{OP} were computed as functions of Δ and then $\Omega(\Delta_{\text{OP}})$ was plotted. In this thesis, Δ shall always refer to the variational parameter appearing in the quadratic Hamiltonian: Δ_{OP} corresponds to the parameters in $\mathbf{F}_{\int}^{+}$.

4.2.2 Standard BCS Superfluidity

The standard BCS picture emerges when both species have the same dispersion relationships: $\varepsilon^a = \varepsilon^b$. In this case, $E_- = 0$ and so the quasiparticle dispersions are always of different sign:

$$\omega_\pm = \pm\eta = \pm\sqrt{E_+^2 + \Delta^2}. \tag{4.28}$$

We immediately see that, once we fill in all the negative energy states, the quasiparticle dispersions $\eta = \sqrt{E_+^2 + \Delta^2}$ have a gap in the spectrum of magnitude Δ at the non-interaction (renormalized) Fermi surface where $E_+ = 0$. We also see $\theta_+ + \theta_- = 1$, and so there is an equal density of each species:

$$n_a = n_b = \frac{1 - \xi(\theta_+ - \theta_-)}{2} = \frac{1 - \xi \tanh(\beta\eta/2)}{2}. \tag{4.29}$$

The gap equation assumes the familiar form

$$1 = -g \int \mathrm{d}^3\vec{\mathbf{p}} \, \frac{1}{2\sqrt{E_+^2 + \Delta_T^2}} \tanh\Big(\eta/(2T)\Big) \tag{4.30}$$

In the zero temperature limit, $\tanh(\beta\eta/2) \to 1$ for all non-zero Δ. Thus, one sees that the integral has a divergence as $\Delta \to 0$ along the Fermi surface where $E_+ = 0$. Because of this, for arbitrarily weak attractions, there is always a solution Δ_0 to the zero temperature gap equation.

At finite temperatures, however, $\tanh(\beta\eta/2) \approx \beta\eta/2$ near the Fermi-surface and so the divergence is rendered finite even as $\Delta_T \to 0$. Thus, there is a minimum value of coupling required to sustain superfluidity at finite temperatures. In particular, there is a critical temperature T_c at which the gap vanishes $\Delta_{T_c} = 0$, which is given by the solution to

$$1 = -g \int \mathrm{d}^3\vec{\mathbf{p}} \, \frac{1}{2|E_+|} \tanh\Big(|E_+|/(2T_c)\Big) \tag{4.31}$$

The zero-temperature gap and the critical temperature are thus related:

$$\int \mathrm{d}^3\vec{\mathbf{p}} \left[\frac{1}{2\sqrt{E_+^2 + \Delta_0^2}} - \frac{\tanh\Big(|E_+|/(2T_c)\Big)}{2|E_+|} \right] = 0. \tag{4.32}$$

For typical dispersions, in both the large and small momentum regions, $T_c \sim \Delta_0 \ll |E_+|$. As a result, the integral is self-regulated in these regions and the only non-trivial contribution comes from the region about the Fermi-surface.

A common technique to study the relationship between Δ_0 and T_c to use the identity

$$\int \mathrm{d}^3\vec{\mathbf{p}} \, h(E_+) = \int \mathrm{d}\epsilon \int \mathrm{d}^3\vec{\mathbf{p}} \, h(\epsilon)\delta(E_+ - \epsilon) = \int \mathrm{d}\epsilon \, N(\epsilon)h(\epsilon) \tag{4.33a}$$

where

$$N(\epsilon) = \int \mathrm{d}^3\vec{\mathbf{p}} \, \delta(E_+ - \epsilon) \tag{4.33b}$$

is the density of states at energy ϵ of the non-interacting (but renormalized) system. To this end, one often introduces a cutoff so that the integrals only contribute from a region near the Fermi-surface where $E_+^2 < \omega_D^2$. With this

approximation, the relationship between the zero-temperature gap Δ_0 and the critical temperature T_c becomes

$$\int_0^{\omega_D} \mathrm{d}\epsilon\, N(\epsilon) \left[\frac{1}{2\sqrt{\epsilon^2+\Delta_0^2}} - \frac{\tanh\left(\epsilon/(2T_c)\right)}{2\epsilon} \right] = 0. \tag{4.34}$$

If $\Delta_0 \sin T_c \ll p_F$ and the dispersions are smooth enough over the scale set by Δ_0 and T_c, then the dominant portion of this integral is in the region where $\epsilon < \Delta_0$. In particular, as long as the dispersions are sufficiently flat, this may be approximated by the constant $N(0)$ over the region of interaction, which simply represents the effective low-energy properties of the fermions at the Fermi surface. One may also take the cutoff to infinity. The resulting solution is thus quite insensitive to both the regularization scheme *and* to the properties of the Fermi surface.

Before we derive this relationship, we consider the solution to the gap equation. This *is* sensitive to the ultraviolet physics and acquires an explicit dependence on the regulator ω_D:

$$1 \approx \frac{-g}{2} N(0) \int_0^{\omega_D} \mathrm{d}\epsilon\, \frac{1}{\sqrt{\epsilon^2+\Delta_T^2}} \tanh\left(\sqrt{\epsilon^2+\Delta_0^2}/(2T_c)\right). \tag{4.35}$$

In the zero temperature limit, we may directly integrate this to find the gap:

$$1 = \frac{-g}{2} N(0) \ln\left[\frac{\omega_D}{\Delta_0} + \sqrt{1+\left(\frac{\omega_D}{\Delta_0}\right)^2} \right]. \tag{4.36}$$

The usual separation of scales is $\Delta_0 \ll \omega_D \ll p_F$ through which the last term simplifies to give the familiar result

$$\Delta_0 = 2\omega_D e^{-2/(|g|N(0))} \tag{4.37}$$

which emphasizes the non-perturbative nature of superfluidity: The gap Δ_0 in the spectrum of quasiparticle cannot be represented as a power-series in the coupling g.

To determine the relationship between Δ_0 and T_c, we introduce the dimensionless variable $x = \epsilon/\Delta_0$. The relevant relation becomes

$$0 = \int_0^{\omega_D/\Delta_0} \mathrm{d}x\, \frac{N(\Delta_0 x)}{2} \left[\frac{1}{\sqrt{x^2+1}} - \frac{1}{x} \tanh\left(\tfrac{x}{2}\tfrac{\Delta_0}{T_c}\right)\right], \tag{4.38a}$$

$$\approx \frac{N(0)}{2} \lim_{X\to\infty} \int_0^X \mathrm{d}x \left[\frac{1}{\sqrt{x^2+1}} - \frac{1}{x} \tanh\left(\tfrac{x}{2}\tfrac{\Delta_0}{T_c}\right)\right]. \tag{4.38b}$$

Dropping the constant and integrating the last term by parts, we have

$$\begin{aligned}
0 &\approx \lim_{X\to\infty}\left[\sinh^{-1}(X) - \ln(X)\tanh\left(\frac{X\Delta_0}{2T_c}\right) + \int_0^X \mathrm{d}x\ \ln(x)\frac{\mathrm{d}}{\mathrm{d}x}\tanh\left(\frac{x\Delta_0}{2T_c}\right)\right], \\
&= \ln(2) + \left[\int_0^\infty \mathrm{d}y\ \left[\ln(y) + \ln\left(\frac{2T_c}{\Delta_0}\right)\right]\frac{\mathrm{d}}{\mathrm{d}y}\tanh(y)\right)\Bigg], \\
&= \ln(2) + \ln\left(\frac{2T_c}{\Delta_0}\right) + \int_0^\infty \mathrm{d}y\ \ln(y)\frac{\mathrm{d}}{\mathrm{d}y}\tanh(y), \\
&= \ln\left(\frac{4T_c}{\Delta_0}\right) + \ln\left(\frac{\pi}{4e^\gamma}\right),
\end{aligned}$$

where $\gamma = 0.5772157\ldots$ is the Euler-Mascheroni constant. From this, we find the following well-known and robust prediction of mean-field BCS theory:

$$\frac{T_c}{\Delta_0} \approx \frac{e^\gamma}{\pi} \approx 0.567. \tag{4.39}$$

4.2.3 Asymmetric BCS Superfluidity

Now consider the BCS picture but when the two species have different dispersions (for example, if they have different masses). The gap equation becomes

$$\frac{-1}{g} = \int \mathrm{d}^3\vec{\mathbf{p}}\ \frac{1}{4\sqrt{E_+^2+\Delta^2}}\left(\tanh\left(\frac{E_-+\sqrt{E_+^2+\Delta^2}}{2T}\right) - \tanh\left(\frac{E_--\sqrt{E_+^2+\Delta^2}}{2T}\right)\right).$$

If we assume that we remain in the BCS region where $\omega_- < 0 < \omega_+$ for all momenta, then we have the following relationship between Δ_0 and T_c:

$$0 = \int \mathrm{d}^3\vec{\mathbf{p}}\left(\frac{1}{2\sqrt{E_+^2+\Delta_0^2}} - \frac{1}{4|E_+|}\left(\tanh\left(\frac{E_-+|E_+|}{2T_c}\right) - \tanh\left(\frac{E_--|E_+|}{2T_c}\right)\right)\right).$$

The first term is the same as in the symmetric case, but the latter terms are complicated by the presence of a non-zero difference in dispersions E_-. In general, the relationship between Δ_0 and T_c is complicated, but, as was pointed out in [41], there is a special exception. To see this, write $E_- = E_-(E_+)$ as a function of E_+, and perform the same transformation as above to the variable $x = \epsilon/\Delta_0$. The second term becomes

$$-\int \mathrm{d}x\ \frac{N(\Delta_0 x)}{4x}\left(\tanh\left[\frac{\Delta_0}{2T_c}\left(x + \frac{E_-(\Delta_0 x)}{\Delta_0}\right)\right] + \tanh\left[\frac{\Delta_0}{2T_c}\left(x - \frac{E_-(\Delta_0 x)}{\Delta_0}\right)\right]\right).$$

If the energy difference $E_-(E_+) = aE_+$ is a homogeneous function, then $E_-(\Delta_0 x) = \Delta_0 E_-(x)$ and everything, except the density of states, may be expressed in terms of the ratio Δ_0/T_c:

$$0 = \int \mathrm{d}x \, \frac{N(\Delta_0 x)}{2} \left(\frac{1}{\sqrt{x^2+1}} - \frac{1}{2x} \left(\tanh\left[\tfrac{(1+a)x\Delta_0}{2T_c} \right] + \tanh\left[\tfrac{(1-a)x\Delta_0}{2T_c} \right] \right) \right).$$

If the coefficient a is small, then, under the same conditions as before, one may replace $N(\Delta_0 x) \approx N(0)$ with the value at the Fermi surface and perform the integrals, obtaining:

$$\begin{aligned} 0 &\approx \ln(2) + \frac{1}{2} \int_0^\infty \mathrm{d}y \left(\ln\left(\tfrac{2yT_c}{(1+a)\Delta_0} \right) \frac{\mathrm{d}}{\mathrm{d}y} \tanh(y) + \ln\left(\tfrac{2yT_c}{(1-a)\Delta_0} \right) \frac{\mathrm{d}}{\mathrm{d}y} \tanh(y) \right), \\ &= \ln(2) + \frac{1}{2} \ln\left(\tfrac{2T_c}{(1+a)\Delta_0} \tfrac{2T_c}{(1-a)\Delta_0} \right) + \int_0^\infty \mathrm{d}y \left(\ln(y) \frac{\mathrm{d}}{\mathrm{d}y} \tanh(y) \right), \\ &= \ln\left(\tfrac{4T_c}{\sqrt{1-a^2}\Delta_0} \right) + \ln\left(\frac{\pi}{4e^\gamma} \right). \end{aligned}$$

Thus, we have the result

$$\frac{T_c}{\Delta_0} \approx \frac{\sqrt{1-a^2}e^\gamma}{\pi} \approx 0.567\sqrt{1-a^2}. \tag{4.40}$$

Let us review the conditions on this result:

- The energy difference between the two species $E_- \approx aE_+$ must be approximately a homogeneous function of the energy sum E_+ in the vicinity of the common Fermi-surface. In particular, it must vanish with E_+ indicating that $E_a = E_b = 0$ so that the two species must share the same Fermi-surface.
- The magnitude of the coefficient a must be less than 1.
- The quasiparticle dispersions must have the opposite sign, $\omega_- < 0 < \omega_+$ near the Fermi-surface.
- The density of states $N(\epsilon)$ must not vary appreciable over the region near the Fermi-surface where the integral is dominant.

All of these conditions are actually very similar. The homogeneity requirement is simply the statement that the dispersions are smooth over a scale of order $\Delta_0/(1-|a|)$ and that the Fermi-surfaces are equal. The condition that $|a| < 1$ is simply the local manifestation that $\omega_- < 0 < \omega_+$ at the Fermi-surface.

The special case considered in [41] was that of non-relativistic fermions:

$$E_{a,b} = p^2/(2m_{a,b}) - \mu_{a,b}, \tag{4.41}$$

with equal Fermi-momenta

$$p_F = \sqrt{2\mu_a m_a} = \sqrt{2\mu_b m_b}. \tag{4.42}$$

In this case, we have

$$E_- = \frac{m_+}{m_-}(|E_+| + \mu_+) - \mu_- = \frac{m_b - m_a}{m_b + m_a}|E_+| - \frac{2m_b\mu_b - 2m_a\mu_a}{m_a + m_b}, \tag{4.43}$$

where

$$\frac{1}{m_\pm} = \frac{1}{m_a} \pm \frac{1}{m_b}, \qquad \text{and} \qquad \mu_\pm = \mu_a \pm \mu_b. \tag{4.44}$$

Thus, the required conditions are satisfied if the Fermi surfaces are equal, $m_a\mu_a = m_b\mu_b$, and the scales separate as

$$\Delta_0 \ll (1 - |a|)\mu_+. \tag{4.45}$$

As emphasized in [41], although the solution to the zero-temperature gap equation Δ_0 is unchanged by a large mass asymmetry $r = m_a/m_b < 1$, the critical temperature may be significantly reduced:

$$\frac{T_c}{\Delta_0} \approx 0.567\frac{\sqrt{2r}}{1+r}. \tag{4.46}$$

Chapter 5

Breached Pair Superfluidity

Breached Pair superfluids embody the notion of phase separation in momentum space: some regions of momentum space exhibit pairing contributing to the superfluid properties, while other regions remain unpaired maintaining properties of a Fermi liquid. These exotic superfluids are characterized by the coexistence of a superfluid and a normal component in a translationally invariant and isotropic state. Both components are accommodated in different regions of momentum space with the normal component residing in the "breaches", bounded by gapless Fermi surfaces. In position space, these superfluid phases remain spatially homogeneous and isotropic.[1]

The pairing correlations lead to spontaneously broken U(1) symmetries as with conventional fermion superfluids. This admits the usual Goldstone modes and topological vortex properties. In addition, the presence of gapless Fermions maintain some normal Fermi-liquid properties. For example, thermodynamic properties such as the heat capacity that are dominated by the low-energy degrees of freedom will more closely resemble those of Fermi-liquids than those of superfluids.

Many of the characteristic properties of Breached Pair superfluids can be understood from an analysis of the quasiparticle properties given by the quadratic Hamiltonian (4.4) that defines the variational ensemble. In particular, the Breached Pair states are characterized by gapless fermionic excitations where $\omega_{\pm}(p) = 0$.

Even though the quadratic Hamiltonian (4.4) admits such states, these states do not necessarily minimize the free-energy of some "realistic" model. Indeed, Sarma's original calculations [16] found that the states with gapless fermionic excitations are unstable. We shall defer the discussion about the stability of these states to Section 5.2. We simply note here that they can be stabilized with appropriate interactions, thus we proceed to discuss the quasiparticle properties.

[1] There is also the possibility of Breached Pair superfluidity with P-wave dominated interactions that are not isotropic and homogeneous [42, 43]. In this thesis we shall only consider the S-wave case.

5.1 Quasiparticle Properties

For illustrative purposes, we consider only non-relativistic dispersions

$$\varepsilon_p^{a,b} = \frac{p^2}{2m_{a,b}} - \mu_{a,b}. \tag{5.1}$$

5.1.1 Dispersions

Most of the quasiparticle properties follow from the dispersions

$$\omega_\pm = E_- \pm \sqrt{E_+^2 + \Delta^2} \tag{5.2}$$

where

$$E_\pm(p) = \frac{p^2}{2m_\pm} - \mu_\pm, \qquad \frac{1}{m_\pm} = \frac{1}{m_a} \pm \frac{1}{m_b}, \qquad \text{and,} \qquad \mu_\pm = \mu_a \pm \mu_b.$$

At zero-temperature, the signs of the dispersions indicate whether or not the quasiparticle states are occupied. Thus, in regions of momentum space where $\omega_- < 0 < \omega_+$, the properties of the state are very similar to those of conventional BCS superfluids. The deviations occur in the "breach" regions where either $\omega_-, \omega_+ < 0$ or $0 < \omega_-, \omega_+$. In these regions, the properties of the state are similar to that of a Fermi-liquid. Note that the relevant quantity to consider is the sign of $\omega_+\omega_-$.[2] The breach points, which behave as Fermi-surfaces, are thus defined by $\omega_+\omega_- = 0$. If there is no momentum dependence in Δ, μ or m, then analytic formulae can be derived, but the stable solutions will have extra momentum dependence so we do not present these academic results here.

The novel feature of these states is that there are gapless fermionic excitations at the breach momenta: these gapless momenta define Fermi-surfaces and one expects all of the standard properties of Fermi surfaces. For example, there will be a large density of states with very low energy. This will result in a superfluid with an anomalously large heat capacity.[3] It is even possible that a dispersion may be almost quadratic which would give gapless superfluids an even higher heat capacity than a normal Fermi-liquid.

[2] Alternatively, one can think about this in terms of the pole structure of the correlation functions. This approach has been presented in the QCD context: [35].

[3] Conventional superfluids have a gapless Goldstone mode, but, as it is bosonic, only the states near zero momenta are low energy, as opposed to the entire Fermi-surface and the effects are thus suppressed. Breached Pair states have the extra gapless fermion degrees of freedom in addition to the Goldstone boson.

This property has led to an interesting potential signature for gapless colour-superconductors in neutron stars [44].

These dispersions are altered at finite temperature through the temperature dependence of the variational parameters Δ etc. We point out, however, that the Breached Pair and BCS phases may only be rigorously distinguished at zero temperature. In particular, the "gap in the spectrum" is not a sufficient order parameter at finite temperatures $T > 0$ [25, 27]. Indeed, no symmetry distinguishes between the two phases and one expects a smooth crossover at sufficiently high temperatures.

5.1.2 Densities

The occupation numbers as a function of momentum are obtained directly from the coherence factors. We note here, however, that these follow from the construction of the vacuum state from the zero state $|0\rangle$ annihilated by the original operators $\widehat{\mathbf{a}}$ and $\widehat{\mathbf{b}}$. Consider a single degree of freedom (momentum): The vacuum state should be annihilated by the quasiparticle operators $\widehat{\mathbf{c}}_\pm$ or $\widehat{\mathbf{c}}_\pm^\dagger$ respectively depending on whether $\omega_\pm$ are positive or negative. Recall that we have

$$\widehat{\mathbf{c}}_+ = \cos\phi\,\widehat{\mathbf{a}} + \sin\phi\,\widehat{\mathbf{b}}^\dagger, \qquad \widehat{\mathbf{c}}_- = \sin\phi\,\widehat{\mathbf{a}} - \cos\phi\,\widehat{\mathbf{b}}^\dagger \tag{5.3}$$

where

$$2\cos\phi\sin\phi = \frac{\Delta}{\sqrt{E_+^2 + \Delta^2}}.$$

Thus, as long as $\Delta \neq 0$, neither $\widehat{\mathbf{c}}_\pm$ nor $\widehat{\mathbf{c}}_\pm^\dagger$ annihilate the zero state $|0\rangle$. Consider three possible cases:

$\omega_- < 0 < \omega_+$: This is the usual BCS case. The ground state should satisfy $\widehat{\mathbf{c}}_+ |\mathrm{BP}\rangle = \widehat{\mathbf{c}}_-^\dagger |\mathrm{BP}\rangle = 0$. Using the anticommuting properties of the fermion operators, we can construct the following state which satisfies these properties:

$$|\mathrm{BP}\rangle = \mathcal{N}\widehat{\mathbf{c}}_+\widehat{\mathbf{c}}_-^\dagger |0\rangle = (\cos\phi + \sin\phi\widehat{\mathbf{b}}^\dagger\widehat{\mathbf{a}}^\dagger)|0\rangle \tag{5.4}$$

where we have used the properties of $|0\rangle$ being the zero state for operators $\widehat{\mathbf{a}}$ and $\widehat{\mathbf{b}}$ and normalized the state. This is the familiar "pairing" wave function from standard BCS theory.

$\omega_-, \omega_+ < 0$: This is one type of breach. The ground state here should satisfy $\widehat{\mathbf{c}}_+^\dagger |\mathrm{BP}\rangle = \widehat{\mathbf{c}}_-^\dagger |\mathrm{BP}\rangle = 0$. Now $\widehat{\mathbf{c}}_+^\dagger\widehat{\mathbf{c}}_-^\dagger |0\rangle = 0$, but $\widehat{\mathbf{c}}_+^\dagger |0\rangle \propto \widehat{\mathbf{c}}_-^\dagger |0\rangle \propto$

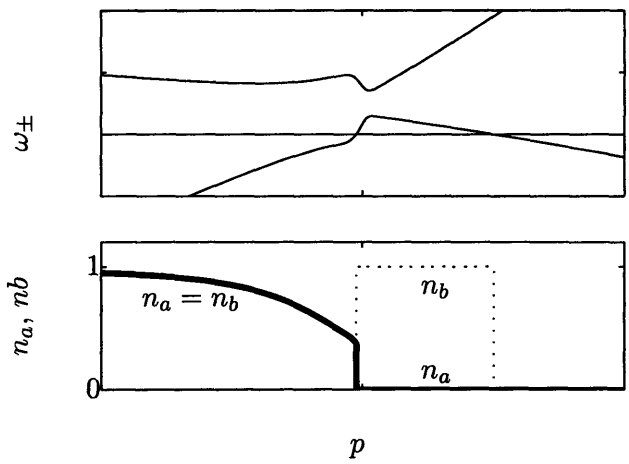

Figure 5.1: Quasiparticle dispersions $\omega_\pm(p)$ (top), and occupation numbers $n_a(p)$ and $n_b(p)$ (middle), in a sample BP state.

$\widehat{\mathbf{a}}^\dagger |0\rangle \neq 0$. Thus, the properly normalized state simply has a fully occupied species $\widehat{\mathbf{a}}$

$$|\mathrm{BP}\rangle = \widehat{\mathbf{a}}^\dagger |0\rangle . \tag{5.5}$$

$0 < \omega_-, \omega_+$: This is the other type of breach. The ground state here should satisfy $\widehat{\mathbf{c}}_+ |\mathrm{BP}\rangle = \widehat{\mathbf{c}}_- |\mathrm{BP}\rangle = 0$. Again, $\widehat{\mathbf{c}}_+ \widehat{\mathbf{c}}_- |0\rangle = 0$, but $\widehat{\mathbf{c}}_+ |0\rangle \propto \widehat{\mathbf{c}}_- |0\rangle \propto \widehat{\mathbf{b}}^\dagger |0\rangle \neq 0$. Thus, the properly normalized state simply has a fully occupied species $\widehat{\mathbf{b}}$

$$|\mathrm{BP}\rangle = \widehat{\mathbf{b}}^\dagger |0\rangle . \tag{5.6}$$

The complete Breached Pair ground state is a tensor product of these states over all momenta. Incidentally, at zero temperature, one can simply construct such a state with the parameters $\phi_{\vec{\mathbf{p}}}$ as variational parameters and minimize. This was the approach taken in the original BCS paper [8]. We reproduce the BCS results at $T = 0$ with equal dispersions $\varepsilon_a = \varepsilon_b$.

The typical situation for a Breached Pair state has regions of both BCS type, and a breach of one or the other Fermi types, depending on which Fermi surface ($\widehat{\mathbf{a}}$ or $\widehat{\mathbf{b}}$) is largest. An example is shown in Figure 5.1. At finite temperature, the slope of the dispersions become important and the sharp features of the Fermi surfaces become smoothed. We make one important remark here: even though the breach region looks like a normal Fermi

sea in terms of occupancy, the quasiparticle operators are the Bogoliubov transformed operators $\widehat{\mathbf{c}}_{\pm}$, not the bare operators $\widehat{\mathbf{a}}$ and $\widehat{\mathbf{b}}$. Thus, the breach is best thought of as a property of the state, rather than of the spectrum. It is simply a filling in of the states that have become negative energy states due to the asymmetry.

5.2 Stability

In the previous section, we discussed many of the properties of Breached Pair superfluids that follow from the spectrum of the variational Hamiltonian $\widehat{\mathbf{H}}_0$. We have not yet verified, however, that the state is stable. First we shall discuss some models where we can demonstrate that the system is thermodynamically stable, and then we discuss some possible physical realizations.

A requirement for thermodynamic stability is that the ensemble be of maximal entropy (see Section A.1.3). This is equivalent to the thermodynamic potential $\Omega(T, \vec{\mu})$ being a convex function: Convexity follows naturally from a proper minimization over a set of variational parameters, but is not guaranteed if this minimization is not fully performed. This can be a problem, for example, when one simply has a solution to the Schwinger-Dyson equations: The solution is only guaranteed to be a stationary point and may correspond to a maximum or a saddle point. This is exactly the type of instability found by Wu and Yip [19] and seems to be related to the chromo-magnetic instabilities discussed first by Shovkovy and Huang [29, 30, 45, 46, 47]. This latter issue arises when the stability is induced by long-range interactions and will be discussed in Section 5.5. The first issue is addressed by properly performing the minimization.

We start our discussion about stability by reminding the reader that, to identify possible phases for thermodynamic systems, one need only consider the phase diagram in the grand canonical ensemble (see Section A.4.6). Thus, we consider here large volumes of extensive phases in systems without long-range interactions. Under these conditions, possible heterogeneous mixed phases will be composed of pure phases found in the grand canonical ensemble using the tangent construction discussed in Section A.4.6. To ensure that we have found a stable Breached Pair state, we must find a model that admits such a state as a minimum of the thermodynamic potential $\Omega(T, \vec{\mu})$ at fixed temperature and chemical potentials. The first explicit examples of such states were presented in [1].

5.2.1 Heuristic Breached Pair Stability

For extensive systems, the thermodynamic potential $\Omega = -PV$ has the interpretation of negative pressure: Thus, the minimization requirement means that we wish to construct a state with maximum pressure for a given set of chemical potentials and temperature. Such a state will "push" out any competing states.

Start with a system of free fermions with unequal Fermi surfaces. In the absence of any interactions, this state minimizes the potential of the system, where the potential is determined solely by the kinetic energy $\int [p^2/(2m) - \mu]$:

$$\Omega = \sum_{a,b} \frac{1}{2\pi^2} \left(\frac{p_F^5}{10m} - \mu \frac{p_F^3}{6} \right) = -\sum_{a,b} \frac{p_F^5}{30m\pi^2}. \tag{5.7}$$

The Fermi-momenta p_F should be thought of as the "variational parameters" that define the occupancy of the state of minimal potential: $p_F = \sqrt{2m\mu}$.

In the presence of an attractive interaction, an increase in the pressure of the phase may be possible due to the condensation energy of the interaction, but this will be balanced by the kinetic energy which must deviate from the free fermion minimum. The cost for changing the occupancy is thus approximately given by the second derivative of Ω with respect to p_F:

$$\frac{\mathrm{d}^2\Omega}{\mathrm{d}p_F^2} = -\frac{p_F^3}{10m\pi^2}. \tag{5.8}$$

As was pointed out in [18], by increasing the mass, one can reduce the kinetic costs for changing the occupancy of a given species. Thus, by increasing the mass of one of the species, one can make it easy for the system to equalize the Fermi surfaces, and thus allow for pairing.

In weak coupling with short range interactions, however, introducing a heavy species is not enough to ensure that a Breached Pair state emerges: By reducing the kinetic costs, one simply allows a fully gapped BCS phase. Thus, Sarma and others found that the gapless state was unstable to a fully gapped BCS state.

To realize a stable Breached Pair state, one must somehow penalize the fully gapped phase. One way of doing this is to consider finite-range interactions. These give rise to a momentum-dependent gap and only support pairing in certain regions of momentum space. Thus, by tuning the masses and chemical potentials of the particles, one can arrange for one Fermi-surface to be in the region of strong pairing and the other to be in a region of weak pairing. After pairing, the Fermi surface in the weak pairing regime

remains gapless. We shall present models that exhibit these types of stable Breached Pair states later in this section. An example is shown in Figure 5.2.

There may be additional ways of stabilizing the state through long-range interactions such as those mediated by gauge bosons. Through suitable neutrality requirements, one might be able to locally enforce a difference in particle number so that fully gapped BCS pairing—which requires equal densities of each species—is prohibited. This is the idea behind the stability of the gapless Colour-Flavour–Locked (gCFL) phase in high density QCD. As mentioned earlier, however, there are still some some unresolved issues about this type of stability (see Section 5.5).

Note that *local* neutrality is required for these types of stability arguments. Global neutrality constraints do not add anything to the stability: if a Breached Pair state is not stable in the grand canonical ensemble with fixed chemical potentials, it will not be stable in the canonical ensemble with fixed particle numbers. This thermodynamic property of the ensembles is discussed in Appendix A.4.2.

Finally, there is evidence that, at strong coupling, the Breached Pair state may become stable, even with equal masses and short-range interactions [24]. This may be pictured as follows: In strong coupling, the fermions tightly pair to form molecular bound states. These bosonic pairs are weakly interaction and form a BEC. If one now increases the chemical potentials for one of the species, then extra fermions will be drawn into the system, but will weakly interact with the boson pairs. The resulting mixture of bosonic pairs and the excess fermions likely has little reason to phase separate and so a homogeneous mixture of bosonic molecular states and excess fermions—the strongly coupled equivalent of the Breached Pair state—may be stable. Indeed, it was this picture that initially stimulated the investigation for a stable Breached Pair state.

5.3 Stable Breached Pair States

We now demonstrate, by example, how to realize pure Breached Pair superfluid states in an extensive systems. We shall consider the mean-field analysis of models of the form (4.1) discussed earlier with non-relativistic dispersions:

$$\widehat{\mathcal{H}} = \int \frac{\mathrm{d}^3\vec{\mathbf{p}}}{(2\pi)^3} \left(\frac{p^2}{2m_a} \widehat{\mathbf{a}}^\dagger_{\vec{\mathbf{p}}} \widehat{\mathbf{a}}_{\vec{\mathbf{p}}} + \frac{p^2}{2m_b} \widehat{\mathbf{b}}^\dagger_{\vec{\mathbf{p}}} \widehat{\mathbf{b}}_{\vec{\mathbf{p}}} \right) + \widehat{\mathcal{H}}_I. \tag{5.9}$$

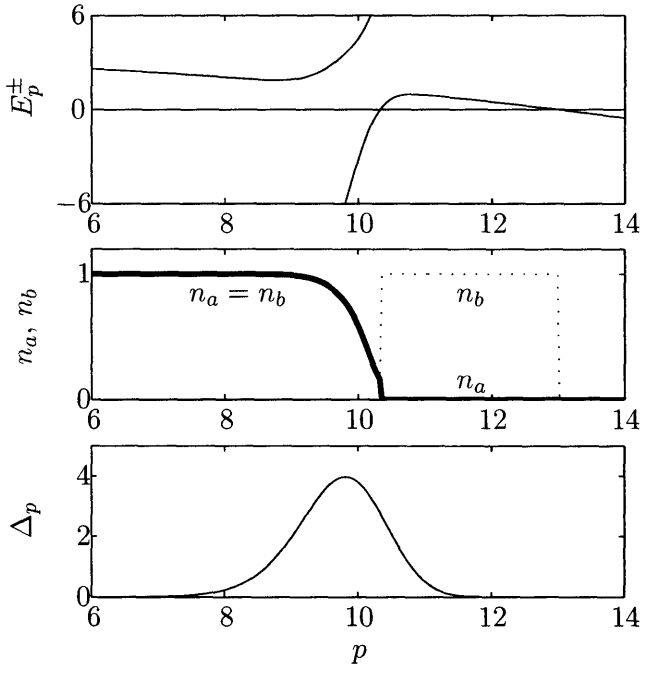

Figure 5.2: Quasiparticle dispersions $E_p^{\pm}$ (top), occupation numbers n_a and n_b (middle), and gap parameter Δ_p for a sample Breached Pair state at $(p_b^F, p_a^F) = (13, 10)$. All momentum scales are in units of $\hbar/\lambda$ and all energy scales are in units of $\hbar^2/(m_+\lambda^2)$. The mass ratio is $m_b/m_a = 50$ and the coupling strength has been chosen so that $2m_+\Delta_{p_0}/p_0^2 = 0.1$ to ensure weak-coupling. Notice that there are two "Fermi" surfaces at $p \approx 10.3$ and $p = 13$. The first occurs where Δ_p becomes too small to support the gap. The second is simply the Fermi surface for b which is virtually unaffected by the pairing. The "breach" occurs between these surfaces and only the region R outside contributes to the gap equation (5.15).

5.3.1 Interaction Structures

Most field theoretic models consider local interactions so that the model has well behaved cluster-decomposition properties, gauge invariance etc. Simple dimensional analysis shows, however, that such an interaction is not renormalizable in three dimensions and requires some sort of ultraviolet regulation. The typical renormalization procedure is to introduce some sort of regulator, compute physical quantities, and then eliminate the regulator and coupling constant in favour of the physical parameters. In principle, one would like to remove all dependence on the cutoff in this manner, but this is only possible for renormalizable theories. In practice, we must be content with a theory that depends on the regulator, or use a physically meaning full regulator.

Potential Scattering For non-relativistic systems, it may be a good approximation to treat the pairing interaction as an instantaneous potential interaction between the two species $\widehat{\mathbf{a}}$ and $\widehat{\mathbf{b}}$:

$$\begin{aligned}\widehat{\mathcal{H}}_I &= \frac{g}{V}\int \mathrm{d}^3\vec{\mathbf{x}}\,\mathrm{d}^3\vec{\mathbf{y}}\;\; V(\vec{\mathbf{x}}-\vec{\mathbf{y}})\;\; \widehat{\mathbf{a}}^\dagger_{\vec{\mathbf{x}}}\,\widehat{\mathbf{b}}^\dagger_{\vec{\mathbf{y}}}\,\widehat{\mathbf{b}}_{\vec{\mathbf{y}}}\,\widehat{\mathbf{a}}_{\vec{\mathbf{x}}},\\ &= \frac{g}{V}\int \text{đ}^3\vec{\mathbf{p}}\,\text{đ}^3\vec{\mathbf{q}}\,\text{đ}^3\vec{\mathbf{k}}\;\; V_{\vec{\mathbf{k}}}\;\; \widehat{\mathbf{a}}^\dagger_{\vec{\mathbf{p}}-\vec{\mathbf{k}}}\,\widehat{\mathbf{b}}^\dagger_{\vec{\mathbf{q}}+\vec{\mathbf{k}}}\,\widehat{\mathbf{b}}_{\vec{\mathbf{q}}}\,\widehat{\mathbf{a}}_{\vec{\mathbf{p}}}. \end{aligned} \tag{5.10}$$

Such a situation would be relevant, for example, in systems of cold atoms where the interactions are tuned to a Feshbach resonance controlled by an external magnetic field.[4] In this case, the resonance between the two different species is typically different from the resonance for intra-particle interactions. Thus, by adjusting the magnetic field, one can obtain a situation in which the inter-particle interaction dominates and in which the intra-particle interactions can be neglected as in our model.

With our restriction to spatially homogeneous and isotropic states, the Schwinger-Dyson self-consistency conditions in this interaction are:

$$\Delta_{\vec{\mathbf{p}}} = -g\int \text{đ}^3\vec{\mathbf{q}}\;\; \frac{V_{\vec{\mathbf{p}}-\vec{\mathbf{q}}}\Delta_{\vec{\mathbf{q}}}}{2\sqrt{E_+^2(\vec{\mathbf{q}})+\Delta^2_{\vec{\mathbf{q}}}}}\left[\theta_+(\vec{\mathbf{q}})-\theta_-(\vec{\mathbf{q}})\right], \tag{5.11a}$$

$$\delta\mu_a = -gV_{\vec{\mathbf{0}}}\int \text{đ}^3\vec{\mathbf{p}}\frac{(\theta_+ + \theta_-) - \xi(\theta_+ - \theta_-)}{2} = -gV_{\vec{\mathbf{0}}}n_b, \tag{5.11b}$$

$$\delta\mu_b = -gV_{\vec{\mathbf{0}}}\int \text{đ}^3\vec{\mathbf{p}}\frac{(2-\theta_+ - \theta_-) - \xi(\theta_+ - \theta_-)}{2} = -gV_{\vec{\mathbf{0}}}n_a. \tag{5.11c}$$

[4] For a description of atomic interactions including Feshbach resonances, see [48] and the references therein.

We consider here only spherically symmetric potentials $V(r)$ between the two species $\widehat{\mathbf{a}}$ and $\widehat{\mathbf{b}}$. Details about the structure of $V_{\vec{\mathbf{k}}}$ for various potentials are given in Appendix C.

Although using the potential scattering model is physically well justified, it is technically challenging, even for homogeneous and isotropic states. The problem is that one must include variational parameters for each momentum: $\Delta_{\vec{\mathbf{p}}}$. Thus, one is trying to minimize over an infinite dimensional functional space. Fortunately, the gap equation seems to converge when treated as an iteration scheme. This allows one to use a discretization to look for solutions. Unfortunately, we are not presently aware of a proof that the stable fixed-points are always minima.

Numerical solutions for certain types of potential scattering models were presented in [1] and will be discussed in Section 5.3.2. To be more certain that we have performed the proper minimization, however, we consider a simplified separable interaction.

Separable Potentials In order to use only a handful of variational parameters, one would like to parametrize the momentum dependence in a definite way. As discussed in Section 3.3, if one uses a separable interaction of the form (3.45), all of the momentum dependence is parametrized by the cutoff function Λ_p^2.

A simplified version of this is the interaction used in the original BCS model [8]. In standard BCS superconductors, the attraction is mediated by a retarded phonon interaction that is screened for energies greater than the Debye frequency ω_D. Thus, one introduces a cutoff $\Lambda_p = \theta(\omega_D^2 - E_+(p)^2)$. This was used in Section 4.2.2 to obtain the gap equation (4.37). While physically motivated and qualitatively accurate, this is not suitable for a proper thermodynamic discussion because the function $E_+(p)$ depends on the variational parameters $\delta\mu$ and chemical potentials μ.

To properly generate the thermodynamic relations—for example (3.32) $N = -\partial\Omega/\partial\mu$—the model must be defined independently of the variational parameters, and the chemical potentials must enter purely as Lagrange multipliers. Thus, one may instead implement the cutoff this through the interaction density (3.44)

$$\frac{\widehat{\mathbf{H}}_I}{V} = g\int đ^3\vec{\mathbf{p}}\, đ^3\vec{\mathbf{p}}'\, đ^3\vec{\mathbf{q}}\, đ^3\vec{\mathbf{q}}'\, V(\vec{\mathbf{p}},\vec{\mathbf{p}}',\vec{\mathbf{q}},\vec{\mathbf{q}}')\widehat{\mathbf{a}}^\dagger_{\vec{\mathbf{p}}}\,\widehat{\mathbf{b}}^\dagger_{\vec{\mathbf{q}}}\,\widehat{\mathbf{b}}_{\vec{\mathbf{q}}'}\,\widehat{\mathbf{a}}_{\vec{\mathbf{p}}'} \tag{5.12}$$

with one of the following separable interactions

$$V_{\rm BCS}(\vec{\mathbf{p}},\vec{\mathbf{p}}',\vec{\mathbf{q}},\vec{\mathbf{q}}') = \Lambda_p^2\Lambda_q^2\ (2\pi)^6\delta^{(3)}_{\vec{\mathbf{p}}+\vec{\mathbf{q}}}\delta^{(3)}_{\vec{\mathbf{p}}'+\vec{\mathbf{q}}'}, \tag{5.13a}$$

$$V_{\rm Contact}(\vec{\mathbf{p}},\vec{\mathbf{p}}',\vec{\mathbf{q}},\vec{\mathbf{q}}') = V\Lambda_p\Lambda_q\Lambda_{p'}\Lambda_{q'}\ (2\pi)^3\delta^{(3)}_{\vec{\mathbf{p}}-\vec{\mathbf{p}}'+\vec{\mathbf{q}}-\vec{\mathbf{q}}'}. \tag{5.13b}$$

The first of these has the computational advantage that the self-energy corrections are suppressed by a factor of the volume. Thus, in the infinite volume limit, there are no renormalizations to the chemical potentials: $\delta\mu = 0$. Thus, there is only a single variational parameter Δ. The second model requires a proper minimization over the three parameters Δ, $\delta\mu_a$ and $\delta\mu_b$.

The idea here is to note that the momentum dependent parameters $\Delta_{\vec{\mathbf{p}}}$ of the potential scattering model are now replaced by

$$\Delta_{\vec{\mathbf{p}}} \to \Lambda_p^2\Delta. \tag{5.14}$$

Thus, the idea is to choose the cutoff function Λ_p to mimic the behaviour of the momentum dependent gap. Another approach would be to simply use the realistic interaction with an ansatz of the form $\Lambda_p^2\Delta$. Unfortunately, this requires numerical minimization because the form of the gap equations derived here are no-longer applicable.

Interactions of this form are also used to model QCD. In the QCD context, the attraction is provided directly by gluon exchange. Due to the asymptotic freedom of QCD, the interaction becomes weak for large momenta. The cutoff is typically taken to fall off for large momenta to simulate the asymptotic freedom of the theory. This will be discussed in Part III. Note, however, that the momentum dependence does not resolve the stability issues in the QCD context. Rather, stability in the QCD context depends on colour and electric neutrality conditions as discussed in Section 5.5.

5.3.2 Solutions

Potential Scattering For the potential scattering model, the non-trivial portion of the Schwinger-Dyson equation has the form

$$\begin{aligned}\Delta_p &= -g\int\frac{\mathrm{d}^3\vec{\mathbf{q}}}{(2\pi)^3}V_{|\vec{\mathbf{p}}-\vec{\mathbf{q}}|}\langle\widehat{\mathbf{b}}_{\vec{\mathbf{q}}}\widehat{\mathbf{a}}_{-\vec{\mathbf{q}}}\rangle = \\ &= \frac{-g}{8\pi^2}\int_0^\infty \mathrm{d}q\ V_{p,q}\frac{q^2\Delta_q}{\sqrt{E_+^2(q)+\Delta_q^2}}[\theta_+(q)-\theta_-(q)].\end{aligned} \tag{5.15}$$

This is similar to a convolution, except that there is a non-linear dependence on the parameters Δ_q. For typical potentials, $V_{p,q}$ is dominant along the

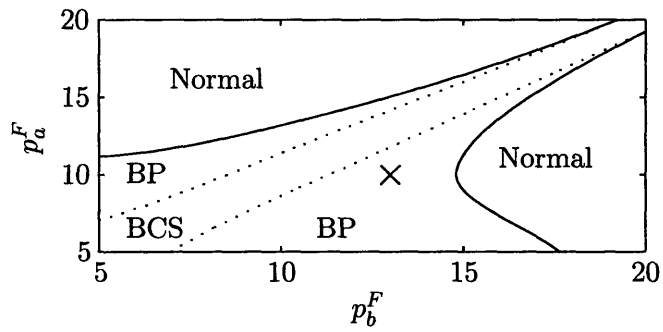

Figure 5.3: Qualitative $T = 0$ phase diagram for interaction (5.10) with a Gaussian potential $V(r) \propto \exp(-r^2/2\lambda^2)$. All momentum scales are in units of $\hbar/\lambda$ and all energy scales are in units of $\hbar^2/(m_+\lambda^2)$. The mass ratio is $m_b/m_a = 50$ and the coupling strength has been chosen so that $2m_+\Delta_{p_0}/p_0^2 = 0.1$ at the point marked "×" where $(p_b^F, p_a^F) = (13, 10)$ to ensure weak-coupling. (This ratio is less that 1 throughout this diagram.) Note that the lower Breached Pair region has more heavy particles b while the upper Breached Pair region has fewer heavy particles. The upper type may be realized in the QCD context [21, 26]. All phase transitions are first order.

diagonal where $p \approx q$. From this, one sees that Δ_p is dominated for $p \approx q$ where the weight is largest. For fully gapped BCS type phases at low temperature, the weight is dominant near the common Fermi surface where $E_+ \sim 0$, thus, Δ_p is largest in this region.

In the presence of a breach, the factor $[\theta_+ - \theta_-]$ may reduce the weight of the gap equations in this region by reducing the contributions to the right-hand side, possibly destroying the correlations altogether. Equation (5.15) can be solved numerically to find stationary points of the thermodynamic potential. Over this set of self-consistent solutions, one can minimize Ω to determine the phase structure.

We have done this for a variety of interactions, and find similar qualitative structure: a central strip of fully gapped BCS-like phase about $p_a^F = p_b^F$, with normal unpaired phases outside (see Fig. 5.3.) Depending on the model parameters, these phases may be separated by a region of Breached Pair superfluid phase. To verify that these indeed contain gapless modes we plot in Fig. 5.4 a sample set of occupation numbers, quasiparticle dispersions, and the gap parameter Δ_p. As our heuristic arguments suggested, the presence of gapless fermion modes depends on two factors: 1) the momentum structure of Δ_p and, 2) the mass ratio.

First, Δ_p must be large in some regions and small in others. If Δ_p is large enough at a Fermi surface, it will induce pairing at that surface and

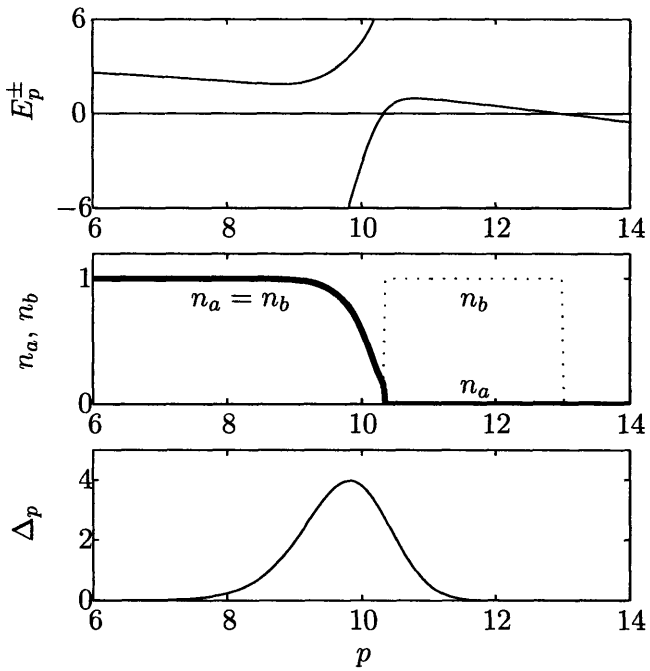

Figure 5.4: Quasiparticle dispersions $E_p^{\pm}$ (top), occupation numbers n_a and n_b (middle), and gap parameter Δ_p for a sample Breached Pair state at $(p_b^F, p_a^F) = (13, 10)$. All units and parameters are described in Fig. 5.3. Notice that there are two "Fermi" surfaces at $p \approx 10.3$ and $p = 13$. The first occurs where Δ_p becomes too small to support the gap. The second is simply the Fermi surface for b which is virtually unaffected by the pairing. The "breach" occurs between these surfaces and only the region R outside contributes to the gap equation (5.15).

support a superfluid. If it is also small enough at the other Fermi surface, it will not appreciably affect the normal free-fermion behaviour. The problem with previous analyses is that they assume point-like interactions, implying a constant $\Delta_p = \Delta$. Physical interactions, however, tend to exhibit more complicated behaviour and suitable Δ_p are quite generic: Δ_p tends to peak about the Fermi surface of the lighter species and fall off to at least one side. The model shown in Fig. 5.3 and Fig. 5.4, for example, has a Gaussian interaction. Longer-range forces (such as a screened Coulomb interaction) tend to plateau to the left of p_0 but still fall to the right.

Second, as was emphasized in [18], one may reduce the cost associated with shifting the Fermi sea p_b^F by increasing the mass m_b. Thus, by choosing a large enough mass ratio, one may always move the Fermi surface for the heavy species to a region where $\Delta_{p_b^F}$ is small enough so as to leave the Fermi

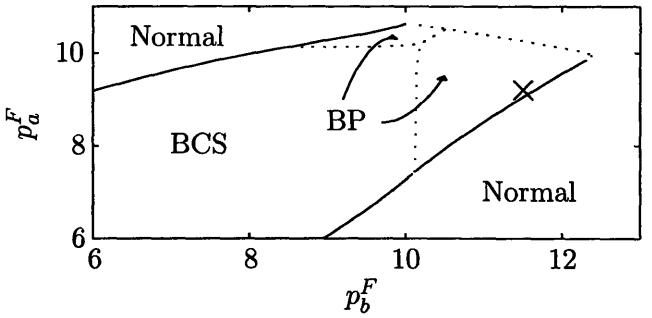

Figure 5.5: $T = 0$ phase diagram for separable potential interaction (5.13a) with a hard cutoff $f(p) \sim \theta(p - 10\sigma)$ that has been smoothed over the range from $p \in (9.7, 10.3)$. All momenta are expressed in units of σ where 10σ is the cutoff scale, and all energies are expressed in units of $\sigma^2/(2m_+)$. The mass ratio is $m_b/m_a = 4$ and the coupling g has been chosen so that $2m_+\Delta/p_0^2 = 0.2$ at $p_a^F = p_b^F = p_0 = 10\sigma$ to ensure weak-coupling. (This ratio is less that 1 throughout this diagram). All phase transitions are first order as discussed in the text. The mixed phases of [23, 49] would be found on the solid lines. The sample state in Fig. 5.6 at $(p_b^F, p_a^F) = (11.5, 9.2)$ is marked "×".

surface undisturbed. The states shown in Fig. 5.3 and Fig. 5.4 have a mass ratio $m_b/m_a = 50$.

Since the variational states of model (5.10) are parametrized by a variable *function* Δ_p, the set of states over which the minimization must consider is enormous, and we cannot be certain to have found the global minimum. We have searched for stable fixed-points of the gap equation (5.15) and compared them, so our results for this model are consistent and plausible, but not rigorous.

Separable Interactions One can now find the *global* minimum by plotting (see Fig. 5.6) the thermodynamic potential density as a function of the single parameter $\Delta_{\rm OP}$

$$\frac{\Omega(\Delta_{\rm OP})}{V} = \min_{\langle\theta|\widehat{\Delta}|\theta\rangle=\Delta_{\rm OP}} \langle\theta|\widehat{\mathcal{H}} - \mu_a\widehat{\mathbf{n}}_a - \mu_b\widehat{\mathbf{n}}_b|\theta\rangle\,, \tag{5.16}$$

where we minimization over all BCS style ansatz $|\theta\rangle$ with given expectation $\Delta_{\rm OP}$. This minimization is equivalent to comparing *all* solutions of the mean-field gap equation

$$\Delta = -\frac{g}{2}\int \mathrm{d}^3\vec{\mathbf{q}}\, \frac{\Delta\Lambda_q^2}{\sqrt{E_+^2(q) + \Lambda_q^4\Delta^2}}[\theta_+(q) - \theta_-(q)] \tag{5.17}$$

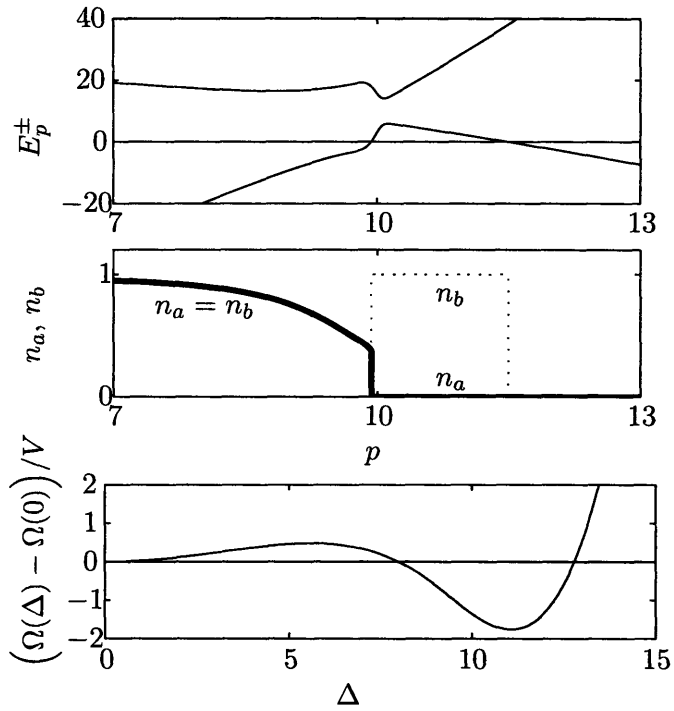

Figure 5.6: Quasiparticle dispersions $E_p^{\pm}$ (top), and occupation numbers n_a and n_b (middle), in a sample Breached Pair state. This state has gap parameter $\Delta \approx 11$ which is the global minimum of the grand thermodynamic potential density $\Omega(\Delta)/V$ (bottom) as defined in (5.16). The maximum at $\Delta \approx 5.6$ corresponds to an unstable Breached Pair state. These figures correspond to the point $(p_b^F, p_a^F) = (11.5, 9.2)$ in Fig. 5.5.

where we have used the notations from Section 4.2. We may thus rigorously conclude that, within the mean-field approximation of homogeneous phases at zero temperature, this model has the phase diagram shown in Fig. 5.5. We plot the properties of a sample Breached Pair state in Fig. 5.6 to illustrate that there are indeed gapless modes.

Finally, we address the issue of the instability discussed by Wu and Yip in [19] where they claim that the superfluid density ρ_S is negative due to a large negative contribution from the diverging density of states at $E = 0$ near the transition to the Breached Pair state. Their calculation is equivalent to calculating $\rho_M = -\mathrm{d}^2\Omega/\mathrm{d}\mu_+^2$, and the condition that the superfluid density be positive is simply the thermodynamic equilibrium condition (A.33) required by a state of maximum entropy. In the presence of gapless modes,

one finds two contributions to ρ_S. The first contribution is positive and is the same as in the usual BCS superfluid state. The second contribution is negative and is proportional to the density of fermionic states at the Fermi surface. This negative contribution arises from differentiating the "blocking" terms θ_+ and θ_- (4.21) that define the breach regions.

Due to the thermodynamic relationships, $\rho_M = -\mathrm{d}^2\Omega/\mathrm{d}\,\mu_+^2$ has the same sign as $\mathrm{d}^2\Omega/\mathrm{d}\,\Delta^2$ (this is shown explicitly in Appendix A.4.6.1). In particular, one finds that the negative superfluid density simply indicates that the Breached Pair solution under consideration is an unstable maximum rather than a stable minimum. The solutions we present here are all global minima, and hence stable in the thermodynamic sense.

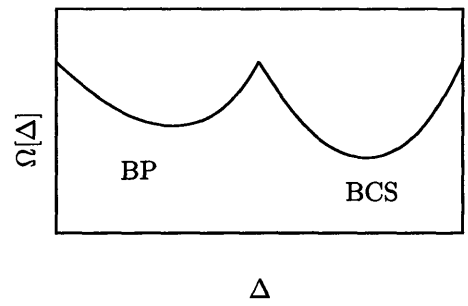

Figure 5.7: Schematic description of the thermodynamic potential $\Omega[\Delta]$ as a function of the variational parameter Δ near the BCS-BP phase transition. (For the actual model shown in Figure 5.6, this behaviour is difficult to resolve numerically for the parameters chosen, but the effects can be seen with a careful analysis.) The presence of a cusp in the thermodynamic potential at some point indicates that the phase transition must be first order in the mean-field approximation.

This raises an interesting point: if the BP/BCS transition were second order, then the fermionic density of states would formally diverge at the transition. A simple calculation (most easily performed analytically using a Hubbard Stratonovich transformation to eliminate the four-fermion interaction and to obtain the effective potential $\Omega[\Delta]$. See [50] for example) shows that at this transition, $\mathrm{d}^2\Omega(\Delta)/\mathrm{d}\Delta^2 \to -\infty$. Near the BP/BCS transitions, $\Omega(\Delta)$ must thus develop a cusp. This means that the are instead, two competing local minima as shown in Figure 5.7. One of these minima is a fully gapped BCS state and the other is Breached Pair. The BCS state is stable because there are no gapless fermions, and thus no negative contributions to the superfluid density. The BP state is stable because the fermion dispersions are sufficiently steep that the conventional superfluid density is larger

than the negative contribution from the fermionic density of states.

Thus, in the $T = 0$ mean-field approximation, the transition must be *first order*. At finite temperature, the cusp is smoothed and we suspect that the transition line ends at a critical point. In this way, the $T = 0$ Breached Pair transition avoids instability. In non-extensive systems such as QCD where gapless states may be stabilized by neutrality constraints, similar instabilities have been noted [29]. The resolution may be the formation of a non-homogeneous phase. This possibility requires further analysis.

5.4 Symmetries and Low-Energy Effective Theory

In this section, we would like to discuss the form of the low-energy effective theory describing Breached Pair states. The exact form and calculational framework for the effective theory is still under development, but we shall present an outline in this section.

The idea of using a low-energy effective theory is one may be able to formulate a simplified theory that contains only the low-energy excitations, but that properly describes low energy physics. To a large extent, the form of such a theory is determined by symmetry and a few unknown coefficients. Once the coefficients are determined, the theory promises to describe well low-energy physics.

The modern idea of effective field theories is that even non-renormalizable theories may be studied as long as, to a certain order in some perturbative expansion parameter, the theory can be described by only a finite number of coefficients. Typically the expansion performed is a low-energy expansion and some sort of weak-coupling expansion. If a theory is describable in this sense, then it has a real predictive power. (For a further discussion of renormalizability, please see the discussion in Section 6.1.6.)

To formulate a low-energy effective theory, there are several well defined steps:

1. Identify the low-energy degrees of freedom.
2. Identify the expansion parameters and the power counting scheme.
3. Construct all terms consistent with symmetries and power counting to a given order.
4. Match the coefficients of the terms. If low-energy experimental data are available, then match to these. Otherwise, match to simulations,

microscopic model calculations, or another effective theory that is applicable in some overlapping regime with the present theory..

We shall apply this procedure again in Section 7.4 to describe the low-energy physics of QCD.

5.4.1 Symmetries

Our models (4.1) admit several symmetries:

Continuous Global Symmetries: The models exhibit at least a continuous global $U_a(1)\otimes U_b(1)$ symmetry:

$$\widehat{\psi} = \begin{pmatrix} \widehat{\mathbf{a}} \\ \widehat{\mathbf{b}}^\dagger \end{pmatrix} \to \begin{pmatrix} e^{i\alpha_a}\widehat{\mathbf{a}} \\ e^{-i\alpha_b}\widehat{\mathbf{b}}^\dagger \end{pmatrix} = e^{i\alpha_- \sigma_0/2 + i\alpha_+ \sigma_3/2}\widehat{\psi}. \tag{5.18}$$

If we take the two species as having the same charge, then the vector symmetry $\alpha_+ = \alpha_a + \alpha_b$ corresponds to the $U_+(1)$ associated with this charge. This symmetry will be spontaneously broken by the pairing condensate that forms. The residual $U_-(1)$ symmetry generated by $\alpha_- = \alpha_a - \alpha_b$ remains unbroken.

The effective theory must respect these symmetries. The effective degrees of freedom may transform under the spontaneously broken $U_+(1)$ symmetry, but the low-energy effective theory must be invariant under this transformation. If it were not, then the degenerate vacua would not be physically identical as dictated by the symmetry. We emphasize this point: even though the $U_+(1)$ symmetry is spontaneously broken by the vacuum state, the original theory respects this symmetry, thus, all vacua related by this transformation must be physically indistinguishable. The effective theory *and* the low-energy degrees of freedom must be invariant under the residual $U_-(1)$ symmetry.

In the standard BCS model, $\varepsilon_a = \varepsilon_b$, and the global symmetry group is expanded to an U(2) spin symmetry. This extra symmetry places extra symmetry constraints on the effective theory. We shall consider the more general case here of the $U_a(1)\otimes U_b(1) = U_-(1)\otimes U_+(1)$ symmetry.

Space-time Symmetries: Our model is also translationally and rotationally invariant. It does not have full relativistic invariance in general, so spatial components will differ from temporal components, but the rotational symmetry must be preserved by the effective theory. It is possible that the

ground state spontaneously breaks translational and rotational symmetries through a crystalline LOFF state (see Section 4.1.1), but we do not consider this possibility here.

A very important symmetry is time-reversal invariance T. This is implemented as an anti-unitary operator[5] taking $t \to -t$. In fact, the "pairing" in a BCS state is fundamentally related to this time-reversal symmetry. This persists, even if the state is not homogeneous and isotropic (see, for example [50, 51]). Our models and states will also preserve parity P.

5.4.2 Degrees of Freedom

The BCS and Breached Pair ground states have correlations of the form $\langle \widehat{\mathbf{a}}\widehat{\mathbf{b}} \rangle \neq 0$. The ground state, thus, breaks the $\mathrm{U}_+(1)$ symmetry:

$$\langle \widehat{\mathbf{a}}\widehat{\mathbf{b}} \rangle \to e^{i\alpha_+} \langle \widehat{\mathbf{a}}\widehat{\mathbf{b}} \rangle . \tag{5.20}$$

If the interaction is local, then one can apply the non-relativistic version of Goldstone's theorem [52, 53] to deduce that there must be a massless collective excitation associated with the broken symmetry. This will turn out to be a real scalar field ϕ that enters as the phase of the condensate

$$\langle \widehat{\mathbf{a}}\widehat{\mathbf{b}} \rangle = \Delta_{\mathrm{OP}} e^{i\phi} \tag{5.21}$$

so that, under the broken symmetry:

$$\phi \to \phi + \alpha_+ . \tag{5.22}$$

In BCS phases, the fermionic excitations are completely gapped (see (4.18) and (4.28)). Thus, as long as we take the scale Λ to be less than the physical gap in the spectrum, the only low-energy excitation is this scalar collective excitation.

In the Breached Pair state, one must also include the gapless quasi-particle excitations. Typically there will be two quasi-particle fields ψ_1 and ψ_2 with linear dispersions about the breach points.[6] Note that all of the $\mathrm{U}_+(1)$ symmetry transformation properties are absorbed into the scalar field

[5] An anti-unitary operator $\widehat{\mathbf{A}}$ acts as:

$$\widehat{\mathbf{A}}\alpha \, |n\rangle = \alpha^* \widehat{\mathbf{A}} \, |n\rangle . \tag{5.19}$$

Thus, in addition to taking $t \to -t$, all factors of i acquire a negative sign.

[6] In principle, with peculiar band structures, one may be able to realize states with more than two breaches in a single band, but we are presently unaware of any situations in which such models might be realized. Typically, each band has two breach points.

ϕ so that the fermionic quasi-particles transform only under the unbroken symmetry U$_-$(1):

$$\psi_i \to e^{i\alpha_-}\psi_i. \tag{5.23}$$

5.4.3 Power Counting

The expansion parameter for our low-energy theory will be energy and momentum. The floating scale for the effective theory is thus an energy scale Λ, and we shall only keep degrees of freedom with energy less than this scale in our theory. When there is a Fermi-surface, this means that we keep modes sufficiently close to the Fermi-surface. For linearly dispersing collective modes, we may simply count in powers of momentum.

To properly account for the Fermionic degrees of freedom, we should introduce a label momentum $\vec{\mathbf{k}}$ describing the location on the Fermi-surface of the particular modes. Thus, for each Fermion, we break the momentum into two parts $\vec{\mathbf{p}} = \vec{\mathbf{k}} + \vec{\mathbf{l}}$ where $\vec{\mathbf{k}}$ is a label momentum on the Fermi surface, and $\vec{\mathbf{l}}$ describes the actual momentum of the field as a deviation from the Fermi surface.

For a spherical Fermi surface, we should now break $\vec{\mathbf{l}}$ into two pieces $\vec{\mathbf{l}} = \vec{\mathbf{l}}_\perp + \vec{\mathbf{l}}_\parallel$, one perpendicular to the Fermi surface (a single degree of freedom) and the other parallel (two degrees of freedom). One introduces two cutoffs, $\Lambda_\perp$ and $\Lambda_\parallel$ so that momenta integrals have the form:

$$\sum_{\vec{\mathbf{k}}} \int_{\Lambda_\perp} \text{đ}\vec{\mathbf{l}}_\perp \int_{\Lambda_\parallel} \text{đ}^2\vec{\mathbf{l}}_\parallel \tag{5.24}$$

where the momenta are limited by the cutoff. Thus, the momenta integrals cover regions of the Fermi surface ("patches") of area $\pi{\Lambda_\parallel}^2$. There must thus be on the order of $N \approx 4k_F^2\Lambda_\parallel^{-2}$ patches to cover the whole Fermi surface. The sum over $\vec{\mathbf{k}}$ counts each of these patches. If the Fermi surface remains spherical, then one has a nice "large N" limit here in which the renormalization group may be carefully applied (see [51] for further details applied to condensed matter physics and [54] for a review of applications to high-density QCD).

It is beyond the scope of this thesis to properly implement this patch summation. We simply point out that this is the correct way to proceed to properly realize the power counting. The important point for constructing the effective theory is that each degree of freedom has an additional vector parameter $\vec{\mathbf{k}}$—the label—that may enter the Lagrangian. In particular, this may be coupled with derivatives to restore rotational invariance.

Instead, we proceed to construct the effective theory in terms of gradient terms $\vec{\nabla}\psi_i$. This gradient will pull out momenta $\vec{\mathbf{p}} = \vec{\mathbf{k}} + \vec{\mathbf{l}}$ which contains both the label momentum of order k_F and the kinetic piece of order Λ. Thus, our expansion will not properly count powers. It will, however, contain all of the low-order pieces, and the proper power counting can be easily extracted.

5.4.4 Effective Lagrangian

We may now construct the effective action. We start with the bosonic pieces. Invariance under the spontaneously broken $U_+(1)$ symmetry tells us that the field ϕ must only enter with derivative couplings. This, along with time-reversal and rotational invariance dictate that the kinetic term must have the form to lowest order:

$$\mathcal{L}_\phi = \frac{f^2}{2}\left(\dot{\phi}^2 - v^2(\vec{\nabla}\phi)^2\right) + \mathrm{O}(\Lambda^3). \tag{5.25}$$

There are thus two unknown parameters, the decay constant f and the speed of sound v. In a fully gapped BCS theory, this is the complete description of the low energy physics. Note how the linear dispersion of the scalar field follows from the symmetries.[7] The fermions also have a kinetic term

$$\mathcal{L}_\psi = \sum_{n=\pm}\left(i\psi_n^\dagger\dot{\psi}_n - \psi_n^\dagger\omega_n(-i\vec{\nabla})\psi_n\right) + \mathrm{O}(\Lambda^2). \tag{5.26}$$

where, as a starting point, the dispersions are given by the expressions (5.2). In principle, the dispersions $\omega_\pm$ should be power-expanded in each patch. The effective theory parameters will be the coefficients in this expansion. In principle, there will be a set of coefficients for each patch—instead of a single parameter, there is an unknown "function" over the Fermi-surface—but this simplifies if the surfaces is not distorted.

[7] In addition to the symmetries, one must also ensure that:

1. Terms are Hermitian.
2. Terms are non-trivial using the (anti)-commutation relations.
3. Terms are invariant when integrating by parts. This assumes that there are no boundary terms and thus implicitly assumes that there are no anomalies. In theories with anomalies, total derivatives may be important. See (6.15c) for an example of an important total derivative term. This prohibits terms like $\phi i\dot{\phi} = i\partial_t(\phi^2)/2$ which are total derivatives for bosons but not for Fermions.

The interactions are a bit more complicated

$$\mathcal{L}_{\phi,\psi} = \sum_{n=\pm} g_n^{(1)} \left[\psi_n^\dagger \left(i\overleftarrow{\nabla} - i\overrightarrow{\nabla}\right) \psi_n\right] \cdot \vec{\nabla}\phi +$$
$$- \frac{1}{2} \sum_{n=\pm} \left(h_n^{(1)} \nabla^2\phi + h_n^{(2)} (\vec{\nabla}\phi)^2 + h_n^{(3)} \ddot{\phi} + h_n^{(4)} (\dot{\phi})^2\right) \psi_n^\dagger \psi_n + \mathrm{O}(\Lambda^3). \quad (5.27)$$

One may take the mean-field as a starting point, match to determine the initial values of these coefficients and then perform a renormalization group analysis to see how the interactions scale as one lowers the cutoff. We are currently performing such an analysis and hope to publish results soon.

5.5 Long-Range Interactions

As we have discussed, extensive Breached Pair superfluids must be stable in the grand-canonical ensemble for fixed chemical potentials if they are to be stable at all: Imposing global particle number constraints will only lead to the formation of mixed phases in accordance with the Gibbs' phase rule A.4.3. For non-extensive systems, however, the situation may be markedly different. In particular, the presence of long-range interactions—such as those mediated by massless gauge bosons, or a static $1/r$ Coulomb interaction—can change the global particle number constraint to a local charge neutrality constraint.

In the presence of long-range interactions, complete phase separation will not be permitted. The non-neutral constituent phases will have a non-extensive Coulomb energy that limits the size of the domains. This must be balance against the interface energy costs and an equilibrium mixed phase will consist of "bubbles" of one phase embedded in the other [55, 56]. The size and shape of the bubbles will depend on the competition between the surface energy and the bulk Coulomb energy.

If the long-range interaction is weak, then the bulk Coulomb cost will be weak and a mixed phase may still be allowed. This has been considered in the QCD context for example [57]. In principle, however, as one increases the strength of the long-range interaction, the bubble size must shrink. There is thus, the distinct possibility that, for large enough interactions, mixed phases are prohibited, and local neutrality constraints may stabilize Breached Pair type states. This is the fundamental idea behind the gapless colour-superconducting states that have been proposed to date [20, 21]. In particular, the QCD interactions are very strong: this has been used as

the basis for the argument about the stability of the gapless colour-flavour locked (gCFL) state against the formation of mixed phases [58].

Despite this apparent resolution to the mixed-phase instability issue, these colour-superconducting states still appear to have an instability. In particular, the computation of some of the the gluon propagators in the random-phase approximation appears to yield negative squared Meissner masses $M_m^2 < 0$ [29, 30, 31]. This type of instability is identical with the instability described by Wu and Yip [19] for the Sarma state. In that case, the instability was simply the statement that the thermodynamic stability requirement (A.33) that

$$\frac{\partial^2 \Omega}{\partial \mu_a \partial \mu_b} \tag{5.28}$$

is negative definite for all external sources μ_i. For the Sarma solution this is not surprising because the state is not a minimum, but a maximum of the thermodynamic potential; thus, all of the convexity arguments that follow from the variational principle (see Sections A.4.1 and A.4.6) are invalid.

The situation with the local neutrality enforcement is somewhat more puzzling because the Breach Pair solution *is* a minimum if one only considers neutral and homogeneous states, and only these state should be considered in the limit of infinite coupling to the long-range interaction. Somehow, the calculation of the Meissner masses is insensitive to the neutrality constraint. One possibility is that it might be necessary to consider inhomogeneous states in the variational formalism to properly capture the effects of the Meissner mass. In the high-density QCD context this is being explored as the possibility of a LOFF type state [46, 47]. Other possibilities include considering additional "gluon" condensation in the gauge fields. A complete resolution of this problem is still outstanding.

5.6 Experimental Realizations

We have shown that it is likely that Breached Pair states are thermodynamically stable with suitable finite-range interactions and sufficiently large mass ratios. Furthermore, there is both heuristic and numeric [24] evidence that at stronger couplings, Breached Pair states may be stable even with equal masses and short-range interactions. Here we discuss a few situations in which Breached Pair states might be realized.

Cold Atoms Systems One of the most promising places to find Breached Pair states is in cold atom traps. Several experimental groups have been able

to cool systems of fermions to the point where Bose-Einstein condensation has been observed [59, 60, 61, 62, 63, 64, 65, 66].

The possibility for obtaining conditions favourable for Breached Pair superfluidity arise through the phenomenon of Feshbach resonance [67]. The presence of a bound state in a closed channel with an energy close to the scattering energy can give rise to a resonance and lead to an infinite scattering length.[8] The effective strength of the fermion-fermion interactions can thus be carefully controlled by adjusting an external magnetic field. Even with similar masses, one might be able to probe the strong coupling regime and see Breached Pair phases. Moderate mass ratios may also be achievable by using different species.

The challenge here is determining a clear signature, but, in principle, Time Of Flight (TOF) imaging should be able to resolve the momentum distribution. The idea here is to turn off the trapping potential and let the atomic cloud expand. The high-momentum degrees of freedom have greater velocity and thus expand more rapidly. In this way, the momentum distribution is translated to a spatial distribution that can be imaged.

A clear signature would thus be the occupancy profile with distinct Fermi surfaces. If one images only the species with a smaller Fermi surface, then one would expect to see a ring indicating the high momentum components resulting from pairing about the larger Fermi surface.

If a large mass ratio is required, then these may be effected through an optical lattice [70]. The optical lattice traps different hyperfine states, which then "hop" throughout the lattice by tunnelling. The tunnelling rate is highly sensitive to the depth of the lattice, and one thus is able to adjust the effective masses of the species. One may also be able to realize appropriate conditions in systems of trapped ions with dipolar interactions [71].

The requirement of a finite effective range at weak coupling may be more difficult to achieve because the natural length-scale for the interactions (primarily Van der Waals) is much smaller than the inter-atomic spacing. There are suggestions, however, that the effective range near resonance may actually be quite large for narrow resonance even though the bare range is small [72, 73]. For example, the 543.25 G resonance of ^{6}Li has an effective range of $R^* \approx 19000$ Å even though the bare interaction range is $R_e \approx 30$ Å [72, 74].

[8] The technique to study this resonance phenomenon amounts to forming projection operators for the subspace of the closed channel and using these to "integrate out" the subspace, thereby inducing an effective resonant potential. The technique—the Feshbach-Fano partitioning method [67, 68, 69]—is quite general. For a review see [48].

Liquid Hydrogen Liquid hydrogen [75] may provide another arena for observing Breached Pair superfluidity. The Coulomb interactions are certainly long-ranged, and the proton/electron mass ratio ~ 1800 is huge. The idea here (due to Ryan Barnett [76]) would be to consider small spin splittings in a magnetic field so that there are essentially four interacting species. In this way, there are simultaneously two pairing channels: $e_\uparrow$ with $p_\downarrow$, and $e_\downarrow$ with $p_\uparrow$. These channels may each support Breached Pair superfluidity with an excess of one spin state. Together, the two channels, however, balance charges so that neutrality is ensured.

Semiconductors Breached Pair superconductors may be realized in solid state physics. Several possibilities occur here. One option, through which differing mass ratios may be achieved is to consider pairing between different bands [77, 78]. The effective dispersions for the quasi-electrons is determined by the band structure: thus, the effective mass may be very different from the bare particle mass.

Another possibility might be to form a superfluid between particle and hole excitations [79, 80]. If it becomes feasible to realize pairing between carriers of opposite charge, then one may be able to directly test the stability issues that arise from the consideration of unstable gapless phases in the presence of local neutrality constraints. The idea would be to dope a material so that neutrality requires an unequal number of species.

Neutron Stars There is still a possibility that Breached Pair states may be stabilized through neutrality constraints. This has led to the conjecture that gapless phases of colour-flavour locked matter (g2SC [20] and gCFL [21, 26] phases) may be found in the cores of neutron stars [20, 21, 25, 26, 27].

It turns out that, in such phases, the requirements of electrical neutrality force one of the gapless fermion modes to remain almost quadratic. This results in a large density of low-energy excitations, and an unusually high heat capacity. Recently, the heat capacity and cooling properties of such a phase have been calculated [44]. The result is that such a gapless superfluid core would act as a "hot water bottle", keeping old stars with a gapless phase much warmer than regular neutron stars. If abnormally warm old neutron stars are observed, then this would be good evidence for the existence of these gapless phases.

Part III

QCD

Chapter 6

Introduction

The techniques developed in the previous chapters for studying weakly interacting fermionic systems can be applied in another context: high density quantum chromodynamics (QCD). In this part of the thesis, we shall analyze an NJL model to study qualitative features of QCD that may be realized in neutron stars. The structure of the NJL model fits within general framework presented, so the analysis will follow with little formal development. The additional symmetries and degrees of freedom, however, allow for a much richer structure than the simple two-species models considered so far. In particular, the non-Abelian nature of the underlying symmetries gives rise to a much richer theory of low-energy collective excitations. Understanding this structure will be our motivation. We start, however, with an overview of QCD and the standard model of particle physics.

6.1 The Standard Model of Particle Physics

Quantum Chromodynamics (QCD) is the presently accepted theory of the strong interactions and forms a cornerstone of the currently accepted standard model of particle physics. One of the beautiful aspects of the standard model is that it is almost uniquely determined by a few basic principles and a set of observations about the matter content of our universe:

Quantum Field Theory: The standard model is a relativistic quantum field theory, built on the principles of quantum mechanics and special relativity in $3+1$ dimensional space-time.

Symmetries: The fundamental structure of the standard model is dictated by symmetry. This include the Poincare invariance of relativity, the gauge invariance of the interactions and various global symmetries. All matter can be classified by representations of these symmetry groups. Although the symmetries are somewhat limited by self-consistency requirements, (such as the absence of certain anomalies), the choice of symmetries are essentially an empirical input.

Renormalizability: While the symmetry principles greatly restrict the possible interactions in the theory, there are still infinitely many. It is the requirement of renormalizability that renders the number of interactions finite. Although we know that the standard model as limited to strictly renormalizable interactions is incomplete, the renormalizable theory is remarkably accurate: this greatly simplifies our analysis.

6.1.1 Space-time Symmetries

The standard model is a four-dimensional relativistic quantum field theory respecting the Poincare group of space-time transformations. Certain fields also obey various discrete symmetries of charge conjugation (C), parity (P) and time reversal invariance (T). The probabilistic interpretation of quantum mechanics, however, requires that all relativistic field theories respect the combination PCT.

All of the matter in the standard model can be classified by irreducible representations of the Poincare algebra. All known fundamental matter transforms under one of four spin representations: spin 0 (Higgs boson), spin 1/2 (quarks, leptons), spin 1, (vector gauge bosons: photons, gluons, W and Z bosons), and spin 2 (gravitons). Through a limited set of assumptions, the spin representation is linked to the statistics of the particles: half-integer spins are fermionic while integer spins are bosonic. This is the celebrated spin-statistics theorem [81]. 5

6.1.2 Gauge Symmetries

Due to the signature of the metric, spin 1 particles generically have an unphysical degree of freedom with negative energy: the naïve Hamiltonian is not bounded below and the theory is sick. A resolution is to decouple the unphysical degrees of freedom from the rest of the theory. The only known way of doing this is to introducing a gauge symmetry: the unphysical degrees of freedom become simply a redundant reparametrization of the theory under this symmetry.

Another way of thinking about the introduction of gauge fields is to start with some global symmetry, for example: $\psi_x \to \mathbf{U}\psi_x$. Local interactions (such as $\psi_x^\dagger \psi_x$ for a U(N) symmetry) that preserve this global symmetry also admit the extension to a local symmetry: $\psi_x \to \mathbf{U}(x)\psi_x$. This local symmetry, however, is spoiled by derivatives which only transform covariantly for the global symmetry:

$$\partial\psi_x \to \mathbf{U}_x \partial\psi_x + \partial\mathbf{U}_x\psi_x \neq \mathbf{U}_x\partial\psi_x. \tag{6.1}$$

The local symmetry can be restored by introducing a spin 1 gauge field. Although, naïvely, these fields have four degrees of freedom, two components become manifestations of the local symmetry: by fixing the gauge, only two degrees of freedom remain and the resulting spectrum is bounded below.

To formally introduce the gauge field, it is useful to think about the situation geometrically. The gauge field acts precisely as a geometric connection that makes the operation of differentiation covariant under the gauge transformation. Although this is well known, we shall review the process here because we will make use of it again in Section 7.4.4.1 to connect properties of a microscopic model with those of the low-energy effective theory.

Covariant Derivatives Many physical properties, such as the energy associated with a field, depend in some way on the derivatives of the fields. The requirement of gauge invariance is that the gauge transformation should have no effect on the physical properties of the system.

As already mentioned, local quantities such as $\psi_x^\dagger \psi_x$ are naturally gauge invariant, but to construct quantities involving derivatives, we must construct a derivative that transforms covariantly

$$\nabla\psi_x \rightarrow \mathbf{U}(x)\nabla\psi_x. \tag{6.2}$$

If such an object can be constructed, then quantities such as $\psi_x^\dagger \nabla\psi_x$ and $(\nabla\psi_x)^\dagger \nabla\psi_x$ will be gauge invariant.

One can think of a field ψ_x as a slice through a complex vector bundle over space-time $\mathbb{R}^{3+1}$. The gauge transformation is an automorphism of this bundle that preserves the projection onto the space-time. The fibre that projects onto a given point x of space-time transforms definitely as $\mathbf{U}(x)$: local comparisons, such as $\psi_x^\dagger \psi_x$, can be thus be made in a gauge invariant way. Derivatives are non-local and compare the field on two different fibres above the points x and $x+h$. The transformations of different fibres are completely unrelated: $\psi_x \rightarrow \mathbf{U}(x)\psi_x$ while $\psi_{x+h} \rightarrow \mathbf{U}(x+h)\psi_{x+h}$ with no relationship between $\mathbf{U}(x)$ and $\mathbf{U}(x+h)$.

We need a prescription for transporting the field at x to $x+h$ so that a proper comparison can be made. This prescription for such "parallel transport" must change with the gauge transformation in such a way that this comparison remains independent of the transformation. Such a prescription is provided through a geometric "connection": this is exactly how gauge fields enter into the theory.

The connection $i\mathbf{A}_\mu(x)$ is a geometric object that maps space-time tangents h^μ (which specify the desired direction in which to "transport" the

field) to matrices that effect the appropriate transformation. The field ψ_x may thus be compared with the field ψ_{x+h} only through this parallel transport:

$$\nabla_\mu \psi_x = \lim_{\|h\|\to 0} \frac{\psi_{x+h} - h^\mu i\mathbf{A}_\mu(x)\psi_x}{\|h\|}. \tag{6.3}$$

The transformation properties of the connection $i\mathbf{A}_\mu(x)$ may be simply deduced by the requirement that (6.3) transform covariantly:

$$\nabla_\mu \psi_x \to \mathbf{U}(x)\nabla_\mu \psi_x. \tag{6.4}$$

This means that the connection $\mathbf{A}_\mu(x) \to \mathbf{A}'_\mu(x)$ must satisfy:

$$\mathbf{U}(x)(\psi_{x+h} - h^\mu i\mathbf{A}_\mu(x)\psi_x) = \mathbf{U}(x+h)\psi_{x+h} - h^\mu i\mathbf{A}'_\mu(x)\mathbf{U}(x)\psi_x. \tag{6.5}$$

Expanding, for infinitesimal h, $\mathbf{U}(x+h) = \mathbf{U}(x) + h^\mu \partial_\mu \mathbf{U}(x)$, and $\psi_{x+h} = \psi_x + h^\mu \partial_\mu \psi_x$, we find

$$-h^\mu i\mathbf{A}_\mu(x)\psi_x = h^\mu \left[\mathbf{U}^{-1}(x)\partial_\mu \mathbf{U}(x) - \mathbf{U}^{-1}(x) i\mathbf{A}'_\mu(x)\mathbf{U}(x)\right]\psi_x. \tag{6.6}$$

This must hold for all tangents h^μ and field values ψ_x, thus we find the connection transformation properties:[1]

$$\mathbf{A}_\mu \to \mathbf{A}'_\mu = \mathbf{U}\left(\mathbf{A}_\mu + i\partial_\mu\right)\mathbf{U}^{-1}. \tag{6.7}$$

Similarly, one may construct a covariant combination of the connection coefficients by parallel transporting ψ around a closed loop or plaquette defined by two orthogonal tangent vectors h_1^μ and h_2^ν. It turns out that this comparison does not depend on ψ_x and thus defines a covariantly transforming object containing only the connection field. This "field strength" tensor acts as a kinetic term for the gauge field:

$$\mathbf{A}_{\mu\nu} = [\nabla_\mu, \nabla_\nu] = \partial_\mu \mathbf{A}_\nu - \partial_\nu \mathbf{A}_\mu + [\mathbf{A}_\mu, \mathbf{A}_\nu]. \tag{6.8}$$

In differential geometry, $\mathbf{A}_{\mu\nu}$ is analogous to the four index curvature tensor: two of the indices are the space-time indices and the other two are the field component indices. For pure geometry and general relativity, the field components are also space-time indices describing how "tangents" transform.

[1]The factor of i was introduced in the definition of $i\mathbf{A}$ so that $\mathbf{A}$ is Hermitian. In mathematical literature, $\mathbf{A}$ is often defined to be anti-Hermitian without this factor.

6.1.3 Gauge Group of the Standard Model

The gauge group of G_{SM} the standard model has been empirically determined[2] to be:[3]

$$G_{\text{SM}} = (\text{SU}_C(3) \otimes \text{SU}(2) \otimes \text{U}(1))/\text{Z}_6. \tag{6.9}$$

All of the fundamental gauge bosons transform under the adjoint representations of these groups. Thus, there are thus 8 $\text{SU}_C(3)$ gauge bosons called gluons that mediate the strong interaction. The two SU(2) generators and the single U(1) generator mix, giving rise to the physical W and Z bosons and the electromagnetic photon as discussed in Section 6.1.7.

6.1.4 Matter Content

The matter content of the standard model has also been empirically determined.[4] Although the Higgs particle has also not been conclusively detected, it forms such an integral part of the theory that few physicists doubt its existence.

We label the matter content by denoting how it transforms under the gauge group G_{SM}. Note that since the U(1) hypercharge group is Abelian, it has a continuum of representations represented by real numbers (the Hypercharge "Y" of the particle). The other groups have only countably many representations labelled by integers (their dimension).[5] In addition, matter

[2]There are certain restrictions placed on the gauge group to ensure that the theory is self-consistent, anomaly free, etc. Perhaps some underlying "unified" theory can uniquely determine the gauge structure, but to date, the gauge group must be taken empirically.

[3]The Z_6 factor follows from the charge assignments of the matter fields: all matter is charged in such a way as to remain invariant under a certain Z_6 subset of the centre of the full gauge group. In particular, the U(1) hypercharge assignments must be carefully chosen to maintain this invariance. On of the triumphs of the Georgi-Glashow SU(5) unification model [82] was that it explained the observed hypercharge pattern: the full gauge group $\text{SU}_C(3) \otimes \text{SU}(2) \otimes \text{U}(1) \not\subset \text{SU}(5)$ only fits into the unification scheme if the hypercharges are chosen correctly so that the Z_6 centre factors out. Unfortunately, SU(5) unification predicts proton decay in contradiction with experiment.

[4]The standard model is certainly not complete. The additional matter, however, has not been directly detected and does not seem to greatly affect low-energy physics, though it may play a profound cosmological role, as "dark matter" for example. New particles must have a large enough mass to evade production in particle collisions, or must be too weakly coupled to be easily detected. Possibilities include sterile neutrinos, supersymmetric partners, axions, Kaluza-Klein modes etc.

[5]One should be careful about labelling the irreducible representations by dimension alone as this characterization is not always unique: there are, for example, four inequivalent 15 dimensional representations of SU(3). For low dimensional representations, however, this labelling is sufficient.

should be labelled by its Poincare. It suffices here to use a broad classification based on statistics. The only distinction that needs to be made is the chirality of the fermions: "left" (L) or "right" (R).

The standard model has the following matter content: the Lorentz structure is explicitly indicated (with subscripts to specify the fermion chirality) and the gauge structure is displayed as a triplet (C, I, Y) denoting the $\mathrm{SU}_C(3)$ colour (C), SU(2) isospin (I) and U(1) hypercharge (Y) representations respectively.

Fermions The fermions are divided into baryons (quarks) Q_L, U_R and D_R, and leptons L_L and E_R.

Q_L: $(3, 2, \frac{1}{6})$
U_R: $(3, 1, \frac{2}{3})$
D_R: $(3, 1, -\frac{1}{3})$
L_L: $(1, 2, -\frac{1}{2})$
E_R: $(1, 1, -1)$

For each of these are three duplicate copies or "families". The first family consists of the up (u) and down (d) quarks, the electron (e) and the electron neutrinos (ν_e):

$$Q_L = \begin{pmatrix} u_L^a \\ d_L^a \end{pmatrix}, \quad L_L = \begin{pmatrix} e_L^a \\ \nu_{eL}^a \end{pmatrix}, \tag{6.10a}$$

$$U_R = u_R^a, \quad D_R = d_R^a, \quad E_R = e_R^a, \tag{6.10b}$$

The second family consists of the charm (c) and strange quarks (s), the muon (μ) and the muon neutrino (ν_μ). The third family consists of the top (t) and bottom quarks (b), the tau meson (τ) and the tau meson neutrino ν_τ.

Scalars The only scalar is the Higgs particle of which there is only one family:

Φ: $(1, 2, \frac{1}{2})$.

Vector Bosons The vector bosons are the mediators of the gauge interactions: they transform under the adjoint representation of the respective component of the gauge group and are singlets under the others:

G_μ: $(8, 1, 0)$
A_μ: $(1, 3, 0)$
B_μ: $(1, 1, 1)$

6.1.5 Standard Model Lagrangian

Conforming to the principle of gauge invariance, the gauge fields enter through the covariant derivative

$$\mathbf{D}_\mu = \partial_\mu - ig_s\mathbf{G}_\mu - ig\mathbf{A}_\mu - ig'\mathbf{B}_\mu \tag{6.11}$$

where $\mathbf{A}_\mu = A^a_\mu \mathbf{T}^a$ and the matrices $\mathbf{T}^a$ generate the appropriate representation of the gauge group. Usually one fixes the normalization $\mathrm{Tr}[\mathbf{T}^a\mathbf{T}^b] = \delta^{ab}/2$. To which representation the generators $\mathbf{T}^a$ belong depends on the matter content as specified above. We have included here universal coupling constants g_s, g and g' which define the normalizations of the dimensionful gauge fields. Note, however, that once the representations are chosen, the same coupling constant must be used for all matter: In this sense, the coupling constants are universal.

The kinetic term for the gauge fields are expressed in terms of the field strength tensors:

$$\mathbf{G}^{\mu\nu} = \partial^\mu \mathbf{G}^\nu - \partial^\nu \mathbf{G}^\mu + g_s[\mathbf{G}^\mu, \mathbf{G}^\nu], \tag{6.12a}$$

$$\mathbf{A}^{\mu\nu} = \partial^\mu \mathbf{A}^\nu - \partial^\nu \mathbf{A}^\mu + g[\mathbf{A}^\mu, \mathbf{A}^\nu], \tag{6.12b}$$

$$\mathbf{B}^{\mu\nu} = \partial^\mu \mathbf{B}^\nu - \partial^\nu \mathbf{B}^\mu. \tag{6.12c}$$

The full standard model Lagrangian contains kinetic pieces and interactions:

$$\mathcal{L}_{\mathrm{SM}} = \mathcal{L}_{\mathrm{K}} + \mathcal{L}_{\mathrm{I}} \tag{6.13}$$

The kinetic terms are

$$\begin{aligned}\mathcal{L}_K = &-\frac{1}{4}\mathrm{Tr}[\mathbf{G}^{\mu\nu}\mathbf{G}_{\mu\nu}] - \frac{1}{4}\mathrm{Tr}[\mathbf{A}^{\mu\nu}\mathbf{A}_{\mu\nu}] - \frac{1}{4}\mathrm{Tr}[\mathbf{B}^{\mu\nu}\mathbf{B}_{\mu\nu}] + \\ &+ \bar{Q}\not{\mathbf{D}}Q + \bar{U}\not{\mathbf{D}}U + \bar{D}\not{\mathbf{D}}D + \bar{L}\not{\mathbf{D}}L + \bar{E}\not{\mathbf{D}}E + (\mathbf{D}_\mu\Phi)^\dagger\mathbf{D}^\mu\Phi\end{aligned} \tag{6.14}$$

where $\not{\mathbf{D}} = \gamma^\mu \mathbf{D}_\mu$ is the covariant derivative and $\bar{Q} = Q^\dagger\gamma^0$ to preserve the Poincare invariance of the theory for fermions (this is just the covariant generalization of the kinetic term from the Dirac equation.)

These terms are all diagonal in structure and summed over all particles and multiplets. It is not required that the kinetic terms initially be diagonal, but one can perform a field redefinition to obtain this form with any complications being put into the interaction terms. These kinetic terms are said to be in canonical form and this fixes the physical dimensions of the various fields.

The interaction Lagrangian has the following form:

$$\mathcal{L}_I = -\frac{\mu^2}{2}\Phi^\dagger\Phi + \frac{\lambda}{4!}(\Phi^\dagger\Phi)^2 \tag{6.15a}$$

$$+ h_{ij}\bar{Q}_L^i D_R^j \Phi + k_{ij}\bar{Q}_L^i U_R^j \Phi^\dagger + l_{ij}\bar{L}_L^i E_R^j \Phi \tag{6.15b}$$

$$+ \frac{\theta\epsilon_{\mu\nu\rho\sigma}}{32\pi^2}\,\mathrm{Tr}[\mathbf{G}^{\mu\nu}\mathbf{G}^{\rho\sigma}]. \tag{6.15c}$$

The first line consists of the scalar self couplings for the Higgs field. The second line are the Yukawa couplings and the last line is the so-called theta term. There are similar theta terms for the other gauge groups, but they can be removed via field redefinitions. This exhausts all possible terms consistent with the symmetry, renormalizability requirements, and observed matter content (assuming the existence of a single Higgs field).

This description of the standard model predicts that the neutrinos are massless. Recent data, however, strongly indicates that at least some of the neutrinos are massive. To account for this, an additional right-handed neutrino $N_R = \nu_{eR}^a$ should be included in the previous theory with charge assignments $(1, 1, 0)$. Along with the kinetic term, one is allowed the additional interaction $n_{ij}\bar{L}_L^i N_R^j \Phi^\dagger$ which generates neutrino masses. There are several unanswered questions about the nature of neutrino masses, however. For example: Why are the neutrinos so light? They should naturally be of the same scale as the other fermions. One explanation lies in the so-called see-saw mechanism which requires a non-renormalizable interaction at a higher scale (possibly associated with unification). We mention the right-handed neutrinos as there is good evidence for their existence, but they will have little no role in our analysis of dense QCD matter. For a more detailed review, please see [83].

Finally, we comment on the so-called theta term. This term is allowed by all symmetries of the theory except that it violates CP in the strong interaction. Such a violation is not seen (measurements of the neutron electric dipole moment, for example, limit $|\theta| < 10^{-9}$). One cannot simply impose $\theta = 0$ as a symmetry requirement, however, because many different contributions to the effective θ arise through the anomaly: An extremely unnatural fine-tuning of the bare parameter would be required to cancel these contributions. This so-called "strong CP" problem has been around for many years and may require new physics such as the introduction of an axion field to solve [6] We shall not further address the strong CP problem

[6]For reviews, please see [84, 85, 86] and the references therein. See [87] for a current attempt to resolve this problem and for some references of recent discussions.

in this work, but the underlying physics of the anomaly and the presence of instantaneous in QCD may have an important effect on the structure of dense matter. We shall discuss this later.

6.1.6 Renormalizability

As mentioned, the requirement of renormalizability prohibits any additional interactions. In quantum field-theories, renormalization is required to remove ultraviolet divergences from the theory. This is done by introducing additional parameters (counterterms) to the theory and then setting these to match experimental results. (See [88] for a lucid discussion of this type of renormalization.)

The old notion of a renormalizable theory is that, all divergences that arise must be absorbed into a finite number of (bare) parameters describing the theory. In this way, once the finite number of parameters are determined, the theory has predictive power. This is the type of renormalizability required by a fundamental theory if it is to stand on its own, and is the type of renormalizability that nature fortuitously seems to prefer for fundamental theories. Including additional terms in (6.15) would spoil this renormalizability.

The modern notion of effective field theories, however, is much more accommodating: if, at any given order in some expansion parameter, only a finite number of parameters are required to absorb all divergences, then the theory has a definite predictive power, even if it is not formally renormalizable in the old sense. This notion is not sufficient for a truly fundamental theory as it allows for the possibility that the theory requires infinitely many parameters in its non-perturbative definition. However, it allows one to work with effective theories that can answer questions within a certain restricted domain. For example, with a finite number of parameters, one may define a very useful low-energy effective theory.

The remarkable property of nature is that the standard model appears to satisfy the more restrictive notion of renormalizability to a high degree of accuracy. There may well be non-renormalizable interactions, but they are suppressed by a very high energy scale as discussed below. In the case of QCD proper, the theory is both renormalizable and asymptotically free. This admits the possibility that QCD is a complete and self-consist fundamental theory to arbitrarily small length scales. Such a theory is said to be ultraviolet (UV) complete.

The requirement of renormalizability is not tautological. Low-energy effective theories of QCD—containing hadrons as the degrees of freedom—

contain non-renormalizable terms. The remarkable thing about nature's renormalizability is that this seems to result from the hadrons being composite particles. Once the constituent degrees of freedom—quarks and gluons—were identified, the renormalizability emerged. The resulting renormalizable theory described in Section 6.1.5 is incredibly accurate over virtually all observable energy scales: one must probe very high energy scales with high precision to find deviations (though they must exist for the theory to be self-consistent). In condensed matter systems, virtually everything is composite in nature, and only the less restrictive notion of renormalizability is typically of use.

In the case of QED, the theory is still renormalizable, but not asymptotically free: at some small but finite length scale, the coupling constant diverges (often referred to as a "Landau pole") and the standard model becomes sick. Our present understanding is that standard model, including QED, arises as the low energy expansion of some more fundamental UV complete theory. The renormalizability of QED is the observation that the low-energy description decouples from the microscopic theory. Thus, after measuring a finite number of parameters, one can make low-energy predictions without further knowledge of the microscopic theory.

If the standard model requires a UV completion, then there seems to be no justification for the omission of terms based on the old-fashioned renormalizability requirement. Why then does (6.15) work so well in their absence?

Additional terms may indeed exist that describe physics above some energy scale Λ. Such terms would require coupling constants of negative energy dimension. These couplings should have a "natural size" governed by some dimensionless number g of order unity at the scale Λ. Upon "integrating out" the heavy[7] degrees of freedom, one obtains the low energy effective description we call the standard model. Such terms, however, will end up with the dimensionful coupling g/Λ^n of the appropriate negative mass dimension. If the scale Λ is large compared with the scales of interest E, then the effects of these terms are suppressed by factors of E/Λ. The statement of old-fashioned renormalizability thus translates to a statement about the decoupling of low-energy physics from the details of high-energy physics.

[7]By "heavy", we mean particles of such mass that they cannot be produced in low-energy collisions. "Integrating them out" means to formally re-express the theory without these degrees of freedom by performing the appropriate path integral. In practice, this process starts with the much less sophisticated process of replacing the fields with vacuum expectation values and replacing propagators with factors of the particle's mass. Upon this, various levels of improvement can be made to capture higher order effects.

If the scale Λ is not too large, then the neglected contributions may have a noticeable effect. Present high-precision tests, however, push the scale for new physics to above the TeV scale. Well below this scale—especially in the GeV regime that we shall consider—the standard model as expressed in (6.15) works remarkably well.

One final example of non-renormalizability in nature is gravity. One can formulate a quantum theory of gravity, but it requires an infinite number of parameters to define the low-energy expansion. Thus, the predictive power of this theory is somewhat lacking unless one finds a consistent way to organize corrections to the theory.

6.1.7 Higgs Mechanism

A consequence of the gauge symmetry is that all gauge bosons are initially massless: the symmetry is said to protect the mass. Two of the observed gauge bosons, however—the W and Z bosons—are massive. This is explained through the Anderson-Higgs mechanism [89, 90, 91, 92, 93, 94, 95], and is the same mechanism responsible for the Meissner effect in superconductors (which results from the photons acquiring a mass).

It would seem from the present form of the standard model that all of the fermions and gauge bosons should be massless: mass terms are forbidden by the symmetries. This is in stark contrast with the observed reality where virtually all of the fermions have masses. The resolution to this apparent problem is due to spontaneous symmetry breaking.

The present theory admits two distinct phases. The coefficient $\lambda \geq 0$ must be positive to ensure the potential is bounded, but the parameter μ^2 may be either positive or negative. For $\mu^2 < 0$, the vacuum expectation value of the scalar field Φ is zero and the ground state has the same symmetry as the Lagrangian.

For $\mu^2 > 0$, however, the scalar field Φ may Bose-condense and acquire a non-zero vacuum expectation value. In this case, the gauge SU(2)×U(1) symmetry is spontaneously broken by the vacuum state at sufficiently low temperatures. This is analogous to the spontaneous breaking of the U(1) phase symmetry in superfluids.

Were the broken symmetry global, the ground state would have gapless collective excitations[8] in accordance with Goldstone's theorem [52, 53]. In

[8]In local relativistic theories these collective excitations are called Nambu-Goldstone modes [52, 53, 96, 97, 98]. The number of modes is equal to the number of spontaneously broken continuous symmetry generators. Collective modes also occur in local non-relativistic theories where they are sometimes referred to as Bogoliubov-

the presence of gauge fields,[9] however, these modes do not remain massless. Instead, they are "eaten" by the gauge field which acquires three degrees of freedom and becomes a massive excitation. In this way, two of the three generators of the broken SU(2)⊗U(1) group become the massive third component of gauge bosons: this is known as the Higgs mechanism [94]. The massive eigenstates of the gauge fields are the physical W and Z bosons with masses of 80 and 100 GeV respectively. The remaining unbroken $U(1)_{EM}$ symmetry is associated with electromagnetism. This symmetry protects the associated gauge field, ensuring that the electromagnetic photon remains massless.

At high enough temperatures, the full symmetry is restored. Below the electroweak phase transition at $T_{EW} \sim 100$ GeV, however, the Higgs field assumes the following vacuum expectation value (VEV)

$$\langle \Phi \rangle = \begin{pmatrix} 0 \\ v \end{pmatrix} \tag{6.16}$$

where $v = \sqrt{3!\mu^2/\lambda} \sim 200$ GeV. We have used the gauge symmetry to rotate all of the other components away: this is the sense in which these degrees of freedom are "eaten" by the gauge bosons.

As a result of expanding the Higgs field about its vacuum expectation value, quadratic fermionic couplings are generated that couple left and right-handed fermions. Through these terms, the fermions acquire masses. The magnitude of the fermion masses is determined by the Higgs vacuum expectation value v, and by the various Yukawa couplings h, k, and l. It is due to the large variations in these Yukawa couplings that the fermions have such different masses. The origin and nature of these parameters is still one of physics' great mysteries.

As will be discussed below, the energy scales of relevance for neutron star are on the scale of 500 MeV or so. The QCD scale is also on the same order. As a result, the charm, bottom, and top quarks play little role. The up and down quarks play an important role, but for many purposes may be considered massless. It is the strange quark that complicates the situation: for very large densities, it may also be treated as light and a very nice symmetric theory of three massless quarks results. For realistic densities, however, the effects of m_s must be considered: It is this that strains the fermionic system giving rise to a diverse and interesting phase structure.

Anderson [89, 99, 100] modes, though the counting can differ in this context.

[9]The modes also do not appear if there are long-range interactions such as a Coulomb interaction. In this case, they become a massive charge-density (plasmon) excitation.

Particle:		Mass:	Electric Charge:
Leptons:	e^-	$m_e = 0.51$ MeV	$Q = -1$
	μ^-	$m_\mu = 106$ MeV	$Q = -1$
	τ^-	$m_\tau = 1777$ MeV	$Q = -1$
	ν_e, ν_μ, ν_τ	m_ν small but finite	$Q = 0$
Quarks:	u	$m_u = 1.5$–4 MeV	$Q = \frac{2}{3}$
	d	$m_d = 4$–8 MeV	$Q = -\frac{1}{3}$
	s	$m_s = 80$–130 MeV	$Q = -\frac{1}{3}$
	c	$m_c = 1.15$–1.35 GeV	$Q = \frac{2}{3}$
	b	$m_b = 4.1$–4.9 GeV	$Q = -\frac{1}{3}$
	t	$m_t = 170$–180 GeV	$Q = \frac{2}{3}$

Table 6.1: Fermion masses in the standard model [101].

6.1.8 Energy Scales

As we are interested in the properties of condensed matter, it is interesting to estimate an upper limit of the types of densities that could be encountered. Objects that are too massive will undergo gravitational collapse. Neutron stars approach this upper limit, and exhibit typical energy scales of the GeV order. The gravitational limit is not too far above this scale.

For example,[10] the requirement of gravitational stability gives a mass-radius bound of $M \leq 4Rc^2/(9G)$ [103] which requires the average density to be less than $\rho_{\text{avg}} \leq 64c^6/(729G^3M^2)$. Inserting typical neutron star masses of the order $1M_\odot \sim 2 \times 10^{30}$ kg, one obtains a bound of $\rho_{\text{avg}} \leq 64c^6/(729G^3M^2) \lesssim 10^{17}$ g/cm^3. Core densities may be an order of magnitude or so larger. To translate this to an estimate of the typical energy scale, we consider a degenerate Fermi-liquid of quarks with a density $\rho \sim m_q p_F^3$ where $m_q \sim 100$ MeV.[11] This gives a energy scale on the order of $p_F \sim 500$ MeV. Neutron stars in thermal equilibrium typically have temperatures of the much smaller than $T \ll 10^{10}$ K~ 1 MeV and are thus always "cold". Even during formation in a supernovae, temperatures do not appear to exceed 50 MeV.

Thus, we are well below the onset of new physics at the TeV scale and several orders of magnitude below the electroweak restoration scale of 100 GeV. The relevant physics in neutron star cores is thus described by QCD with

[10] For some more precise calculations, see [102] and the references therein.

[11] Although the current quark masses are very light 6.1, the relevant parameter here is the constituent quark mass which is typically of this order. See Table E.3 for example.

low energy electroweak contributions. The latter play an important role in the bulk physics of neutron stars, especially in their thermal evolution, but are weakly coupled to the QCD effects and so can be treated as part of a weakly coupled thermodynamic ensemble in determining the equilibrium properties. In practice this means that one can approximate the detailed microscopic interactions between QCD matter and electroweak matter by simply adjusting the thermodynamic parameters to meet the appropriate thermodynamic equilibrium conditions (neutrality, electroweak equilibrium etc. See Section 7.4.5 for details).

6.1.9 Asymptotic Freedom: Weak Coupling

We have now justified that QCD and low-energy electroweak physics are the appropriate tools to describes the correct physics in neutron stars. Can we compute with it? One of the difficulties of QCD is that it is a strongly coupled theory at low energy scales. One manifestation of this is that, although the theory contains only quarks and gluons, these particles have never been observed in nature. This aspect of the theory—known as confinement—which was a major hurdle to the acceptance of the theory. In a strongly coupled theory, the fundamental degrees of freedom may not be free to propagate.

In QCD, confinement is related to the fact that the coupling constant gets *stronger* at low-energy scales (large distances): if one tries to pull two quarks apart, the forces become very large and one must eventually put enough energy into the system to form a quark-antiquark pair from the vacuum. The result is that, instead of ending up with two free quarks, one ends up with two hadrons: the new quark and anti-quark combine with the original quarks to screen the colour. The problem with—and ultimate beauty of—QCD is that the theory is asymptotically free: the coupling constant get large at long distance scales but small at short distances.

In a quantum field theory, the couplings of the theory depend on the scale at which one works. For example, consider a stationary electric charge (point source). At long distances, a test charge will experience a Coulomb force proportional to $1/r^2$ where the proportionality constant describes the strength of the electromagnetic coupling (fine-structure) constant $\alpha \sim e^2$. In a polarizable medium, however, the charge will be screened because dipoles in the medium align with the electric field, reducing the effective charge of the source. This results in a lower effective charge, or smaller effective coupling. As one moves closer to the source, less material is available to screen the source and the effective coupling gets larger.

The vacuum may contain no matter, but it is still filled with quantum fluctuations. One may picture this with the energy-time uncertainty principle: for short periods of time, particle-antiparticle pairs have a finite probability of forming. These pairs have a dipole moment and allow the vacuum to act as a polarizable medium. The effect of this screening is interpreted as a dependence of the coupling constant on the separation scale. Thus, the fine-structure constant $\alpha(\Lambda)$ depends on the energy scale (inverse distance scale). For low energies, α asymptotes to the familiar value $\alpha \to 1/137$, but for high energies (short distances) it becomes very large (less screening). Without modification, this coupling diverges at a finite energy scale: In this way we know that QED is sick and needs some other form of ultraviolet completion beyond the standard model.

QCD, on the other hand, exhibits anti-screening: the coupling $g_s(\Lambda)$ becomes small at high energy scales. This is due fundamentally to its non-Abelian nature (Abelian theories can only screen). At sufficiently short distance scales, the interactions vanish, the theory becomes free and there are no divergence. Such theories are said to be asymptotically free [104, 105, 106, 107, 108] and are highly desirable because they may exist as complete, self-consistent theories of microscopic physics.

At low energies and large distances, QCD is strongly coupled, and there is no reason to expect that the fundamental degrees of freedom persist to low energies: collective phenomena may dominate. Indeed, this is the case for QCD: all coloured degrees of freedom are confined and the low-energy states are all colour singlets. The resulting low-energy spectrum includes a veritable zoo of particles [101], none of which carries colour charge.

The problem is that there are very few tools to study strongly interacting systems: a particle physicist's primary toolbox is founded on perturbation theory, which requires a small expansion parameter: typically a weak coupling.[12] Thus, there is little hope of being able to calculate low-energy physics from first principles without using the massive simulations of lattice QCD. These simulations typically involve a Monte-Carlo integration of an Euclidean path-integral for the lattice theory, and have enjoyed a reasonable amount of success in describing vacuum QCD and the properties of hadrons. The success of the Monte-Carlo algorithm, however, depends on its convergence properties.

When generalized to finite densities (through the introduction of a chemical potential), the weights of the path-integral become complex. The result

[12]There are several examples of exactly solvable models, but these are often one dimensional or tend to be quite artificial.

is that the Monte-Carlo algorithm must now average over wildly oscillating functions. The favourable convergence properties thus vanish and the problem becomes exponentially hard. While there have been advances in solving certain problems using clustering techniques, the general problem is believed to be formally NP-hard [109]. There may still be approximate solutions, or techniques for solving specific problems of physical interest, but a tractable solution in the specific case of QCD is one of the outstanding problems in QCD today.

The second result of asymptotic freedom, however, is that at *high* enough energies, one *can* use perturbative and weak-coupling techniques. At temperatures or energies much higher than 500 MeV one may use perturbative QCD to establish asymptotic properties of the theory. Typically, however, one must be at scales above 10 GeV for perturbative QCD to become accurate. This allows one to apply QCD in high-energy collisions, the early universe, and at extremely high densities. Once these perturbative calculations are used to determine the general structure of the theory in the asymptotic regime, one can extrapolate to reasonable energy scales and use this as a starting point for other weak-coupling analysis

As we discussed in Section 6.1.8, the typical energy scale of neutron star cores may be about 500 GeV: this is right about the point at which QCD goes from being strongly coupled to weakly coupled ($\Lambda_{\mathrm{QCD}} \sim 500$ MeV where $\alpha_s(\Lambda_{\mathrm{QCD}}) \sim 1$). Thus, one can make strong statements about the behaviour of QCD at much larger densities, and then try to extrapolate down to physical densities. This extrapolation is difficult, however, because on is starting to leave the weakly coupled regime. The main approach of our analysis is to use a model to qualitatively capture the interesting physics in this non-perturbative regime.

6.1.10 Low Energy Effective Theories

Despite the complexities involved with trying to solve a strongly coupled theory from first principles, an incredible amount can be learned from the symmetries of the underlying theory (indeed, it was through the patterns found in the data that the underlying theory of QCD was deduced). The reason is that the low-energy physics is, to lowest order, almost completely and uniquely determined by symmetry.

This has several important implications:

1. Once the proper symmetry pattern is deduced, the low energy physics can be well described without reference to a microscopic theory. To

lowest order, everything can be formulated in terms of a handful of constants that can, in principle, be computed from the microscopic theory. In practice, they are "matched" onto results from lattice QCD, from experiment, or other effective theory calculations. In high density QCD one typically forms a chain of effective theories. If the range of validity of these theories overlap, then they can be matched at these overlapping scales. Thus, one typically starts with perturbative QCD, then matches this to High Density Effective Theory (HDET), and finally matches HDET to the low-energy Chiral Perturbation Theory (ChPT or χPT).

2. Many different microscopic theories lead to the same low-energy effective theory: the only difference is that values of the the effective parameters differ from one theory to the other. The only requirement is that the microscopic theories have the same symmetry structure.

We shall make use of the second point to motivate studying a simpler family of Nambu–Jona-Lasinio (NJL) models [97, 98] rather than the full theory of QCD. These models reproduce some of the low-energy physics associated with QCD but are much more easily dealt with using the techniques developed here. They do not match all of the low-energy physics, however. For example, they describe the pattern of chiral symmetry breaking, and even the formation of "nucleon droplets" [110], but do not capture confinement properly, or explain the structure of nucleons as triplets of three quarks.

Chapter 7

High Density QCD

We shall now proceed to apply the techniques from earlier parts of this thesis to study QCD at the high densities that might be found in the cores of neutron stars. This work was first presented in [2]. At large enough densities, the nucleons are crushed together and the quarks become the relevant degrees of freedom. The asymptotic freedom of QCD ensures that at high-enough densities the theory is weakly coupled. This allows one to perform weak-coupling calculations at asymptotically high densities. Such calculations have established that the structure of the ground state of quark matter is a colour superconductor (see for example [37, 110, 111, 112, 113, 114, 115, 116, 117, 118, 119, 120, 121, 122, 123]). In particular, at densities high enough that the three lightest quarks can be treated as massless, the ground state is the colour-flavour–locked (CFL) state in which all three colours and all three flavours participate in maximally (anti)-symmetric pairing [116, 119, 124, 125].

Determination of the QCD phase structure at moderate densities and in the presence of non-zero quark masses has proceeded in several ways. One approach has been to formulate a chain of effective theories, and then to match coefficients across several energy scales through these effective theories to perturbative calculations. Coefficients in the low-energy chiral effective theory [126] are matched to calculations performed in high-density effective theories (HDET) [118, 127, 128] which in turn are matched to weakly-coupled QCD. This allows one to determine the properties of the Goldstone bosons and determine the effects of small quark masses [129, 130, 131, 132, 133, 134, 135, 136, 137, 138]. Within this framework, it has been noted that, in the presence of a finite strange quark mass, neutral "kaons" (the lightest pseudo-Goldstone modes at high density with the same quantum numbers as their vacuum counterpart) can Bose-condense in the CFL state to form a kaon-condensed CFLK^0 phase with lower condensation energy [139, 140, 141].

Unfortunately, the low-energy effective theory is only reliable for small perturbations and at moderate densities the strange quark mass is not a small perturbation. A recent attempt has been made to extrapolate to

large strange quark mass (m_s) [142], but this approach has not dealt with additional complications in the condensate structure that allow different gap parameters for each pair of quarks.

To deal with moderate quark masses, another approach has been to study Nambu–Jona-Lasinio (NJL) models [97, 98] of free quarks with contact interactions that model instanton interactions or single gluon exchange. These models are amenable to the mean-field techniques presented earlier in this thesis and exhibit a similar symmetry breaking pattern to QCD which results in CFL ground states [110, 115].

Within this model, one can study the effects of moderate quark masses through self-consistent solutions of the mean-field gap equations. This has led to a plethora of phases. In particular, several analyses show a transition to a colour-flavour locked phase with gapless fermionic excitations (the gCFL phase) [21, 25, 26]. This gapless phase has the same structure as the Breached Pair state we discussed in Part II, except that: 1) there are many more species participating, 2) the state is stabilized only when colour and electric neutrality constraints are imposed, and 3) the neutrality constraints cause one of the fermion branches to maintain almost quadratic dispersions.

The CFL/gCFL transition has been analyzed with both NJL based calculations [21, 25, 26, 27] and effective theory based calculations [142, 143]. Until recently, however, the NJL calculations have excluded the possibility of kaon condensation (see however [144] which considers kaon condensation in the NJL model at low density), while the effective theories do not consider the complicated patterns in which the condensate parameters evolve at finite quark masses. The first attempts to consider both the NJL analysis with kaon condensation were [2, 145].

The goal of this thesis is to show how to use low-energy effective theories to organize the results of the self-consistent mean-field analysis of the NJL model which accounts for the full condensate structure. In particular, we use an NJL model based on single gluon exchange to find self-consistent solutions that correspond to the CFLK^0 phase; we show that these phases agree with the predictions of the low-energy effective theory; and we determine how and where the zero temperature phase transition to a gapless CFL phase occurs as one increases the strange quark mass. In addition, unlike previous work on the NJL model, our numerical solutions are *fully* self-consistent: we include *all* condensates and self-energy corrections required to close the gap equations.

We first describe the pattern of symmetry breaking that leads to the CFL and CFLK^0 states (Section 7.1). Then we present our numerical results, demonstrating some properties of these states and determining the locations

of the zero-temperature phase transitions (Section 7.2). After a careful description of our model (Section 7.3) we derive the low-energy effective theory, paying particular attention to the differences between QCD and the NJL model (Section 7.4). Here we demonstrate that, for small perturbations, our numerical solutions are well described by the effective theory, and we use our numerical results to compute the pion decay constant f_π which agrees with the perturbative QCD results. Specific numerical details about our calculations and a full description of our self-consistent parametrization are given in Appendix E.

We leave for future work the consideration of finite temperature effects, the analysis of the gapless CFLK^0 (gCFLK^0), the inclusion of instanton effects, the inclusion of up and down quark mass effects and the possibility of other forms of meson condensation.

7.1 Colour Flavour Locking (CFL)

QCD has a continuous symmetry group of $\mathrm{U(1)_B}\otimes\mathrm{SU(3)_L}\otimes\mathrm{SU(3)_R}\otimes\mathrm{SU(3)_C}$. In addition, there is an approximate $\mathrm{U(1)_A}$ axial flavour symmetry that is explicitly broken by anomalies. At sufficiently high densities, however, the instanton density is suppressed and this symmetry is approximately restored.

The CFL ground state spontaneously breaks these continuous symmetries through the formation of a diquark condensate [116]

$$\langle \bar{\psi}^{c\dagger}_{\alpha a}\gamma_5\psi_{\beta b}\rangle \propto \Delta_3\epsilon^{\alpha\beta k}\epsilon_{abk} + \Delta_6(\delta^\alpha_a\delta^\beta_b + \delta^\alpha_b\delta^\beta_a). \tag{7.1}$$

The symmetry breaking pattern (include the restored axial $\mathrm{U(1)_A}$ symmetry) is thus[1]

$$\frac{\mathrm{U(3)_L}\otimes\mathrm{U(3)_R}\otimes\mathrm{SU(3)_C}}{\mathrm{Z_3}} \to \mathrm{SU(3)_{L+R+C}}\otimes\mathrm{Z_2}\otimes\mathrm{Z_2} \tag{7.2}$$

where the $\mathrm{Z_2}$ symmetries corresponds to $\psi_L \to -\psi_L$ and $\psi_R \to -\psi_R$. It has been noted that the symmetry breaking pattern at high density (7.2) is the same as that that for hyper-nuclear matter at low density [146]. This leads one to identify the low-energy pseudo-scalar degrees of freedom in both theories. We shall refer to the pseudo-scalar Goldstone bosons in the high density phase as "pions" and "kaons" etc. when they have the same flavour quantum numbers as the corresponding low-density particles.

The CFL state (7.1) preserves parity, and is preferred when instanton effects are considered. Excluding instanton effects, there is an uncountable

[1]The $\mathrm{Z_3}$ factor mods out the common centres. See (7.11) for the explicit representation.

degeneracy of physically equivalent CFL ground states that violate parity. These are generated from the parity even CFL by the broken symmetry generators.

The symmetry breaking pattern (7.2) breaks 18 generators. The quarks, however, are coupled to the eight gluons associated with the $SU(3)_C$ colour symmetry and to the photon of the $U(1)_{EM}$ electromagnetism (which is a subgroup of the vector flavour symmetry). Eight of these gauge bosons acquire a mass through the Higgs mechanism and the coloured excitations are lifted from the low-energy spectrum. There remain 10 massless Nambu-Goldstone excitations: a pseudo-scalar axial flavour octet of mesons, a scalar superfluid boson associated with the broken $U(1)_B$ baryon number generator, and a pseudo-scalar η' boson associated with broken axial $U(1)_A$ generator. There remains one massless gauge boson that is a mixture of the original photon and one of the gluons [116, 147]. With respect to this "rotated electromagnetism" $U(1)_{\tilde{Q}}$ the CFL state remains neutral [148].

The degeneracy of the vacuum manifold is lifted by the inclusion of a non-zero strange quark mass m_s. In the absence of instanton effects and other quark masses, the ground state is not near to the parity even CFL state (7.1), but rather, is a kaon rotated state $CFLK^0$. As $m_s \to 0$ this state approaches a state on the vacuum manifold that is a pure kaon rotation of the parity even CFL (7.1).

Even in the absence of quark masses, the vacuum manifold degeneracy is partially lifted by the anomalous breaking of the $U(1)_A$ axial symmetry which we have neglected: Instanton effects tend to disfavour kaon condensation by favouring parity even states, and thus delay the onset of the $CFLK^0$ until m_s reaches a critical value (possibly excluding it). The effects of anomaly and instanton contributions have been well studied [115, 124, 134, 149, 150, 151] and play an important quantitative role in the phase structure of QCD. Non-zero up and down quark masses also tend to disfavour kaon condensation.

For the purposes of this chapter, we shall neglect both the effects of instantons, and the effects of finite up and down quark masses. This will ensure that kaon condensation occurs for arbitrarily small m_s. Both of these effects open the possibility of a much richer phase structure, including condensation of other mesons (see for example [141, 152]). Future analyses should take these numerically important effects into account, both in the effective theory and in the NJL model.

The primary source of for kaon condensation is the finite strange quark mass. To lowest order, this behaves as a chemical potential [139, 140, 141] (see (7.3) and (7.4)). In this chapter, we also consider the addition of a hy-

percharge chemical potential as this removes many complications associated with masses and leads to a very clean demonstration of kaon condensation.

7.2 Self-Consistent Solutions

We consider four qualitatively different phases: Two are self-consistent mean-field solutions to the NJL model with a finite hypercharge chemical potential parameter μ_Y; the other two are self-consistent mean-field solutions to the NJL model with a finite strange-quark mass parameter m_s. In each of these cases, one solution corresponds to a parity even CFL phase and the other corresponds to a kaon condensed CFLK^0 phase. Our normalizations and a complete description of the model are presented in Section 7.3. A full description of all the parameters required to describe these phases along with some typical values is presented in Appendix E.

7.2.1 Finite Hypercharge Chemical Potential

The CFL phase in the presence of a hypercharge chemical potential corresponds to the fully gapped CFL phase discussed in [21]. Here one models the effects of the strange quark through its shift on the Fermi surface $p_F \approx \mu_q$ of the strange quarks. This can be seen by expanding the free-quark dispersion

$$\sqrt{p^2 + M_s^2} \approx |p| + \frac{M_s^2}{2\mu_q} + \cdots \tag{7.3}$$

or, more carefully, by integrating out the antiparticles to formulate the High Density Effective Theory. See for example [118, 127, 128, 138]).

These leading order effects are equivalent to adding a hypercharge chemical potential of magnitude

$$\mu_Y = \frac{M_s^2}{2\mu_q}. \tag{7.4}$$

and a baryon chemical potential shift of

$$\delta\mu_B = -\frac{M_s^2}{\mu_q}. \tag{7.5}$$

We consider only the effect of the hypercharge chemical potential here, holding μ_B fixed. Note that the relevant parameters here are M_s and μ_q rather than m_s and $\mu_s = \mu_B/3$. M_s is the constituent quark mass that appears in

the dispersion relation whereas m_s is the bare quark mass parameter; likewise, μ_q is the corrected quark chemical potential that determines the Fermi surface whereas $\mu_s = \mu_B/3$ is the bare baryon chemical potential. (These distinctions are important because our model takes into account self-energy corrections.)

The CFL phase responds in a trivial manner to a hypercharge chemical potential: the quasiparticle dispersions shift such that the physical gap in the spectrum becomes smaller; none of the other physical properties change. In particular, as the hypercharge chemical potential increases, the coloured chemical potential $\mu_8 = -\mu_Y$ decreases to maintain neutrality. The values of all of the gap parameters, the self-energy corrections, the densities and the thermodynamic potential remain unchanged until the physical gap in the spectrum vanishes. (The apparent change in the magnitude of the gap parameters in the first figure of [21] is due to the shift in the baryon chemical (7.5) which occurs if one uses the strange quark chemical potential shift μ_s rather than a hypercharge shift μ_Y.) This is a consequence of the $\tilde{Q}$ neutrality of the CFL state [153]. In particular, the electric chemical potential remains zero $\mu_e = 0$ and the state remains an insulator until the onset of the gapless modes. The same phenomena has also been noticed in the two-flavour case [36, 154, 155].

As such, we can analytically identify the phase transition to the gCFL phase which occurs for the critical chemical potential

$$\mu_Y^c = \Delta_0 \tag{7.6}$$

where $\Delta_0 = \Delta_3 - \Delta_6$ is the physical gap in the spectrum in the absence of any perturbations. Throughout this chapter we use parameter arbitrarily chosen so that $\mu_Y^c = \Delta_0 = 25$ MeV to correspond with the parameter values in [21, 26, 27]. We show typical quasiparticle dispersion relations for this state in Figure 7.1.

The splitting of the dispersions can also be easily understood from the charge neutrality condition (7.58) and the leading order effects are summarized in Table 7.1. After setting $\mu_8 = -\mu_Y$, the chemical potentials for the rs and gs quarks shift by $-\mu_Y$ whereas for the bu and bd quarks it shifts by $+\mu_Y$. Thus, the (gs,bd) and (rs,bu) pairs are the first to become gapless.

The kaon condensed hypercharge state is more complicated. One can again use the appropriate charge neutrality conditions (7.58) to estimate how the quarks will be affected by μ_Y, but the naïve results hold only to lowest order. In particular, the condensates of the CFLK^0 state also vary as μ_Y increases (see Table E.2). These higher order effects break all the

	ru	gd	bs	rd	gu	rs	bu	gs	bd
CFL	0	0	0	0	0	-1	$+1$	-1	$+1$
CFLK^0	0	$+\frac{1}{2}$	$-\frac{1}{2}$	0	$+\frac{1}{2}$	-1	$+\frac{1}{2}$	$-\frac{1}{2}$	$+\frac{1}{2}$

Table 7.1: Leading order shifts in the chemical potentials of the various quarks in the CFL and CFLK^0 states in the presence of a hypercharge chemical potential shift μ_Y. This follows directly from (7.58).

degeneracy between the quark species and Figure 7.3 has nine independent dispersions.

We shall compare the thermodynamic potentials of these two states later (see Figures 7.7 and 7.8), but we point out here that the transition to a gapless colour-flavour–locked state with kaon condensation (gCFLK^0) occurs at a larger hypercharge chemical potential than the CFL/gCFL transition. This can be most easily seen in Figure 7.5. This is in qualitative agreement with [142] and [143], but in quantitative disagreement.

In the CFL/gCFL transition, two modes become gapless simultaneously: the lower branches of the (rs,bu) and (gs,bd) pairs. One of these modes is electrically neutral (gs,bd) and it crosses the zero-energy axis giving rise to a "breach" in the spectrum. The other mode is electrically charged: as soon as in crosses, the electric chemical potential must rise to enforce neutrality. The state now contains gapless charged excitations and becomes a conductor. The result is that the the neutral gapless mode has two linear dispersions while the charged gapless mode has a virtually quadratic dispersion when electric neutrality is enforced. (This was discovered in [21] and is explained in detail in [26].)

In the CFLK^0/gCFLK^0 transition, a single charged mode becomes gapless.[2] Thus, immediately beyond the transition, the corresponding gCFLK^0 state will also be a conductor but there will be a single charged gapless mode with almost quadratic dispersion. Additional modes will continue to lower until either more modes become gapless, or a first order phase transition to a competing phase occurs.

[2]This mode pairs rs, gu, and bu quarks in quite a non-trivial manner. In the CFL, the quasiparticles form a nice block-diagonal structure in which the quarks exhibit definite pairing between two species, In the CFLK0, the block structure is more complicated and the pairing cannot be simply described: the lowest lying quasiparticle is simple a linear combination of the three rs, gu, and bu quark.

7.2.2 Finite Strange Quark Mass

The second pair of CFL/CFLK^0 states that we consider are self-consistent solutions to the gap equation in the presence of a finite strange quark mass. Qualitatively we expect to see similar features to the states at finite hypercharge chemical potential and indeed we do as shown in Figures 7.2 and 7.4.

Quantitatively, we notice a few differences with previous analyses concerning the locations of the phase transitions to gapless states. Our parameters have been chosen to match the parameters in [27]. They find that $M_s^2/\mu = 46.8$ MeV, but the CFL/gCFL transition happens noticeably earlier with our model at $M_s^2/\mu = 43.9$ MeV. This is due to a corresponding six-percent reduction in the condensate parameters and represents the effects of performing a fully self-consistent calculation.

Another difference concerns the appearance of gapless modes in the CFLK^0 state. This transition occurs at $M_s^2/\mu = 52.5$ MeV in our model—a factor of 1.2 larger than the CFL/gCFL transition. This is some ten percent smaller than the factor of 4/3 derived in [142]. This is likely due to the more complicated condensate structure we consider.

7.3 NJL Model

We base our analysis on the following Hamiltonian density for the NJL model

$$\widehat{\mathbf{H}} = \int \mathrm{d}^3\vec{\mathbf{p}}\, \widehat{\psi}^\dagger_{\vec{\mathbf{p}}} \left(\vec{\alpha}\cdot\vec{\mathbf{p}} - \mu + \gamma_0 \mathbf{M}\right) \widehat{\psi}_{\vec{\mathbf{p}}} + \widehat{\mathbf{H}}_{\text{int}}. \tag{7.7}$$

Here we consider 9 species of quarks = 3 colours × 3 flavours: Including the relativistic structure, there are 36 quark operators in the vector ψ. The matrices μ and $\mathbf{M}$ are the quark chemical potentials and masses respectively.

We take the interaction to be a four-fermion contact interaction with the quantum numbers of single gluon exchange:[3]

$$\widehat{\mathbf{H}}_{\text{int}} = g \int \left(\overline{\widehat{\psi}}\gamma^\mu \boldsymbol{\lambda}^A \widehat{\psi}\right)\left(\overline{\widehat{\psi}}\gamma_\mu \boldsymbol{\lambda}^A \widehat{\psi}\right). \tag{7.8}$$

[3]Here the matrices $\boldsymbol{\lambda}^A$ are the eight 3×3 Gell-Mann matrices and the γ^μ are the Dirac matrices which we take in the chiral basis. Our normalizations and conventions are

$$\mathrm{Tr}[\boldsymbol{\lambda}^A\boldsymbol{\lambda}^B] = \tfrac{1}{2}\delta^{AB},$$
$$\gamma_5 = i\gamma_0\gamma_1\gamma_2\gamma_3 = \begin{pmatrix} -\mathbf{1} & \mathbf{0} \\ \mathbf{0} & \mathbf{1}\end{pmatrix},$$
$$\gamma_C = i\gamma_2\gamma_0.$$

We also use natural units where $c = \hbar = k_B = 1$.

This is exactly a sum of terms of the form (3.44) with interaction matrices:

$$\mathbf{\Gamma}^A_\mu = \gamma_0\gamma_\mu \otimes \mathbf{1} \otimes \boldsymbol{\lambda}^A. \tag{7.9}$$

The only added complication is that, to the spatial terms $\mu \in \{1,2,3\}$, a negative sign from the metric must be added. The Gell-Mann matrices act on the colour space and the flavour structure is diagonal. We point out that this form of NJL interaction has the desirable feature of explicitly breaking the independent colour $\mathrm{SU(3)_{CL}}$ left and $\mathrm{SU(3)_{CR}}$ right symmetries that some NJL models preserve. This is important because the condensation pattern (7.1) does not explicitly link left and right particles: Our model thus has the same continuous symmetries as QCD, and the only complication to deal with is the gauging of the single colour $\mathrm{SU(3)_C}$ symmetry.

Our goal here is to provide a non-perturbative model to discuss the qualitative features of QCD at finite densities. We model the finite density by working in the grand thermodynamic ensemble by introducing a baryon chemical potential for all of the quarks:

$$\boldsymbol{\mu} = \frac{\mu_B}{3}\mathbf{1}. \tag{7.10}$$

With only this chemical potential and no quark masses, our model has an $\mathrm{U(3)_L} \otimes \mathrm{U(3)_R} \otimes \mathrm{SU(3)_C}/\mathrm{Z_3}$ continuous global symmetry in which the left-handed quarks transform as $(\bar{\mathbf{3}}, \mathbf{1}, \mathbf{3})$ and the right handed quarks transform as $(\mathbf{1}, \bar{\mathbf{3}}, \mathbf{3})$. In the chiral basis we have explicitly[4]

$$\begin{pmatrix} \psi_L \\ \psi_R \end{pmatrix} \to \begin{pmatrix} e^{-i\theta_L}\mathbf{F}_L^* \otimes \mathbf{C} & \mathbf{0} \\ \mathbf{0} & e^{-i\theta_R}\mathbf{F}_R^* \otimes \mathbf{C} \end{pmatrix} \begin{pmatrix} \psi_L \\ \psi_R \end{pmatrix} \tag{7.11}$$

where $\mathbf{F}$ and $\mathbf{C}$ are SU(3) matrices. For an attractive interaction, this NJL model exhibits the same symmetry breaking pattern as QCD (7.2) with a restored axial symmetry. The difference between this NJL model and QCD is that the NJL model contains no gauge bosons. Thus, there are 18 broken generators which correspond to massless Goldstone bosons, and none of these is eaten. To effectively model QCD, we must remove the extra coloured Goldstone bosons. At the mean-field level, this is done by imposing gauge neutrality conditions [148, 156, 157]. Once the appropriate chemical potentials are introduced, the dependence on the vacuum expectation values of the coloured Goldstone modes is cancelled and the low-energy physics of the NJL model matches that of QCD.

[4] From this explicit representation we can see how the centres of the colour and flavours overlap giving rise to the $\mathrm{Z_3}$ factor.

The usual NJL model has a local interaction, but this is not renormalizable and needs regulation. For the purposes of this chapter, we introduce a hard cutoff on each of the momenta $\Lambda_{\vec{\mathbf{p}}} = \theta(\Lambda - \|\vec{\mathbf{p}}\|)$ to mimic the effects of asymptotic freedom at large momenta. This potential is separable and has exactly the same form as (3.45):

$$\begin{aligned}\widehat{\mathcal{H}}_{\text{int}} = gV \int \mathrm{d}^3\vec{\mathbf{p}}\mathrm{d}^3\vec{\mathbf{p}}'\mathrm{d}^3\vec{\mathbf{q}}\mathrm{d}^3\vec{\mathbf{q}}'\ \Lambda_p\Lambda_{p'}\Lambda_q\Lambda_{q'} \times \\ \times (2\pi)^3\delta^{(3)}(\vec{\mathbf{p}} - \vec{\mathbf{p}}' + \vec{\mathbf{q}} - \vec{\mathbf{q}}')\left(\overline{\widehat{\psi}}_{\vec{\mathbf{p}}}\gamma^\mu\lambda^A\widehat{\psi}_{\vec{\mathbf{p}}'}\right)\left(\overline{\widehat{\psi}}_{\vec{\mathbf{q}}}\gamma_\mu\lambda^A\widehat{\psi}_{\vec{\mathbf{q}}'}\right). \quad (7.12)\end{aligned}$$

To study this model we perform a variational calculation by introducing the quadratic model

$$\widehat{\mathcal{H}}_0 = \int \mathrm{d}^3\vec{\mathbf{p}}\ \left(\widehat{\psi}^\dagger_{\vec{\mathbf{p}}}\mathbf{E}(\vec{\mathbf{p}})\widehat{\psi}_{\vec{\mathbf{p}}} + \widehat{\psi}^T_{\vec{\mathbf{p}}}\mathbf{B}_{\vec{\mathbf{p}}}\widehat{\psi}_{\vec{\mathbf{p}}} + \widehat{\psi}^\dagger_{\vec{\mathbf{p}}}\mathbf{B}^\dagger_{\vec{\mathbf{p}}}\widehat{\psi}^*_{\vec{\mathbf{p}}}\right) \quad (7.13)$$

where

$$\mathbf{E}(\vec{\mathbf{p}}) = \vec{\alpha}\cdot\vec{\mathbf{p}} - \mu + \gamma_0\mathbf{M} - \mathbf{A} \quad (7.14)$$

and then computing the variational upper bound on the thermodynamic potential Ω of the full system as discussed in Chapter 2:

$$\frac{\Omega}{V} \leq \frac{\Omega_0}{V} + \langle\mathcal{H} - \mathcal{H}_0\rangle_0. \quad (7.15)$$

The condition for the right hand side of (7.15) to be stationary with respect to the variational parameters is equivalent to the self-consistent gap equation.

As discussed in Section 3.3.2, with our separable interaction (7.12), all of the momentum dependence is contained within the cutoff function Λ_p. Thus, the task for finding mean-field solutions consists of choosing reasonable parametrizations of $\mathbf{A}$ (which includes the chemical potentials, masses and related corrections) and $\mathbf{B}$ (which includes the gap parameters Δ) that are closed under the self-consistency condition, and numerically finding stationary points of this system of equations.

There are only two difference here from the techniques previously discussed:

1. $\mathbf{A}$ and $\mathbf{B}$ are arbitrary 36×36 matrices subject to $\mathbf{A} = \mathbf{A}^\dagger$ and $\mathbf{B} = -\mathbf{B}^T$. A full parametrization thus consists of 2556 parameters and is costly to fully explore. Instead, we choose a partial parametrization that is physically natural and *fully* closed under the self-consistency

conditions. While we cannot be certain that we have considered all possible condensation patterns, we are pretty confident that we have identified the principle states.

2. In the previous two-species systems, one only needs to consider *either* $\langle \widehat{\mathbf{a}}\widehat{\mathbf{b}} \rangle$ condensates *or* $\langle \widehat{\mathbf{a}}^\dagger \widehat{\mathbf{b}} \rangle$ condensates. Here we must allow for the possibility of both. Thus, the formalism developed in Sections 3.1, 3.2, and 3.3 is not sufficient: we must use the more general results presented in Appendix B.

As discussed in Section 7.4.5 and [148], we must impose the appropriate gauge charge neutrality conditions. This is done by introducing bare gauge chemical potentials into the model and choosing these to ensure the final solution is neutral.

To impose a charge neutrality condition, we instead vary μ_R (along with with the other parameters) to obtain a neutral solution (again we note that the total charge and other correlations of the state depend only on the corrected parameters μ_R). Once this solution is found, $\delta\mu$ is computed and the required bare chemical potential $\mu = \mu_R - \delta\mu$ determined. Despite the fact that the self-energy corrections depend only on the corrected parameters (μ_R etc.), the thermodynamic potential depends on both the corrected and the bare parameters and so this last step is important.

One must also be careful about which thermodynamic potential is used to compare states when neutrality conditions are enforced as we are no-longer in the grand ensemble. The differences between the potentials of the relevant ensembles are proportional to terms of the form $Q\mu$, however, so for neutrality conditions, $Q = 0$ and the thermodynamic potential may still be used to compare states.

7.3.1 CFL at $m_s = 0$.

As an example, consider the parity even CFL state. The self-consistency conditions are fully closed when one includes four variational parameters. There are two gap parameters Δ_3 and Δ_6 corresponding to the diquark condensate (7.1), one chemical potential correction $\delta\mu_B$ to the baryon chemical potential and and induced off-diagonal chemical potential μ_{oct}. The quadratic Hamiltonian (7.13) can thus be expressed

$$\widehat{\mathcal{H}}_0 = \widehat{\psi}^\dagger \left(\vec{\alpha} \cdot \vec{\mathbf{p}} - \tfrac{1}{3}\mu_B - \boldsymbol{\delta\mu} \right) \widehat{\psi} + \tfrac{1}{2}\widehat{\psi}^T \gamma_C \gamma_5 \boldsymbol{\Delta} \widehat{\psi} \; + \; \text{h.c.}$$

where

$$[\boldsymbol{\Delta}]^{\alpha a}{}_{\beta b} = \Delta_3 \epsilon^{\alpha\beta k} \epsilon_{abk} + \Delta_6 (\delta^\alpha_a \delta^\beta_b + \delta^\alpha_b \delta^\beta_a), \tag{7.16}$$

and

$$\boldsymbol{\delta\mu} = \tfrac{1}{3}\delta\mu_B + \boldsymbol{\mu}_{\rm oct}. \tag{7.17}$$

Most of this structure is all well-known and discussed many times in the literature, however, there has been no mention of the parameter $\boldsymbol{\mu}_{\rm oct}$ because most analyses neglect the self-energy corrections.

Neglecting the correction to the baryon chemical potential is reasonable since it has little physical significance: it simply enters as a Lagrange multiplier to establish a finite density. As such, the effective common quark chemical potential

$$\mu_q = \tfrac{1}{3}\mu_B^{\rm eff} = \tfrac{1}{3}\left(\mu_B + \delta\mu_B\right) \tag{7.18}$$

is the relevant physical parameter defining the Fermi surface. To compare states in the grand ensemble, however, one must fix the bare rather than the effective chemical potentials. This is what we have done in our calculations. Numerically, we find that the corrections $\delta\mu_B$ cause μ_q to vary by only a few percent as we vary the perturbation parameters μ_Y and m_s.

There is no bare parameter corresponding to $\mu_{\rm oct}$. Thus, it is spontaneously induced and should be treated on the same footing as Δ. To see that such a parameter must exist, consider changing to the "octet" basis using the augmented Gell-Mann matrices

$$\tilde{\psi}_A = 2[\boldsymbol{\lambda}^A]_{\alpha a}\psi_{(\alpha a)} \tag{7.19}$$

where $\boldsymbol{\lambda}^0 = \mathbf{1}/\sqrt{6}$. In this basis, the off-diagonal condensate becomes diagonal with one singlet parameter $4\Delta_6 + 2\Delta_3$ and eight octet parameters $\Delta_6 - \Delta_3$:

$$\tilde{\boldsymbol{\Delta}} = \begin{pmatrix} 4\Delta_6 + 2\Delta_3 & & & \\ & \Delta_6 - \Delta_3 & & \\ & & \ddots & \\ & & & \Delta_6 - \Delta_3 \end{pmatrix} \tag{7.20}$$

It is clear that in the CFL, the singlet channel decouples from the octet channel: there is no symmetry relating these and the two gap parameters are related by the numerical value of the coupling g. This decoupling is also present in the chemical potential corrections. One linear combination corresponds to the identity: this corrects the baryon chemical potential $\delta\mu_B$. The other is the induced $\mu_{\rm oct}$. Explicitly

$$[\boldsymbol{\mu}_{\rm oct}]^{\alpha a}{}_{\beta b} = \mu_{\rm oct}\left(\sum_{A=1}^{8}[\boldsymbol{\lambda}^A]_{\alpha a}[\boldsymbol{\lambda}^A]_{\beta b} - 8[\boldsymbol{\lambda}^0]_{\alpha a}[\boldsymbol{\lambda}^0]_{\beta b}\right)$$

Numerically, we calibrate our model with this CFL solution. In particular, we chose our parameters to reproduce the results of [27]. We use a hard cutoff at $\Lambda = 800$ MeV, and a coupling constant chosen so that, with an effective quark chemical potential of $\mu_q = 500$ MeV one has a physical gap in the spectrum of $\Delta_0 = \Delta_3 - \Delta_6 = 25$ MeV. This fixes the following parameter values which we hold fixed for all of our calculations:

$$\Lambda = 800 \text{ MeV}, \tag{7.21a}$$
$$g\Lambda^2 = 1.385, \tag{7.21b}$$
$$\mu_B/3 = 549.93 \text{ MeV}. \tag{7.21c}$$

With these parameters fixed, the fully self-consistent mean-field CFL solution has the following variational parameters:

$$\begin{aligned} \Delta_3 &= 25.6571 \text{ MeV}, \\ \Delta_6 &= 0.6571 \text{ MeV}, \\ \delta\mu_B/3 &= -49.93 \text{ MeV}, \\ \mu_{\text{oct}} &= -0.03133 \text{ MeV}. \end{aligned}$$

Note as first noted in [116], and discussed in [158], the parameter Δ_6 is required to close the gap equation, but is small because the sextet channel is repulsive. In weakly-coupled QCD, Δ_6 is suppressed by an extra factor of the coupling. This effect is numerically captured in the NJL model. The parameter μ_{oct} is also required to close the gap equation when the Hartree-Fock terms are included, and was first introduced in [2]. It is also numerically suppressed. Recent calculations often omit Δ_6 and μ_{oct}: we see that this is generally justified.

The physical gap in the spectrum also defines the critical hypercharge chemical potential for the CFL/gCFL transition (7.6):

$$\mu_Y^c = \Delta_0 = 25.00 \text{ MeV}. \tag{7.23}$$

7.3.2 CFL at $\mu_Y, m_s \neq 0$

Once one introduces a strange quark mass, one must introduce additional parameters. A simple way to determine which parameters are required is to add the mass, then compute the gap equation and see which entries in the self-energy matrix are non-zero. By doing this for a variety of random values of the parameters, one can determine the dimension of the subspace required to close the gap equation and introduce the required parameters.

In the case of the CFL state with non-zero hypercharge chemical potential, one only needs to introduce the parameters μ_Y and μ_8 to ensure gauge neutrality: As discussed in 7.2.1 none of the other parameters change. To go beyond the transition into the gCFL phase, however, or to extend the results to non-zero temperature, one must introduce additional parameters. These include the perturbation μ_Y, the gauge chemical potentials μ_3 and μ_8 and μ_e required to enforce neutrality, as well as nine gap parameters ϕ_i, φ_i and σ_i that fully parametrize the triplet and sextet diquark condensates (these latter nine parameters correspond to the same parameters defined in reference [25]). The additional parameters are chemical potentials similar to μ_{oct} which are induced by the gap equations. The full set of parameters in discussed in Appendix E.

Adding a strange quark mass is more complicated. First of all, we need to introduce additional Lorentz structure. For homogeneous and isotropic systems, there are eight possible relativistic structures:

$$\mathbf{A} = \mathbf{1} \otimes \delta\boldsymbol{\mu} + \gamma_5 \otimes \delta\boldsymbol{\mu}_5 - \gamma_0 \otimes \delta\mathbf{m} - \gamma_0\gamma_5 \otimes \delta\mathbf{m}_5,$$
$$\mathbf{B} = \gamma_C\gamma_5 \otimes \boldsymbol{\Delta} + \gamma_C \otimes \boldsymbol{\Delta}_5 + \gamma_0\gamma_C\gamma_5 \otimes \boldsymbol{\kappa} + \gamma_0\gamma_C \otimes \boldsymbol{\kappa}_5.$$

Introducing quark masses requires one to introduce the additional Lorentz structure $\boldsymbol{\kappa}$ [158] to close the gap equations, but these are found to be small. In total, one requires about 20 parameters to fully parametrize the CFL in the presence of a strange quark mass (see Table E.3).

With the inclusion of a bare quark mass m_s one induces a chiral condensate $\langle\bar{\psi}\psi\rangle$ which in turn generates a correction to the quark mass. The resulting parameter in $\mathbf{A}$ is the constituent quark mass M_s which appears in the dispersion relationships for the quarks. It is this constituent quark mass that must be used when calculating the effective chemical potential shift (7.4). Generally the constituent quark mass is quite a bit larger than the bare quark mass parameter m_s. For example, close to the phase transition, we have $m_s \approx 83$ MeV while the constituent quark mass is $M_s \approx 150$ MeV (see Table E.3). We have checked that our calculations are quantitatively consistent with the calculations presented in [14] in this regard.

7.3.3 Meson Condensed CFL: CFLK^0 etc.

Applying a meson rotations to the CFL state breaks the parity of the state, and mixes the parity even parameters $\boldsymbol{\mu}$, $\mathbf{m}$, $\boldsymbol{\Delta}$ and $\boldsymbol{\kappa}$ with their parity odd counterparts $\boldsymbol{\mu}_5$, $\mathbf{m}_5$, $\boldsymbol{\Delta}_5$ and $\boldsymbol{\kappa}_5$. The full set of parameters and typical numerical values is presented in Appendix E.

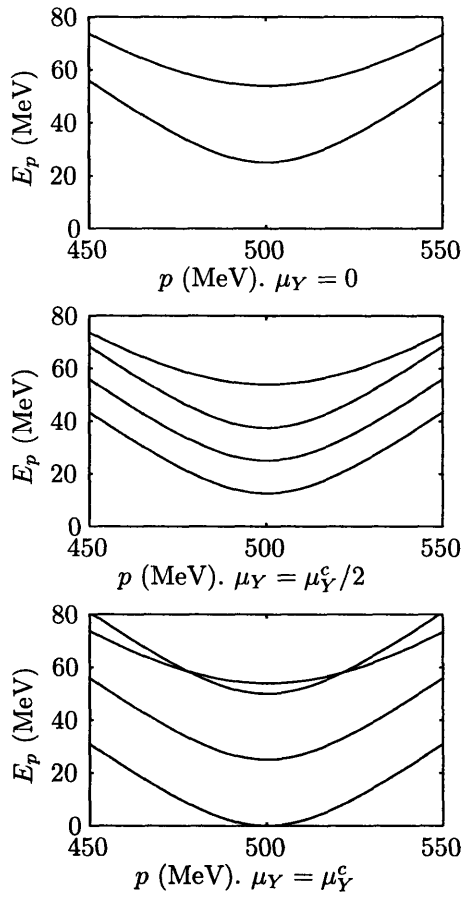

Figure 7.1: Lowest lying quasiparticle dispersion relations near the Fermi momentum $p_F = \mu_q = 500$ MeV for the CFL phase with three different values of the hypercharge chemical. All dispersion relations have left-right degeneracy: we now consider the colour-flavour degeneracy. In the top plot at $\mu_Y = 0$, the bottom dispersion has an eight-fold degeneracy and a gap of $\Delta_0 = 25$ MeV. The top band contains a single quasiparticle pairing (ru,gd,bs) with a gap of $4\Delta_6 + 2\Delta_3 = 54$ MeV. In the middle plot at $\mu_Y = \mu_Y^c/2 = 12.5$ MeV, the (rs,bu) and (gs,bd) pairs are shifting as indicated in Table 7.1. In the bottom plot, two pairs have become gapless marking the CFL/gCFL transition.

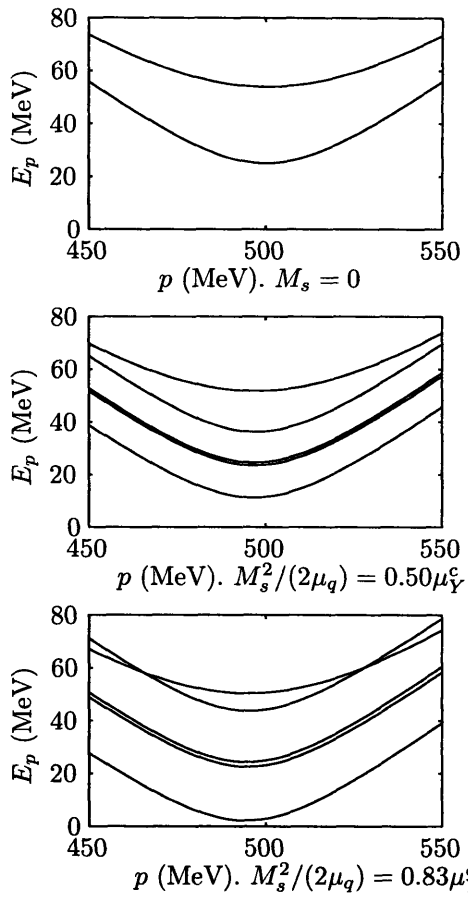

Figure 7.2: Lowest lying quasiparticle dispersion relationships about the Fermi momentum $p_F = \mu_q = 500$ MeV for the CFL phase with two different values of the strange quark mass. (The $M_s = 0$ dispersions are the same as in the top of Figure 7.1.) Qualitatively this has the same structure as Figure 7.1 except that middle dispersion is now split by higher order mass effects.

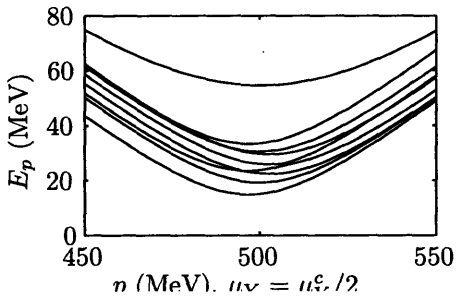

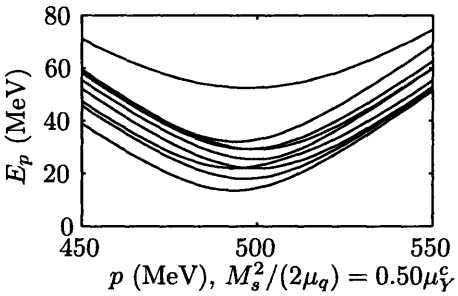

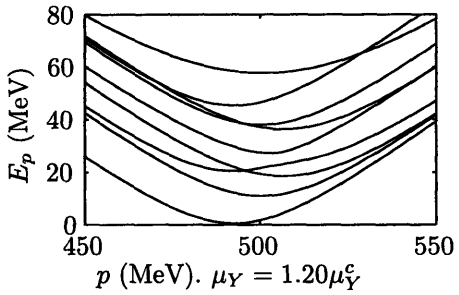

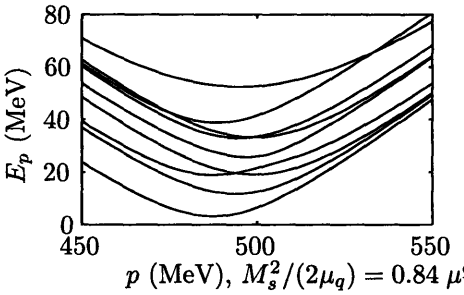

Figure 7.3: Lowest lying quasiparticle dispersion relationships about the Fermi momentum $p_F = \mu_q = 500$ MeV for the CFLK^0 phase with two different values of the hypercharge chemical. (The $\mu_Y = 0$ dispersions are the same as in the top of Figure 7.1.) Again, all dispersion have a left-right degeneracy. In the top plot at $\mu_Y = \mu_Y^c/2 = 12.5$ MeV, the eightfold degenerate lowest band has split into eight independent dispersions. To leading in the perturbation, the splitting is described by Table 7.1, but the lack of degeneracy indicates that there are also higher order effects. The lower plot at at $\mu_Y \approx 1.20\mu_Y^c \approx 30$ MeV is close to the CFLK^0/gCFLK^0 transition. The gapless band now contains only a single mode and is charged.

Figure 7.4: Lowest lying quasiparticle dispersion relationships about the Fermi momentum $p_F = \mu_q = 500$ MeV for the CFLK^0 phase with two different values of the strange quark mass. (The $M_s = 0$ dispersions are the same as in the top of Figure 7.1.) Qualitatively this has the same structure as Figure 7.3.

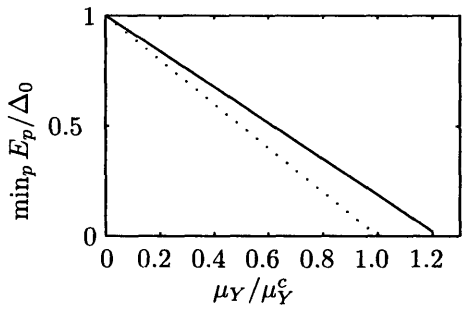

Figure 7.5: Physical gap of the lowest lying excitation as a function of the hypercharge chemical potential. The dotted line corresponds to the CFL phase: the phase transition to the gCFL occurs at $\mu_Y = \mu_Y^c$ where the gap vanishes. The solid line corresponds to the CFLK^0 state. The transition to a gapless phase is delayed by a factor of 1.22.

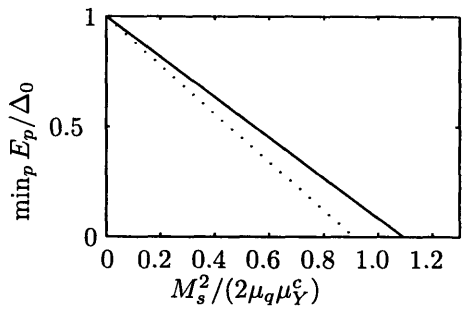

Figure 7.6: Physical gap of the lowest lying excitation as a function of the strange quark mass. The dotted line corresponds to the CFL phase and the solid line corresponds to the CFLK^0 phase. We have normalized the axes in terms of $\mu_Y^c = \Delta_0$ for comparison with the hypercharge chemical potential case. The CFL/gCFL transition occurs at a slightly smaller value of $M_s^2/\mu_q \approx 45.5$ MeV than the value of 46.8 MeV in [21, 26, 27]. This is due to the effects of the other parameters on the quasiparticle dispersion relations. We note that, as with μ_Y, the transition from the CFLK^0 to a gapless phase is delayed relative to the CFL/gCFL transition, but by a slightly reduced factor of 1.2. This is in qualitative agreement but quantitative disagreement with the factor of 4/3 found in [142]. The is most-likely the result of our fully self-consistent treatment of the condensate parameters.

7.4 Low-Energy Effective Theory

To describe the low energy physics of these models, we follow a well established procedure: identify the low-energy degrees of freedom and their transformation properties, identify the expansion parameters (power counting scheme), write down the most general action consistent with the symmetries and power counting, and determine the arbitrary coefficients by matching to experiment or another theory. In our case, we will match onto the mean-field approximation of the NJL model. The resulting low energy effective theory has been well studied [126, 159]: we use this presentation to establish our conventions, and to contrast the effective theory of QCD with that of the microscopic NJL model.

In this section we consider only the low-energy effective description of the fully gapped CFL and meson condensed phases such as the CFLK^0. The gapless phases also have a low-energy description which is similar to that discussed in Section 5.4, although, at this point, the mesons are sufficiently massive that one must reconsider whether or not the low-energy description is still valid. This shall be considered in future work.

7.4.1 Degrees of Freedom

The coset space in the NJL model is isomorphic to U(3)⊗U(3). This can be fully parametrized with two SU(3) matrices $\mathbf{X}$ and $\mathbf{Y}$ and two physical phases A and V which we physically one can identify with the condensates:

$$\sqrt{V^\dagger A}[\mathbf{X}]_{c\gamma} \propto \epsilon_{abc}\epsilon_{\alpha\beta\gamma}\langle\psi_L^{a\alpha}\psi_L^{b\beta}\rangle\,, \tag{7.24a}$$

$$\sqrt{V^\dagger A^\dagger}[\mathbf{Y}]_{c\gamma} \propto \epsilon_{abc}\epsilon_{\alpha\beta\gamma}\langle\psi_R^{a\alpha}\psi_R^{b\beta}\rangle\,. \tag{7.24b}$$

Thus, these transform as follows:

$$\mathbf{X} \to \mathbf{F}_L\mathbf{X}\mathbf{C}^\dagger, \tag{7.25a}$$

$$\mathbf{Y} \to \mathbf{F}_R\mathbf{Y}\mathbf{C}^\dagger, \tag{7.25b}$$

$$A \to e^{2i(\theta_R-\theta_L)}A, \tag{7.25c}$$

$$V \to e^{2i(\theta_R+\theta_L)}V \tag{7.25d}$$

Note that the condensation pattern $\mathbf{X} = \mathbf{Y} = \mathbf{1}$, $A = V = 1$ is unbroken by the residual symmetry where $\mathbf{F}_L = \mathbf{F}_R = \mathbf{C}$ and also by the Z_2 symmetries where $\theta_L, \theta_R = \pm\pi$. This is the reason for the extra factor of two in the phases. In QCD the degrees of freedom are similar, but one must consider

only colour singlet objects. Thus, the low-energy theory for QCD should include only the colour singlet combination

$$\mathbf{\Sigma} = \mathbf{X}\mathbf{Y}^\dagger \to \mathbf{F}_L \mathbf{\Sigma} \mathbf{F}_R^\dagger \tag{7.26}$$

and the colour singlet phases A and V. Note also that these have the following transformation properties under parity

$$\mathbf{X} \to \mathbf{A}^\dagger \mathbf{Y}, \tag{7.27a}$$
$$\mathbf{Y} \to \mathbf{A}\mathbf{X}, \tag{7.27b}$$
$$\mathbf{A} \leftrightarrow \mathbf{A}^\dagger, \tag{7.27c}$$
$$\mathbf{\Sigma} \leftrightarrow \mathbf{\Sigma}^\dagger. \tag{7.27d}$$

The field content of the effective theories is thus

H, η': Two singlet fields corresponding to the U(1) phases of A and V. The field associated with V is a scalar boson associated with the superfluid baryon number condensation. We shall denote this field H.

The field associated with A is a pseudo-scalar boson associated with the axial baryon number symmetry and shall be identified with the η' particle. As discussed in Section 7.1, the axial symmetry symmetry is anomalously broken in QCD and the η' is not strictly massless due to instanton effects, but these are suppressed at high density. We ignore these effects. Our NJL model thus contains no instanton vertex and our low-energy theory will contain no Wess-Zumino-Witten terms [160, 161]. It would be interesting to include both of these terms and repeat this calculation as these effects are likely not small [151].

π^a: Eight pseudo-scalar mesons π^a corresponding to the broken axial flavour generators. As colour singlets these remain as propagating degrees of freedom in both QCD and NJL models. These have the quantum numbers of pions, kaons and the eta and transform as an octet under the unbroken symmetry.

ϕ^a: Eight scalar bosons ϕ^a corresponding to the broken coloured generators. These are eaten by the gauge bosons in QCD and are removed from the low energy theory. This gives masses to eight of the gauge bosons and decouples them from low-energy physics. In the NJL model these bosons still remain as low energy degrees of freedom, but decouple from the colour singlet physics when one properly enforces colour neutrality.

There are additional fields and effects that should be considered as part of a complete low-energy theory, but that we neglect:

1. The appropriately "rotated electromagnetic field" associated with the unbroken $\mathrm{U}(1)_{\tilde{Q}}$ symmetry remains massless. Both the CFL and CFLK^0 states remain neutral with respect to this field, however, and we do not explicitly include it in our formulation.

2. The leptons are not strictly massless, but the electron and muon are light enough to consider in the low-energy physics. In particular, they contribute to the charge density in the presence of an electric chemical potential and at finite temperature. In this chapter, leptonic excitations play no role since we consider only $T = 0$ and both CFL and CFLK^0 quark matter is electrically neutral for $\mu_e = 0$. The leptons play an implicit role in fixing $\mu_{\tilde{Q}}$ such that $\mu_e = 0$ in both insulating phases.

To be explicit, we relate all of the dimensional physical fields H, η', ϕ^a and π^a to the phase angles through their decay constants: $H = f_H \tilde{H}$, $\eta' = f_{\eta'}\tilde{\eta}'$, $\phi^a = f_\phi \tilde{\phi}^a$, and $\pi^a = f_\pi \tilde{\pi}^a$. The two U(1) phases angles have a slightly different normalization because of the normalization of the generators. This normalization is chosen to match the kinetic terms in the original theory and matches [130, 131]: $\tilde{\eta}' = \sqrt{6}(\theta_R - \theta_L)$, and $\tilde{H}' = \sqrt{6}(\theta_R + \theta_L)$. The realization of these transformations in the microscopic theory is

$$\psi \to \exp\left\{ i \left[\frac{-\tilde{H}\mathbf{1} - \tilde{\eta}'\gamma_5}{2\sqrt{6}} + \tilde{\phi}^a \mathbf{r}^a + \tilde{\pi}^a \mathbf{f}_A^a \right] \right\} \psi \tag{7.28}$$

where

$$\mathbf{f}_{R,L}^a = (\mathbf{1} \pm \gamma_5) \otimes (-\boldsymbol{\lambda}_a^*) \otimes \mathbf{1}/2, \tag{7.29a}$$
$$\mathbf{c}^a = \mathbf{1} \otimes \mathbf{1} \otimes \boldsymbol{\lambda}_a, \tag{7.29b}$$
$$\mathbf{f}_A^a = \mathbf{f}_R^a - \mathbf{f}_L^a = \gamma_5 \otimes (-\boldsymbol{\lambda}_a^*) \otimes \mathbf{1}, \tag{7.29c}$$
$$\mathbf{f}_V^a = \mathbf{f}_R^a + \mathbf{f}_L^a = \mathbf{1} \otimes (-\boldsymbol{\lambda}_a^*) \otimes \mathbf{1}, \tag{7.29d}$$
$$\mathbf{r}^a = (\mathbf{f}_V^a - \mathbf{c}^a)/2 \tag{7.29e}$$

and the corresponding realization in the effective theory is

$$\mathbf{X} = \exp\{-i\tilde{\pi}^a \boldsymbol{\lambda}_a\} \exp\left\{i\tilde{\phi}^a \boldsymbol{\lambda}_a\right\}, \tag{7.30a}$$

$$\mathbf{Y} = \exp\{i\tilde{\pi}^a \boldsymbol{\lambda}_a\} \exp\left\{i\tilde{\phi}^a \boldsymbol{\lambda}_a\right\}, \tag{7.30b}$$

$$A = \exp\left\{2i\tilde{\eta}'/\sqrt{6}\right\}, \tag{7.30c}$$

$$V = \exp\left\{2i\tilde{H}/\sqrt{6}\right\}, \tag{7.30d}$$

$$\boldsymbol{\Sigma} = \exp\{-2i\tilde{\pi}^a \boldsymbol{\lambda}_a\}. \tag{7.30e}$$

7.4.2 Power Counting

In addition to Λ_{QCD} which separates the three light quarks from the heavy quarks, there are two primary scales in high density QCD: the quark chemical potential μ_q and the gap Δ. In the NJL model there is also a cutoff and the coupling constant: these are related by the gap equation when one holds μ and Δ fixed and the qualitative physics is not extremely sensitive to the remaining renormalization parameter.

Our low-energy theory is an expansion in the energy/momentum of the Goldstone fields. Thus, the expansion is in powers of the derivatives with respect to the scales μ and Δ. In this chapter, we shall only consider leading order terms: Systematic expansions have been discussed elsewhere (see for example [162]).

7.4.3 Kinetic Terms

To construct the low-energy theory we follow [126] and introduce coloured currents

$$\begin{aligned}
\mathbf{J}^\mu_X &= \mathbf{X}^\dagger \partial^\mu_{(v)} \mathbf{X} \to \mathbf{C}\mathbf{J}^\mu_X \mathbf{C}^\dagger, \\
\mathbf{J}^\mu_Y &= \mathbf{Y}^\dagger \partial^\mu_{(v)} \mathbf{Y} \to \mathbf{C}\mathbf{J}^\mu_Y \mathbf{C}^\dagger, \\
\mathbf{J}^\mu_\pm &= \mathbf{J}^\mu_X \pm \mathbf{J}^\mu_Y \to \mathbf{C}\mathbf{J}^\mu_\pm \mathbf{C}^\dagger.
\end{aligned}$$

In the presence of a finite density, we no longer have manifest Lorentz invariance and must allow for additional constants into our spatial derivatives

$$\partial^\mu_{(v)} = (\partial^0, v\partial^i)$$

to account for the differing speeds of sound. This chapter will be concerned with static properties, so we can neglect these. In principle, one must also

match these coefficients v. In QCD this matching, along with other coefficients, has been made with perturbative calculations at asymptotic densities [130, 131]. Our theory and states still maintain rotational invariance. Thus, to lowest order we have [126]

$$\begin{aligned}\mathcal{L}_{\text{eff}} =& \mathcal{L}_{\eta'} + \mathcal{L}_{\Sigma} + \mathcal{L}_{H} + \mathcal{L}_{\phi} + \cdots, \\ =& \frac{3f_{\eta'}^2}{4}\partial^{\mu}_{(v_{\eta'})}A^{\dagger}\partial_{(v_{\eta'})\mu}A - \frac{f_{\pi}^2}{4}\operatorname{Tr}[\mathbf{J}_{-}^{\mu}\mathbf{J}_{-\mu}] + \\ &+ \frac{3f_{H}^2}{4}\partial^{\mu}_{(v_H)}V^{\dagger}\partial_{(v_H)\mu}V - \frac{f_{\phi}^2}{4}\operatorname{Tr}[\mathbf{J}_{+}^{\mu}\mathbf{J}_{+\mu}] + \cdots, \\ =& \tfrac{1}{2}\partial^{\mu}_{(v_{\eta'})}\eta'\partial_{(v_{\eta'})\mu}\eta' + \tfrac{1}{2}\partial^{\mu}_{(v_{\pi})}\pi^{a}\partial_{(v_{\pi})\mu}\pi^{a} + \\ &+ \tfrac{1}{2}\partial^{\mu}_{(v_H)}H\partial_{(v_H)\mu}H + \tfrac{1}{2}\partial^{\mu}_{(v_{\phi})}\phi^{a}\partial_{(v_{\phi})\mu}\phi^{a} + \cdots.\end{aligned}$$

The neglected terms are of higher order in the derivative expansion. Note that our normalizations have been chosen so that this expression is canonically normalized to quadratic order in terms of the dimensionful fields.

The division of $\mathcal{L}_{\text{eff}}$ is natural [126] because it separates out the colour singlets. $\mathcal{L}_{\Sigma}$ depends only on $\boldsymbol{\Sigma}$ for example:

$$\mathcal{L}_{\Sigma} = -\frac{f_{\pi}^2}{4}\operatorname{Tr}[\mathbf{J}_{-}^{\mu}\mathbf{J}_{-\mu}] = \frac{f_{\pi}^2}{4}\operatorname{Tr}[\partial^{\mu}_{(v_{\pi})}\boldsymbol{\Sigma}^{\dagger}\partial_{(v_{\pi})\mu}\boldsymbol{\Sigma}].$$

Thus, with the exceptions noted above, the lowest-order low-energy effective theory of massless $N_f = 3$ QCD is

$$\mathcal{L}_{\text{QCD}} = \mathcal{L}_{\Sigma} + \mathcal{L}_{H} + \mathcal{L}_{\eta'} + \cdots \tag{7.31}$$

whereas the NJL model proper must also include $\mathcal{L}_{\phi}$.

7.4.4 Perturbations

We shall now consider two types of perturbations: chemical potentials and quark masses. To deal with these perturbations, we note that they enter the microscopic Lagrangian as

$$\mathcal{L}_{\text{SB}} = \psi_{L}^{\dagger}\boldsymbol{\mu}^{L}\psi_{L} + \psi_{R}^{\dagger}\boldsymbol{\mu}^{R}\psi_{R} + \psi_{R}^{\dagger}\mathbf{M}\psi_{L} + \psi_{L}^{\dagger}\mathbf{M}^{\dagger}\psi_{R}.$$

These terms break the original symmetries of the theory, but one can restore these symmetries by imparting the following spurion transformations to the masses and chemical potentials

$$\mathbf{M} \to \pm\sqrt{A^{\dagger}}(\mathbf{F}_{R}^{*} \otimes \mathbf{C})\mathbf{M}(\mathbf{F}_{L}^{*} \otimes \mathbf{C})^{\dagger}, \tag{7.32a}$$

$$\boldsymbol{\mu}^{L} \to (\mathbf{F}_{L}^{*} \otimes \mathbf{C})\boldsymbol{\mu}^{L}(\mathbf{F}_{L}^{*} \otimes \mathbf{C})^{\dagger}, \tag{7.32b}$$

$$\boldsymbol{\mu}^{R} \to (\mathbf{F}_{R}^{*} \otimes \mathbf{C})\boldsymbol{\mu}^{R}(\mathbf{F}_{R}^{*} \otimes \mathbf{C})^{\dagger}. \tag{7.32c}$$

The transformation $\mathbf{M} \to -\mathbf{M}$ preserves the residual Z_2 symmetries. This prevents odd powers of the mass terms from appearing in the chiral effective theory. In particular, the linear term dominant in the vacuum is forbidden resulting in an inverse mass-ordering of the mesons [130, 131] with the kaon being the lightest particle at high density. Finally, to preserve parity, we must have that

$$\mathbf{M} \to \mathbf{M}^\dagger. \tag{7.33}$$

All these symmetries must be restored in the effective theory: we are only allowed to couple these parameters to the fields in ways that preserve the global symmetries. To lowest order, this greatly limits the possible terms in the effective theory.

7.4.4.1 Chemical Potentials

In the case of the chemical potentials, we can go one step further by noting that the perturbations always appears in combination with the time derivative

$$\mathcal{L} = \psi^\dagger (i\partial_0 + \boldsymbol{\mu})\psi + \cdots . \tag{7.34}$$

One can thus promote the chemical potentials to a temporal component of a spurion gauge field and render the symmetries local in time:

$$\boldsymbol{\mu} \to (\mathbf{F}^* \otimes \mathbf{C})\,(\boldsymbol{\mu} + i\partial_0)\,(\mathbf{F}^* \otimes \mathbf{C})^\dagger. \tag{7.35}$$

The effective theory must also maintain these local symmetries. One concludes that the chemical potential perturbations can only appear through the introduction of covariant derivatives in the effective theory. In particular, consider adding independent colour and flavour chemical potential terms:

$$\boldsymbol{\mu}^{L,R} = \mu_{L,R}\mathbf{1} \otimes \mathbf{1} + \boldsymbol{\mu}_F^{L,R} \otimes \mathbf{1} + \mathbf{1} \otimes \boldsymbol{\mu}_C \tag{7.36}$$

where $\boldsymbol{\mu}_F$ and $\boldsymbol{\mu}_C$ are traceless 3×3 matrices. From these we may construct the following quantities that transform covariantly:

$$\nabla_0 \mathbf{X} = \partial_0 \mathbf{X} + i[\boldsymbol{\mu}_F^L]^* \mathbf{X} + i\mathbf{X}\boldsymbol{\mu}_C^\dagger, \tag{7.37a}$$

$$\nabla_0 \mathbf{Y} = \partial_0 \mathbf{Y} + i[\boldsymbol{\mu}_F^R]^* \mathbf{Y} + i\mathbf{Y}\boldsymbol{\mu}_C^\dagger, \tag{7.37b}$$

$$\nabla_0 \boldsymbol{\Sigma} = \partial_0 \boldsymbol{\Sigma} + i[\boldsymbol{\mu}_F^L]^* \boldsymbol{\Sigma} - i\boldsymbol{\Sigma}[\boldsymbol{\mu}_F^R]^T, \tag{7.37c}$$

$$\nabla_0 V = (\partial_0 + 2i\mu_V)\, V, \tag{7.37d}$$

$$\nabla_0 A = (\partial_0 + 2i\mu_A)\, A, \tag{7.37e}$$

where $\mu_V = \mu_R + \mu_L$ is a small adjustment of the baryon chemical potential $\mu_B/3$ and $\mu_A = \mu_R - \mu_L$ is the "axial baryon" chemical potential. For the rest of this chapter, we shall only consider vector chemical potentials that are real and symmetric: $\boldsymbol{\mu}_F^{L,R} = \boldsymbol{\mu}_F = \boldsymbol{\mu}_F^* = \boldsymbol{\mu}_F^\dagger$ etc. With these restrictions, the static potential in the effective theory is

$$V = \frac{f_\pi^2}{2}\operatorname{Tr}[\boldsymbol{\Sigma}^\dagger \boldsymbol{\mu}_F \boldsymbol{\Sigma} \boldsymbol{\mu}_F - \boldsymbol{\mu}_F^2] - 3f_H^2[\mu_V]^2 - 3f_{\eta'}^2[\mu_A]^2 + \\ + \frac{f_\phi^2}{4}\operatorname{Tr}\left[\left(\mathbf{X}^\dagger \boldsymbol{\mu}_F \mathbf{X} + \mathbf{Y}^\dagger \boldsymbol{\mu}_F \mathbf{Y} + 2\boldsymbol{\mu}_C\right)^2\right] + \cdots \quad (7.38)$$

to lowest order. The terms omitted include terms of higher order in the perturbation and small corrections due to the explicit violation of the "local" spurion symmetries by the cutoff.

From this expansion, we see that, by considering the dependence of the thermodynamic potential Ω on the various chemical potentials in different phases, one may extract all of the parameters of the effective potential. The do this, we simply add small perturbations to our model, compute Ω and fit the dependencies to the effective theory. The symmetry arguments here are very general. If the functional form is not correct, then we may conclude that: 1) We have missed important contributions to the effective theory, 2) there are errors in the microscopic calculation, or 3) there is a large amount of cutoff sensitivity (i.e. the cutoff breaks the symmetries badly).

7.4.4.2 Mass Terms

We now start a systematic expansion in the mass perturbations. First we note that terms linear in masses are forbidden by the residual Z_2 symmetry. This excludes the usual mass term found in chiral perturbation theory about the vacuum.

There are four terms quadratic in the quark masses allowed by the symmetries:

$$V_M^{(2)} = a_0 \operatorname{Tr}[\mathbf{M}^\dagger \mathbf{M}] + \quad (7.39)$$

$$+ a_3 A^\dagger \left(\operatorname{Tr}[\mathbf{M}\boldsymbol{\Sigma}\mathbf{M}\boldsymbol{\Sigma}] - \operatorname{Tr}[\mathbf{M}\boldsymbol{\Sigma}]\operatorname{Tr}[\mathbf{M}\boldsymbol{\Sigma}]\right) + \text{h.c.} + \quad (7.40)$$

$$+ a_6 A^\dagger \left(\operatorname{Tr}[\mathbf{M}\boldsymbol{\Sigma}\mathbf{M}\boldsymbol{\Sigma}] + \operatorname{Tr}[\mathbf{M}\boldsymbol{\Sigma}]\operatorname{Tr}[\mathbf{M}\boldsymbol{\Sigma}]\right) + \text{h.c.} + \quad (7.41)$$

$$+ a_8 \operatorname{Tr}[\boldsymbol{\Sigma}\mathbf{M}]\operatorname{Tr}[\boldsymbol{\Sigma}^\dagger \mathbf{M}^\dagger]. \quad (7.42)$$

Each of these has an undetermined coefficient. Our notations are consistent with the definitions given in [152] except for the the term a_8 which they neglect because it is suppressed in perturbative QCD.

To forth order, there is a rapid proliferation of possible terms. Only one is dominant for physics, however: this is the term that causes masses to act as chemical potential shifts. The other terms should be suppressed by Δ/μ. However, it is easy to check that this assumption is justified: missing dominant terms will appear clearly in the microscopic calculations.

$$V_M^{(4)} = c_{01}\,\mathrm{Tr}[\mathbf{M}^\dagger\mathbf{M}]\,\mathrm{Tr}[\mathbf{M}^\dagger\mathbf{M}] + c_{02}\,\mathrm{Tr}[\mathbf{M}^\dagger\mathbf{M}\mathbf{M}^\dagger\mathbf{M}] + \tag{7.43}$$

$$-c\,\mathrm{Tr}\left([\mathbf{M}^\dagger\mathbf{M},\mathbf{\Sigma}]^\dagger[\mathbf{M}^\dagger\mathbf{M},\mathbf{\Sigma}]\right) + \cdots, \tag{7.44}$$

where the last term is the piece that behaves as a chemical potential shift. In Appendix D we expand these expressions to determine the explicit form of the effective potential in terms of various perturbations and meson fields. The easiest way to extract the parameters is to use the expressions (D.15) in Appendix D.1 for maximal meson condensation with various mass parameters. Linear combinations of these are taken to subtract off undesired coefficients (such as c_{01} and c_{02} for example) and the remaining data are fitted to polynomials to extract the coefficients. Note that one should fit somewhat higher-order polynomials as there are definitely higher-order terms that we have neglected in these expressions.

To gain some idea of the scales involved, we note the results from perturbative QCD. These are obtained by matching the low-energy theory onto the high-density effective theory (HDET) formulation of perturbative QCD [130, 131, 138, 152]:

$$c \approx \frac{f_\pi^2}{8\mu^2} \sim 1/180 \approx 0.0056 > 0, \tag{7.45a}$$

$$a_3 \approx \frac{3\Delta_3^2}{4\pi^2} \sim 50\ \mathrm{MeV}^2 > 0, \tag{7.45b}$$

$$a_6 \approx \frac{3\Delta_6^2}{8\pi^2} \sim 5\ \mathrm{MeV}^2 > 0, \quad \text{and} \tag{7.45c}$$

$$a_8 \approx 0. \tag{7.45d}$$

These results can be compared with our numerical results obtained as described above by matching the effective theory to the NJL model with the

parameters (7.21) $\Lambda = 800$ MeV, $g\Lambda^2 = 1.385$, and $\mu_B/3 = 549.93$ MeV:

$$c = 0.03, \tag{7.46a}$$
$$a_0 = -0.05 \text{ GeV}^2, \tag{7.46b}$$
$$a_3 = 90 \text{ MeV}^2, \tag{7.46c}$$
$$a_6 = 0.1 \text{ MeV}^2, \tag{7.46d}$$
$$a_8 = -0.3 \text{ MeV}^2. \tag{7.46e}$$

These agree qualitatively with the perturbative QCD results, except that the a_8 term is quite significant. A similar type of matching procedure will be used to determine the coefficient coefficient f_π, and will be discussed in detail in Section 7.5.

The previous discussion has been focused on the effective potential where only static configurations are considered. There are a few terms that must also be considered in the full theory. In particular, the term with coefficient c should be roughly equivalent to adding chemical potentials $\boldsymbol{\mu}_F \approx \mathbf{M}^\dagger\mathbf{M}/(2\mu_q)$. The chemical potentials, however, always enter with time derivatives. Thus there are mixed terms that follow from the expansion of the covariant derivatives with a single time derivative.

There must be similar mass terms, and indeed, the following term is allowed:

$$c'i\left(\text{Tr}[\boldsymbol{\Sigma}^\dagger\dot{\boldsymbol{\Sigma}}\mathbf{M}\mathbf{M}^\dagger] - \text{Tr}[\dot{\boldsymbol{\Sigma}}\boldsymbol{\Sigma}^\dagger\mathbf{M}^\dagger\mathbf{M}]\right). \tag{7.47}$$

Note that these two terms must always appear in this combination to restore parity. The coefficient c' should be approximately related to c:

$$c' \approx 4\mu_q c. \tag{7.48}$$

This follows from identifying the terms with the chemical potential expansion. One may also explain this in terms of an approximate gauge symmetry [140] whereby the combination $\mathbf{M}^\dagger\mathbf{M}$ spuriously restores (approximately) the local flavour symmetry.

7.4.5 Charge Neutrality

As discussed in [148, 156, 157], the gauge invariance of QCD implies that homogeneous states must be colour neutral. This arises through tadpole diagrams that act as static colour sources $\mathbf{A}^0_C(\vec{\mathbf{p}} = 0)$ that ensure colour neutrality. These sources enter the NJL calculation as Lagrange multipliers to enforce neutrality.

One can see explicitly how these arise in the context of the effective theory. The gauge fields effect the local symmetry and thus couple through the derivatives in exactly the same way as the spurion coloured chemical potentials: $\mu_C \propto g_s \mathbf{A}_C^0$. Enforcing gauge-invariance induces an effective coloured chemical potential that makes (7.38) stationary with respect to variations of the gauge field, and thus equivalently,with respect to traceless variations of μ_C. Thus, we see that, to lowest order [126, 156, 157]

$$\mu_C = -\tfrac{1}{2}\left(\mathbf{X}^\dagger \mu_F \mathbf{X} + \mathbf{Y}^\dagger \mu_F \mathbf{Y}\right). \tag{7.49}$$

Inserting this into the (7.38), and considering only traceless perturbations, we see that the colour dependence drops out of the effective theory and we are left with the static effective potential involving only the colour singlet fields:

$$V = \frac{f_\pi^2}{2}\mathrm{Tr}[\mathbf{\Sigma}^\dagger \mu_F \mathbf{\Sigma} \mu_F - \mu_F^2] + V_M^{(2)} + V_M^{(4)} + \cdots. \tag{7.50}$$

In order to reproduce the physics of this in the NJL model, however, we must remove the coloured degrees of freedom. This is done by introducing colour chemical potentials to the NJL model as Lagrange multipliers and using them to impose colour neutrality [148, 156, 157]. This removes the colour dependence in the NJL model to all orders in the same way as it removes the colour dependence in (7.49) to lowest order. (In general, it is not sufficient to impose colour neutrality: one must also project onto colour singlet states (as well as states of definite baryon number). This projection is important for small systems, but likely has negligible cost for thermodynamically large systems such as neutron stars. See [163] for an explicit demonstration of this in the two-flavour case.)

The quarks also couple to the photon, and so we also must enforce electric neutrality. Enforcing electromagnetic gauge invariance will likewise induce an electric chemical potential μ_e that ensures electric neutrality. It turns out that both the CFL and the CFLK^0 quark matter are neutral under a residual charge $\tilde{Q}$ (both are $\tilde{Q}$ insulators). This means that one has some freedom in choosing the chemical potentials used to enforce neutrality. In particular, prior to the onset of gapless modes, one may choose these combinations so that $\mu_e = 0$. This is naturally enforced by including charged leptons in the calculation.

Once a charged excitation becomes gapless and the material becomes a conductor and a non-zero μ_e is required to enforce neutrality. The phase transition to the gCFL and gCFLK^0 is defined by exactly such a charged excitation. In chapter, we shall only consider the insulating phases, and thus

simply set $\mu_e = 0$. For further discussions of the metal/insulator properties of the CFL and gCFL we refer the reader to [21, 25, 27].

7.5 Kaon Condensation

We are now in a position to argue for the existence of a kaon condensed state. Consider performing an axial K^0 rotation on the parity-even CFL state. This is effected using (7.28) in the microscopic theory and using (7.30) in the effective theory with the parameter $\tilde{\pi}^6 = \theta$. Such a state is now described by

$$\Sigma = e^{2i\theta\lambda_6} = \begin{pmatrix} 1 & & \\ & \cos(\theta) & i\sin(\theta) \\ & i\sin(\theta) & \cos(\theta) \end{pmatrix}. \tag{7.51}$$

In the presence of a hypercharge chemical potential, the effective potential becomes [139, 140, 141]

$$V(\theta) = \frac{f_\pi^2 \mu_Y^2}{2}\left(\cos^2(\theta) - 1\right) + \cdots . \tag{7.52}$$

We see that this has a minimum for $\theta = \pm\pi/2$: this is the state with maximal K^0 condensation. We can also directly compute the difference in the thermodynamic potential densities between the CFL state and the $CFLK^0$ state:

$$\Omega_{CFLK^0} - \Omega_{CFL} = -\frac{f_\pi^2 \mu_Y^2}{2}. \tag{7.53}$$

Armed with this relationship, we can now turn to the microscopic calculation and determine the coefficient f_π. In Figure 7.7 we plot our numerical results so that the linear relationship (7.53) is evident. From the slope of the relationship we find that

$$f_\pi \approx 0.19\mu_q. \tag{7.54}$$

We note that this is in good numerical agreement with the perturbative QCD result [130, 131] of $f_\pi = 0.209\mu_q$. This striking agreement between two very different models arises from the fact that this coefficient is not very sensitive to the effects of the cutoff (which is different in the two theories) and gives encouraging support to the use of the NJL model to study QCD.

The equivalent relationship in the case of a strange quark mass requires one to include mass terms in the effective theory (see for example [138]), but the leading order effect can be determined by using the "effective" strange

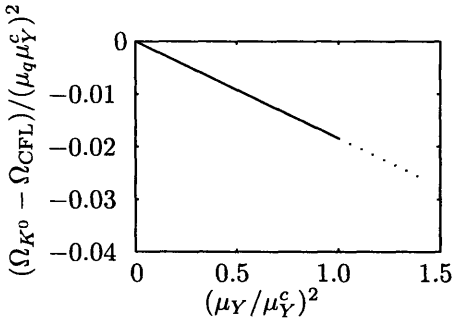

Figure 7.7: Numerical difference in energy densities between the kaon condensed CFLK^0 state and the CFL state at finite hypercharge potential μ_Y obtained from our microscopic NJL calculation. The units are scaled in terms of the quark chemical potential $\mu_q = 500$ MeV and the critical hypercharge chemical potential $\mu_Y^c = 25$ MeV. The quantities plotted were chosen so that the relationship will be linear if our calculation agrees with the effective theory result (7.53). The slope of the line is $m = -f_\pi^2/2\mu_q^2 \approx -0.018$ from which we can determine the effective theory parameter $f_\pi \approx 0.19\mu_q$. This is in good numerical agreement with the perturbative QCD result $f_\pi \approx 0.209\mu_q$ [130, 131]. The dashed extension shows the comparison between the CFLK^0 potential and the CFL potential, but beyond 1.0, the CFL becomes the gCFL and the energy dependence changes. We have not calculated the gCFL potential in this chapter, but plot this extension to emphasis that the CFLK^0 persists beyond the CFL/gCFL transition point at 1.0.

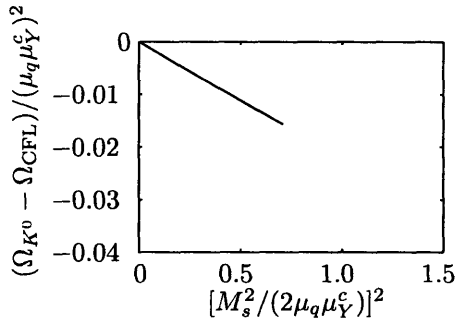

Figure 7.8: Numerical difference in energy densities between the kaon condensed CFLK^0 state and the CFL state at finite strange quark mass m_s obtained from our microscopic NJL calculation. The units are scaled in terms of the renormalized quark chemical potential $\mu_q \approx 500$ MeV and the critical hypercharge chemical potential $\mu_Y^c = 25$ MeV to facilitate comparison with Figure 7.7 and to emphasize the linear relationship implicit in (7.55). The slope of the line is $m \approx -f_\pi^2/2\mu_q^2 \approx -0.028$ which gives an effective $f_\pi \approx 0.21\mu_q$ which is consistent with our previous results. In comparison with Figure 7.7, the CFL→gCFL transition occurs somewhat earlier because the gap parameters are reduced with increasing strange quark mass. The curve cannot be extended as in Figure 7.7 because the free-energy of the CFL is no longer a constant as it was with a hypercharge perturbation.

quark chemical potential $\mu_Y \approx M_s^2/(2\mu_q)$ that follows from (7.3):

$$\Omega_{\mathrm{CFLK^0}} - \Omega_{\mathrm{CFL}} = -\frac{f_\pi^2}{2}\left(\frac{M_s^2}{2\mu_q}\right)^2. \tag{7.55}$$

It is important here to note, however, that the strange quark mass affects the solution in such a way that the gap parameters change and self-energy corrections modify the quark chemical potential and the constituent quark mass. It is the renormalized parameters that appear in this relation and in the perturbative QCD result. Thus, as a function of the bare parameters m_s, we have $M_s \propto m_s$ and $\mu_q - \mu_s \propto m_s^2$. Thus, we should see a linear relationship between $\Omega_{\mathrm{CFLK^0}} - \Omega_{\mathrm{CFL}}$ and M_s^4. We plot this relationship in Figure 7.8 and extract the slope which gives the relationship $f_\pi \approx 0.21\mu_q$. This is in qualitative agreement with our previous result. The slight numerical disagreement is due to effects of the strange quark mass that are not captured bu the chemical potential shift (7.3).

We pause here to point out a discrepancy between our results and similar work by Buballa [145]. Our results shown in Figure 7.8 suggests that kaon condensation occurs for all values of m_s in this simple model with $m_u = m_d = 0$ whereas Buballa finds that kaon condensation is only favoured for m_s sufficiently large. If the chemical potential shift were the only effect of a strange quark mass, then this would be inconsistent with (7.38). This is not, however, the correct expansion. Instead, one has, for maximal kaon condensation and $m_u = m_d = 0$:

$$\Omega_{\mathrm{CFLK^0}} - \Omega_{\mathrm{CFL}} = -(4a_6 + a_8)m_s^2 - 2cm_s^4 + \mathrm{O}(m_s^6). \tag{7.56}$$

This follows from expanding the second order and selected fourth order mass perturbation terms (D.5).

Buballa's results are consistent with the effective theory. The discrepancy is due to a different choice of parameters $\Delta \sim 100$ MeV and $\Lambda = 600$ MeV compared with our parameters $\Delta \sim 25$ MeV and $\Lambda \sim 800$ MeV. With the large gap, one is further from the perturbative QCD regime and the quadratic term appears to play a significant role. For example, using his parameters, we find $a_3 \approx 270$ MeV^2 which about a factor of 1/3 of the asymptotic QCD result of $a_3 \approx 760$ MeV^2 [145].

One can start to see this in our data (7.46): the coefficient a_8 is negative and comparable to a_6. The combination $4a_6 + a_8$ is still positive for our parameters, but as one moves away from the perturbative QCD regime, it appears to become larger so that the quadratic term dominates for small

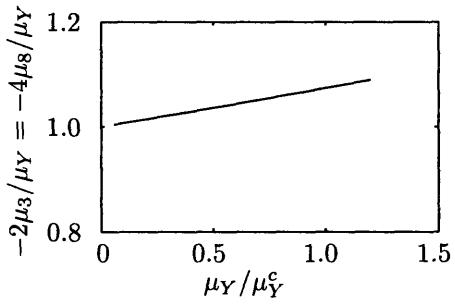

Figure 7.9: Chemical potentials required by the NJL model to enforce colour neutrality in the CFLK^0 phase with finite hypercharge chemical potentials. Note that the effective theory relationship (7.58) is satisfied from small chemical potentials. The linear deviation seen here reflects the missing terms in the effective theory that are of higher order in the perturbation μ_Y with a linear deviation here corresponds to μ_Y^2 terms missing in (7.58).

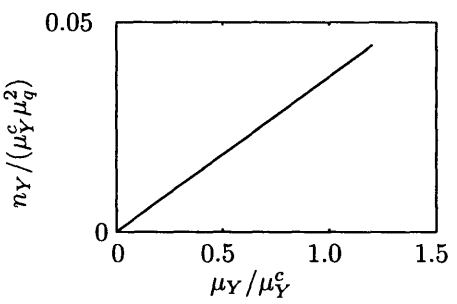

Figure 7.10: Hypercharge density of the CFLK^0 state in the presence of a hypercharge chemical potential μ_Y as obtained from our microscopic NJL model calculation. The units are scaled as in Figure 7.7 so that the relationship will be linear if the NJL model calculation agrees with the effective theory prediction (7.59). By determining the slope of this relationship we have another way of determining the coefficient f_π in the effective theory. The slope is $f_\pi^2/\mu_q^2 \approx 0.037$ which agrees with our previous determination of $f_\pi \approx 0.19\mu_q$.

m_s. Using Buballa's parameters, we qualitatively reproduce his results. A further discussion of these effects will be presented shortly [164].

There are a couple of other consequences that follow directly from the effective theory. One is the value of the coloured chemical potentials required to enforce neutrality. In our microscopic model, we have fixed the gauge (unitary gauge) by setting $\mathbf{X} = \mathbf{Y}^\dagger = \sqrt{\Sigma}$ for the axial rotations. The CFL state has $\mathbf{X} = \mathbf{Y} = \mathbf{1}$ while the CFLK^0 state has

$$\mathbf{X} = \mathbf{Y}^\dagger = \frac{1}{\sqrt{2}} \begin{pmatrix} \sqrt{2} & & \\ & 1 & i \\ & i & 1 \end{pmatrix}. \tag{7.57}$$

From (7.49) we have the following relationships required to enforce neutrality [156]

$$\mu_8 = -\mu_Y, \qquad \mu_3 = 0, \qquad \text{(CFL)}, \tag{7.58a}$$

$$\mu_8 = -\frac{1}{4}\mu_Y, \qquad \mu_3 = -\frac{1}{2}\mu_Y, \qquad \text{(CFLK}^0\text{)}. \tag{7.58b}$$

We plot these relationships in Figure 7.9. Note that they only hold for small perturbations where the effective theory is valid: this plot also demonstrates a departure from the lowest order effective theory as the perturbation is increased.

As a final demonstration of the effective theory, we calculate the hypercharge density. This is obtained by varying the thermodynamic potential with respect to the hypercharge chemical potential:

$$n_Y = -\frac{\partial \Omega}{\partial \mu_Y} \approx -f_\pi^2 \mu_Y (\cos^2(\theta) - 1). \tag{7.59}$$

There should be no hypercharge density in the CFL state and a density of $n_Y = f_\pi^2 \mu_Y$ in the CFLK^0 state. Indeed, the CFL supports no hypercharge density with $n_u = n_d = n_s$. The hypercharge density of the CFLK^0 phase is shown in Figure 7.10 and provides another method of extracting $f_\pi = 0.19\mu_q$.

7.5.1 A Note on the Meaning of $V(\theta)$

We make a few remarks here about the meaning of the effective potential $V(\theta)$. In particular, one might be tempted to try and compute the functional form of $V(\theta)$ in the microscopic theory to facilitate matching with the effective theory. Such an approach will generally fail because one is allowed to pick an arbitrary parametrization of the Goldstone fields as long as they

leave the kinetic terms unaltered [165, 166]. Physical quantities must be invariant under this change of parametrization: thus the spectrum about the minimum, densities, and energy differences are reasonable quantities to compare in each theory. The general form of the effective potential away from the stationary points, however, is rather arbitrary.

As an example: consider starting with the parity even CFL state in the presence of a finite μ_Y. This state corresponds to a stationary point of the effective potential and is a self-consistent solution to the gap-equations. One can then form a continuum of "kaon rotated" states $|\theta\rangle$ by applying the broken symmetry generators to this state. One might expect to find $V(\theta)$ by computing the energy of these states, but instead one finds an expression that is only valid locally about the stationary point. The reason is twofold: First, there is not a unique "kaon rotated" state $|\theta\rangle$. This state has many other parameters corresponding to other "directions" (such as the gap parameters Δ, the chemical potential corrections etc.) The only way to uniquely determine these is to solve the gap-equations, and these only have well-defined solutions at stationary points. Second, the generators of the pseudo-Goldstone bosons in the presence of perturbations are not the same as the generators of the true Goldstone bosons in the unbroken model: the pseudo-Goldstone bosons have some admixture of these other "directions".

This becomes even more evident when you analyze the CFLK^0 state with a large perturbation: one can try to "undo" the kaon rotation by applying the appropriate symmetry generators to minimize the parity violating condensates, but one finds that there is no way to do this. One must also transform the other parameters in order convert a CFLK^0 state back to a parity even CFL state.

7.6 Conclusion

We have explicitly found self-consistent solutions within a microscopic NJL model exhibiting the feature of kaon condensation in a colour-flavour–locked state. Using these solutions, we have demonstrated that by properly enforcing gauge neutrality, one can remove the extraneous coloured degrees of freedom from the NJL model and effectively model kaon condensation in high-density QCD. In particular, the microscopic calculations can be matched onto the low-energy effective theory of QCD. Using this matching procedure and considering states of maximal meson condensation, we determined the following parameters of the low-energy effective theory when we

fix $\Lambda = 800$ MeV, $g\Lambda^2 = 1.385$, and $\mu_B/3 = 549.93$ MeV:

$$f_\pi = 0.19\mu_q, \tag{7.60a}$$
$$c = 0.03, \tag{7.60b}$$
$$a_0 = -0.05 \text{ GeV}^2, \tag{7.60c}$$
$$a_3 = 90 \text{ MeV}^2, \tag{7.60d}$$
$$a_6 = 0.1 \text{ MeV}^2, \tag{7.60e}$$
$$a_8 = -0.3 \text{ MeV}^2. \tag{7.60f}$$

Of these, f_π is in good quantitative agreement and c, a_3, and a_6 are in good qualitative agreement with the perturbative QCD results. The parameter a_8 seems somewhat larger than expected from QCD. Furthermore, there is evidence [145] that as one moves further from the perturbative regime, a_8 becomes larger leading to a qualitatively different picture.

Furthermore, our solutions are fully self-consistent: no approximations have been made beyond the mean-field approximation and restricting our attention to isotropic and homogeneous states. We find that our results agree qualitatively with both the expected properties of the CFLK^0 phase based on effective theory calculations, and with the previous numerical calculations of the CFL/gCFL transition.

Quantitatively we find that the phase transitions occur at slightly smaller parameter values than previously found in the literature. Concerning the CFL/gCFL transition, we find that the gap parameters are reduced by a few percent compared with those presented in [21, 26, 27], and subsequently, the critical M_s is also a few percent lower. Concerning the CFLK^0/gCFLK^0 transition, we find that the transition occurs about a factor of 1.2 higher than the CFL/gCFL transition. This is in qualitative agreement but quantitative disagreement with the factor of 4/3 calculated in [142].

The next step is to use this microscopic model to determine the phase structure of high-density QCD in the region where the gapless modes appear. We suspect that the gCFLK^0 state will survive somewhat longer than the gCFL state on account of its lower condensation energy, but a quantitative comparison is required. Extrapolation to finite temperature is also a trivial extension in our formalism. What makes the excursion to finite temperatures and into the gCFLK^0 non trivial is the fact that a non-zero electric chemical potential μ_e will be required to enforce neutrality. This will also induce further condensation of the charged mesons that must be included to obtain self-consistent solutions. In the presence of several simultaneous meson condensates, the number of variational parameters increases

dramatically, limiting the effectiveness of our fully self-consistent methods.

A somewhat more challenging direction is to consider the effects of instantons and finite up and down quark masses and investigate other forms of meson condensation. Preliminary investigations indicate, however, that the number of parameters required to close the gap equations in the presence of arbitrary meson rotations may be prohibitively large to continue with fully self-consistent calculations. This should still be tractable with carefully made approximations, and is worth considering as the effects are large enough to qualitatively alter the results.

Part IV

Appendix

Appendix A

Thermodynamics and Statistical Mechanics

In this chapter, we review some notions about thermodynamics and statistical mechanics. Much of this material is based on the account by Sewell [167]. This gives a very nice modern account of the formal aspects of thermodynamics and statistical mechanics. It is mathematical, but uses as little math as needed to make accurate claims.

A.1 Quantum Statistical Mechanics

Consider a system and a some experiments that can be performed with a set of possible outcomes $\{e_1, e_2, \cdots\}$. Suppose, further, that we have many "identical" copies of this system. If we repeat the experiment N times, then an outcome can be labelled by the numbers $(n_1, n_2, \cdots)$ where n_i describes how many times outcome e_i was obtained. Our best description of the system (without discovering further observables) is to associate with each state e_n the probability

$$\lim_{N\to\infty} \frac{n_i}{N} = p_i. \tag{A.1}$$

We call such a description—the set of outcomes $\{e_1, e_2, \cdots\}$ and the probability measure over this set of outcomes $p \equiv (p_1, p_2, \cdots)$—a "state" ρ. The utility of this probabilistic description is that it allows use to characterize systems without complete knowledge. Classically, one might only have access to a limited number of observables. The dynamics of the unknown degrees of the system are thus responsible for the different possible outcomes which we must describe probabilistically. Another possibility is that one might only have access to part of a system—it might be coupled to a large and complex "heat bath" for example—and interactions with the environment prevent complete knowledge.

A.1.1 Expectation Values

Given a state ρ, one can compute the expectation value of some observable $\widehat{\mathbf{A}}$

$$\langle \widehat{\mathbf{A}} \rangle = \rho(\widehat{\mathbf{A}}) = \sum_n p_n A_n \tag{A.2}$$

where A_n is the result of measuring $\widehat{\mathbf{A}}$ on the pure state defined by e_n.

To formalize the notion of incomplete states for a quantum mechanical system, we assume that the set of outcomes corresponds to a set of commuting operators such that each outcome e_n is associated with an eigenstate $|n\rangle$. The state of a thermodynamic ensemble can thus be described by the density operator (density matrix)

$$\widehat{\boldsymbol{\rho}} \sum_n p_n |n\rangle \langle n| . \tag{A.3}$$

Mathematically, the set of all states $\mathcal{P}$—the set of all density matrices in quantum mechanics—is convex and the extremal points are pure states π_i which have exactly one non-zero $p_i = 1$. The quantum mechanical expectation value is thus given by

$$\langle \widehat{\mathbf{A}} \rangle_\rho = \mathrm{Tr}[\widehat{\mathbf{A}} \widehat{\boldsymbol{\rho}}]. \tag{A.4}$$

A.1.2 Degrees of Freedom: Finite vs. Infinite

We shall consider quantum systems defined by their Hamiltonian $\widehat{\mathbf{H}}$. If the system is finite, then all computations with the density operator $\widehat{\boldsymbol{\rho}}$ are finite and everything is well defined. There are subtleties when working with the thermodynamics of quantum systems that are discussed carefully in [167]. For example, to properly discuss "phase transitions", one must formally consider systems with infinitely many degrees of freedom: in finite systems, tunnelling ensures that all phase transitions are formally smooth. As what we do here is fairly standard, we shall not be concerned with these subtleties, but they should be considered whenever less conventional systems are analyzed.

A.1.3 Entropy

Entropy is a bit of an elusive concept. One concrete way of understanding entropy comes from information theory. The entropy of a state $p \in \mathcal{P}$ is a measure of the "impurity" of the state,

$$S(p) = -\sum_i p_i \ln p_i : \tag{A.5}$$

Pure states have zero entropy while mixed states have positive entropy. The quantum mechanical version of this for finite systems is

$$S(\widehat{\rho}) = -\operatorname{Tr}[\widehat{\rho}\ln\widehat{\rho}]. \tag{A.6}$$

A.2 Ensembles

Statistical mechanics is founded on the idea that one can describe a complicated system with a small number of macroscopic variables which represent measurable quantities. The idea is that there are many microscopic configurations (states) that will yield the same macroscopic measurements and hence will be indistinguishable to the observer. We now make an assumption:[1]

Assum$^{\underline{n}}$ A.2.1: *We assume that all states with a given fixed set of measurable properties are equally likely to occur, and thus should be equally weighted in the ensemble.*

Using this assumption, one can perform well-defined statistical averaging of quantities over an ensemble of states to approximate the time averaging effected by the measurement of equilibrium properties. This statistical averaging can performed over one of several types of ensembles depending on the appropriate physical system in question:

Micro-canonical Ensemble: This ensemble is relevant for completely isolated systems where the energy, particle number and other conserved quantities are held fixed.

Macro-canonical (Gibbs) Ensemble: This ensemble is allowed to exchange energy with other systems in such a way that the "temperature" is help fixed rather than the energy. The inverse-temperature β enters as a Lagrange multiplier. As we shall discuss below, this has several important theoretical advantages over the micro-canonical ensemble.

Grand-canonical Ensemble: In this ensemble, all of the conserved quantities (particle number in particular) are allowed to fluctuate in the same manner as the energy in the macro-canonical ensemble. Instead,

[1] This assumption is justified by ergodic properties of the time-evolution of the system. In particular, it fails if there are conserved quantities. These are dealt with specially as discussed in Section A.3.1. Ergodicity is a rather strong assumption, and not required. Chaotic systems with strange attractors for example fail in this respect. See for example http://tsallis.cat.cbpf.br/TEMUCO.pdf for an updated bibliography.

the respective Lagrange multipliers (the chemical potentials for example) are held fixed. This ensemble is particularly useful for discussing phase structures as the relevant phase diagram comprises only pure states.

We shall now discuss the details of these ensembles.

A.2.1 Micro-canonical Ensemble

Systems where one holds all of the conserved quantities, (energy, particle number etc.) fixed are said to be in the micro-canonical ensemble. Systems that are perfectly isolated from their environment are best described by micro-canonical ensembles.

Suppose that the quantity N is measure of the "size" of the system (for example, the number of particles in the system). One can argue that, for large ergodic systems, the statistical averages are dominated by the state with maximal entropy (we shall perform this minimization later when we can justify the $N \to \infty$ limit):

$$S(E) \approx \max_{\substack{\rho(\widehat{\mathbf{H}})=E \\ \rho(\widehat{\mathbf{N}})=N \\ \rho(\widehat{\mathbf{1}})=1 \\ \vdots}} S(\widehat{\boldsymbol{\rho}}). \tag{A.7}$$

If this is true, then one can simply work with the state of maximal entropy. This approach, however, is typically only useful for gases as the system "size" itself must be taken to be very large in order justify the maximal entropy principle.[2]

Another problem with the micro-canonical ensemble for non-gaseous phases is that isolated systems have a tendency to phase separate. Liquids, for example, do not expand to fill their container. Thus, one ends up studying the equilibrium of a gas and a liquid: each pure phase is no-longer described as an isolated system (they exchange energy, particle number etc.), but is actually more appropriately described by another ensemble. The appearance of "mixed" phases—heterogeneous mixtures of different phases—on the phase diagram of micro-canonical ensembles can greatly complicate the analysis of the phase structure. The grand-canonical ensemble alleviates this problem.

[2]One may always solve the problem with "brute force" methods rather that employing a maximal entropy principle. For these techniques, often applicable for small systems, the micro-canonical ensemble can be very useful, but this is best done numerically.

A.2.2 Macro-canonical (Gibbs) Ensemble

There is another reason to disfavour the micro-canonical ensemble: It is very difficult in practice to make a perfectly isolated system. Instead, it is easier to consider systems in contact with a thermal bath. Empirically, we know that the composition of a thermal bath makes little difference, as long as it is large and has a quasi-continuous spectrum. This led Gibbs to suggest that one consider a heat bath as $N-1$ copies of the system under consideration weakly coupled such that they can exchange energy.

One advantage of this approach is that the limit $N \to \infty$ represents the limit of an ideal heat bath which is quite realistic and attainable in practice. In this setup, we imagine distributing a fixed amount of energy NE over the ensemble of N systems. Again, we maximize entropy, but now over the entire ensemble. We now require the total ensemble energy NE to be fixed, but the energy of any individual system need not be fixed. As a result, we only restrict that the average energy $E = \langle \widehat{\mathbf{H}} \rangle$ be fixed over the ensemble. To do this, we introduce a Lagrange multiplier β. Thus, we now maximize the function

$$f = \max_{\substack{\rho(\widehat{\mathbf{N}})=N \\ \rho(\widehat{\mathbf{1}})=1 \\ \vdots}} (S - \beta E) = \max_{\substack{\rho(\widehat{\mathbf{N}})=N \\ \rho(\widehat{\mathbf{1}})=1 \\ \vdots}} \mathrm{Tr}\left(-\widehat{\boldsymbol{\rho}} \ln \widehat{\boldsymbol{\rho}} - \beta \widehat{\boldsymbol{\rho}} \widehat{\mathbf{H}}\right). \tag{A.8}$$

Instead of maximizing the function f, one usually scales this and instead minimizes the function $F = -f/\beta$ which is known as the Helmholtz free energy. Thus, we arrive at the statistical formulation of equilibrium thermodynamics that one can represent the equilibrium properties of a system coupled to an ideal thermal bath at temperature T by the normalized state $\widehat{\boldsymbol{\rho}}_\beta$ that minimizes the Helmholtz free energy F:

$$F(T) = \min_{\substack{\rho(\widehat{\mathbf{N}})=N \\ \rho(\widehat{\mathbf{1}})=1 \\ \vdots}} \mathrm{Tr}[\widehat{\boldsymbol{\rho}} \widehat{\mathbf{H}} + T \widehat{\boldsymbol{\rho}} \ln \widehat{\boldsymbol{\rho}}]. \tag{A.9}$$

A.2.3 Grand-canonical (Thermodynamic) Ensemble

The macro-canonical ensemble gives us a justification of the maximal entropy principle through the $N \to \infty$ limit of an ideal thermal bath. Unfortunately, the analysis of the phase structure in the macro-canonical ensemble may still be complicated by the presence of mixed phases due to the constraints on the conserved quantities. We may alleviate this by using Gibbs'

construct, but allowing the other conserved quantities (especially particle number) to fluctuate throughout the ensemble. For each conserved quantity, we introduce an additional Lagrange multiplier (for particle number we introduce the chemical potential μ) to fix the ensemble average. In the following, we consider only particle number, but the other conserved quantities should be dealt with similarly. Finally, we should also only consider properly normalized states $\mathrm{Tr}\,\widehat{\boldsymbol{\rho}} = 1$. This constraint is also dealt with by introducing the Lagrange multiplier λ. The result is that we minimize the "thermodynamic potential" Ω

$$\Omega = \min_{\widehat{\boldsymbol{\rho}}} (F - \lambda \,\mathrm{Tr}\,\widehat{\boldsymbol{\rho}} - \mu N) = \min_{\widehat{\boldsymbol{\rho}}} \mathrm{Tr}\left[\frac{\widehat{\boldsymbol{\rho}} \ln \widehat{\boldsymbol{\rho}}}{\beta} + \lambda \widehat{\boldsymbol{\rho}} + \widehat{\boldsymbol{\rho}}\left(\widehat{\mathbf{H}} - \mu \widehat{\mathbf{N}}\right)\right]. \tag{A.10}$$

The minimization is now with respect to an unconstrained density operator $\widehat{\boldsymbol{\rho}}$. Assuming that S, E and N are differentiable functions of the density operator, the condition for this to be an extremum $\partial\Omega/\partial\widehat{\boldsymbol{\rho}} = 0$ gives us

$$\widehat{\boldsymbol{\rho}} = e^{-(1+\lambda/\beta)} e^{-\beta(\widehat{\mathbf{H}} - \mu\widehat{\mathbf{N}})}. \tag{A.11}$$

The normalization condition simply defines the partition function:

$$e^{1+\lambda/\beta} = Z = \mathrm{Tr}[e^{-\beta(\widehat{\mathbf{H}} - \mu\widehat{\mathbf{N}})}]. \tag{A.12}$$

Using this to eliminate λ, we have the following state with maximal entropy

$$\widehat{\boldsymbol{\rho}}(\beta) = \frac{e^{-\beta\widehat{\mathbf{H}}}}{\mathrm{Tr}[e^{-\beta\widehat{\mathbf{H}}}]}. \tag{A.13}$$

We identify the parameter[3] $\beta = 1/T$ in terms of the absolute temperature.

Note that we now have a well-defined state of maximal entropy at fixed temperature and chemical potential that may be used to performing statistical averages. This is applicable when considering systems coupled to an ideal heat bath of fixed temperature T and an ideal particle bath of fixed chemical potential μ.

In terms of the partition function, we have[4]

$$F = -T \ln(Z). \tag{A.15}$$

[3]We use natural units such that Boltzmann's constant $k_B = 1$ here: $\beta = 1/(k_B T)$

[4]Note that this relationship is easy to remember in this form:

$$e^{-\beta\Omega} = \mathrm{Tr}[e^{-\beta(\widehat{\mathbf{H}} - \mu\widehat{\mathbf{N}})}]. \tag{A.14}$$

Finally, one can view the unnormalized density operator $\widehat{\boldsymbol{\rho}}_0(\beta) = \exp(-\beta\widehat{\mathbf{H}})$ as a function of β, in which case, it satisfies the differential equation

$$\frac{\partial\widehat{\boldsymbol{\rho}}_0}{\partial\beta} = -\widehat{\mathbf{H}}\widehat{\boldsymbol{\rho}}_0 \tag{A.16a}$$

with the initial condition at $\beta = 0$ ($T = \infty$)

$$\widehat{\boldsymbol{\rho}}_0(0) = \widehat{\mathbf{1}}. \tag{A.16b}$$

This provides a starting point for defining the perturbative expansion of the partition function. Integrating this differential equation in the interaction picture gives rise to the "time" ordering etc.

The thermodynamic limit that justifies the maximal entropy principle is the limit of an ideal thermodynamic bath of fixed temperature and chemical potential rather than properties of the system. Thus, there is no problem in principle with the thermodynamic limit: even a system containing only a few particles can be studied as long as it can be weakly coupled to a large bath. To compare, the use of a maximal entropy principle in the micro-canonical ensemble can only be justified if the size of the system itself is large.

One might argue that many of the systems that we shall discuss in this thesis (neutron stars and cold atom systems) are well-described by the micro-canonical ensemble. For the entire system, this may be true (though it is very difficult to achieve isolation in practise), but consider a finite region in the interior of such a system. This finite region may exchange both energy and particles with the surrounding regions. Furthermore, for large systems, the collection of "surrounding regions" behaves very much like Gibbs' collection of systems. Thus, one may do very well by studying the phases in the grand-canonical ensemble and then patching them together to form the entire system.

A.3 Thermodynamic Variables

We summarize here the first two laws of thermodynamics. The first law states that energy is conserved. This can be formulated by saying that there is a differential form for the heat required by a system to change:

$$\mathrm{d}Q = \mathrm{d}E + P\mathrm{d}V + \vec{\boldsymbol{\Theta}} \cdot \mathrm{d}\vec{\mathbf{N}}. \tag{A.17}$$

The second law says that for adiabatic changes of state, this can be written as a form $T\mathrm{d}S$ where $T = \beta^{-1}$ is the temperature and S is extensive (the

thermodynamic entropy). Combining these, we have

$$T\mathrm{d}S = \mathrm{d}E + P\mathrm{d}V + \vec{\Theta} \cdot \mathrm{d}\vec{\mathbf{N}}. \tag{A.18}$$

Putting $Q_0 = E$, $\Theta_0 = 1$, $\theta_k = \beta\Theta_k$ and $p = \beta P$ we have the familiar thermodynamic relationship

$$\mathrm{d}S = p\mathrm{d}V + \vec{\theta} \cdot \vec{\mathbf{N}} \tag{A.19}$$

where the variables θ are intensive "potentials" (these include the chemical potentials for example) and the variables $\vec{\mathbf{N}}$ are the conserved "charges" for the system.

A.3.1 Conserved Quantities

The reason that the energy E has been singled out in the previous discussion is because it is a conserved quantity of the system (as long as the Hamiltonian is time-independent). If there are conserved quantities such as particle number, volume etc. then the assumption A.2.1 that all micro-states states are equally likely is clearly false. It is only possibly to justify this assumption when one only considers states that have held fixed these conserved quantities.

Suppose one wants to study a box which contains N particles and has volume V. The Hamiltonian for this system will conserve both N and V, and so we must only consider states which have a definite volume and particle number. The formalism is the same as before, but now one considers the Helmholtz free energy as a function of these parameters as well: $F(T, V, N, \cdots)$ and one minimizes over configurations where these quantities are well-defined. This is how standard thermodynamics proceeds.

Generically, these quantities are properties of the system as specified in the Hamiltonian. We shall refer to them as Q_i where Q_0 is the energy of the system. To each of these we can defined the thermodynamical conjugate θ_i. These appear as the Lagrange multipliers introduced to enforce the appropriate constraint while maximizing the entropy. Thus, we have seen that $\theta_0 = \beta$. In this formalism, one finds that $p = \beta P$—the reduce pressure—is conjugate to the volume V etc.

Introducing all appropriate multipliers, we determine the thermodynamic state by maximizing:

$$\max_{\mathrm{Tr}[\vec{\rho}]=1} S - pV - \vec{\theta} \cdot \vec{\mathbf{N}}. \tag{A.20}$$

This expression follows the maximum entropy reasoning very nicely, but the quantity (A.20) turns out to be zero for extensive systems (see Section A.4.5) and is thus not of much use physically. Instead, we use other Legendre transforms which represent physical quantities as thermodynamic potentials.

A.4 Thermodynamic Potentials

To carefully define the thermodynamic variables for quantum systems and the resulting thermodynamics is a bit involved due to the requirement of working with systems containing infinitely many degrees of freedom.[5] We proceed a little less carefully and refer the reader to [167] Chapter 6.4 for a more thorough discussion.

We start with the Helmholtz free energy F defined by (A.9). This is to be minimized at fixed temperature, volume and particle number. From this, we can Legendre transform to one of several thermodynamic potentials to remove constraints by introducing Lagrange multipliers. One of the most useful is to form the Gibbs free energy:

$$\Omega(T, \vec{\mu}) = \min \left(F - \vec{\mu} \cdot \vec{\mathbf{N}} \right). \tag{A.21}$$

The minimization is over all physical states. This can be related to the expression (A.20). The appropriate Legendre transform is

$$-\beta\Omega = pV = \beta PV = \max_{\substack{\mathrm{Tr}[\widehat{\rho}]=1 \\ V(\widehat{\rho})=V}} S - \vec{\theta} \cdot \vec{\mathbf{Q}} \tag{A.22}$$

where one includes the energy (one of the conserved quantities $Q_0 = E$) and the inverse temperature (one of the generalized "potentials" $\theta_0 = \beta$). The combination $S - \beta E = -\beta F$ defines the Helmholtz free-energy F.

A.4.1 Convexity

As a result of the minimization principles, one can prove that Ω is a convex function of the temperature and chemical potentials. Here we prove convexity over $\vec{\mu}$: the extension to include T can be done similarly by returning to the maximum entropy principle (where T enters as a Lagrange multiplier). Let $\Omega(\rho, \vec{\mu}) = F - \vec{\mu} \cdot \vec{\mathbf{N}}$ be the minimand for an arbitrary state ρ.

[5] In finite systems, for example, there is always a unique ground state which is fully symmetric due to the possibility of tunnelling. There is no possibility for spontaneous symmetry breaking, or phase transitions.

The convexity of $\Omega(\vec{\mu})$ requires that, the affine combination of $x\Omega_1 + (1-x)\Omega_2$ where $\Omega_1 = \Omega(\vec{\mu}_1)$ etc. be less than $\Omega(\vec{\mu})$ at the actual intermediate chemical potential $\vec{\mu} = x\vec{\mu}_1 + (1-x)\vec{\mu}_2$ for all points $\vec{\mu}_1$ and $\vec{\mu}_2$. This follows naturally from the minimization:

$$\begin{aligned} x\Omega_1 + (1-x)\Omega_2 &= x \min_\rho [F(\rho) - \vec{\mu}_1 \cdot \vec{\mathbf{N}}(\rho)] + (1-x) \min_\rho [F(\rho) - \vec{\mu}_2 \cdot \vec{\mathbf{N}}(\rho)], \\ &\leq \min_\rho \Big(x[F(\rho) - \vec{\mu}_1 \cdot \vec{\mathbf{N}}(\rho)] + (1-x)[F(\rho) - \vec{\mu}_2 \cdot \vec{\mathbf{N}}(\rho)] \Big), \\ &= \min_\rho F(\rho) - (x\vec{\mu}_1 + (1-x)\vec{\mu}_2)\vec{\mathbf{N}}(\rho), \\ &= \Omega(x\vec{\mu}_1 + (1-x)\vec{\mu}_2). \end{aligned}$$

The convexity is equivalent to the matrix of partials $\partial^2\Omega/\partial\mu_a\partial\mu_b$ being negative semi-definite and is required for thermodynamic stability. Thus, one often sees stability conditions expressed in terms of such partials.

The convexity also allows one to determine properties of other ensembles. For example, if the system is extensive, then one can show that in the thermodynamic limit, the ensembles are equivalent. Consider for example a two-component system subject to constraints of fix particle number and volume. Generically such a system may contain multiple phases as described by Gibb's phase rule.

A.4.2 Equivalence of Ensembles

Physically, the various thermodynamic ensembles are not equivalent. In the micro-canonical ensemble, the energy is exactly fixed, whereas it fluctuates in the other ensembles. The fluctuations in the conserved quantities, however, typically scale as $\sqrt{N}$ where N describes the size of the ensemble (number of particles, volume etc.). Thus, in the thermodynamic limit—infinite size—the fluctuations become insignificant: $\delta E/E \sim \sqrt{N}/N \to 0$. In this sense, the ensembles are equivalent in the thermodynamic limit.

When discussing large volumes of a substance in equilibrium, then, we prefer to use the grand-canonical ensemble for the reasons discussed in Section A.2.3. One of the main benefits is that one need not consider the complications associated with mixed phases in this ensemble.

A.4.3 Mixed Phases and the Phase Rule

Mixtures of phases occur when one fixes too many properties of a system and are characterized by the Gibbs Phase Rule (see [168] for some extensive

applications of this). The phase rule relates the number of chemically independent components of a system c, the number of coexisting phases p and the number of degrees of freedom f:

$$f = c - p + 2. \tag{A.23}$$

For example, consider water ($C = 1$). The possible degrees of freedom are the temperature T, pressure P, volume V and particle number N. Consider vapour in a closed system with fixed N and V. As a vapour, the pressure and temperature can still vary. There are thus $f = 2$ degrees of freedom when there is a single phase $f = 1 - 1 + 2 = 2$. Now consider the container with a mixture of water and vapour. The pressure will now be fixed by the vapour pressure of the system and given as a function of the temperature $P(T)$, thus, only the temperature of the system may be varied independently and there is only one degree of freedom $f = 1 - 2 + 2$. Finally, at the triple point with ice, liquid, and vapour, both the temperature and pressure are fixed and there are no degrees of freedom $f = 1 - 3 + 2 = 0$.

The phase rule is simply specifies the dimensions of the coexistence manifolds in phase space and follows from simply counting the number of variables describing the system and the number of equilibrium constraint and the equation of state. We have the following variables: volume V, pressure P, temperature T, and the various particle numbers $(N_1, N_2, \ldots, N_c)$: (2+c) variables per phase in total. Equilibrium between phases requires equal P, T, and $(\mu_1, \mu_2, \ldots, \mu_c)$. Each phase is also described by an equation of state. Thus, for a system with p phases, there are $p(2 + c)$ variables describing the volumes, temperatures etc. of each phase. There are $p - 1$ interfaces at which each of the $(2 + c)$ intensive variables must be equilibrated. Finally, there are p equations of state. Counting, we have

$$f = p(2 + c) - (p - 1)(2 + c) - p = (2 + c) - p. \tag{A.24}$$

We now consider a specific example to show how this works. Consider a system with two species a and b as we consider for Breached Pair superfluids in Part II. It was pointed out in [23] that a mixed phase could occur when particle numbers N_a and N_b were fixed. This follows directly from the phase rule: $P = C - F + 2 = 2 - 2 + 2$. The two degrees of freedom are the pressure and temperature.

The beauty of the grand-canonical ensemble is that one explicitly fixes all of the equilibrium conditions (chemical potentials and temperature) but none of the other thermodynamic degrees of freedom, thus one maximizes f and minimizes $p = 1$ the number of phases. The phase diagram in this

ensemble thus consists of pure phases, with mixed phases occurring only along phase boundaries. In contrast, in the other ensembles, mixed phases can occupy large volumes of the phase diagram. These phase structures, however, can be directly constructed from the grand-canonical ensemble.

A.4.4 Tangent Construction for Switching Ensembles

Suppose that one has computed the phase diagram in the grand-canonical ensemble. This means we have the function $\Omega(T, \vec{\mu}) = \Omega(\vec{\mu})$. (For simplicity, we consider only fixed temperature here and thus ignore the T dependence: it can be analyzed in a similar manner.) Suppose we now want to study a system with a fixed particle number constraint in the macro-canonical ensemble. How do we go about determining the solution?

First we note that the thermodynamic relations imply a one-to-one correspondence between tangents Ω and states of fixed particle number:

$$\vec{\mathbf{N}} = -\frac{\partial \Omega}{\partial \vec{\mu}}. \tag{A.25}$$

When Ω is not differentiable, there is a cone of possible tangent hyperplanes which contact Ω and which bound Ω from above (see Figure A.1). This cone of tangents describes various possible mixed phases composed of the pure phases (where Ω is differentiable) that intersect at the singularity. To find the state that minimizes H for some fixed constraint $\vec{\mathbf{N}} = \vec{\mathbf{N}}_0$ one simply forms the hyperplane with gradient $\vec{\mathbf{N}}_0$ and drops this until it contacts the surface Ω. The first point of contact will define either a pure or mixed state which satisfies the appropriate constraints. Since this state also lies on Ω, it minimizes Ω for the fixed chemical potentials defined by the contact point. No matter what constraints we apply, there is always a stable state in the grand canonical ensemble.

This is easiest to visualize with a single parameter $\Omega(\mu)$ as drawn in Figure A.1. First we specify the particle number N. We must find the point on $\Omega(\mu)$ where the slope $\Omega' = -N$: The hyperplane is now just a line of slope $-N$. Simply hold a ruler above Ω with the appropriate slope and bring it down until it contacts Ω. The convexity of Ω ensures that there will be a point of contact. If this is in a region where there is a pure phase, the Ω will have exactly this slope at this point and one has a description of a pure phase with a given chemical potential that satisfies the number constraints. Again, by the convexity of the potential, this state is guaranteed to have minimum free-energy $F = \Omega + \mu N$.

If the contact point is at a cusp as at the top of Figure A.1, then the solution lies on a phase boundary and at fixed N the system will consist of a mixed phase. One can also see how the mixed phase occupies a large region of the phase space at fixed N: there are many slopes which will intersect at the same cusp. This argument is valid only for extensive thermodynamic

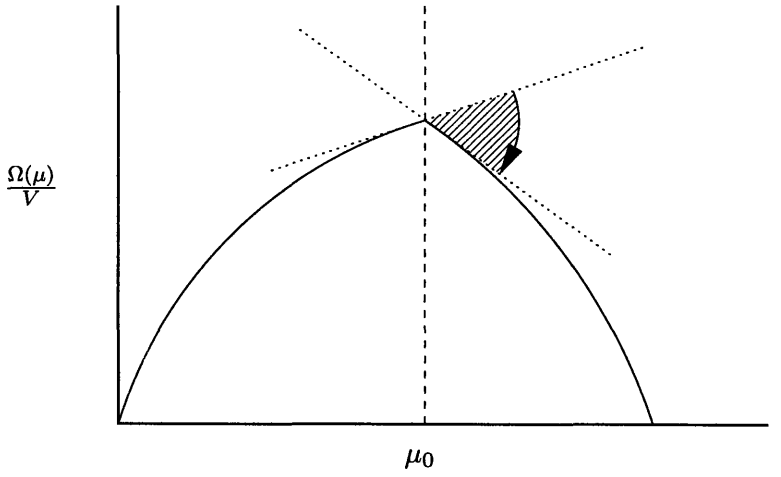

Figure A.1: The cone of tangent (hyper)planes to a thermodynamic potential density $-P = \Omega(\mu)/V$. Immediately to the left of μ_0 is a pure phase with density n_L while immediately to the right is another pure phase with density n_R. The densities are the negative slopes of the tangents at μ_0 according to (A.25). At $\mu = \mu_0$ there is a continuum of mixed phases: These consist of a volume fraction x at density n_L and the remaining fraction $1 - x$ at density n_R. The average density over all space, $n = xn_L + (1 - x)n_R$, lies within $n \in (n_L, n_R)$.

systems. Long-range interactions can render the energy of some pure phases non-extensive (due, for example, to the rapidly diverging Coulomb energy per unit volume V as $V \to \infty$). In such cases, a mixed phase would contain bubbles of limited size. The surface energy of these phase boundaries becomes a volume effect and must therefore be taken into account, even in the thermodynamic limit (see for example [57]). This complicates the relation between $\vec{\mathbf{N}}$ and $\vec{\mu}$, however, one may be able to restore the description if one suitable averages. This is discussed in Section A.4.5.

A.4.5 Extensivity

Consider two copies of a system, both in the same thermodynamic state, but far from each other so that they only exchange heat (as in Gibbs' ensemble). All additive quantities for this combined system such as the entropy, energy,

volume, particle numbers etc. have twice the values of a single system. Now consider bringing the two systems into a single container of twice the volume. If, for the resulting system, the additive quantities are all still twice the value of a single system, then the system is said to be *extensive*.

Extensivity is important because it allows us to take the thermodynamic limit of a particular system by combining many copies. In this limit the ensembles are equivalent and one can work exclusively with the grand-canonical ensemble which has many computational advantages. There are cases, however, when extensivity fails. One example is if there are long-range forces: In this case, the energy of the combined system would be less/greater than twice the original system depending on whether the long-range force is repulsive or attractive. One usually makes the assumption of extensivity to ensure that the assumption A.2.1 holds. It does not hold in general for non-extensive systems.[6]

Extensivity also fails if there are substantial finite-size effects: In this case, one alters the properties of the system by removing the barrier between them. Often, however, extensivity can be returned by considering very large systems: regions in the centre of a large system will generally not be sensitive to the details of the boundaries unless there are long-range forces.

Even in the case of long-range forces, extensivity might be restored. Consider for example the Coulomb interaction. The long-range force requires that the system be neutral overall. On a short distance scale, the system may not be neutral (there may be charge domains for example), but suitable averaged over a large enough distance scale, the system will be neutral and the overall system will be extensive. The difficulty with this is that, the "components" of the system will now be composite objects—the neutral domains—rather than the original microscopic degrees of freedom. This make the analysis difficult and application of the phase rule challenging because one must carefully determine what c means. This is also seen in QCD: An extensive description of the theory must be built out of colour neutral components rather than the fundamental degrees of freedom.

We set aside these exceptions for now and consider purely extensive systems. The entropy, volume and all of the measurable conserved quantities N_i are additive. Additivity implies extensivity.[7] The thermodynamic entropy

[6] See also [169, 170, 171, 172] for a generalization of the notion of entropy that is useful for non-extensive systems.

[7] For two non-interacting systems, the doubled system is represented by $\widehat{\rho} \otimes \widehat{\rho}$ (this neglects possible symmetrization conditions, but for spatially well-separated systems the overlap is negligible) while the measurable operator is a linear combination $\widehat{\mathbf{N}}_i \otimes \widehat{\mathbf{1}} + \widehat{\mathbf{1}} \otimes \widehat{\mathbf{N}}_i$. The additivity follows trivially.

is thus a homogeneous function of its arguments:

$$S(\alpha V, \alpha \vec{\mathbf{N}}) = \alpha S(V, \vec{\mathbf{N}}). \tag{A.26}$$

This implies that[8]

$$S = pV + \vec{\theta} \cdot \vec{\mathbf{N}} \tag{A.28}$$

where p and $\vec{\theta}$ are *intensive* quantities (independent of the size of the system).

Now, the thermodynamical law (A.19) can be expressed in terms of the densities $s = S/V$ and $\vec{\mathbf{n}} = \vec{\mathbf{N}}/V$:

$$V(\mathrm{d}s - \vec{\theta} \cdot \mathrm{d}\vec{\mathbf{n}}) + (s - p - \vec{\theta} \cdot \vec{\mathbf{n}})\mathrm{d}V = 0. \tag{A.29}$$

Since all of the volume dependence is explicit, this implies that

$$\mathrm{d}s = \vec{\theta} \cdot \mathrm{d}\vec{\mathbf{n}}, \tag{A.30a}$$

$$p = s - \vec{\theta} \cdot \vec{\mathbf{n}}. \tag{A.30b}$$

From this we can see that (A.20) is zero for extensive thermodynamics systems. Instead of using this quantity for physical purposes, we introduce the Legendre transform of the entropy density to define the reduced pressure p:

$$p(\vec{\theta}) = \max_{\vec{\mathbf{n}}} \left[s(\vec{\mathbf{n}}) - \vec{\theta} \cdot \vec{\mathbf{n}} \right]. \tag{A.31}$$

A.4.6 Thermodynamic Stability

The basic requirement for thermodynamic stability is that the representative state ρ be the state of maximal entropy. We saw that this is equivalent to ensuring that the thermodynamic potential is a true minimum

$$-PV = \Omega(\vec{\mu}) = \min(H - \vec{\mu} \cdot \vec{\mathbf{N}}), \tag{A.32}$$

where the minimization is over all possible states. Thus, Ω must be a concave function of the chemical potentials $\vec{\mu} = (\mu_a, \mu_b)$ (see Section A.4.1).

Often the calculation proceeds without explicitly performing this minimization, but by making some approximation, or looking for self-consistent

[8] If $f(ax) = af(x)$ for all x, then

$$\frac{\mathrm{d}f(ax)}{\mathrm{d}a} = x\frac{\mathrm{d}f(ax)}{\mathrm{d}ax} = f(x) = \frac{f(ax)}{a} \qquad \Rightarrow \qquad \frac{\mathrm{d}f}{\mathrm{d}x} = \frac{f}{x}. \tag{A.27}$$

This has the family of solutions $f(x) = \lambda x$.

solutions. In these cases, it is a non-trivial check of convexity that the matrix of partials

$$\frac{\partial^2 \Omega}{\partial \mu_a \partial \mu_b} \tag{A.33}$$

is negative definite. While this may not be sufficient (the state may only be metastable for example) it is a necessary condition. This condition is automatically satisfied, however, if a proper minimization is performed, even if it is only performed over a limited set of states.

A.4.6.1 Two Parameter Example

Here we present a simple example of how the thermodynamic stability relationship (A.33) is related to the minimization. This relationship was used toward the end of Section 5.3.2. Consider a thermodynamic potential

$$\Omega[\mu] = \min_{\Delta}(F[\Delta] - \mu N[\Delta]) \tag{A.34}$$

where the state is described by a single variational parameter Δ and the external chemical potential μ which enters as a Lagrange multiplier. This is the form of the separable model considered in Section 5.3.2.

Consider solving this problem through the self-consistency equations. We first form $\Omega[\mu, \Delta] = F[\Delta] - \mu N[\Delta]$ and then solve the self-consistency condition (gap equation)

$$\frac{\partial \Omega[\mu, \Delta]}{\partial \Delta} = F' - \mu N' = 0. \tag{A.35}$$

The solution to this equation implicitly defines the function $\Delta[\mu]$. The derivative of this relationship may also be computed:

$$(F'' - \mu N'')\frac{\mathrm{d}\Delta}{\mathrm{d}\mu} = N'. \tag{A.36}$$

The self-consistent solution is a local minimum if and only if the second derivative is greater than zero:

$$\frac{\partial^2 \Omega[\mu, \Delta]}{\partial \Delta^2} = F'' - \mu N'' > 0. \tag{A.37}$$

Now consider the criterion for thermodynamic stability. This can be re-expressed in terms of the minimization condition (A.37) using the implicit

relationships:

$$\frac{\mathrm{d}^2\Omega[\mu]}{\mathrm{d}\mu^2} = (F'' - \mu N'')(\Delta')^2 + (F' - \mu N')\Delta'' - 2N'\Delta', \tag{A.38}$$

$$= (F'' - \mu N'')(\Delta')^2 + (0)\Delta'' - 2(F'' - \mu N'')(\Delta')^2, \tag{A.39}$$

$$= -(F'' - \mu N'')(\Delta')^2, \tag{A.40}$$

$$= -\frac{\partial^2\Omega[\mu, \Delta]}{\partial\Delta^2}(\Delta')^2 < 0. \tag{A.41}$$

Thus, we see that the thermodynamic stability criterion (A.33) and the minimization condition (A.37) are equivalent.

Appendix B

Generalized Quadratic Fermions

In this section, we present all of the details required when actually computing with the techniques outlined in Section 3.1. In particular, we include the generalization that allows for simultaneously including the pairing *and* Hartree-Fock terms.

B.1 Quadratic Fermions

We start by considering the most general quadratic Hamiltonian:

$$\widehat{\mathbf{H}} = \widehat{\boldsymbol{\psi}}^\dagger \mathbf{A} \widehat{\boldsymbol{\psi}} + \widehat{\boldsymbol{\psi}}^\dagger \mathbf{B} \widehat{\boldsymbol{\psi}}^* + \widehat{\boldsymbol{\psi}}^T \mathbf{B}^\dagger \widehat{\boldsymbol{\psi}} \tag{B.1}$$

where

$$\widehat{\boldsymbol{\psi}} = \begin{pmatrix} \widehat{\mathbf{a}}_1 \\ \widehat{\mathbf{a}}_2 \\ \vdots \\ \widehat{\mathbf{a}}_n \end{pmatrix} \tag{B.2}$$

satisfy canonical commutation relations

$$\{\widehat{\psi}_a, \widehat{\psi}_b^*\} = \delta_{ab}, \qquad \{\widehat{\psi}_a^*, \widehat{\psi}_b^*\} = \{\widehat{\psi}_a, \widehat{\psi}_b\} = 0. \tag{B.3}$$

Note that we have included all possible bilinear fermion operators whereas in Chapter 3 we only included the single term $\widehat{\boldsymbol{\psi}}^\dagger \mathbf{A}_0 \widehat{\boldsymbol{\psi}}$. We can simplify the formulation if we introduce an augmented collection of fermions

$$\widehat{\boldsymbol{\Psi}} = \begin{pmatrix} \widehat{\boldsymbol{\psi}} \\ \widehat{\boldsymbol{\psi}}^* \end{pmatrix}. \tag{B.4}$$

The Hamiltonian (B.1) can now be written

$$\widehat{\mathbf{H}} = \widehat{\boldsymbol{\Psi}}^\dagger \tilde{\mathbf{E}} \boldsymbol{\Psi} \tag{B.5}$$

where

$$\tilde{\mathbf{E}} = \begin{pmatrix} \mathbf{A} & \mathbf{B} \\ \mathbf{B}^\dagger & \mathbf{0} \end{pmatrix}. \tag{B.6}$$

This formalism with "augmented" spinors allows for all possible quadratic forms, but has a potential "double counting" problem. To deal with this, first note that the usual diagonal commutation relations are still satisfied:

$$\{\widehat{\mathbf{\Psi}}_a, \widehat{\mathbf{\Psi}}_b^*\} = \delta_{ab}, \tag{B.7}$$

but that there is an additional "conjugation matrix" $\mathbf{C} = \mathbf{C}^T = \mathbf{C}^\dagger$

$$\mathbf{C} = \begin{pmatrix} \mathbf{0} & \mathbf{1} \\ \mathbf{1} & \mathbf{0} \end{pmatrix} \tag{B.8}$$

which acts to conjugate the spinors:

$$\widehat{\mathbf{\Psi}}^* = \mathbf{C}\widehat{\mathbf{\Psi}}. \tag{B.9}$$

This means that the off-diagonal commutation relations are no-longer trivially zero:

$$\{\widehat{\mathbf{\Psi}}_a^*, \widehat{\mathbf{\Psi}}_b^*\} = \{\widehat{\mathbf{\Psi}}_a, \widehat{\mathbf{\Psi}}_b\} = [\mathbf{C}]_{ab}. \tag{B.10}$$

Since the model is quadratic, we can diagonalize it, but we must take care, however, to preserve the conjugation properties. We start by rearranging the Hamiltonian using the conjugation and anticommutation relations,

$$\widehat{\mathbf{H}} = \widehat{\mathbf{\Psi}}^\dagger \mathbf{E} \mathbf{\Psi} + \frac{\mathrm{Tr}[\tilde{\mathbf{E}}]}{2}, \tag{B.11}$$

where

$$\mathbf{E} = \frac{\tilde{\mathbf{E}} - \mathbf{C}\tilde{\mathbf{E}}^T\mathbf{C}}{2}. \tag{B.12}$$

The structure of $\mathbf{E}$ ensures that all of the eigenvalues are real and occur in pairs of opposite sign. We comment without proof that it is thus always possible to diagonalize $\mathbf{E}$ with a unitary transformation $\mathbf{Q}$ so that

$$\mathbf{Q}^\dagger \mathbf{E} \mathbf{Q} = \begin{pmatrix} \mathbf{D} & \mathbf{0} \\ \mathbf{0} & -\mathbf{D} \end{pmatrix} \tag{B.13}$$

where $2\mathbf{D} = \mathrm{diag}(\omega_1, \cdots, \omega_n)$ and which satisfies $\mathbf{CQC} = \mathbf{Q}^*$. This latter property ensures that the transformed fermion operators (which create and annihilate the Bogoliubov quasiparticles) $\widehat{\mathbf{c}} = \mathbf{Q}^\dagger \widehat{\mathbf{\Psi}}$ also satisfy the

conjugation properties $\widehat{\mathbf{c}}^* = \mathbf{C}\widehat{\mathbf{c}}$. All this follows from the property that $\mathbf{C}\mathbf{E}^T\mathbf{C} = -\mathbf{E}$.

Note that the diagonalization of $\mathbf{E}$ is not unique. As a result, numerical algorithms are not guaranteed to generate the appropriately transforming $\mathbf{Q}$, even though it exists. One must also permute the eigenvalues so they line up and include a factor of the appropriate phases. Thus, for an arbitrary diagonalization matrix $\mathbf{U}$, one has $\mathbf{Q} = \mathbf{U}\mathbf{P}\exp(i\phi)$ where $\mathbf{P}$ is a permutation matrix chosen to arrange the eigenvalues in pairs and $\exp(2i\phi) = \mathbf{C}\mathbf{P}^\dagger\mathbf{U}^\dagger\mathbf{C}\mathbf{U}^*\mathbf{P}^*$.

This may not be a sufficient algorithm if there are degenerate eigenvalues. A better solution is just be to identify all the eigenvectors corresponding to positive eigenvalues and conjugate them to find the remaining conjugated eigenvectors. This should work unless there are multiple zero eigenvalues (rare in practice). Note that $\mathbf{Q}$ will then have the following structure

$$\mathbf{Q} = \begin{pmatrix} \mathbf{Q}_1 & \mathbf{Q}_2^* \\ \mathbf{Q}_2 & \mathbf{Q}_1^* \end{pmatrix}. \tag{B.14}$$

The final step is to use the anticommutation relations for the new fields to write the Hamiltonian as

$$\widehat{\mathbf{H}} = 2\widehat{\mathbf{c}}^\dagger\mathbf{D}\widehat{\mathbf{c}} + \mathrm{Tr}[\tilde{\mathbf{E}}/2 - \mathbf{D}] \tag{B.15}$$

where only a single set of Bogoliubov quasiparticle operators $\widehat{\mathbf{c}}$ now explicitly enter. In this form, there are no double counting problems: $\widehat{\mathbf{c}}$ comprises exactly a single complete set of operators. From this we see that the matrix $2\mathbf{D} = \mathrm{diag}(\omega_1, \cdots, \omega_n)$ contains the quasiparticle dispersions. The system is now diagonal and one can solve it explicitly using the results of Section 3.1.

B.1.1 Vacuum Expectation Values

As before, with this formalism, we can deduce the vacuum expectation values (VEV) of any composite operator made of $\langle\widehat{\mathbf{\Psi}}\rangle$. Recall that in the ground state of a purely quadratic Hamiltonian, only the two-point correlation functions are non-trivial: all higher order correlations are given in terms for these by using Wick's theorem. All that is left is to deduce the two-point correlators which are trivial in the diagonal basis:

$$\langle\widehat{\mathbf{c}}\widehat{\mathbf{c}}^\dagger\rangle = f_\beta(-2\mathbf{Q}^\dagger\mathbf{E}\mathbf{Q}) \tag{B.16}$$

where $f_\beta(E)$ is the Fermi distribution function (3.12)

$$f_\beta(x) = \frac{1}{1 + e^{\beta E}}. \tag{B.17}$$

Since this is analytic, it is trivial to return to the the original basis:

$$\langle \widehat{\Psi}\widehat{\Psi}^\dagger \rangle = \mathbf{Q}\,\langle \widehat{c}\widehat{c}^\dagger \rangle\,\mathbf{Q}^\dagger = f_\beta(-2\mathbf{E}) = \frac{\mathbf{1}}{\mathbf{1}+e^{-2\beta\mathbf{E}}}, \tag{B.18a}$$

$$\langle \widehat{\Psi}^*\widehat{\Psi}^T \rangle = \mathbf{1} - \langle \widehat{\Psi}\widehat{\Psi}^\dagger \rangle^T = f_\beta(2\mathbf{E}^T) = \frac{\mathbf{1}}{\mathbf{1}+e^{2\beta\mathbf{E}^T}}. \tag{B.18b}$$

These may also be directly derived from the partition function by performing the appropriate derivatives as we discussed in Section 3.1.1. These matrices will be used frequently in the following analysis, so we give them special names:

$$\mathbf{F}^\pm = \frac{\mathbf{1}}{\mathbf{1}+e^{\pm 2\beta\mathbf{E}}}. \tag{B.19}$$

These satisfy have the following properties:

$$\mathbf{F}^+ + \mathbf{F}^- = 1, \qquad \mathbf{C}[\mathbf{F}^\pm]^T\mathbf{C} = \mathbf{F}^\mp, \tag{B.20a}$$

$$\mathbf{F}^\pm = [\mathbf{F}^\pm]^\dagger, \qquad [\mathbf{F}^+, \mathbf{F}^-] = 0. \tag{B.20b}$$

Note that the matrices $\mathbf{F}^\pm$ play the same role as the matrices with the same name in Chapter 3, but they are not formally equivalent. In particular, in this appendix, $\mathbf{F}^\pm$ correspond to the augmented structure including the extra degree of freedoms. Thus, one must be careful about double counting. This is the price that we pay to include both the pairing and Hartree-Fock terms. Similar results to those in Chapter 3 will be derived, but factors of 2 will be required to account for this double counting.

Keeping this in mind, we can work out the thermodynamic potential from the fully diagonalized Hamiltonian (B.15):

$$\Omega = -\frac{1}{\beta}\sum_{j=1}^{n} \ln[2\cosh(\beta D_j)] + \frac{\mathrm{Tr}[\tilde{\mathbf{E}}]}{2}, \tag{B.21a}$$

$$= -\frac{1}{2\beta}\sum_{j=1}^{n} \ln[2\cosh(\beta D_j)] - \frac{1}{2\beta}\sum_{j=1}^{n} \ln[2\cosh(-\beta D_j)] + \frac{\mathrm{Tr}[\tilde{\mathbf{E}}]}{2}, \tag{B.21b}$$

$$= -\frac{1}{2\beta}\,\mathrm{Tr}\ln[2\cosh(\beta\mathbf{E})] + \frac{1}{2}\,\mathrm{Tr}[\tilde{\mathbf{E}}], \tag{B.21c}$$

$$= \frac{1}{2\beta}\,\mathrm{Tr}\ln[\mathbf{F}^-] + \frac{1}{2}\,\mathrm{Tr}[\tilde{\mathbf{E}}]. \tag{B.21d}$$

Note we have used the fact that $\mathrm{Tr}[\mathbf{E}] = 0$ in the simplification. Compare this with (3.22): the extra factor of 2 prevents double counting.

B.1.1.1 Normal Ordering

When computing charges, there is an issue of normal ordering which we omitted in Chapter 3. For example, when working with relativistic systems, on often write the charge density as

$$\widehat{\mathbf{Q}} = \widehat{\bar{\psi}}\gamma_0\widehat{\psi} = \widehat{\psi}^\dagger\widehat{\psi}. \tag{B.22}$$

However, this has the form

$$\widehat{\mathbf{Q}} = \sum_{L,R}\left(\widehat{\mathbf{a}}^\dagger\widehat{\mathbf{a}} + \widehat{\mathbf{b}}\widehat{\mathbf{b}}^\dagger\right) \tag{B.23}$$

which is non-zero in the vacuum. The desired operator is normal ordered:

$$:\widehat{\mathbf{Q}}:= \sum_{L,R}\left(\widehat{\mathbf{a}}^\dagger\widehat{\mathbf{a}} - \widehat{\mathbf{b}}^\dagger\widehat{\mathbf{b}}\right) = \widehat{\mathbf{Q}} - \{\widehat{\mathbf{b}}, \widehat{\mathbf{b}}^\dagger\}. \tag{B.24}$$

Related is the question: what is the density of free fermions as a function of momentum? The question as posed is ambiguous. Does one want the density of massless fermions or the density of massive fermions? These give different answers in general. In order to specify, one must first supply a quadratic Hamiltonian that defines which operators are creation operators and which operators are annihilation operators. Once this is done, one can reorder the operators in a well-defined way, and compute the appropriate charges and densities.

Suppose we are given a quadratic model with the augmented Hamiltonian matrix $\mathbf{E}_{\text{NO}}$ as discussed above. We wish to normal order quadratic forms with respect to the eigenstates of the Hamiltonian $\widehat{\mathbf{\Psi}}^\dagger\mathbf{E}_{\text{NO}}\widehat{\mathbf{\Psi}}$. To do this, consider the quasiparticle operators $\widehat{\mathbf{c}}_{\text{NO}} = \mathbf{Q}_{\text{NO}}^\dagger\widehat{\mathbf{\Psi}}$ of the normal ordering Hamiltonian. The operators which annihilate the vacuum state are those with positive energy: i.e. those corresponding to the non-zero diagonal entries of:

$$\boldsymbol{\theta}\left(\mathbf{Q}_{\text{NO}}^\dagger\mathbf{E}_{\text{NO}}\mathbf{Q}_{\text{NO}}\right). \tag{B.25}$$

Furthermore, since we have restricted ourselves to canonical transformations, the commutation relations still apply:

$$\{\widehat{\mathbf{c}}_a^\dagger, \widehat{\mathbf{c}}_b\} = \delta_{ab}. \tag{B.26}$$

Thus, the normal ordered operator product is[1]

$$:\widehat{\mathbf{c}}\widehat{\mathbf{c}}^\dagger: = \widehat{\mathbf{c}}\widehat{\mathbf{c}}^\dagger - \boldsymbol{\theta}\left(\mathbf{Q}_{\text{NO}}^\dagger\mathbf{E}_{\text{NO}}\mathbf{Q}_{\text{NO}}\right). \tag{B.27}$$

[1] As a quick check, consider the one-dimensional case. If $D > 0$, then $\widehat{\mathbf{a}}^\dagger\widehat{\mathbf{a}}$ is normal ordered as is $\widehat{\mathbf{a}}\widehat{\mathbf{a}}^\dagger - 1 = -\widehat{\mathbf{a}}^\dagger\widehat{\mathbf{a}}$.

In terms of the original operators $\widehat{\Psi} = \mathbf{Q}_{\mathrm{NO}}\widehat{\mathbf{c}}_{\mathrm{NO}}$, we have

$$:\widehat{\Psi}\widehat{\Psi}^{\dagger}: = \widehat{\Psi}\widehat{\Psi}^{\dagger} - \theta(\mathbf{E}_{\mathrm{NO}}), \tag{B.28}$$

$$:\widehat{\Psi}^{*}\widehat{\Psi}^{T}: = \widehat{\Psi}^{*}\widehat{\Psi}^{T} - \theta(-\mathbf{E}_{\mathrm{NO}}^{T}). \tag{B.29}$$

Note that in this equation $\mathbf{E}_{\mathrm{NO}}$ refers to the quadratic Hamiltonian with respect to which to normal order. Finally, note that the normal ordered version of $\mathbf{F}^{\pm}$ are given by

$$:\mathbf{F}^{\pm}:= \mathbf{F}^{\pm} - \theta(\mp\mathbf{H}_{\mathrm{NO}}) \tag{B.30}$$

so that

$$:\mathbf{F}^{+}: + :\mathbf{F}^{-}:= \mathbf{1} - \mathbf{1} = \mathbf{0}. \tag{B.31}$$

This is indicative of a general result: any time the constant $\mathbf{1}$ appears due to commutation relations, this term should be removed from the corresponding normal ordered expressions. When momenta are introduced, this term $\mathbf{1}$ will be replaced by the momentum space volume term $\mathbf{V}_p$ (3.49). Again, this will drop out of normal ordered expressions.

B.2 Interactions

As a specific example (and because the models of interest have this form) consider the general Hamiltonian

$$\widehat{\mathbf{H}} = \widehat{\Psi}^{\dagger}\tilde{\epsilon}\widehat{\Psi} + g(\widehat{\Psi}^{\dagger}\gamma^{\dagger}\widehat{\Psi})(\widehat{\Psi}^{\dagger}\gamma\widehat{\Psi}). \tag{B.32}$$

To preserve the structure of the augmented spinors $\widehat{\Psi}$, we must ensure that the Hamiltonian has the following form

$$\widehat{\mathbf{H}} = \widehat{\Psi}^{\dagger}(\epsilon + \mathbf{X})\widehat{\Psi} + g(\widehat{\Psi}^{\dagger}\Gamma^{\dagger}\widehat{\Psi})(\widehat{\Psi}^{\dagger}\Gamma\widehat{\Psi}) + \mathrm{const} \tag{B.33}$$

where

$$\epsilon = -\mathbf{C}\epsilon^{T}\mathbf{C}, \qquad \mathbf{X} = -\mathbf{C}\mathbf{X}^{T}\mathbf{C}, \qquad \text{and} \qquad \Gamma = -\mathbf{C}\Gamma^{T}\mathbf{C}. \tag{B.34}$$

To do this, we use the commutation and conjugation relations to define

$$\Gamma = \frac{\gamma - \mathbf{C}\gamma^{T}\mathbf{C}}{2}, \quad \epsilon = \frac{\tilde{\epsilon} - \mathbf{C}\tilde{\epsilon}^{T}\mathbf{C}}{2},$$

$$\mathbf{X} = g\frac{\mathrm{Tr}[\gamma^{\dagger}]\Gamma}{2} + g\frac{\mathrm{Tr}[\gamma]\Gamma^{\dagger}}{2},$$

$$\mathrm{const} = \frac{\mathrm{Tr}[\tilde{\epsilon}]}{2} + g\frac{\mathrm{Tr}[\gamma^{\dagger}]\,\mathrm{Tr}[\gamma]}{4}.$$

For symmetry reasons—and to keep track of the double counting—it is preferable to perform calculations with the Hamiltonian (B.33) rather than trying to use (B.32). This introduces the complication of including the term $\mathbf{X}$ in the full propagator. One way to avoid this is to only consider properly normal ordered Hamiltonians as discussed in Section B.2.1.1.

B.2.1 Variational Hamiltonian

The variational Hamiltonian with the augmented structure is

$$\widehat{\mathbf{H}}_0 = \widehat{\mathbf{\Psi}}^\dagger(\boldsymbol{\epsilon} + \mathbf{X} + \boldsymbol{\Sigma})\widehat{\mathbf{\Psi}} = \widehat{\mathbf{\Psi}}^\dagger \mathbf{E} \widehat{\mathbf{\Psi}}. \tag{B.36}$$

where the variational parameters are the elements of the matrix $\boldsymbol{\Sigma}$ which must be constrained to satisfy

$$\boldsymbol{\Sigma} = \boldsymbol{\Sigma}^\dagger, \tag{B.37a}$$

$$\boldsymbol{\Sigma} = -\mathbf{C}\boldsymbol{\Sigma}^T\mathbf{C}. \tag{B.37b}$$

The latter condition implies that $\mathrm{Tr}[\boldsymbol{\Sigma}] = 0$. Note that the matrix $\boldsymbol{\Sigma}$ should be thought of as containing the corrections or "renormalizations" to the chemical potentials, masses etc. as well as the gap parameters. The quadratic portion of the free energy is given by (B.21),

$$\Omega_0 = \frac{1}{2\beta}\,\mathrm{Tr}\ln[\mathbf{F}^-] \tag{B.38}$$

while the expectation value of the residual quadratic piece is

$$\langle \widehat{\mathbf{H}} - \widehat{\mathbf{H}}_0 \rangle_0 = \langle \widehat{\mathbf{H}}_{\mathrm{int}} \rangle_0 - \mathrm{Tr}[\boldsymbol{\Sigma}\mathbf{F}^+], \tag{B.39}$$

and the expectation of the interaction—now including both Hartree and Fock terms—is

$$\langle \widehat{\mathbf{H}}_{\mathrm{int}} \rangle_0 = g\left(\mathrm{Tr}[\boldsymbol{\Gamma}^\dagger\mathbf{F}^+]\,\mathrm{Tr}[\boldsymbol{\Gamma}\mathbf{F}^+] + \mathrm{Tr}[\boldsymbol{\Gamma}^\dagger\mathbf{F}^-\boldsymbol{\Gamma}\mathbf{F}^+] - \mathrm{Tr}[\boldsymbol{\Gamma}^\dagger\mathbf{F}^-\mathbf{C}\boldsymbol{\Gamma}^T\mathbf{C}\mathbf{F}^+]\right).$$

Including all of the constants, we have

$$\begin{aligned}\Omega \leq \Omega[\boldsymbol{\Sigma}] = \frac{1}{2\beta}\,\mathrm{Tr}\ln[\mathbf{F}^-] - \mathrm{Tr}[\boldsymbol{\Sigma}\mathbf{F}^+] + \frac{\mathrm{Tr}[\tilde{\boldsymbol{\epsilon}}]}{2} + g\frac{\mathrm{Tr}[\boldsymbol{\gamma}^\dagger]\,\mathrm{Tr}[\boldsymbol{\gamma}]}{4} + \\ + g\left(\mathrm{Tr}[\boldsymbol{\Gamma}^\dagger\mathbf{F}^+]\,\mathrm{Tr}[\boldsymbol{\Gamma}\mathbf{F}^+] + 2\,\mathrm{Tr}[\boldsymbol{\Gamma}^\dagger\mathbf{F}^-\boldsymbol{\Gamma}\mathbf{F}^+]\right).\end{aligned} \tag{B.40}$$

B.2.1.1 Normal Ordering

If the original Hamiltonian is to be normal ordered, then we may completely neglect the term $\mathbf{X}$ because

$$:(\widehat{\boldsymbol{\Psi}}^\dagger \boldsymbol{\Gamma}^\dagger \widehat{\boldsymbol{\Psi}})(\widehat{\boldsymbol{\Psi}}^\dagger \boldsymbol{\Gamma} \widehat{\boldsymbol{\Psi}}):=::\widehat{\boldsymbol{\Psi}}^\dagger \boldsymbol{\Gamma}^\dagger \widehat{\boldsymbol{\Psi}}::\widehat{\boldsymbol{\Psi}}^\dagger \boldsymbol{\Gamma} \widehat{\boldsymbol{\Psi}}::=:(\widehat{\boldsymbol{\Psi}}^\dagger \boldsymbol{\gamma}^\dagger \widehat{\boldsymbol{\Psi}})(\widehat{\boldsymbol{\Psi}}^\dagger \boldsymbol{\gamma} \widehat{\boldsymbol{\Psi}}):\,. \tag{B.41}$$

The quadratic part (without $\mathbf{X}$ now), however, still needs to be reordered:

$$:\widehat{\boldsymbol{\Psi}}^\dagger \boldsymbol{\epsilon} \widehat{\boldsymbol{\Psi}}:= \widehat{\mathbf{H}} - \mathrm{Tr}\left[\boldsymbol{\theta}(-\mathbf{E}_{NO})\boldsymbol{\epsilon}\right]. \tag{B.42}$$

The normal ordered free-energy is thus

$$\begin{aligned}\Omega \leq \Omega[\boldsymbol{\Sigma}] = \frac{1}{2\beta}\mathrm{Tr}\ln[\mathbf{F}^-] - \mathrm{Tr}[\boldsymbol{\theta}(-\mathbf{E}_{NO})\tilde{\boldsymbol{\epsilon}}]+ \\ - \mathrm{Tr}[\boldsymbol{\Sigma}\mathbf{F}^+] + \frac{\mathrm{Tr}[\tilde{\boldsymbol{\epsilon}}]}{2} + g\frac{\mathrm{Tr}[\boldsymbol{\gamma}^\dagger]\,\mathrm{Tr}[\boldsymbol{\gamma}]}{4}+ \\ + g\left(\mathrm{Tr}[\boldsymbol{\Gamma}^\dagger :\mathbf{F}^+:]\,\mathrm{Tr}[\boldsymbol{\Gamma} :\mathbf{F}^+:] + 2\,\mathrm{Tr}[\boldsymbol{\Gamma}^\dagger :\mathbf{F}^-: \boldsymbol{\Gamma} :\mathbf{F}^+:]\right).\end{aligned} \tag{B.43}$$

B.2.2 Self-Consistent Schwinger-Dyson Equations

In this new formalism, we can use the same techniques of Section 3.2.2 to compute the self-consistency conditions in the form of the Schwinger-Dyson equations.

$$\boldsymbol{\Sigma} = g\left(\boldsymbol{\Gamma}^\dagger\,\mathrm{Tr}[\boldsymbol{\Gamma}\mathbf{F}^+] + \boldsymbol{\Gamma}\,\mathrm{Tr}[\boldsymbol{\Gamma}^\dagger\mathbf{F}^+] + 2\boldsymbol{\Gamma}^\dagger\mathbf{F}^-\boldsymbol{\Gamma} - 2\boldsymbol{\Gamma}\mathbf{F}^+\boldsymbol{\Gamma}^\dagger\right). \tag{B.44}$$

This expression satisfies the appropriate constraints (B.37), thus, no additional Lagrange multipliers need be introduced. The Schwinger-Dyson equation for the normal ordered Hamiltonian has exactly the same form (B.44) except that the quantities $\mathbf{F}^\pm \rightarrow :\mathbf{F}^\pm:$ must be replaced by the normal ordered versions.

B.2.2.1 Free Energy

Finally, we present an expression for the free-energy bound by using the Schwinger-Dyson equation (B.44) to eliminate $\boldsymbol{\Sigma}$ from (B.40):

$$\begin{aligned}\Omega[\mathbf{F}^+] = \frac{1}{2\beta}\mathrm{Tr}\ln[\mathbf{F}^+] + \frac{\mathrm{Tr}[\tilde{\boldsymbol{\epsilon}} - \boldsymbol{\mu}]}{2} + g\frac{\mathrm{Tr}[\boldsymbol{\gamma}^\dagger]\,\mathrm{Tr}[\boldsymbol{\gamma}]}{4}+ \\ - g\left(\mathrm{Tr}[\boldsymbol{\Gamma}^\dagger\mathbf{F}^+]\,\mathrm{Tr}[\boldsymbol{\Gamma}\mathbf{F}^+] + 2\,\mathrm{Tr}[\boldsymbol{\Gamma}^\dagger\mathbf{F}^-\boldsymbol{\Gamma}\mathbf{F}^+] - 2\,\mathrm{Tr}[\mathbf{F}^+\boldsymbol{\Gamma}^\dagger\boldsymbol{\Gamma}]\right)\end{aligned} \tag{B.45}$$

and for normal ordered Hamiltonians

$$\Omega[\mathbf{F}^+] = \frac{1}{2\beta}\,\mathrm{Tr}\ln[\mathbf{F}^+] - \mathrm{Tr}[\boldsymbol{\theta}(-\widehat{\mathbf{E}}_{NO})\tilde{\boldsymbol{\epsilon}}]+ \\ + \frac{\mathrm{Tr}[\tilde{\boldsymbol{\epsilon}} - \boldsymbol{\mu}]}{2} + g\frac{\mathrm{Tr}[\boldsymbol{\gamma}^\dagger]\,\mathrm{Tr}[\boldsymbol{\gamma}]}{4}+ \\ - g\left(\mathrm{Tr}[\boldsymbol{\Gamma}^\dagger{:}\mathbf{F}^+{:}]\,\mathrm{Tr}[\boldsymbol{\Gamma}{:}\mathbf{F}^+{:}] + 2\,\mathrm{Tr}[\boldsymbol{\Gamma}^\dagger{:}\mathbf{F}^-{:}\boldsymbol{\Gamma}{:}\mathbf{F}^+{:}] - 2\,\mathrm{Tr}[{:}\mathbf{F}^+{:}\boldsymbol{\Gamma}^\dagger\boldsymbol{\Gamma}]\right). \quad \text{(B.46)}$$

Appendix C

Potential Scattering

In this appendix we present the detailed forms for several potential scattering models as described Section 5.3.1. The Fourier transform thus simplifies:

$$V_{\vec{\mathbf{k}}} = V_k = \int \mathrm{d}^3\vec{\mathbf{r}}\, e^{-i\vec{\mathbf{r}}\cdot\vec{\mathbf{k}}} V(r),$$
$$= 2\pi \int_0^\infty \mathrm{d}r \int_{-1}^1 \mathrm{d}x\, r^2 e^{-irkx} V(r) = \frac{4\pi}{k}\int_0^\infty \mathrm{d}r\, r\sin(rk)V(r). \quad \text{(C.1)}$$

In this case of s-wave scattering, the variational parameters depend only on the magnitude Δ_p and the gap equation becomes

$$\Delta_p = \frac{-g}{4\pi^2}\int_0^\infty \mathrm{d}q \int_{-1}^1 \mathrm{d}x\, V_{p^2+q^2-2pqx} \frac{q^2\Delta_q}{2\sqrt{E_+^2(q)+\Delta_q^2}}(\theta_+ - \theta_-), \quad \text{(C.2)}$$

$$= \frac{-g}{4\pi^2}\int_0^\infty \mathrm{d}q\, \frac{V_{pq}q^2\Delta_q}{2\sqrt{E_+^2+\Delta_q^2}}(\theta_+ - \theta_-), \quad \text{(C.3)}$$

where

$$V_{pq} = \int_{-1}^1 \mathrm{d}x\, V_{\sqrt{p^2+q^2-2pqx}}. \quad \text{(C.4)}$$

Here we explicitly calculate the transform of several potentials. The forms given may be used in numerical code to determine the matrix V_{pq}.

$V(r) = e^{-r/\lambda}/r^2$: This is a long-range interaction that is cutoff with a length scale λ.

$$V_k = \frac{4\pi\tan^{-1}(\lambda k)}{k}. \quad \text{(C.5)}$$

For this potential,

$$V_{pq} = \frac{2\pi}{pq}[A(p+q) - A(p-q)]$$
$$\text{where} \qquad A(p) = 2p\tan^{-1}(\lambda p) - \frac{\ln(1+\lambda^2p^2)}{\lambda}. \quad \text{(C.6)}$$

The only trick here is evaluating this at $p = q = 0$. In the limit $q \to 0$ we have

$$V_{p0} = \frac{8\pi \tan^{-1}(\lambda p)}{p}, \qquad V_{00} = 8\lambda\pi.$$

Yukawa $V(r) = e^{-r/\lambda}/r$**:** This is a long-range Coulomb interaction that is cutoff with a length scale (Debye screening) λ.

$$V_k = \frac{4\pi^2\lambda^2}{1+\lambda^2 k^2}. \tag{C.7}$$

For this potential,

$$V_{pq} = \frac{2\pi}{pq}[A(p+q) - A(p-q)]$$
$$\text{where} \qquad A(p) = \pi \ln(1+\lambda^2 p^2). \tag{C.8}$$

Here we have also

$$V_{p0} = \frac{8\pi^2\lambda^2}{1+\lambda^2 p^2}, \qquad V_{00} = 8\lambda^2\pi^2.$$

Gaussian $V(r) = e^{-r^2/2\lambda^2}/\sqrt{2\pi}/\lambda$**:** This is a Gaussian interaction which has a nice Fourier transform. This was used in the paper [1].

$$V(r) = \frac{1}{\lambda\sqrt{2\pi}} e^{-r^2/(2\lambda^2)},$$
$$V_k = 2\pi^2\lambda^2 e^{-p^2\lambda^2/2},$$
$$V_{pq} = \frac{2\pi}{pq}[A(p+q) - A(p-q)], \qquad A(p) = -\pi e^{-p^2\lambda^2/2},$$
$$V_{p0} = 4\pi^2\lambda^2 e^{-p^2\lambda^2/2},$$
$$V_{00} = 4\lambda^2\pi^2.$$

Appendix D

Effective Potentials for Meson Condensation

Here we give some explicit forms for the effective potential (7.50). We use the parametrization

$$\Sigma = \exp\left\{\frac{-i}{f_\pi}\begin{pmatrix} \frac{\pi_8}{\sqrt{3}}+\pi_3 & \pi_1-i\pi_2 & \pi_4-i\pi_5 \\ \pi_1+i\pi_2 & \frac{\pi_8}{\sqrt{3}}-\pi_3 & \pi_6-i\pi_7 \\ \pi_4+i\pi_5 & \pi_6+i\pi_7 & -\frac{2\pi_8}{\sqrt{3}} \end{pmatrix}\right\} \tag{D.1a}$$

$$= \exp\left\{\frac{-i\sqrt{2}}{f_\pi}\begin{pmatrix} \frac{\eta}{\sqrt{6}}+\frac{\pi^0}{\sqrt{2}} & \pi^- & K^- \\ \pi^+ & \frac{\eta}{\sqrt{6}}-\frac{\pi_0}{\sqrt{2}} & \overline{K}_0 \\ K^+ & K_0 & -\frac{2\eta}{\sqrt{6}} \end{pmatrix}\right\}, \tag{D.1b}$$

where

$$\pi^0 = \pi_3, \qquad \eta^0 = \pi_8, \tag{D.1c}$$

$$\pi^\pm = (\pi_1 \pm i\pi_2)/\sqrt{2}, \qquad K^\pm = (\pi_4 \pm i\pi_5)/\sqrt{2}, \tag{D.1d}$$

$$K^0 = (\pi_6 + i\pi_7)/\sqrt{2}, \qquad \overline{K}^0 = (\pi_6 - i\pi_7)/\sqrt{2}. \tag{D.1e}$$

D.1 Single Meson Condensates

If we consider only condensation of a single meson field (which is the easiest thing to do numerically), then we can derive four different forms of potential. From the mass dependencies of these potentials we can extract some of the coefficients. All of the mesons π^1, π^2, π^4, π^5, π^6, and π^7 are related by flavour symmetries so we only need to consider a single type if we allow arbitrary mass parameters. We choose π^6 corresponding to K^0 condensation. The other forms are for π^3, η and η'. We list the complete potentials below:

Neutral Kaon Condensation: Here we consider a condensate of the form

$$\Sigma = e^{-2i\tilde{\pi}_6\lambda^6} = \begin{pmatrix} 1 & & \\ & \cos(\tilde{\pi}_6) & -i\sin(\tilde{\pi}_6) \\ & -i\sin(\tilde{\pi}_6) & \cos(\tilde{\pi}_6) \end{pmatrix}. \tag{D.2}$$

Let $x = \cos(\tilde{\pi}_6)$. The effective potential becomes

$$\begin{aligned} V = {} & x^2\left[(2c(m_s^2-m_d^2)^2+(4a_6+a_8)(m_d+m_s)^2)\right]+ \\ & +x\left[-2(2a_3-a_8-2a_6)m_u(m_d+m_s)\right]+ \qquad \text{(D.3)} \\ & +\Big[a_0(m_u^2+m_d^2+m_s^2)-2c(m_s^2-m_d^2)^2+ \\ & \quad -4a_3m_dm_s+4a_6(m_u^2-m_dm_s)+a_8m_u^2+ \\ & \quad +c_{00}(m_u^2+m_d^2+m_s^2)^2+c_{01}(m_u^4+m_d^4+m_s^4)\Big]+\cdots. \qquad \text{(D.4)} \end{aligned}$$

Stationary points with maximal kaon condensation occur when $m_u = 0$:

$$\begin{aligned} V|_{m_u=0} = {} & x^2\left[(2c(m_s^2-m_d^2)^2+(4a_6+a_8)(m_d+m_s)^2)\right]+ \\ & +\Big[a_0(m_d^2+m_s^2)-2c(m_s^2-m_d^2)^2+ \\ & \quad -4a_3m_dm_s-4a_6m_dm_s+ \\ & \quad +c_{00}(m_d^2+m_s^2)^2+c_{01}(m_d^4+m_s^4)\Big]+\cdots. \qquad \text{(D.5)} \end{aligned}$$

Neutral Pion Condensation: Here we consider a condensate of the form

$$\Sigma = e^{-2i\tilde{\pi}_3\lambda^3} = \begin{pmatrix} e^{-i\tilde{\pi}_3} & & \\ & e^{i\tilde{\pi}_3} & \\ & & 1 \end{pmatrix}. \tag{D.6}$$

Let $x = \cos(\tilde{\pi}_3)$. The effective potential becomes

$$\begin{aligned} V = {} & x^2\left[8\left(m_u^2+m_d^2\right)a_6+4a_8m_um_d\right]+ \\ & +x\left[2m_s(m_d+m_u)(-2a_3+2a_6+a_8)\right]+ \\ & +\Big[a_0(m_u^2+m_d^2+m_s^2)-4a_3m_um_d+ \\ & \quad +4(m_s^2-m_d^2-m_u^2+m_um_d)a_6+ \\ & \quad +(m_s^2+(m_d-m_u)^2)a_8+ \\ & \quad +c_{00}(m_u^2+m_d^2+m_s^2)^2+c_{01}(m_u^4+m_d^4+m_s^4)\Big]+\cdots. \end{aligned}$$

Stationary points with maximal condensation occur when $m_s = 0$:

$$\begin{aligned} V|_{m_s=0} = x^2 &\left[8\left(m_u^2 + m_d^2\right) a_6 + 4a_8 m_u m_d\right] + \\ &+\Big[a_0(m_u^2 + m_d^2) - 4a_3 m_u m_d + \\ &\quad - 4(m_d^2 + m_u^2 - m_u m_d)a_6 + \\ &\quad + (m_d - m_u)^2 a_8 + \qquad \text{(D.7)} \\ &\quad + c_{00}(m_u^2 + m_d^2)^2 + c_{01}(m_u^4 + m_d^4)\Big] + \cdots . \qquad \text{(D.8)} \end{aligned}$$

Eta Condensation: Here we consider a condensate of the form

$$\boldsymbol{\Sigma} = e^{-2i\tilde{\pi}_8 \boldsymbol{\lambda}^8} = \begin{pmatrix} e^{-i\tilde{\pi}_8/\sqrt{3}} & & \\ & e^{-i\tilde{\pi}_8/\sqrt{3}} & \\ & & e^{2i\tilde{\pi}_8/\sqrt{3}} \end{pmatrix}. \qquad \text{(D.9)}$$

Let $x = \cos(\tilde{\pi}_8/\sqrt{3})$. Then

$$\begin{aligned} V = x^4 &\left[32 a_6 m_s^2\right] + \\ &+x^3 \left[8 a_8 m_s \left(m_u + m_d\right)\right] + \\ &+x^2 \left[8\left((m_u^2 + m_u m_d + m_d^2 - 4m_s^2)a_6 - m_u m_d a_3\right)\right] + \\ &+x \left[2(m_u + m_d)\left(2m_s a_6 - 3m_s a_8 - 2m_s a_3\right)\right] + \\ &+\Big[a_0(m_u^2 + m_d^2 + m_s^2) + 4a_3 m_u m_d + \\ &\quad - 4a_6(m_u^2 + m_u m_d + m_d^2 - m_s^2) + \\ &\quad + a_8[(m_u + m_d)^2 + m_s^2] + \\ &\quad + c_{00}(m_u^2 + m_d^2 + m_s^2)^2 + c_{01}(m_u^4 + m_d^4 + m_s^4)\Big] + \cdots . \qquad \text{(D.10)} \end{aligned}$$

Stationary points with definite condensation occur when $m_u = m_d = 0$, and $m_s = 0$:

$$\begin{aligned} V|_{m_s=0} = x^2 &\left[8\left((m_u^2 + m_u m_d + m_d^2)a_6 - m_u m_d a_3\right)\right] + \\ &+\Big[a_0(m_u^2 + m_d^2) + 4a_3 m_u m_d + \\ &\quad - 4a_6(m_u^2 + m_u m_d + m_d^2) + \\ &\quad + a_8(m_u + m_d)^2 + \\ &\quad + c_{00}(m_u^2 + m_d^2)^2 + c_{01}(m_u^4 + m_d^4)\Big] + \cdots . \qquad \text{(D.11)} \end{aligned}$$

$$V|_{m_u=m_d=0} = 32a_6 m_s^2(x^4 - x^2) + (a_0 + 4a_6 + a_8)m_s^2 + \\ + (c_{00} + c_{01})m_s^4. \tag{D.12}$$

Eta Prime Condensation: Here we consider a condensate of the form

$$A = e^{2i\tilde{\eta}'/\sqrt{6}}. \tag{D.13}$$

Let $x = \cos(2\tilde{\eta}'/\sqrt{6})$. Then

$$\begin{aligned} V = x\Big[&-4(m_u m_d + m_d m_s + m_u m_s)(a_3 - a_6) + \\ &+ 4(m_u^2 + m_d^2 + m_s^2)a_6\Big] + \\ +\Big[&a_0(m_u^2 + m_d^2 + m_s^2) + a_8(m_u + m_d + m_s)^2 + \\ &+ c_{00}(m_u^2 + m_d^2 + m_s^2)^2 + c_{01}(m_u^4 + m_d^4 + m_s^4)\Big] + \cdots . \end{aligned} \tag{D.14}$$

This already has stationary points with definite condensation.

D.2 Effective Potentials with Mass Perturbations

One can, in principle, start to consider multiple condensations, but this becomes quite tedious. For the purposes of extract the leading order coefficients, these single meson condensation results are sufficient. Here is a summary of the forms of the potentials that can be used to compute the coefficients. These are for maximal condensation of the mesons given as arguments. The first three potentials are for pure CFL with no meson condensation. We use the notation V^{m_u,m_d,m_s} to indicate which masses are non-zero and specify the maximal meson condensate as a subscript.

$$V_{\text{CFL}}^{0,0,m} = (a_0 + 4a_6 + a_8)m^2 + (c_{01} + c_{02})m^4, \tag{D.15a}$$

$$V_{\text{CFL}}^{m,m,0} = (2a_0 - 4a_3 + 12a_6 + 4a_8)m^2 + (4c_{01} + 2c_{02})m^4, \tag{D.15b}$$

$$V_{\text{CFL}}^{m,m,m} = 3\,(a_0 - 4a_3 + 8a_6 + 3a_8)\,m^2 + (9c_{01} + 3c_{02})m^4, \tag{D.15c}$$

$$V_{\tilde{\eta}'=\sqrt{3}\pi/\sqrt{2}}^{0,0,m} = (a_0 - 4a_6 + a_8)m^2 + (c_{01} + c_{02})m^4, \tag{D.15d}$$

$$V_{\tilde{\eta}'=\sqrt{3}\pi/\sqrt{2}}^{m,m,m} = 3(a_0 + 4a_3 - 8a_6 + 3a_8)m^2 + (9c_{01} + 3c_{02})m^4, \tag{D.15e}$$

$$V_{\tilde{\pi}_8=\sqrt{3}\pi/4}^{0,0,m} = (a_0 - 4a_6 + a_8)m^2 + (c_{01} + c_{02})m^4, \tag{D.15f}$$

$$V_{\tilde{\pi}_3=\pi/2}^{m,m,0} = (2a_0 - 4a_3 - 4a_6)m^2 + (4c_{01} + 2c_{02})m^4, \tag{D.15g}$$

$$V_{\tilde{\pi}_6=\pi/2}^{0,0,m} = a_0 m^2 + (c_{01} + c_{02} - 2c)m^4. \tag{D.15h}$$

By fitting polynomials to the numerical potential as a function of the mass parameter m, we can extract the various coefficients. Note, we can also check to see if neglected terms are important as they will appear as higher-order mass dependencies.

Appendix E

Full Meson Condensation Parametrizations

In this appendix, we give the full parametrization used to analyze the K^0 condensed states. First, we must introduce a full set of diagonal chemical potentials. One approach would be to introduce the 9 individual quark chemical potentials, but certain linear combinations couple to relevant physics. We fix the overall density by fixing the baryon chemical potential μ_B. Then we must enforce gauge neutrality, so we introduce μ_e which couples to the electromagnetic field, and the diagonal colour chemical potentials μ_3 and μ_8. The rest of the chemical potentials are chosen to be orthogonal to these. Here then are the diagonal elements of the diagonal chemical potentials expressed as tensor products of the flavour and colour structure :

$$\mu_B \times [1, \quad 1, \quad 1] \otimes [1, \quad 1, \quad 1]/3, \tag{E.1a}$$
$$\mu_e \times [2, -1, -1] \otimes [1, \quad 1, \quad 1]/3, \tag{E.1b}$$
$$\mu_3 \times [1, \quad 1, \quad 1] \otimes [1, -1, \quad 0]/2, \tag{E.1c}$$
$$\mu_8 \times [1, \quad 1, \quad 1] \otimes [1, \quad 1, -2]/3, \tag{E.1d}$$
$$\mu_f \times [0, \quad 1, -1] \otimes [1, \quad 1, \quad 1], \tag{E.1e}$$
$$\mu_{e3} \times [2, -1, -1] \otimes [1, -1, \quad 0], \tag{E.1f}$$
$$\mu_{e8} \times [2, -1, -1] \otimes [1, \quad 1, -2], \tag{E.1g}$$
$$\mu_{f3} \times [0, \quad 1, -1] \otimes [1, -1, \quad 0], \tag{E.1h}$$
$$\mu_{f8} \times [0, \quad 1, -1] \otimes [1, \quad 1, -2]. \tag{E.1i}$$

An alternative set of chemical potentials includes the hypercharge chemical potential μ_Y instead of μ_f. These are no longer orthogonal, but are still

linearly independent.

$$\mu_B \times [1,\ 1,\ 1] \otimes [1,\ 1,\ 1]/3, \tag{E.2a}$$
$$\mu_e \times [2,-1,-1] \otimes [1,\ 1,\ 1]/3, \tag{E.2b}$$
$$\mu_3 \times [1,\ 1,\ 1] \otimes [1,-1,\ 0]/2, \tag{E.2c}$$
$$\mu_8 \times [1,\ 1,\ 1] \otimes [1,\ 1,-2]/3, \tag{E.2d}$$
$$\mu_Y \times [1,\ 1,-2] \otimes [1,\ 1,\ 1]/3, \tag{E.2e}$$
$$\mu_{e3} \times [2,-1,-1] \otimes [1,-1,\ 0], \tag{E.2f}$$
$$\mu_{e8} \times [2,-1,-1] \otimes [1,\ 1,-2], \tag{E.2g}$$
$$\mu_{f3} \times [0,\ 1,-1] \otimes [1,-1,\ 0], \tag{E.2h}$$
$$\mu_{f8} \times [0,\ 1,-1] \otimes [1,\ 1,-2]. \tag{E.2i}$$

The diagonal mass corrections (chiral condensates) do not couple to any external physics, so we simply use the nine quark mass corrections (δm_{ur}, δm_{ug}, δm_{ub}, δm_{dr}, δm_{dg}, δm_{db}, δm_{sr}, δm_{sg}, δm_{sb}).

The rest of the parameters are described in the following matrices. These appear more condensed when expressed in the basis described in [27] where the quarks are ordered (ru, gd, bs, rd, gu, rs, bu, gs, bd). In this basis, the matrices corresponding to the variational parameters

$$\mathbf{A} = \mathbf{1} \otimes \delta\boldsymbol{\mu} + \gamma_5 \otimes \delta\boldsymbol{\mu}_5 - \gamma_0 \otimes \delta\mathbf{m} - \gamma_0\gamma_5 \otimes \delta\mathbf{m}_5, \tag{E.3a}$$
$$\mathbf{B} = \gamma_C\gamma_5 \otimes \boldsymbol{\Delta} + \gamma_C \otimes \boldsymbol{\Delta}_5 + \gamma_0\gamma_C\gamma_5 \otimes \boldsymbol{\kappa} + \gamma_0\gamma_C \otimes \boldsymbol{\kappa}_5. \tag{E.3b}$$

In order to allow for a computer to enumerate the parameters, we introduce a systematic method for labelling the parameters. First, we use one of the names μ, μ^5, m, m^5, Δ, Δ^5, κ, or κ^5 corresponding to the structure given in (E.3). We then use a two-digit index to specify which elements are non-zero and an i indicates that the specified element is i rather than simply 1. The symmetric entry must also be set so that the resulting matrix $\gamma \otimes \mu$ is either Hermitian or anti-symmetric depending on whether or not it parametrizes $\mathbf{A}$ or $\mathbf{B}$ respectively. In total, there are 666 independent

matrices. For example

$$\mu_{12} = \mu_{12}^5 = \mathbf{m}_{12} = \Delta_{12} = \Delta_{12}^5 = \kappa_{12} = \begin{pmatrix} 0 & 1 & 0 & \cdots \\ 1 & 0 & 0 & \\ 0 & 0 & 0 & \\ \vdots & & & \ddots \end{pmatrix}, \tag{E.4a}$$

$$\mathbf{m}_{12}^5 = \kappa_{12}^5 = \begin{pmatrix} 0 & 1 & 0 & \cdots \\ -1 & 0 & 0 & \\ 0 & 0 & 0 & \\ \vdots & & & \ddots \end{pmatrix}, \tag{E.4b}$$

$$\mu_{12i} = \mu_{12i}^5 = \mathbf{m}_{12i} = \kappa_{12i}^5 = \begin{pmatrix} 0 & i & 0 & \cdots \\ -i & 0 & 0 & \\ 0 & 0 & 0 & \\ \vdots & & & \ddots \end{pmatrix}, \tag{E.4c}$$

$$\mathbf{m}_{12i}^5 = \Delta_{12i} = \Delta_{12i}^5 = \kappa_{12i} = \begin{pmatrix} 0 & i & 0 & \cdots \\ i & 0 & 0 & \\ 0 & 0 & 0 & \\ \vdots & & & \ddots \end{pmatrix}. \tag{E.4d}$$

The reason that $\mathbf{m}^5$ and κ^5 behave differently than the others is that, while $\mathbf{1}$, γ_5, and γ_0 are Hermitian, $\gamma_0\gamma_5$ is anti-Hermitian. Likewise, while $\gamma_C\gamma_5$, γ_C, and $\gamma_0\gamma_C\gamma_5$ are anti-symmetric, $\gamma_0\gamma_C$ is symmetric. Again, recall that these are all specified in the "unlocking" basis which is ordered as

$$\text{ru, gd, bs, rd, gu, rs, bu, gs, bd.} \tag{E.5}$$

The parity even CFL state with no mass or hypercharge is expressed in terms of this parametrization as

$$\Delta_{12} = \Delta_{13} = \Delta_{23} = (\Delta_3 + \Delta_6)/2, \tag{E.6a}$$

$$\Delta_{45} = \Delta_{67} = \Delta_{89} = (\Delta_6 - \Delta_3)/2, \tag{E.6b}$$

$$\Delta_{11} = \Delta_{22} = \Delta_{33} = \Delta_6, \tag{E.6c}$$

$$\mu_{12} = \mu_{13} = \mu_{23} = -3\mu_{\text{oct}}, \tag{E.6d}$$

$$\mu_{e3} = 3\mu_{e8} = -\mu_{f3} = \mu_{f8} = -3\mu_{\text{oct}}/4. \tag{E.6e}$$

Here are some comparisons with other conventions in the literature. Alford, Kouvaris, and Rajagopal [21] introduce Δ_1, $\Delta 2$ and Δ_3 which are all related

to the attractive anti-symmetric $\bar{3}$ channel:

$$\Delta_{23} = \Delta_{89} = \Delta_1, \tag{E.7a}$$
$$\Delta_{13} = \Delta_{67} = \Delta_2, \tag{E.7b}$$
$$\Delta_{12} = \Delta_{45} = \Delta_3. \tag{E.7c}$$

Rüster, Shovkovy, and Rischke [25] introduces the parameters ϕ, φ and σ which include the repulsive symmetric 6 channel parameters:

$$\Delta_{23} = \varphi_1, \quad \Delta_{13} = \varphi_2, \quad \Delta_{12} = \varphi_3, \tag{E.8a}$$
$$\Delta_{89} = \phi_1, \quad \Delta_{67} = \phi_2, \quad \Delta_{45} = \phi_3, \tag{E.8b}$$
$$\Delta_{11} = \sigma_1, \quad \Delta_{22} = \sigma_2, \quad \Delta_{33} = \sigma_3. \tag{E.8c}$$

Finally, Buballa [145] uses only the following parameters to parametrize the meson condensed phases:

$$-\Delta_{12} = \Delta_{45} = s_{22}/4, \tag{E.9a}$$
$$-\Delta_{13} = \Delta_{67} = s_{55}/4, \tag{E.9b}$$
$$-\Delta_{23} = \Delta_{89} = s_{77}/4, \tag{E.9c}$$
$$-\Delta^5_{19i} = \Delta^5_{47i} = p_{25}/4, \tag{E.9d}$$
$$-\Delta^5_{18i} = \Delta^5_{56i} = p_{52}/4. \tag{E.9e}$$

In Tables E.1, E.2, E.3, and E.4 we give the numerical values of the parameters for each of the states displayed in Figures 7.1, 7.3, 7.2, and 7.4 respectively. We only list the non-zero parameters: the other parameters are zero.

Param.	$\mu_Y = 0.50\mu_Y^c$		$\mu_Y = \mu_Y^c$	
	Bare	Correction	Bare	Correction
$\mu_B/3$	+549.93	−49.93	+549.93	−49.93
μ_8	−12.5	0	−25	0
μ_Y	+12.5	0	+25	0
μ_{oct}	0	−0.031332	0	−0.031332
Δ_3	0	+25.657	0	+25.657
Δ_6	0	+0.65709	0	+0.65709

Table E.1: Parameters required for a self-consistent parity-even CFL solution in the presence of a hypercharge chemical potential. These values correspond to the dispersions shown in Figure 7.1. All values are in MeV. The first column labelled "Bare" gives the fixed bare parameters that enter the Hamiltonian (7.7). The column labelled "Correction" is the contribution from the self-energy. The sum of the columns is the value that enters the quadratic Hamiltonian (7.13).

	$\mu_Y = 0.50\mu_Y^c$		$\mu_Y = 1.20\mu_Y^c$	
Param.	Bare	Correction	Bare	Correction
$\mu_B/3$	+549.93	−49.932	+549.93	−49.947
μ_Y	+12.5	−1.0687	+30	−2.5931
μ_e	0	+0.53436	0	+1.2965
μ_3	−6.4772	−0.00000	−16.346	-3.331×10^{-7}
μ_8	−3.2386	−0.00000	−8.1729	-1.665×10^{-7}
μ_{e3}	0	+0.02421	0	+0.027856
μ_{e8}	0	+0.0080699	0	+0.0092853
μ_{f3}	0	+0.035998	0	+0.084801
μ_{f8}	0	+0.011999	0	+0.028267
$\mu_{12} = \mu^5_{18i}$	0	+0.016852	0	−0.047357
$\mu_{13} = \mu^5_{19i}$	0	+0.11902	0	+0.19694
$\mu_{23} = \mu_{89}$	0	+0.046967	0	+0.046617
μ^5_{28i}	0	+0.088616	0	+0.14526
$\mu^5_{29i} = \mu^5_{38i}$	0	+0.046967	0	+0.046617
μ^5_{39i}	0	+0.0030234	0	−0.065811
μ^5_{46i}	0	+0.11479	0	+0.27514
Δ_{11}	0	+0.64468	0	+0.5851
$\Delta_{22} = -\Delta_{88} = -\Delta^5_{28i}$	0	+0.32265	0	+0.31566
$\Delta_{33} = -\Delta_{99} = -\Delta^5_{39i}$	0	+0.33523	0	+0.34523
$\Delta_{12} = -\Delta^5_{18i}$	0	+9.6383	0	+10.138
$\Delta_{13} = -\Delta^5_{19i}$	0	+8.9893	0	+8.5746
$\Delta_{23} = -\Delta_{89}$	0	+12.789	0	+12.605
$\Delta_{45} = -\Delta^5_{56i}$	0	−9.1811	0	−9.7012
$\Delta_{67} = -\Delta^5_{47i}$	0	−8.5229	0	−8.1128
$\Delta^5_{29i} = \Delta^5_{38i}$	0	−0.33242	0	−0.35025

Table E.2: Parameters required for a self-consistent CFLK0 solution in the presence of a hypercharge chemical potential. These values correspond to the dispersions shown in Figure 7.3. All values are in MeV. The first column labelled "Bare" gives the fixed bare parameters that enter the Hamiltonian (7.7). The column labelled "Correction" is the contribution from the self-energy. The sum of the columns is the value that enters the quadratic Hamiltonian (7.13).

	$M_s^2/(2\mu) = 0.50\mu_Y^c$		$M_s^2/(2\mu) = 0.83\mu_Y^c$	
Param.	Bare	Correction	Bare	Correction
$\mu_B/3$	+549.93	−48.952	+549.93	−48.316
μ_8	−12.649	−0.00000	−20.95	$+1.469 \times 10^{-7}$
μ_{e3}	0	+0.022617	0	+0.022026
μ_{e8}	0	+0.0074542	0	+0.0072087
μ_{f3}	0	−0.022617	0	−0.022026
μ_{f8}	0	+0.022362	0	+0.021626
μ_{12}	0	+0.090467	0	+0.088103
$\mu_{13} = \mu_{23}$	0	+0.088963	0	+0.085669
$m_{ur} = m_{dg}$	0	+0.15778	0	+0.19366
$m_{ug} = m_{dr}$	0	+0.17255	0	+0.2117
$m_{ub} = m_{db}$	0	+0.15604	0	+0.19155
$m_{sr} = m_{sg}$	+61.843	+50.029	+80	+64.267
m_{sb}	+61.843	+50.079	+80	+64.329
m_{12}	0	−0.014765	0	−0.018037
$m_{13} = m_{23}$	0	+0.026496	0	+0.032723
$\Delta_{11} = \Delta_{22}$	0	−0.62077	0	−0.59745
Δ_{33}	0	−0.64043	0	−0.62926
Δ_{12}	0	−12.914	0	−12.753
$\Delta_{13} = \Delta_{23}$	0	−12.639	0	−12.302
Δ_{45}	0	+12.293	0	+12.155
$\Delta_{67} = \Delta_{89}$	0	+12.011	0	+11.693
κ_{11}	0	$+3.8762 \times 10^{-6}$	0	$+5.1011 \times 10^{-6}$
κ_{22}	0	$+3.8762 \times 10^{-6}$	0	$+5.0102 \times 10^{-6}$
κ_{33}	0	+0.078913	0	+0.098773
κ_{12}	0	+0.0017234	0	+0.0020923
$\kappa_{13} = \kappa_{23}$	0	+0.52751	0	+0.66061
κ_{45}	0	−0.0017195	0	−0.0020872
$\kappa_{67} = \kappa_{89}$	0	−0.48835	0	−0.61184

Table E.3: Parameters required for a self-consistent parity even CFL solution in the presence of a strange quark mass. These values correspond to the dispersions shown in Figure 7.2. All values are in MeV. The first column labelled "Bare" gives the fixed bare parameters that enter the Hamiltonian (7.7). The column labelled "Correction" is the contribution from the self-energy. The sum of the columns is the value that enters the quadratic Hamiltonian (7.13). For example, the right set of data (just slightly before the CFL/gCFL transition) has a bare (current) strange quark mass of 0 MeV. This corresponds to a constituent quark mass of $80+64 \approx 144$ MeV. (Note that there is a slight difference for the blue constituent quark masses because of the presence of the coloured chemical potential μ_8 required to enforce neutrality.)

	$M_s^2/(2\mu) = 0.50\mu_Y^c$		$M_s^2/(2\mu) = 0.84\mu_Y^c$	
Param.	Bare	Correction	Bare	Correction
$\mu_B/3$	+549.93	−48.951	+549.93	−48.09
μ_3	−6.6057	−0.00000	−13.002	-8.7×10^{-8}
μ_8	−3.3029	−0.00000	−6.5008	-4.35×10^{-8}
μ_f	0	−0.53978	0	−1.0238
μ_{e3}	0	+0.023555	0	+0.025582
μ_{e8}	0	+0.0078516	0	+0.0085274
μ_{f3}	0	+0.035852	0	+0.066184
μ_{f8}	0	+0.011951	0	+0.022061
$\mu_{12} = \mu^5_{18i}$	0	+0.014623	0	−0.026924
$\mu_{13} = \mu^5_{19i}$	0	+0.11615	0	+0.16265
$\mu_{23} = \mu_{89}$	0	+0.044694	0	+0.042908
μ^5_{28i}	0	+0.086431	0	+0.11903
$\mu^5_{29i} = \mu^5_{38i}$	0	+0.044644	0	+0.042927
μ^5_{39i}	0	−0.001146	0	−0.047235
μ^5_{46i}	0	+0.11528	0	+0.21622
$m_{ug} = -m_{ub}$	0	+0.0077476	0	+0.0093125
m_{dr}	0	+0.17093	0	+0.21503
$m_{dg} = m_{db}$	0	+0.15529	0	+0.19536
m_{sr}	+61.637	+50.279	+85	+69.188
$m_{sg} = m_{sb}$	+61.637	+50.335	+85	+69.301
$m_{12} = -m^5_{18i}$	0	−0.010709	0	−0.013162
$m_{13} = -m^5_{19i}$	0	+0.029548	0	+0.053931
$m_{23} = m_{89}$	0	+0.0134	0	+0.017695
$m^5_{29i} = -m^5_{38i}$	0	−0.012525	0	−0.01659
m^5_{46i}	0	−0.0077707	0	−0.009337
Δ_{11}	0	+0.60701	0	+0.53896
$\Delta_{22} = -\Delta_{88}$	0	+0.30409	0	+0.28263
$\Delta_{33} = -\Delta_{99}$	0	+0.32668	0	+0.32494
$\Delta_{12} = -\Delta^5_{18i}$	0	+9.4718	0	+9.6392
$\Delta_{13} = -\Delta^5_{19i}$	0	+8.614	0	+8.0104
$\Delta_{23} = -\Delta_{89}$	0	+12.282	0	+11.726
$\Delta_{45} = -\Delta^5_{56i}$	0	−9.0411	0	−9.2445
$\Delta_{67} = -\Delta^5_{47i}$	0	−8.1684	0	−7.5847
Δ^5_{28i}	0	−0.30382	0	−0.28208
$\Delta^5_{29i} = \Delta^5_{38i}$	0	−0.31799	0	−0.31604
Δ^5_{39i}	0	−0.32038	0	−0.31321
$\kappa_{22} = -\kappa_{88}$	0	-1.7029×10^{-5}	0	-1.3167×10^{-5}
$\kappa_{33} = -\kappa_{99}$	0	−0.040639	0	−0.055178
$\kappa_{12} = \kappa^5_{18i}$	0	−0.00066095	0	−0.00090186
$\kappa_{13} = \kappa^5_{19i}$	0	−0.36095	0	−0.46324
$\kappa_{23} = -\kappa_{89}$	0	−0.50626	0	−0.66374
$\kappa_{45} = -\kappa^5_{56i}$	0	+0.00075037	0	+0.001152
$\kappa_{67} = \kappa^5_{47i}$	0	+0.33313	0	+0.4268
$\kappa^5_{29i} = -\kappa^5_{38i}$	0	−0.019786	0	−0.026852

Table E.4: Parameters required for a self-consistent CFLK0 solution in the presence of a strange quark mass. These values correspond to the dispersions shown in Figure 7.4. All values are in MeV.

Bibliography

[1] M. M. Forbes, E. Gubankova, W. V. Liu, and F. Wilczek, Phys. Rev. Lett. **94**, 017001 (2005), `hep-ph/0405059`.

[2] M. M. Forbes (2004), `hep-ph/0411001`.

[3] F. Wilczek, Phys. Rev. Lett. **48**, 1144 (1982).

[4] F. J. Dyson, Journal of Mathematical Physics **8**, 1538 (1967).

[5] F. Wilczek, arXiv:hep-ph/0502113 (2005), lecture on receipt of the 2004 Nobel Prize.

[6] E. H. Lieb and M. Loss, arXiv:math-ph/0408001 (2004).

[7] E. H. Lieb, arXiv:math-ph/0401004 (2004).

[8] J. Bardeen, L. N. Cooper, and J. R. Schrieffer, Phys. Rev. **108**, 1175 (1957).

[9] R. P. Feynman, *Statistical Mechanics*, Advanced Book Classics (Perseus Books, Reading, Massachusetts, 1998), 2nd ed.

[10] R. W. Richardson, Phys. Lett. **3**, 277 (1963).

[11] J. Dukelsky, S. Pittel, and G. Sierra (2004), `nucl-th/0405011`.

[12] G. Ortiz, R. Somma, J. Dukelsky, and S. Rombouts, Nucl. Phys. **B707**, 421 (2005), `cond-mat/0407429`.

[13] G. Ortiz and J. Dukelsky (2005), `cond-mat/0503664`.

[14] M. Buballa and M. Oertel, Nucl. Phys. **A703**, 770 (2002), `hep-ph/0109095`.

[15] A. J. Leggett, Rev. Mod. Phys. **47**, 331 (1975).

[16] G. Sarma, Phys. Chem. Solid **24**, 1029 (1963).

[17] M. G. Alford, J. Berges, and K. Rajagopal, Phys. Rev. Lett. **84**, 598 (2000), hep-ph/9908235.

[18] W. V. Liu and F. Wilczek, Phys. Rev. Lett. **90**, 047002 (2003), cond-mat/0208052.

[19] S.-T. Wu and S. Yip, Phys. Rev. **A67**, 053603 (2003), arXiv: cond-mat/0303185.

[20] I. Shovkovy and M. Huang, Phys. Lett. **B564**, 205 (2003), hep-ph/0302142.

[21] M. Alford, C. Kouvaris, and K. Rajagopal, Phys. Rev. Lett. **92**, 222001 (2004), hep-ph/0311286.

[22] E. Gubankova, W. V. Liu, and F. Wilczek, Phys. Rev. Lett. **91**, 032001 (2003), hep-ph/0304016.

[23] P. F. Bedaque, H. Caldas, and G. Rupak, Phys. Rev. Lett. **91**, 247002 (2003), cond-mat/0306694.

[24] J. Carlson and S. Reddy (2005), cond-mat/0503256.

[25] S. B. Ruster, I. A. Shovkovy, and D. H. Rischke, Nucl. Phys. **A743**, 127 (2004), hep-ph/0405170.

[26] M. Alford, C. Kouvaris, and K. Rajagopal (2004), hep-ph/0406137.

[27] K. Fukushima, C. Kouvaris, and K. Rajagopal, Phys. Rev. **D71**, 034002 (2005), arXiv:hep-ph/0408322.

[28] S. B. Ruster, V. Werth, M. Buballa, I. A. Shovkovy, and D. H. Rischke (2005), hep-ph/0503184.

[29] M. Huang and I. A. Shovkovy, Phys. Rev. D **70**, 051501 (2004), hep-ph/0407049.

[30] R. Casalbuoni, R. Gatto, M. Mannarelli, G. Nardulli, and M. Ruggieri, Phys. Lett. **B605**, 362 (2005), hep-ph/0410401.

[31] M. Alford and Q.-h. Wang (2005), hep-ph/0501078.

[32] A. I. Larkin and Y. N. Ovchinnikov, Sov. Phys. JETP **20**, 762 (1965), zh. Eksper. Teoret. Fiz. 47 1136-1146.

[33] P. Fulde and R. A. Ferrell, Phys. Rev. **135**, A550 (1964).

[34] M. G. Alford, J. A. Bowers, and K. Rajagopal, Phys. Rev. **D63**, 074016 (2001), hep-ph/0008208.

[35] J. A. Bowers, J. Kundu, K. Rajagopal, and E. Shuster, Phys. Rev. **D64**, 014024 (2001), hep-ph/0101067.

[36] J. Kundu and K. Rajagopal, Phys. Rev. **D65**, 094022 (2002), hep-ph/0112206.

[37] G. Nardulli, Riv. Nuovo Cim. **25N3**, 1 (2002), hep-ph/0202037.

[38] J. A. Bowers and K. Rajagopal, Phys. Rev. **D66**, 065002 (2002), hep-ph/0204079.

[39] J. A. Bowers (2003), hep-ph/0305301.

[40] R. Casalbuoni et al., Phys. Rev. **D70**, 054004 (2004), hep-ph/0404090.

[41] H. Caldas, C. W. Morais, and A. L. Mota (2005), hep-ph/0502003.

[42] E. Gubankova, F. Wilczek, and E. G. Mishchenko, Phys. Rev. Lett. **94**, 110402 (2005), cond-mat/0409088.

[43] E. Gubankova, E. Mishchenko, and F. Wilczek (2004), cond-mat/0411238.

[44] M. Alford, P. Jotwani, C. Kouvaris, J. Kundu, and K. Rajagopal (2004), astro-ph/0411560.

[45] M. Huang and I. A. Shovkovy, Phys. Rev. **D70**, 094030 (2004), hep-ph/0408268.

[46] I. Giannakis and H.-C. Ren, Phys. Lett. **B611**, 137 (2005), hep-ph/0412015.

[47] I. Giannakis and H.-C. Ren (2005), hep-th/0504053.

[48] C. J. Pethick and H. Smith, *Bose-Einsten Condensation in Dilute Gases* (Cambridge University Press, Cambridge, 2002).

[49] H. Caldas, Phys. Rev. A **69**, 063602 (2003), hep-ph/0312275.

[50] S. Weinberg, Nucl. Phys. **B413**, 567 (1994), cond-mat/9306055.

[51] R. Shankar, Rev. Mod. Phys. **66**, 129 (1994).

[52] J. Goldstone, Nuovo Cim. **19**, 154 (1961).

[53] J. Goldstone, A. Salam, and S. Weinberg, Phys. Rev. **127**, 965 (1962).

[54] T. Schafer, ECONF **C030614**, 038 (2003), hep-ph/0310176.

[55] N. K. Glendenning, Phys. Rev. **D46**, 1274 (1992).

[56] N. K. Glendenning and S. Pei, Phys. Rev. **C52**, 2250 (1995).

[57] S. Reddy and G. Rupak, Phys. Rev. **C71**, 025201 (2005), nucl-th/0405054.

[58] M. Alford, C. Kouvaris, and K. Rajagopal (2004), hep-ph/0407257.

[59] S. Jochim, M. Bartenstein, A. Altmeyer, G. Hendl, S. Riedl, C. Chin, J. H. Denschlag, and R. Grimm, Science **302**, 2101 (2003).

[60] M. Greiner, C. A. Regal, and D. S. Jin, Nature **426**, 537 (2003).

[61] M. W. Zwierlein, C. A. Stan, C. H. Schunck, S. M. F. Raupach, S. Gupta, Z. Hadzibabic, and W. Ketterle, Phys. Rev. Lett. **91**, 250401 (2003).

[62] C. A. Regal, M. Greiner, and D. S. Jin, Phys. Rev. Lett. **92**, 040403 (2004).

[63] M. Bartenstein, A. Altmeyer, S. Riedl, S. Jochim, C. Chin, J. H. Denschlag, and R. Grimm, Phys. Rev. Lett. **92**, 120401 (2004).

[64] M. W. Zwierlein, C. A. Stan, C. H. Schunck, S. M. F. Raupach, A. J. Kerman, and W. Ketterle, Phys. Rev. Lett. **92**, 120403 (2004), arXiv:cond-mat/0403049.

[65] C. A. Stan, M. W. Zwierlein, C. H. Schunck, S. M. F. Raupach, and W. Ketterle, Phys. Rev. Lett. **93**, 143001 (2004), arXiv:cond-mat/0406129.

[66] C. H. Schunck, M. W. Zwierlein, C. A. Stan, S. M. F. Raupach, W. Ketterle, A. Simoni, E. Tiesinga, C. J. Williams, and P. S. Julienne, arXiv:cond-mat/0407373 (2004), arXiv:cond-mat/0407373.

[67] H. Feshbach, Ann. Phys. **5**, 357 (1958).

[68] U. Fano, Nuovo Cimento **12**, 154 (1935), arXiv:cond-mat/0502210.

[69] U. Fano, Phys. Rev. **124**, 1866 (1961).

[70] W. V. Liu, F. Wilczek, and P. Zoller, Phys. Rev. A **70** (2004), cond-mat/0404478.

[71] J. I. Cirac and P. Zoller, Physics Today **57**, 38 (2004).

[72] D. S. Petrov, Phys. Rev. Lett. **93**, 143201 (2004), arXiv:cond-mat/0404036.

[73] D. S. Petrov, C. Salomon, and G. V. Shlyapnikov, arXiv:cond-mat/0502010 (2005), arXiv:cond-mat/0502010.

[74] *Three-boson problem near a narrow feshbach resonance*, Talk given at Strongly Interacting Quantum Gases: 18-21 April 2005. Ohio Center for Theoretical Science (OCTS) at The Ohio State University, Columbus, Ohio (2005), URL http://octs.osu.edu/images/Gases/Abstracts/Petrov.pdf.

[75] J. E. Jaffe and N. W. Ashcroft, Phys. Rev. **B23**, 6176 (1981).

[76] R. L. Barnett, Private Communication (2005).

[77] H. H. Suhl, B. T. Matthias, and L. R. Walker, Phys. Rev. Lett. **3**, 552 (1959).

[78] J. Kondo, Prog. Theor. Phys. **29**, 1 (1963).

[79] G. Vignale and K. S. Singwi, Phys. Rev. **B31**, 2729 (1985).

[80] C. W. Lai, J. Zoch, A. C. Gossard, and D. S. Chemla, Science **303**, 503 (2004).

[81] R. F. Streater and A. S. Wightman, *PCT, spin and statistics, and all that*, Mathematical physics monograph series (Benjamin/Cummings, Reading, Mass., 1978).

[82] H. Georgi and S. L. Glashow, Phys. Rev. Lett. **32**, 438 (1974).

[83] S. F. King, Rept. Prog. Phys. **67**, 107 (2004), hep-ph/0310204.

[84] H.-Y. Cheng, Phys. Rept. **158**, 1 (1988).

[85] R. D. Peccei, in *CP violation*, edited by C. Jarlskog (World Scientific, Singapore, 1989).

[86] J. E. Kim (1999), `arXiv:astro-ph/0002193`.

[87] S. D. H. Hsu and F. Sannino, Phys. Lett. **B605**, 369 (2005), `hep-ph/0408319`.

[88] S. Coleman, *Aspects of symmetry: Selected Erice Lectures of Sidney Coleman* (Cambridge University Press, Cambridge, 1988).

[89] P. W. Anderson, Phys. Rev. **110**, 827 (1958).

[90] P. W. Anderson, Phys. Rev. **130**, 439 (1963).

[91] F. Englert and R. Brout, Phys. Rev. Lett. **13**, 321 (1964).

[92] G. S. Guralnik, C. R. Hagen, and T. W. B. Kibble, Phys. Rev. Lett. **13**, 585 (1964).

[93] P. W. Higgs, Phys. Lett. **12**, 132 (1964).

[94] P. W. Higgs, Phys. Rev. Lett. **13**, 508 (1964).

[95] P. W. Higgs, Phys. Rev. **145**, 1156 (1966).

[96] Y. Nambu, Phys. Rev. Lett. **4**, 380 (1960).

[97] Y. Nambu and G. Jona-Lasinio, Phys. Rev. **122**, 345 (1961).

[98] Y. Nambu and G. Jona-Lasinio, Phys. Rev. **124**, 246 (1961).

[99] P. W. Anderson, Phys. Rev. **112**, 1900 (1958).

[100] N. N. Bogoliubov, Nuovo Cimento **7**, 794 (1958).

[101] S. Eidelman, K. Hayes, K. Olive, M. Aguilar-Benitez, C. Amsler, D. Asner, K. Babu, R. Barnett, J. Beringer, P. Burchat, et al. (Particle Data Group), Phys. Lett. **B592**, 1+ (2004), URL `http://pdg.lbl.gov`.

[102] J. M. Lattimer and M. Prakash, Phys. Rev. Lett. **94**, 111101 (2005), `astro-ph/0411280`.

[103] H. A. Buchdahl, Phys. Rev. **116**, 2013 (1959).

[104] D. J. Gross and F. Wilczek, Phys. Rev. Lett. **30**, 1343 (1973).

[105] H. D. Politzer, Phys. Rev. Lett. **30**, 1346 (1973).

[106] D. J. Gross and F. Wilczek, Phys. Rev. **D8**, 3633 (1973).

[107] D. J. Gross and F. Wilczek, Phys. Rev. **D9**, 980 (1974).

[108] H. Georgi and H. D. Politzer, Phys. Rev. **D9**, 416 (1974).

[109] M. Troyer and U.-J. Wiese (2004), `cond-mat/0408370`.

[110] M. Alford, K. Rajagopal, and F. Wilczek, Phys. Lett. **B422**, 247 (1998), `arXiv:hep-ph/9711395`.

[111] B. C. Barrois, Nucl. Phys. **B129**, 390 (1977).

[112] S. Frautschi (Erice, 1978), proceedings of workshop on hadronic matter at extreme density.

[113] B. C. Barrois, Ph.D. thesis, Caltech (1979), UMI 79-04847-mc.

[114] D. Bailin and A. Love, Phys. Rept. **107**, 325 (1984).

[115] R. Rapp, T. Schafer, E. V. Shuryak, and M. Velkovsky, Phys. Rev. Lett. **81**, 53 (1998), `arXiv:hep-ph/9711396`.

[116] M. Alford, K. Rajagopal, and F. Wilczek, Nucl. Phys. **B537**, 443 (1999), `arXiv:hep-ph/9804403`.

[117] D. T. Son, Phys. Rev. **D59**, 094019 (1999), `arXiv:hep-ph/9812287`.

[118] D. K. Hong, Nucl. Phys. **B582**, 451 (2000), `hep-ph/9905523`.

[119] N. J. Evans, J. Hormuzdiar, S. D. H. Hsu, and M. Schwetz, Nucl. Phys. **B581**, 391 (2000), `hep-ph/9910313`.

[120] K. Rajagopal and F. Wilczek (2000), `arXiv:hep-ph/0011333`.

[121] M. G. Alford, Ann. Rev. Nucl. Part. Sci. **51**, 131 (2001), `hep-ph/0102047`.

[122] S. Reddy, Acta Phys. Polon. **B33**, 4101 (2002), `nucl-th/0211045`.

[123] T. Schafer (2003), `hep-ph/0304281`.

[124] T. Schafer, Nucl. Phys. **B575**, 269 (2000), `arXiv:hep-ph/9909574`.

[125] I. A. Shovkovy and L. C. R. Wijewardhana, Phys. Lett. **B470**, 189 (1999), hep-ph/9910225.

[126] R. Casalbuoni and R. Gatto, Phys. Lett. **B464**, 111 (1999), hep-ph/9908227.

[127] D. K. Hong, Phys. Lett. **B473**, 118 (2000), hep-ph/9812510.

[128] S. R. Beane, P. F. Bedaque, and M. J. Savage, Phys. Lett. **B483**, 131 (2000), arXiv:hep-ph/0002209.

[129] V. A. Miransky, I. A. Shovkovy, and L. C. R. Wijewardhana, Phys. Lett. **B468**, 270 (1999), arXiv:hep-ph/9908212.

[130] D. T. Son and M. A. Stephanov, Phys. Rev. **D61**, 074012 (2000), erratum: [131], arXiv:hep-ph/9910491.

[131] D. T. Son and M. A. Stephanov, Phys. Rev. **D62**, 059902 (2000), erratum to [130], arXiv:hep-ph/0004095.

[132] M. Rho, A. Wirzba, and I. Zahed, Phys. Lett. **B473**, 126 (2000), hep-ph/9910550.

[133] D. K. Hong, T. Lee, and D.-P. Min, Phys. Lett. **B477**, 137 (2000), hep-ph/9912531.

[134] C. Manuel and M. H. G. Tytgat, Phys. Lett. **B479**, 190 (2000), hep-ph/0001095.

[135] M. Rho, E. V. Shuryak, A. Wirzba, and I. Zahed, Nucl. Phys. **A676**, 273 (2000), hep-ph/0001104.

[136] K. Zarembo, Phys. Rev. **D62**, 054003 (2000), arXiv:hep-ph/0002123.

[137] D. K. Hong, Phys. Rev. **D62**, 091501 (2000), hep-ph/0006105.

[138] T. Schafer, Phys. Rev. **D65**, 074006 (2002), hep-ph/0109052.

[139] T. Schafer, Phys. Rev. Lett. **85**, 5531 (2000), arXiv:nucl-th/0007021.

[140] P. F. Bedaque and T. Schafer, Nucl. Phys. **A697**, 802 (2002), arXiv:hep-ph/0105150.

[141] D. B. Kaplan and S. Reddy, Phys. Rev. **D65**, 054042 (2002), arXiv: hep-ph/0107265.

[142] A. Kryjevski and D. Yamada, Phys. Rev. **D71**, 014011 (2005), hep-ph/0407350.

[143] A. Kryjevski and T. Schafer, Phys. Lett. **B606**, 52 (2005), arXiv: hep-ph/0407329.

[144] A. Barducci, R. Casalbuoni, G. Pettini, and L. Ravagli, Phys. Rev. **D71**, 016011 (2005), hep-ph/0410250.

[145] M. Buballa, Phys. Lett. **B609**, 57 (2005), hep-ph/0410397.

[146] T. Schafer and F. Wilczek, Phys. Rev. Lett. **82**, 3956 (1999), arXiv: hep-ph/9811473.

[147] M. Alford, J. Berges, and K. Rajagopal, Nucl. Phys. **B571**, 269 (2000), arXiv:hep-ph/9910254.

[148] M. Alford and K. Rajagopal, JHEP **06**, 031 (2002), hep-ph/0204001.

[149] R. Rapp, T. Schafer, E. V. Shuryak, and M. Velkovsky, Annals Phys. **280**, 35 (2000), arXiv:hep-ph/9904353.

[150] D. T. Son, M. A. Stephanov, and A. R. Zhitnitsky, Phys. Lett. **B510**, 167 (2001), arXiv:hep-ph/0103099.

[151] T. Schafer, Phys. Rev. **D65**, 094033 (2002), hep-ph/0201189.

[152] A. Kryjevski, D. B. Kaplan, and T. Schafer, Phys. Rev. **D71**, 034004 (2005), arXiv:hep-ph/0404290.

[153] K. Rajagopal and F. Wilczek, Phys. Rev. Lett. **86**, 3492 (2001), hep-ph/0012039.

[154] P. F. Bedaque, Nucl. Phys. **A697**, 569 (2002), hep-ph/9910247.

[155] M. G. Alford, J. A. Bowers, and K. Rajagopal, J. Phys. **G27**, 541 (2001), arXiv:hep-ph/0009357.

[156] A. Kryjevski, Phys. Rev. **D68**, 074008 (2003), hep-ph/0305173.

[157] A. Gerhold and A. Rebhan, Phys. Rev. **D68**, 011502 (2003), hep-ph/ 0305108.

[158] M. G. Alford, J. Berges, and K. Rajagopal, Nucl. Phys. **B558**, 219 (1999), hep-ph/9903502.

[159] D. K. Hong, M. Rho, and I. Zahed, Phys. Lett. **B468**, 261 (1999), arXiv:hep-ph/9906551.

[160] J. Wess and B. Zumino, Phys. Lett. **B37**, 95 (1971).

[161] E. Witten, Nucl. Phys. **B223**, 433 (1983).

[162] T. Schafer, Nucl. Phys. **A728**, 251 (2003), hep-ph/0307074.

[163] P. Amore, M. C. Birse, J. A. McGovern, and N. R. Walet, Phys. Rev. **D65**, 074005 (2002), hep-ph/0110267.

[164] M. M. Forbes and J. Kundu, in progress.

[165] S. R. Coleman, J. Wess, and B. Zumino, Phys. Rev. **177**, 2239 (1969).

[166] J. Callan, Curtis G., S. R. Coleman, J. Wess, and B. Zumino, Phys. Rev. **177**, 2247 (1969).

[167] G. L. Sewell, *Quantum Mechanics and Its Emergent Macrophysics* (Princeton University Press, Princeton, New Jersey, 2002).

[168] A. Findlay, A. N. Campbell, and N. O. Smith, *The Phase Rule and Its Applications* (Dover, New York, 1951), ninth ed.

[169] C. Tsallis and E. Brigatti, Continuum Mech. Thermodyn. pp. 223–235 (2004), arXiv:cond-mat/0305606.

[170] C. Tsallis, J. Stat. Phys. **52**, 479 (1988).

[171] E. M. F. Curado and C. Tsallis, J. Phys. **A24**, L69 (1991).

[172] C. Tsallis, F. Baldovin, R. Cerbino, and P. Pierobon, in *The Physics of Complex Systems: New Advances & Perspectives* (2003), arXiv: cond-mat/0309093.